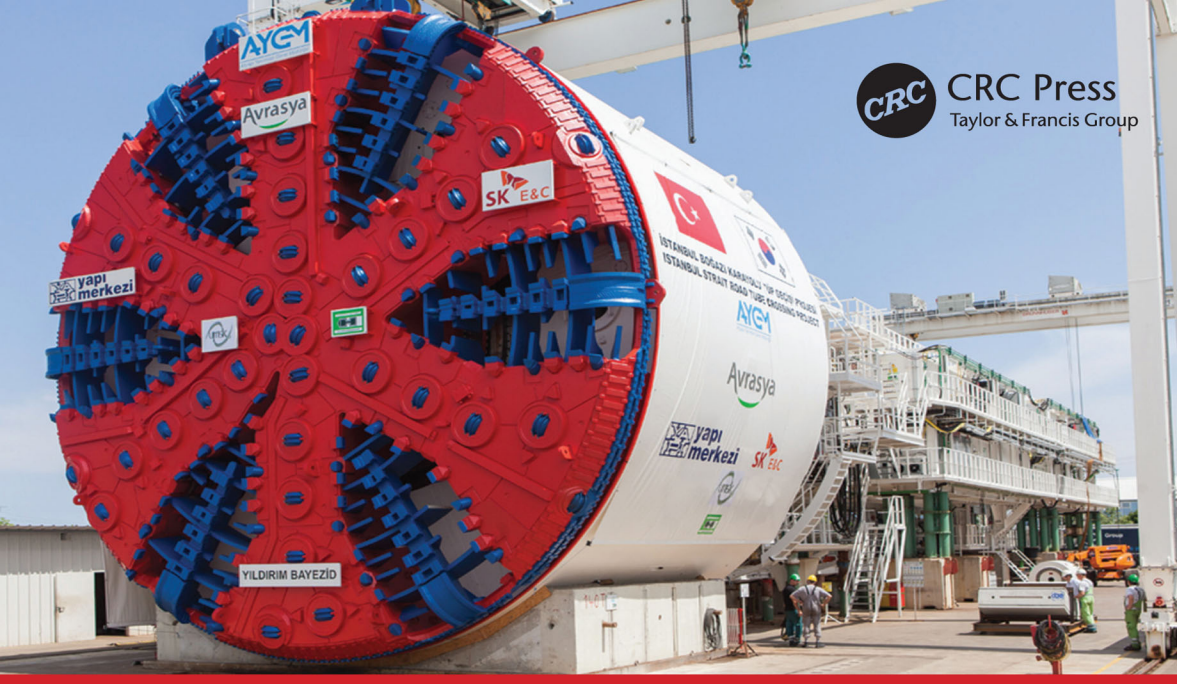

CRC Press
Taylor & Francis Group

Mechanical Excavation in Mining and Civil Industries

Nuh Bilgin | Hanifi Copur | Cemal Balci

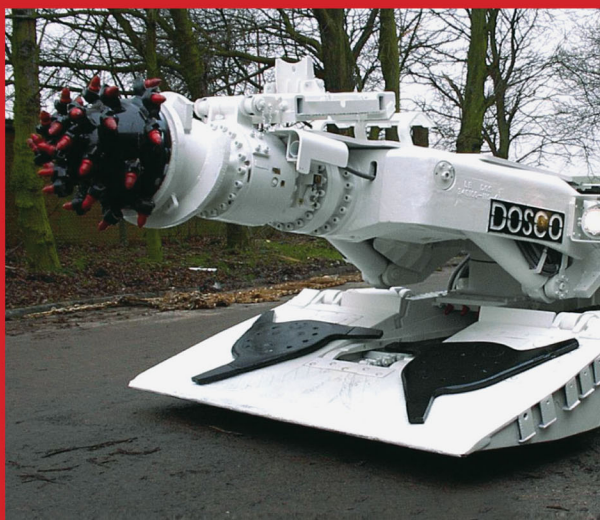

Mechanical Excavation in Mining and Civil Industries

This page intentionally left blank

Mechanical Excavation in Mining and Civil Industries

Nuh Bilgin | Hanifi Copur | Cemal Balci

CRC Press
Taylor & Francis Group
Boca Raton London New York

CRC Press is an imprint of the
Taylor & Francis Group, an **informa** business

CRC Press
Taylor & Francis Group
6000 Broken Sound Parkway NW, Suite 300
Boca Raton, FL 33487-2742

Version Date: 20131009

International Standard Book Number-13: 978-1-4665-8475-4 (eBook - PDF)

This book is dedicated to our lovely wives,

Mrs Ayfer Bilgin, Mrs Nurten Copur, and Mrs Nurgul Celik Balci,

without their patience, tolerance, and help, it would be impossible to write this book.

This page intentionally left blank

Contents

This page intentionally left blank

Preface

This book is intended to reflect several years of experience and accumulated knowledge on mechanized excavation, applied especially in mining and construction industries. First, a brief information and background will be given on site investigation, physical and mechanical properties of rocks, soils, and coal. Then, rock-cutting theories, laboratory rock-cutting tests, wear of cutting tools, roadheaders, impact hammers, hard rock TBMs, soft ground TBMs, microtunnel boring machines, shaft and raise boring machines, large diameter drills, mechanical excavation in coal mines, chain saw machines, and emerging excavation technologies including current research are presented. Almost 50 numerical examples with solutions are included in the book to clarify the topics. It is intended to serve students and practicing engineers in their understanding and decision-making on selecting a proper mechanical excavator for a specific job.

We hope that this book will serve as a sound basis in understanding and applying rapid excavation technologies in construction and mining engineering fields.

Nuh Bilgin
Hanifi Copur
Cemal Balci

This page intentionally left blank

Acknowledgments

Acknowledgments are due to Dr. Sinasi Eskikaya, Dr. Levent Ozdemir, and Dr. Martin Herrenknecht for their contributions on improvement of rapid excavation and tunneling industries in Turkey.

Dr. Hakan Tuncdemir, Dr. Deniz Tumac, and Mr. Emre Avunduk are also acknowledged for their tremendous help in rock-cutting experiments, analyzing, and interpreting the test results.

Some of the figures in Chapter 9 are from Ugur Ates' MSc thesis in interpreted forms, he is also acknowledged for improving the quality of the figures in the book.

This page intentionally left blank

Authors

Nuh Bilgin graduated from the Mining Engineering Department of Istanbul Technical University (ITU). Later he accomplished his PhD studies in the University of Newcastle Upon Tyne, UK in 1977 on "Mechanical Cutting Characteristics of Some Medium and High Strength Rocks." He joined the Mining Engineering Department of ITU in 1978. He was appointed as a full time professor in 1989. He spent one year in the Colorado School of Mines, USA, and one year in Witwatersrand University, SA as a visiting professor. He has published more than a hundred papers on mechanized mining and tunneling technologies. He is currently working in ITU and is chairman of the Turkish Tunnelling Society.

Hanifi Copur graduated from the Mining Engineering Department of ITU. He completed his PhD on rock-cutting mechanics/mechanical excavation of mines and tunnels in the Colorado School of Mines in 1999. He worked as a research engineer in the Excavation Engineering and Earth Mechanics Institute of the Colorado School of Mines between 1995 and 1999. He has been working as an academician in the Mining Engineering Department of ITU since 1999 and currently works as a professor in the same department. He has many national and international scientific and industrial research reports and publications on mechanical mining and tunneling. He is a board member of Turkish Tunnelling Society.

Cemal Balci graduated from the Mining Engineering Department of ITU. In 2004, he received his PhD after completing his thesis on "Comparison of Small and Full Scale Rock Cutting Test to Select Mechanized Excavation Machines" at the Mining Engineering Department of ITU, Mine Mechanization and Technology Division. He joined the research group in Earth Mechanics Institute, Colorado School of Mines in 2001 and remained until 2004 as a researcher. He has published numerous papers on mechanized mining and tunneling technologies and worked in many national and international implementation and research projects. He is currently working in ITU and is a board member of the Turkish Tunnelling Society.

This page intentionally left blank

1

Introduction

1.1 General

Modern society needs excavation of the Earth's crust, especially for mining and construction purposes. The requirement of excavation gradually increases in parallel to the development of the different technologies and the increasing prosperity demand of the societies. This requirement increased tremendously especially after World War II. As a result, many developments were carried out in the excavation industry, particularly in mechanical excavation methods. Drill–blast method is an older excavation method and used very commonly. However, a new scientific discipline called "rock-cutting mechanics" or "mechanical excavation" was born in the early 1950s, and this sped up the competition between mechanical and drill–blast excavation methods. Today, mechanical excavation takes an important share in the excavation industry as an alternative to conventional drill–blast.

Some definition should be well understood to develop a better insight into the rock-cutting mechanics and/or mechanical excavation, which is the main subject of this book. Excavation can be defined as disintegration (breakage, fragmentation, cutting) of the Earth's crust (rocks/rock masses/ground) by means of different methods for economic purposes. Mechanical excavation can be defined as excavation by means of machines transferring the energy as a force from cutting tools (cutters, bits) to the rock/ground by generating concentrated stresses. Rock-cutting mechanics is a scientific discipline that investigates the interaction between cutting tool and rock/ground, the mechanical miner (excavation machine, excavator), and technical–operational–environmental conditions for the purposes of defining the cuttability of rocks. Rock-cutting mechanics also includes designing and selecting mechanical miners, and predicting and optimizing their excavation performance for feasibility and planning purposes.

1.2 Historical Perspective on the Science of Rock-Cutting Mechanics and Mechanical Miners

Most of the scientific development was motivated by the increasing raw material and prosperity requirements in the early 1950s. Early systematic research for rock (coal)-cutting mechanics was begun by the Mining Research Establishment of National Coal Board of England. After a coal plough made in Germany was used for coal winning (Binns and Potts 1955), scientists working in the establishment solved the problems they had encountered, thereby setting the first basic principles of rock-cutting discipline. The first findings, especially for chisel type of cutters, were published in a congress on "Mechanical Properties of Non-Metallic Brittle Materials" (Walton 1958). And then all the studies were gathered in a book (Evans and Pomeroy 1966). These investigations started from drag-type cutting tools to the disk cutters and the machines using them. They were then followed by those carried out in the University of Newcastle Upon Tyne, as well as other universities in England and other European countries up to the 1990s.

One of the most important developments on hard rock excavation was the development of the disk cutter, patented by a mining engineer, James Robbins, from the United States (Stack 2008). This invention caused a rapid increase in the number of the tunneling projects all over the world due to its capability in hard rock cutting. This also caused many new developments, especially in hard rock tunnel boring machine (TBM) technologies. In the 1960s, shielded hard rock TBMs were improved for excavation of the fractured/jointed rock masses in the United States. The improvements in soil excavation machines began during the 1970s, especially in Japan and Germany. Many types of soft ground machines working via face pressure principle were developed in these two countries and are still being developed. Some European countries followed the research trend in soil excavation starting in the 1990s. Scientific investigations currently focus basically on soil and slurry conditioning by chemical additives for improved excavation performance.

Investigations for reaching the underground raw materials as quickly as possible led to the utilization of TBMs in the mining industry. The first TBM application in mining was in Steep Rock underground iron mine in the United States, of which the main development drivages were excavated by a Robbins brand TBM in 1957 (Muirhead 1982). This was followed by many other successful TBM applications in mining such as in many coal mines in England (Tunnicliffe 1982), San Manuel Cooper Mine in Arizona, and Stillwater Platinum and Palladium mine in Montana (Ozdemir 1998).

The U.S. Bureau of Mines started conducting research on rock-cutting mechanics during the 1970s. The first studies were focused on rock cutting with roller cutters and then with drag-type tools. During the same time, the Colorado School of Mines also started conducting research on rock-cutting mechanics and mechanical excavation and the research is still continuing.

Some other universities in the United States followed the Colorado School of Mines by doing research activities on rock cutting.

Research studies in the 1980s were also followed by the universities and private industrial firms or governmental institutions in other countries such as Australia, South Africa, Russia, France, Germany, and Turkey. In some of these countries, the research activities on rock-cutting mechanics and mechanical excavation are still continuing.

1.3 Classification and Comparison of Fragmentation Methods

Currently available are two of the most economical methods of excavation, mechanical excavation and drill and blast methods, used in both mining and construction industries. The mechanical excavation provides an important alternative to drill and blast method and its application and/or market share is gradually increasing in both underground and surface excavations. Mechanical excavation method has some advantages over the conventional drill and blast method as summarized in Table 1.1. There are also some disadvantages/shortcomings of mechanical excavation systems as summarized in Table 1.2. These disadvantages are the main challenges of the mechanical excavation industry.

In addition to the mechanical and drill–blast methods of ground fragmentation, there are some emerging (promising) technologies and novel (in research stage) methods. The novel rock fragmentation/excavation

TABLE 1.1

Basic Advantages of Mechanical Excavation over Drill–Blast

Safer and more environment-friendly operation (no explosive handling–forbidden in urban areas, no blast vibrations in urban areas, no noxious gases, no dust, better workmanship, lesser accidents)
Minimum ground disturbance (lesser overbreak, lesser scaling-support-ventilation requirement, minimized support maintenance, superior ground control in jointed/broken rocks)
Uniform muck size (easy muck/excavated material haulage, no secondary breakage of large rock chunks, lower crushing and mineral processing costs)
Selective mining/excavation capability (minimum ore dilution/minimum mixing with gang, increased ore recovery, separate excavation of rock layers in different strengths making excavation easier)
Continuous operation (not periodic, conducive to automation, excavation–loading–ground supporting simultaneously)
Higher production/excavation rates in favorable ground conditions (higher economical benefits/saving money, earlier mining of high-grade ore, earlier job completion)

Source: Adapted from Ozdemir, L., 1990. Recent developments in hard rock mechanical mining technologies. *Proc. the 4th Canadian Symposium on Mining Automation*, September 16–18, Saskatoon, pp. 143–165; Ozdemir, L., 1992. Mechanical excavation—Today and tomorrow. *Proc. Int. GeoEngineering Conference*, Torino; Ozdemir, L., 1998. Mechanical hard rock mining: Present and future. *Mining Engineering*, March: 36–37.

TABLE 1.2

Basic Disadvantages of Mechanical Excavation Systems over Drill–Blast

Higher initial/capital cost
Lesser flexibility on working conditions
• Very sensitive to ground conditions
• Limited opening cross-section shapes
• Difficult adoptability to a working mine design
Lack of mobility with some underground machines
Inability to cut very hard and very abrasive rock

techniques, such as thermal energy (laser, electric), ultrasound or microwave energy, chemical energy, and water jet cutting, do not currently offer a profitable rock excavation method due to very high specific energy requirements. Emerging technologies have been developed by different manufacturers and are either tested on a limited basis in the laboratory or in the field; none of these systems have been widely accepted so far by the excavation industry, but they are considered as promising or emerging developments.

1.4 Classification of Mechanical Miners

The excavation machines used in mining and civil construction can be classified based on different purposes and/or criterion. They can be classified as surface and underground excavation machines. An excavation machine used in surface operations works in comfortable large areas, is able to use large/heavy machines, requires no illumination during the day light, requires no ventilation, and thus provides safer operations. An excavation machine used in underground operations works in uncomfortable small areas always requires illumination and ventilation, and thus cannot provide a safe operation.

Underground excavation machines can be classified as full-face and partial-face machines based on how they attack the rock face. All the cutters of a full-face machine attack the entire face at the same time; all of them are in contact with the ground simultaneously, the face is excavated as a whole. Tunnel, shaft and raise boring machines, and microtunneling machines are typical full-face machines. Except for borer miners used in the mining of soft minerals such as potash and trona and multihead TBMs used for the excavation of basically soft grounds in short excavation lengths, all the full-face machines create a circular opening. They have very hard rock-cutting abilities due to the roller cutters that they can be used with. However, only a portion of the cutters are in contact with the ground in case of partial-face machines; the face is excavated section by section. These machines can excavate openings other than circular in shape, which is important especially in

TABLE 1.3

General Comparison of Full-Face and Partial-Face Underground Excavation Machines

Criterion	Full-Face	Partial-Face
Cuttable ground types	Very hard rock to soft ground, up to very abrasive rocks.	Medium strength to soft rocks, no or low abrasive rocks.
Mobility	Since they are very large and heavy machines, they are not mobile. It is very difficult or impossible to move these machines from one face to another.	Since they are small machines, they are mobile. It is easy to move these machines from one face to another.
Flexibility	They are not flexible: cannot excavate sharp turns, can excavate only circular cross-section shape, not easily adaptable to a working mine design.	They are flexible: can excavate sharp turns, can excavate any cross-section shapes, easily adaptable to a working mine.
Selective excavation	They are not suitable.	They are suitable.

mining operations requiring a flat-floor. The partial-face machines include roadheaders, continuous miners, shearers, coal ploughs, backhoe excavators, and impact hammers. Some of these machines can be used for both underground and surface excavation operations. Among them, the roadheaders have a special place in terms of flexibility, mobility, and selective excavation ability. The limited strength of drag-type tools is the most important factor affecting the hard-rock-cutting ability of partial-face machines. A general comparison of full-face and partial-face machines is presented in Table 1.3.

Underground excavation machines can be classified based on the inclination of the excavated underground openings, such as horizontal, vertical, or inclined opening excavation machines. All types of excavation machines, used in underground or surface, can be classified based on a number of features: the strength of the excavated ground (such as hard or soft ground excavation machines); their cutterhead motion type (such as machines with axially or transversely rotating cutterheads or linear motion and/or continuous belt-type machines) (Mellor 1976), impact-type machines; preparatory excavation machines (such as drilling machines) or basic excavation machines, or the cutters they use for excavation. As seen, the excavation machines can be classified based on different purposes and/or different features under consideration.

1.5 Classification of Cutting Tools

Today, there are many types of excavation/breakage/disintegration/cutting tools having different geometrical, operational, and material features. The cutting tools have a very special place in mechanical rock excavation since

they are the basic elements transferring the energy of the machines to the ground, generating the required mechanical stresses to break the ground. Therefore, proper selection and design of the cutting tools for any given mechanical miner and geological unit is very important in terms of the economical success of any excavation process.

Many parameters should be considered when choosing a tool for a ground type, such as type, specifications, capacity of the machine; cuttability, strength, abrasiveness, texture, hard mineral content of the ground; tool lacing on cutterhead; tool consumption rate; and cutting capability/performance of the cutting tool. The selection of a suitable cutting tool, which also leads to an optimized design of the cutterhead and mechanical miner, is mainly based on comparison of their cutting performance and tool costs for a given ground/formation.

The cutting tools can be classified based on different purposes and/or different features under consideration. A general classification of cutting tools based on the type of cutting action and application limits in terms of abrasivity and strength of rock masses is given in Table 1.4 (Copur et al. 2012).

The cutting action of drag tools, which limits their utilization up to moderately abrasive medium-strength rocks (up to 100–120 MPa of uniaxial compressive strength), is basically dragging (scratching) with a high friction over the excavated surface, making them prone to wearing out easily. A drag tool keeps its durability mostly up to 4–5 tons of loads. However, the roller cutters are larger/heavier tools that rotate around an axis in cyclic contact with the rock surface, having the unique capability of cutting very hard and abrasive rocks. A roller tool can stand loads up to an average of 20–25 tons, limited by its bearing capacity that is dictated by the cutter diameter.

The common types of drag tools are radial, scraper (wedge, knife, blade, and ripper), chisel (simple chisel), and conical tools (Figure 1.1). All drag tools

TABLE 1.4

General Classification of Cutting Tools Based on Their Action Types

Action	Subaction	Cutting Tools	Operational Limits
Dragging (drag/pick type tools)	Constant (fixed)	Radial	<40–60 MPa UCS,[a] nonabrasive rocks
		Scraper	<60–80 MPa UCS, nonabrasive rocks
		Chisel	<80–100 MPa UCS, low abrasive rocks
	Rotating	Conical	<100–120 MPa UCS, moderately abrasive rocks
Rolling (roller tools)	True rolling	Single-disk	<300 MPa UCS, highly abrasive rocks
	Nontrue rolling	Multidisk	<250 MPa UCS, highly abrasive rocks
		Strawberry	<400 MPa UCS, very high abrasive rocks
Impacting	Impacting	Hammer	<100 MPa UCS, highly fractured rock masses

Source: Adapted from Copur, H. et al. 2012. Predicting cutting performance of chisel tools by using physical and mechanical properties of natural stones. *European Rock Mechanics Symposium (Eurock 2012, ISRM International Symposium)*, May 28–30, Stockholm, 14 p.

[a] UCS: Uniaxial compressive strength.

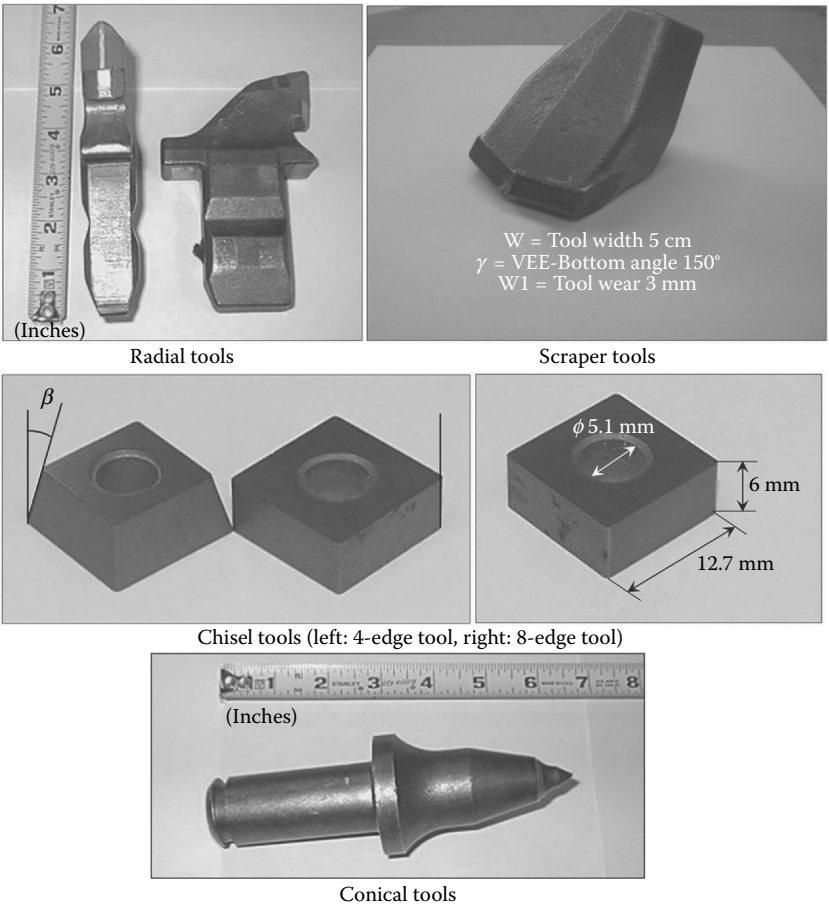

FIGURE 1.1
Common types of drag tools. (Adapted from Copur, H. et al. 2012. Predicting cutting performance of chisel tools by using physical and mechanical properties of natural stones. *European Rock Mechanics Symposium (Eurock 2012, ISRM International Symposium)*, May 28–30, Stockholm, 14 p.)

have a rectangular shank to be fixed on the tool holder, except for conical tools, which have cylindrical shanks that provide an even wearing of tool tips, giving a longer tool life compared to the other types of drag tools.

Radial tools are normally used with continuous miners, shearer-loaders, roadheaders, and trenchers for the excavation of nonabrasive soft grounds and minerals such as coal, salt, and potash (up to 40–60 MPa of uniaxial compressive strength). Their bodies are made of hardened steel and their insert tips are made of tungsten carbide, providing for longer tool life against wearing. Although they are the most efficient tools, their tool shapes make them more prone to wearing and having lower operational life.

Scraper (wedge, knife, blade, ripper) tools with tungsten carbide tip inserts and hardened steel bodies are normally used with full-face TBMs for the excavation of nonabrasive soft-to-medium strength formations up to 60–80 MPa compressive strength (Bilgin et al. 2012). Their tips are preblunted during manufacturing to prevent premature tool breakages. Scraper tools without tungsten carbide tip inserts, which can also be called simple wedge-type tools, are used for the excavation of soft grounds in some mechanical miners such as backhoes, shovels, draglines, and bucket wheel excavators.

The common types of roller tools are single disk (V-type, constant cross-section, or composite shape), multidisk, and strawberry (carbide inserted) tools (Figure 1.2). All roller tools rotate around an axis. Therefore, any point on the cutter ring is in cyclic contact with the rock surface. Constant cross-section single disk cutters are the most effective hard-rock-cutting tools. When another ring is placed on the same tool bearing, such as in the case of multidisk cutters, the force capacity of the bearing is shared by all the rings; therefore, the excavation performance of multidisk cutters is lower compared to that of single-disk cutters. On the other hand, strawberry cutters (with tungsten carbide inserts) crush the rocks instead of chipping them; crushing means spending more energy, as well as lower efficiency (Ozdemir 1995). The multidisk and strawberry cutters can be manufactured as true rolling and nontrue rolling. However, today they are usually manufactured as true rolling type. In nontrue rolling-type cutters, the diameter of one side of the tool is greater than the other side, which requires a dome-shaped cutterhead profile for obtaining evenly distributed tool forces on all rings attached to a bearing. Multidisk cutters are usually preferred in space-limited cutterheads.

Impact tools, which are normally used with impact (hydraulic) breakers, break the rocks by cyclic impacts with high frequency on the rock surface. They can only excavate fractured-jointed-bedded-foliated rock masses having mostly 100 MPa of uniaxial compressive strength. There are different types of impact tools based on the type of ground excavated.

A general comparison of drag and roller-type cutting tools is presented in Table 1.5 (Ozdemir 1997).

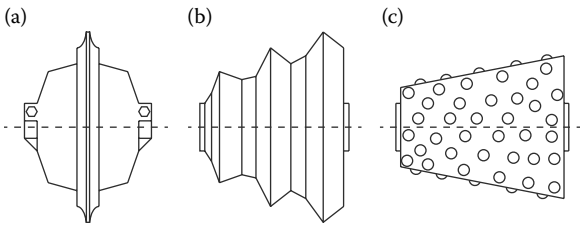

FIGURE 1.2
Sketches of common types of roller tools. (a) Single disk cutter; (b) multi-disk cutter; and (c) strawberry cutter.

TABLE 1.5

General Comparison of Mechanical Fragmentation by Drag and Roller Tools

Criterion	Drag Tools	Roller Tools
Cutting mechanism	Indentation and scratching/ripping of the rock by concentrated loading mainly in the direction of cutting. Picks in the shape of a simple chisel are more efficient than complex shapes, but their use is limited to the excavation of soft and nonabrasive materials. The point attack shape is the least efficient, but its evenly wearing ability elongates tool life; generates more dust.	Inducing high local stresses by rolling/indenting into the rock, mainly normal to the cutting surface. The stress from the pressure bulb that develops under the cutter transfers the load to the rock media and causes chipping. The development of crushed zone takes about 90% of the energy and generates dust and this must be minimized.
Cutting forces	Normal and drag forces are usually in the same range, depending on cutting geometry, tool type, and rock type. Drag forces are higher for radial tools, up to 2 times normal, than for conical tools (between 0.5 and 1.2 times normal). The optimum attack angle for conical tools is along the resultant force.	Normal force is an order of magnitude higher than rolling force. This indicates a need for higher thrust on the machines using roller cutters. Rolling force increases with penetration at higher rate than normal force (rolling/normal force ratio increases).
Cut spacing	Optimum spacing is between 1 and 5 times the depth of cut. The specific energy reduces and the efficiency increases for all types of picks as the spacing and the depth of cut are increased. Shallow cuts are very inefficient. The depth of cut should be as deep as tool load capacity as long as the machine thrust and power would allow.	The optimum spacing between roller tools is usually in the range of 5–25 times the depth of penetration. Groove deepening with a disk is an inefficient process and must be avoided; deeper penetrations and larger spacings provide for higher efficiency.
Cutter speed	Cutting speed, within all realistic practical ranges, has no effect on pick forces and cutting energies. But it can have a significant effect on bit wear due to high heat generation.	Cutting speed appears to have no significant effect on disk performance other than what might occur due to an accelerated wear rate. Bearings normally impose a limit on the allowable linear speed of cutters.
Cutter wear	Mainly due to wear on the carbide tip or wear on the steel jacket. This also limits the linear velocity of tools to prevent heat stresses in the carbide. Better wear and life can be achieved on conical picks due to even wearing of tip.	Failure may occur due to wear on the cutter or bearing. Disk wear causes smaller force increases than might be expected. In cutters featuring carbide, wearing of steel matrix or the breakage of carbide might happen.

continued

TABLE 1.5 (continued)

General Comparison of Mechanical Fragmentation by Drag and Roller Tools

Criterion	Drag Tools	Roller Tools
Rock properties	Very soft and nonabrasive for drag tools and medium rocks for conical tools to achieve highest efficiency and better performance.	Normally medium to hard rock, but can cut any type of rock that does not have plastic behavior.
Rock mass properties	Cutting efficiency is very sensitive to joints and rock mass properties due to the ripping effects of the picks to remove blocks without spending energy for breaking them.	Rock jointing has a beneficial effect on tool performance only if the joints are open and spaced closer than about 1–2 disk diameters.

Source: Modified after Ozdemir, L., 1997. *Mechanical Mining. Short course*. March 19–21, Colorado School of Mines, Golden, Colorado.

1.6 Future of Science of Rock-Cutting Mechanics and Excavation Machines

Independent of the type or the class of the excavation machine, the characteristics of the cutting mechanism are quite complex and any improvement in the mechanical excavation industry requires further research on the understanding of this mechanism and the fundamental principles of the science of rock-cutting mechanics, and, to some extent, soil-cutting mechanics. Although many major improvements were achieved in the last few decades with many robust and versatile machines appearing in the excavation industry, a better understanding of this issue along with the development of more robust, versatile, and automated excavation systems would lead to a safer, faster, more environment-friendly, and cheaper production.

References

Bilgin, N., Copur, H., Balci, C., 2012. Effect of replacing disc cutters with chisel tools on performance of a TBM in difficult ground conditions. *Tunneling and Underground Space Technology*, 27:41–51.

Binns, P.D., Potts, E.L.J., 1955. The ploughability of coal seams. *King's College Mining Society Journal*, 2:69–88.

Copur, H., Balci, C., Bilgin, N., Tumac, D., Avunduk, E., 2012. Predicting cutting performance of chisel tools by using physical and mechanical properties of natural stones. *European Rock Mechanics Symposium (Eurock 2012, ISRM International Symposium)*, May 28–30, Stockholm, 14 p.

Evans, I., Pomeroy, C.D., 1966. *The Strength, Fracture and Workability of Coal*. Pergamon Press, London, 277 p.

Mellor, M., 1976. Mechanics of cutting and boring, Part 3: Kinematics of continuous belt machines. CRREL (US Army, Cold Regions Research and Engineering Laboratory, Hanover, New Hampshire), Special Report, No: 76–17.

Muirhead, I.R., 1982. Mechanized excavation in mining—A challenge for tomorrow. CIM Special Volume 30: Rock Breakage and Mechanical Excavation, pp. 68–75.

Ozdemir, L., 1990. Recent developments in hard rock mechanical mining technologies. *Proc. the 4th Canadian Symposium on Mining Automation*, September 16–18, Saskatoon, pp. 143–165.

Ozdemir, L., 1992. Mechanical excavation—Today and tomorrow. *Proc. Int. GeoEngineering Conference*, Torino.

Ozdemir, L., 1995. Comparison of cutting efficiencies of single-disc, multi-disc and carbide cutters for microtunneling applications. *No-Dig Engineering*, 2(3):18–23.

Ozdemir, L., 1997. *Mechanical Mining. Short Course*. March 19–21, Colorado School of Mines, Golden, Colorado.

Ozdemir, L., 1998. Mechanical hard rock mining: Present and future. *Mining Engineering*, March: 36–37.

Robbins. Product Catalogues.

Sandvik. Product Catalogues.

Stack, B., 2008. Cutting-edge stuff. *World Tunnelling*, December, p. 21.

Tunnicliffe, J.F., 1982. Full-face tunnelling at Selby. *The Mining Engineer*, November: 247–257.

Walton, W.H. (Ed.), 1958. *Congress on Mechanical Properties of Non-Metallic Brittle Materials*. London, Butter Worths Scientific Publications.

This page intentionally left blank

2

Site Investigations for Mechanized Excavation Projects

2.1 Background

Site investigations (geotechnical investigations) resemble blood tests. It involves taking a blood sample from a human body using a syringe. After the blood sample has been taken, it is bottled and labeled to be sent to a laboratory. Depending on what's being checked, the sample is then examined under a microscope, perhaps with the aid of chemicals. The analysis report is written and the results are shared with the patient. The results can be stressful and upsetting for the human. A wrong design and wrong parameters get the wrong answer. If the test and procedure are carried out according to standards there is no need to worry about the results.

Site investigations for mechanical excavation purposes basically define the rock mass conditions in which geological, geotechnical, and other information about the area are to be used by owners, planners, engineers, and contractors. In other words, site investigations are done for mining and tunneling projects in order to (revised from Parker (1996) and Nilsen and Ozdemir (1999a)).

- Define the physical and mechanical properties of the formation
- Provide rock or soil design parameters, stability, and support requirements
- Help define the overall planning, including siting and design optimization
- Remove uncertainties of formation conditions for the bidder
- Estimate cost, schedule, and help to prepare tender documents
- Improve the safety of the work
- Provide experience working with the material, which, in turn will improve the quality of field decisions made during construction
- Decide excavation methods, selection, and performance predictions of the mechanical miners

The general question for many owners is, "How much money should be spent for site investigations in order to provide sufficient information for construction?" The question is not easily answered since there is no single set price, and geological conditions are variable by nature. There is a famous saying that "you pay for a site investigation whether you have one or not." As a general rule of thumb and from previous experience, the cost of the site investigations generally range from 1% to 8% of the total cost of the project. If the project is less complicated, the cost may go as low as 1%; for complicated projects, the cost could go as high as 8%. The price is also changing country by country because of the geological complexity.

The U.S. National Committee on Tunneling Technology USNC/TT (1984) recommends site exploration budgets averaging 3% of the estimated project cost, while in hard rock countries like Norway, site investigation costs typically have been on the order of 0.5–1% of the total construction cost (higher for recent, urban projects) (Nilsen and Ozdemir 1999a).

There has not been an international standard for site investigation procedure and practice, but work has been going on at an accelerating pace to prepare international standards (Norbury 2004). The British site investigation standard, which is called The British Standard Code of Practice BS5930 (2010), generally deals with civil engineering and building works. In the United States, geotechnical investigations by the U.S. Army Corps of Engineers (EM 1110-1-1804, 2001) generally deal with military and civil construction work.

There are some risks using mechanical excavators in tunneling projects due to unexpected geology, wrong machine selection and performance prediction, and insufficient site investigations. These parameters cause an increase in the cost of the project, delays, and claims. The aim of this chapter is to outline site investigation procedures for mechanical excavation projects; not with a comprehensive site investigation manual but by giving basic information to show how it is important for contractors, owners, and engineers. An organization tree of a site investigation and type of techniques can be seen and summarized in Figure 2.1 by Fookes (1967) and Bell (1975).

2.2 Stages of Site Investigations

Site investigation starts with the collection of data about the rock, soil, and geological conditions of the area. Site investigations for tunnel and mining openings are divided into two main stages: preconstruction and construction (Nilsen and Thidemann 1993). These stages of site investigations can be further divided into four substages. Phase I is generally called feasibility and includes desk study or literature review of the project area. Phase II is called preliminary design. Phases III and IV are called final design and

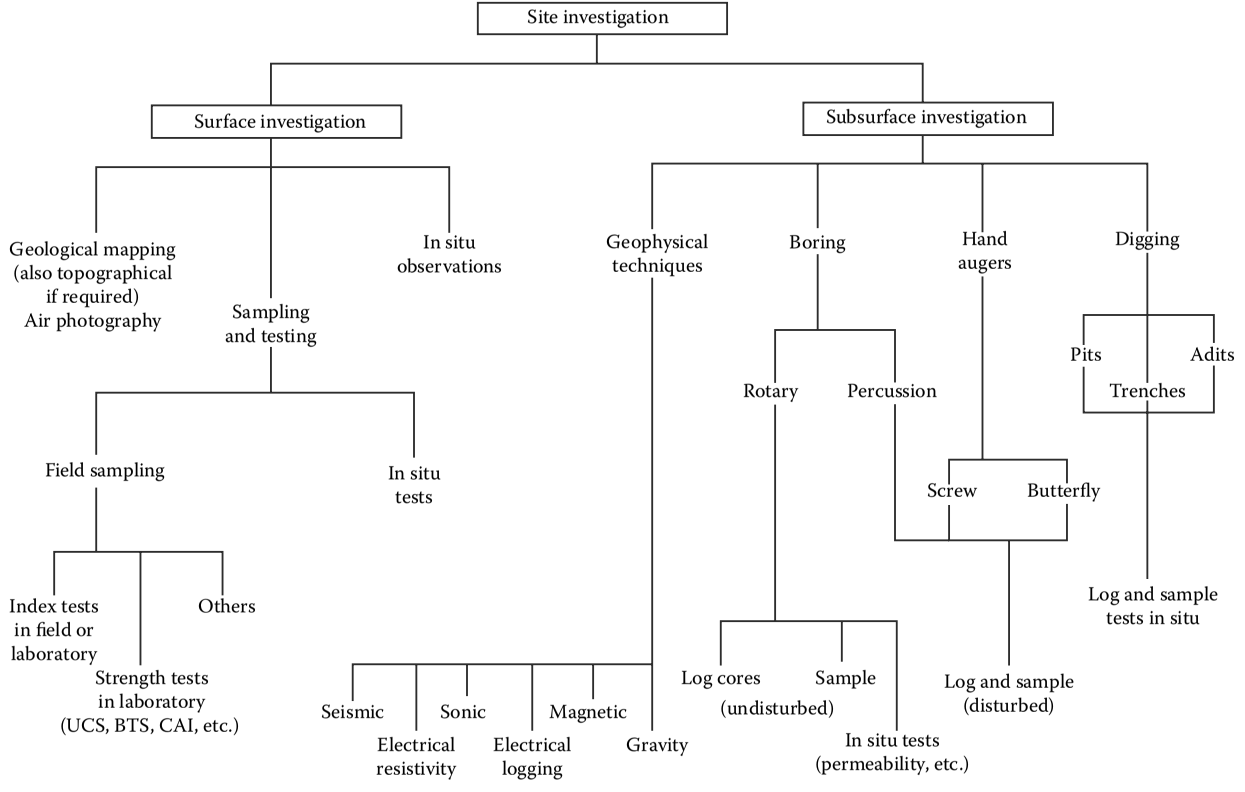

FIGURE 2.1
Site investigation organization tree. (Revised after Fookes, P.G., 1967. *Engineering Geology*, 2:81–106; Bell, F.G., 1975. *Site Investigations in Areas of Mining Subsidence*, ed. F.G. Bell, London, Newnes Butterworth, pp. 1–24.)

construction. Effective and adequate site investigations depend on the information gathered from those stages.

2.2.1 Phase I: Feasibility

Data are collected in this stage of the site investigation for carrying out desk study and walking over to the project area. Some questions related to the project are answered during this stage before going into the other phases. The general steps in this stage including sources for data collection are summarized as:

- Literature Survey of
  - State or Private University Libraries
  - Geological Surveys in different countries
- Local Governmental Publication such as Mineral Research & Exploration General Directorate (MTA); the United States Bureau of Mines (USBM), the United States Bureau of Reclamation (USBR), and so on
- Databases related to project area of
  - Conferences on tunneling such as Rapid Excavation & Tunneling Conference (RETC); North American Tunneling (NAT); World Tunneling Conference (WTC), and so on
  - Conferences on Mining such as World Mining Congress (WMC); Society for Mining, Metallurgy and Exploration Annual Meeting (SME), and so on
- Remote sensing of
  - Black and white air photos
  - Satellite imagery
  - Ground-penetrating radar
- Discussion with engineers, geologist, drillers, and so on
- Topographic map interpretations cross-sections
- Geologic mapping with purpose of
  - Evaluating anticipated geologic conditions
  - Physically observing outcrops in stream beds, road cuts, and natural exposures
  - Observing large-scale rock mass properties

2.2.2 Phases II: Preliminary Design

Phase II, called preliminary design, is the second stage in the site investigation process where field and laboratory studies are generally carried out for pre-design purposes. In this stage, the main program of exploration, planning,

the geotechnical framework, and potential problems are defined. Exploratory drilling or digging is done to get rock core (especially NX size ≈54 mm in diameter) or soil samples during field exploration work. Core logging is very important to define the characteristic of the samples such as: rock type, joint spacing, filling and roughness, weathering, mineralization, faulting, color, hardness, rock quality designation (RQD), and sample photographs. Soil logging is also done to describe soil classification system by doing field index tests. Based on the rock and soil logging, data laboratory testing can be performed by preparing representative samples and standard testing (ASTM, ISRM). Laboratory tests for rock and soil generally include the following tests: unit weight, compressive strength test, tensile strength test, shear strength test, static and dynamic elastic modulus, petrographic analysis, Cerchar abrasivity test, water content, sieve analysis, abrasivity, permeability, standard penetration test (SPT), Atterberg limits, expansion test, compaction tests, shear strength, and unconfined compression test for mechanized excavation projects. Geophysical explorations are performed in this stage, such as doing refraction and reflection seismic, resistivity, magnetic, gravity, electrical and down hole geophysical surveying to define physical properties of soil and rock around the project area. At this stage of the investigation sufficient data for geotechnical analysis should be produced to obtain a geological profile and estimation of the geological characteristics of the rock and soil. Preliminary design data for ground conditions of the area, groundwater inflows and ground classifications, support, muck disposal, and scheduling can be determined in this stage.

2.2.3 Phases III: Final Design

During this stage, the final design of the project must be finished and geotechnical analysis must be refined to determine rock mass classifications, support and lining, water control, handling, and disposal purposes. When the feasibility and the preliminary design stages are completed, the final design of the site investigation can be prepared, exploring some specific problems in detail, such as fault zones, earthquakes, water production, in-situ stresses, and special testing. Predicting the problem areas of the project is very important to explore in this stage: detailed ground characteristics, how much water and where, groundwater level, and material properties such as swelling and abrasiveness of the material. The construction method is also selected and decided in this stage of the phase. Cost estimates and scheduling of the project are reevaluated in this stage so the geotechnical design, summary report, and bid documents can be prepared realistically to accomplish the project.

2.2.4 Phase IV: Construction

The project assignment to the contractor means their work has started. All construction activities must be recorded and kept in a safe place up to the end of the project. In tunneling and mining excavation projects, claims and disputes

are frequently resulted in the court. In this stage of the site investigations, core sampling and testing, tunnel mapping, shift reports and machine data (data logger), instrumentation, and monitoring must be collected by the owner and contractor. In the case of disputes, these data can be very helpful for lawyers.

2.3 Field Investigations

In any excavation project, the first step is to carry out field investigations; search and review existing geological data, papers, and records relating to the project area. Field investigations cover all geological and geophysical data. Geological data should include maps, cross sections, boreholes layout, and hydrogeological conditions. Geophysical data generally includes seismicity of the project area. Geophysical data are used for defining soil and rock interface. An experienced geologist or engineering geologist must perform the geological mapping and data collecting during field investigations. During field work, rock types, and geological conditions, representative sample collection for mechanical tests, and joint mapping are crucial for mechanical excavation projects. After geological mapping and preparing a geological cross section, a general framework is planned of pitting, boring, trenches, and drilling to get samples. Borehole numbers, layout, and depth are always a question for the site investigation. Boreholes will be drilled deeper than the tunnel line. There is no definite rule established for boring spacing and layout. They depend upon many factors, such as the nature and condition of rock and soil, and complexity of the geological conditions. Core drilling (most commonly NX size) is used to obtain rock samples, auger-type of drilling for disturbed soil, and shelby tubes for undisturbed soil sampling.

Core drilling has some important purposes, such as (Nilsen and Ozdemir 1999a)

- To verify the geological interpretation
- To obtain more information on rock-type boundaries and degree of weathering
- To supplement information on orientation and character of weakness zones
- To provide samples for laboratory analyses
- Hydrogeological and/or geophysical testing

During the field investigations, in addition to field mapping, field testing is an important parameter in obtaining rock mass conditions. In situ rock stress measurement by flat jack and hydraulic fracturing testing, are done to define stress conditions of the rock mass. For ground water characteristics of

the rock mass, water injection or pumping test is commonly used for defining ground water conditions of the project area.

2.4 Laboratory Investigations

Laboratory investigations should include standard rock and soil properties testing to prepare the site investigation report. Common laboratory tests are described in Chapter 3 and divided into three categories: physical, mechanical, and chemical tests. The important key role in laboratory studies is the representative sample supply and testing methods for selection and design performance of mechanical excavators. If the sample does not represent the rock mass conditions and is not properly tested in the laboratory, the mechanical excavator selection and performance prediction cannot be reliable. The number of samples required will depend on several factors, such as the complexity of geology, length of the tunnel, intended test methods, type of project, and contract (Nilsen and Ozdemir 1999b).

2.5 Reporting of Site Investigations

Reporting and writing of site investigation reports are still controversial topics in tunneling projects. Owner, designer, contractor, and geotechnical engineers should not take responsibility for problems developing during the construction. *Geotechnical Baseline Reports for Underground Construction* edited by Essex (2007a) are the guidelines most used for tunneling activities, but considerable confusion still exists with respect to the writing of geotechnical reports (Brierley et al. 2000).

For typical mechanized excavation projects, geotechnical engineers prepare different data reports after carrying out site investigation work. The reports, especially in the United States, are generally called geotechnical data report (GDR), geotechnical baseline report (GBR), geotechnical interpretive report (GIR), and geotechnical design summary report (GDSR). The four reports summarize the geological conditions and geotechnical design parameters for soil and rock, as well as provide geotechnical recommendations of which all of them are prepared in different stages of site investigations.

2.5.1 Geotechnical Data Report

The geotechnical data report (GDR) contains only factual data and presents the results of field and laboratory data for the project without including an

interpretation of these data. The GDR should contain the following information (Essex 2007b):

- Descriptions of the geological setting
- Descriptions of the site exploration program(s)
- Logs of all borings, trenches, and other site investigations
- Descriptions/discussions of all field and laboratory test programs
- Results of all field and laboratory testing

2.5.2 Geotechnical Baseline Report

The use of a GIR was first incorporated into a United States construction contract in 1972, for the construction of the Washington, DC, subway system. In the last three decades, the use of such reports has slowly but progressively evolved into what are now termed geotechnical baseline reports (Essex 2007a). The GBR report is generally used for defining the baseline conditions for contractors to select methods, equipment, and risk analysis. It also serves as the basis for bid preparation and is used extensively in resolving disputes during construction.

2.5.3 Geotechnical Interpretive Report

GIR describes geologic background, geologic sections and profiles, and interprets conditions and behavior for assumed construction methods.

2.5.4 Geotechnical Design Summary Report

GDSR is used to identify changed conditions during construction. Besides the other geotechnical reports, the GDSR is helpful in resolving questions of differing site conditions. Groundwater conditions and unexpected geology of the tunnel construction must be investigated and the answers to the questions should be included in this report.

References

Bell, F.G., 1975. Introduction, site investigation. Chapter 1. In *Site Investigations in Areas of Mining Subsidence*, ed. F.G. Bell, London, Newnes Butterworth, pp. 1–24.

Brierley, G.S., Dobbels, D., Howard, A., 2000. Geotechnical report preparation. In *Proceedings of North American Tunneling 2000 Conference and Exhibition Underground Construction: The Revolution Continues,* ed. Ozdemir, Boston, Massachusetts, pp. 1–9. Balkema, Rotterdam, Brookfield.

BS 5930:1999 + A2:2010. Code of practice for site investigations, British Standard, 206.

EM 1110-1-1804, 2001. *Geotechnical Investigations,* U.S. Army Corps of Engineers (USACE), Washington, DC, 103. http://140.194.76.129/publications/eng-manuals/EM_1110-1-1804_sec/EM_1110-1-1804_Sections/basicdoc.pdf (accessed July 22, 2013).

Essex, R.J., 2007a. *Geotechnical Baseline Reports for Construction*, 2nd edition, eds. Roach, M.F., Kritzer, M.R., Ofiara, D., and Townsend, B.F., *North American Tunneling 2008 Proceedings*. Society for Mining, Metallurgy, and Exploration, Inc., Omnipress San Francisco, California, pp. 640–644.

Essex, R.J., 2007b. *Geotechnical Baseline Reports for Construction Suggested Guidelines*, ed. Essex, R.J., ASCE, American Society of Civil Engineers, Virginia, pp. 1–62.

Fookes, P.G., 1967. Planning and stages of site investigation. *Engineering Geology*, 2:81–106.

Nilsen, B., Ozdemir, L., 1999a. Recent developments in site investigation and testing for hard rock TBM projects, In *Rapid Excavation and Tunneling Conference Proceedings*, eds. Hilton, D.E., Samuelson, K. O., Society for Mining, Metallurgy, and Exploration, Inc., Omnipress San Francisco, California, pp. 715–731.

Nilsen, B., Ozdemir, L., 1999b. Recommended laboratory rock testing for TBM projects. *American Underground Association (AUA) News, 14(2)*: 21–35.

Nilsen, B., Thidemann, A., 1993. Engineering geological investigations. In *Rock Engineering, Hydropower Development* Pub. *No 9,* Norwegian Institute of Technology Division of Hydraulic Engineering, Norway, pp. 61–76.

Norbury, D., 2004. Current issues relating to the professional practice of engineering geology in Europe, engineering geology for infrastructure planning in Europe. In *A European Perspective*, eds. Hack, R., Azzam, R., Charlier, R., Liege, Belgium, Springer, pp. 15–30.

Parker, H.W., 1996. *Geotechnical investigations.* Chapter 4 in Tunnel Engineering Handbook, eds. Bickel, I.O., Kuesel, T.R., King, E.H., New York, Chapman & Hall, pp. 46–79.

U.S. National Committee on Tunneling Technology (USNCTT). 1984. *Geotechnical Site Investigations for Underground Projects*. Washington, DC, National Academy Press, Vol. 1, 182 p.

This page intentionally left blank

3

Physical and Mechanical Properties of Rocks, Soils, and Coals

3.1 Rocks

In geology, rocks occur as a solid aggregate of minerals, connected by strong and permanent cohesive forces, and classified according to their origin: igneous, sedimentary, and metamorphic. The major three groups of rocks are subdivided into many groups, and petrology is the scientific study of the rocks. The minerals, grains, and microscopic properties of the rocks give some important information about the rock such as strength, abrasivity, hardness, drillability, and cuttability. In this section, these properties and the methodology of applying the tests will be explained.

Determination of physical and mechanical properties of rocks can be found directly or indirectly. For example, the uniaxial compressive strength (UCS) test can be measured directly or indirectly from point load (PL) strength tests. For mechanical excavation, the most widely used tests are explained in detail in this section.

The first step in sample preparation is coring specimens from blocks of rock obtained from tunnel or mining sites as is seen in Figure 3.1. The core is cut by diamond saw and ground by surface grinder to finish the ends of cylindrical specimens as seen in Figures 3.2 through 3.4. The rock laboratory testing must be based on standards and also conducted according to the guidelines of the standards.

Available standards, suggested methods, and descriptions for rock laboratory testing for mechanical miners are given in Table 3.1. These tests must be carried out for the proper selection and performance prediction of mechanical miners.

3.1.1 Uniaxial Compressive Strength

UCS (σ_c) is one of the most basic parameters of rock strength, and the most common strength determination performed for mining and tunneling projects. It is generally measured in accordance with the procedures recommended in ASTM D2938 or in ISRM, usually with NX-sized core samples

FIGURE 3.1
Typical core drilling machine.

(54 mm in diameter). The samples are prepared to satisfy the requirements of ASTM D4543 or ISRM suggested methods. All core samples are cut and ground to a diameter ratio of 2.0–3.0. A minimum of three to five UCS determinations is recommended for statistical significance of the resulting average.

Compressive strength calculation is formulated below in Equation 3.1.

$$\sigma_c = \frac{F_{\text{Max}}}{A_{\text{Sec}}} \tag{3.1}$$

FIGURE 3.2
Typical core diamond sawing machine.

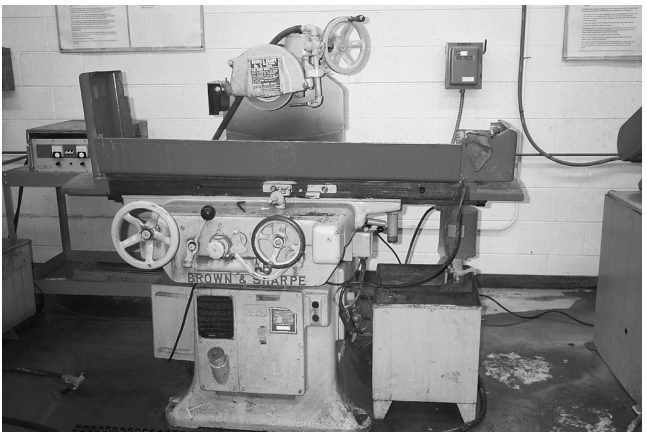

FIGURE 3.3
Typical core surface grinding machine.

where

σ_c = Uniaxial compressive strength, MPa
F_{Max} = Maximum force on the sample before failure, N
A_{Sec} = Cross-sectional area of the sample before testing, mm^2

The foliation and failure type are the most important criteria for UCS testing and influence boreability/cuttability parameters of the mechanical miners. Foliation planes parallel to the loading direction (Figure 3.5a) and perpendicular to the loading direction (Figure 3.5b) are very favorable for crack propagation. Before and after UCS testing, attention should be paid

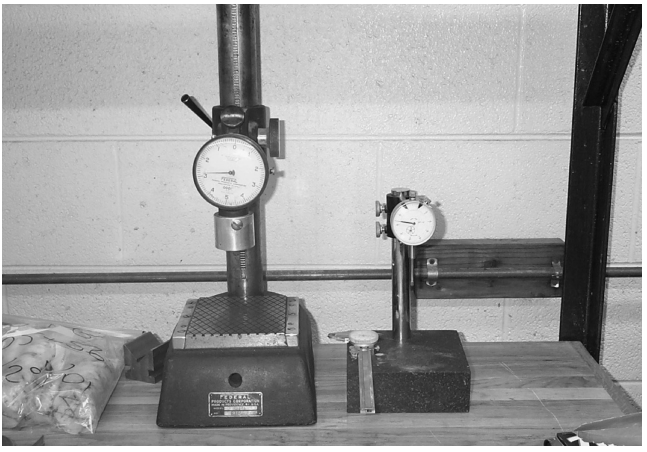

FIGURE 3.4
Core sample's parallel end control devices.

TABLE 3.1

Rock Testing Methods and Standards for Mechanical Miners

Test Name	ISRM (2007) Suggested Methods	ASTM Standards	Other Recommended Methods
Mechanical strength			
UCS	1979	D 2938	
BTS	1978	D 3967	
Static elastic constants	1979	D 3148	
Dynamic elastic constants	1978	D 2845	
Triaxial	1983	D 2664	
Direct shear	1974	D 5607	
Point load	1985	D 5731	
Cone indenter			NCB (1964)
Hardness			
Moh's			Nilsen and Ozdemir (1999)
Vickers			Nilsen and Ozdemir (1999)
Siever's J			Nilsen and Ozdemir (1999)
Shore	2006		
Schmidt hammer	1978	D 5873	
Toughness/brittleness			
Punch penetration test			Nilsen and Ozdemir (1999)
Fracture toughness	1988		Nilsen and Ozdemir (1999)
Brittleness value (S20)			Zare and Bruland (2013)
Sievers' *J*-value (SJ)			Zare and Bruland (2013)
Abrasion value (AV)			Zare and Bruland (2013)
Abrasion value cutter steel (AVS)			Zare and Bruland (2013)
Abrasiveness			
Cerchar		D 7625	CSM (1996)
Schimazek			Schimazek and Knatz (1970)
NTNU AVS			Zare and Bruland (2013)
Taber			Tarkoy (1979)
Rock cutting			
Small-scale linear rock cutting			Fowell and McFeat-Smith (1976); Balci (2004)
Full-scale linear rock cutting			CSM (1996); Eskikaya et al (2000)
Other			
Petrographic analysis	1978		Nilsen and Ozdemir (1999)
X-ray			Nilsen and Ozdemir (1999)

TABLE 3.1 (continued)

Rock Testing Methods and Standards for Mechanical Miners

Test Name	ISRM (2007) Suggested Methods	ASTM Standards	Other Recommended Methods
Sound velocity (P and S waves)	1978	D 2845	
Density	1979		
Porosity	1979		

Source: Based on Nilsen, B. and Ozdemir, L. 1999. *American Underground Association (AUA) News, 14(2)*: 21–35; Bamford, W.E. 1986. Cuttability and drillability of rock, Civil College Technical Report Engineers Australia, July 11, 4; Howarth, D.F. 1987. Mechanical rock excavation—Assessment of cuttability and boreability. In *Rapid Excavation and Tunneling Conference Proceedings*, ed. Society for Mining, Metallurgy, and Exploration, Inc., Vol. 1, pp. 145–164. New York.

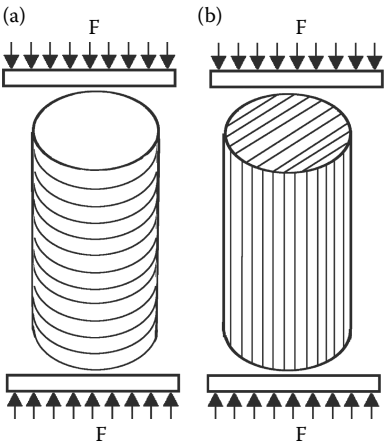

FIGURE 3.5
Foliation effects of the loading direction. (a) Perpendicular to bedding and (b) parallel to bedding.

to how the sample failed. Joints, fractures, bedding, or foliation effects are classified as structural failures and do not represent the real rock strength as seen in Figure 3.6.

3.1.2 Indirect (Brazilian) Tensile Strength

Brazilian tensile strength (BTS, σ_t) provides a measure of rock toughness, as well as strength. This parameter is measured using NX-sized core samples (54 mm in diameter) cut to a 0.5 length:diameter ratio, and follow the procedures of ASTM D3967 or ISRM suggested methods. The diameter is required to change less than 0.5 mm over the length of the sample and the

FIGURE 3.6
An example of the structural failure type of UCS testing.

core ends must be perpendicular to the core axis, up to a precision depending on the standard applied. The Brazilian tensile strength is calculated by using Equation 3.2.

$$\sigma_t = \frac{2P}{\pi LD} \tag{3.2}$$

where
σ_t = Brazilian tensile strength, MPa
D = diameter of the sample before testing, mm
P = maximum force on the sample before failure, N
L = length of the sample before testing, mm

The foliation and failure type are also the most important criteria for BTS testing and should be noted before and after the testing on the report. Foliation planes parallel to the loading direction (Figure 3.7a) and perpendicular to the loading direction (Figure 3.7b) are very favorable for crack propagation. An example of the normal failure type of BTS testing is seen in Figure 3.8.

3.1.3 PL Strength Index

The PL strength is widely used as an accepted index test for strength classification and measure of the strength of a core or irregular piece of rock for

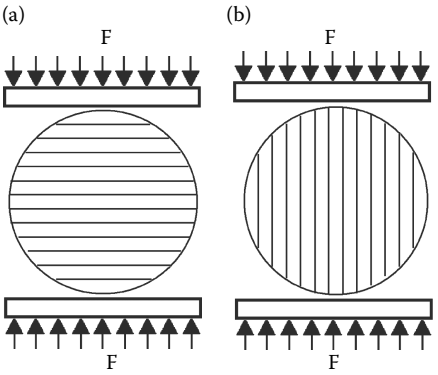

FIGURE 3.7
Foliation effects of the loading direction. (a) Parallel to bedding and (b) perpendicular to bedding.

determination of *UCS*. The test can be performed with portable equipment and so may be conducted either in the field or in the laboratory (Broch and Franklin 1972; Brown 1981). The piece of rock is loaded to failure between two standard conical platens. The uncorrected PL strength (*Is*) is calculated as the ratio of failure load and equivalent core diameter (De). *Is* must be corrected to the standard equivalent diameter (*De*) of 50 mm and called *Is(50)* diameter of 50 mm. The procedure for size correction can be obtained graphically or mathematically as outlined by the standard applied procedures. The device and an example of the normal failure type of PL testing are seen in Figures 3.9 and 3.10, respectively.

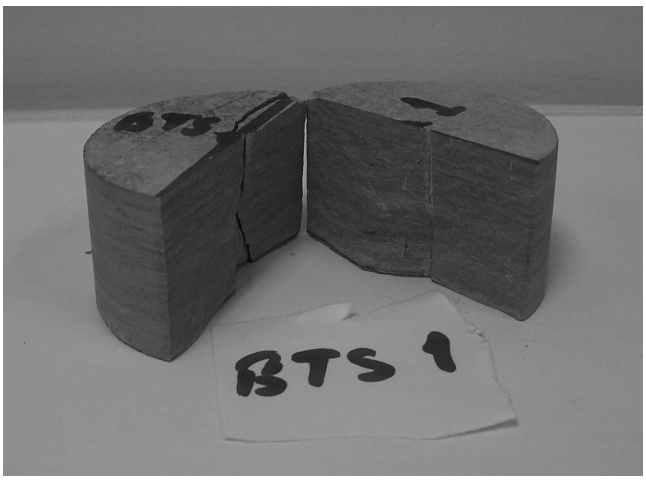

FIGURE 3.8
An example of the normal failure type of BTS testing.

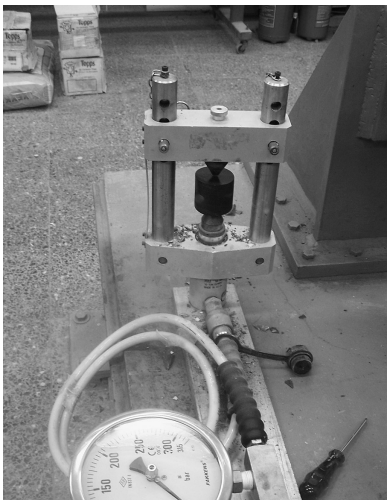

FIGURE 3.9
Typical PL device.

3.1.4 Cerchar Abrasivity Index

The Cerchar Abrasivity Index (*CAI*) indicates the degree of rock abrasivity, for classifying and predicting cutter wear rate and costs. The Cerchar test and associated *CAI* were developed at a time of more demand for application of mechanical excavation machines at the Laboratoire du Center d' Études et Recherches des Charbonnages de France (CERCHAR) and standardized

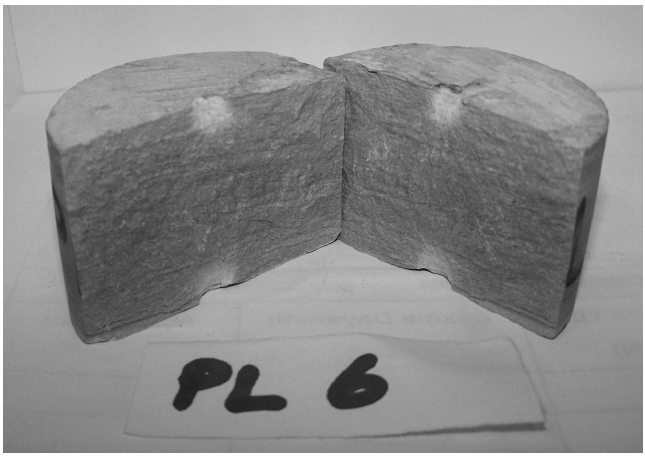

FIGURE 3.10
An example of the normal failure type of PL testing.

FIGURE 3.11
Typical Cerchar abrasivity device.

by ASTM D7625-10 Standard Test Method for Laboratory Determination of Abrasiveness of Rock Using the CERCHAR Method. The tests are performed on freshly broken rock surfaces, free of weathering effects. The remnant pieces from indirect (Brazilian) tensile strength tests are normally used for this purpose. Rock samples are held in a vise with the fresh surface facing upward as seen in Figure 3.11. A conical 90°, hardened steel pin, fastened in a 7 kg head, is set carefully on the fresh surface and drawn 1 cm across it in 1 s. This is repeated for a total of five pins for each sample test. Minimum and maximum wear diameters are measured for each pin, and shape of the wear is recorded. The tips of the pins are then examined under a reticular microscope and two perpendicular diameters of the resulting wear flat are recorded for each pin. Coating the pin tips with a dye prior to testing makes the wear flat more visible. The *CAI* is then calculated by Equation 3.3:

$$CAI = \frac{1}{10}\sum_{i=1}^{10} d_i \tag{3.3}$$

where d_i is the pin wear diameter in (1/10 mm). A general cutter consumption rate (*CAI*) for pick cutters is estimated by Equation 3.4:

$$CAI\ (\text{cutter/m}^3) = 0.25\ CAI \tag{3.4}$$

The lower the CAI, the softer and less abrasive the rock is for cutters. A CAI of 1 is very soft, while 6 is extremely abrasive. The criterion for abrasiveness published by ASTM D7625 is seen in Table 3.2.

TABLE 3.2

Criteria for the CERCHAR Abrasiveness Index ASTM D7625

Classification	Average *CAI* Stylus Rockwell Hardness (HRC) Value 55	Average *CAI* Stylus Rockwell Hardness (HRC) Value 40
Very low abrasiveness	0.30–0.50	0.32–0.66
Low abrasiveness	0.50–1.00	0.66–1.51
Medium abrasiveness	1.00–2.00	1.51–3.22
High abrasiveness	2.00–4.00	3.22–6.62
Extreme abrasiveness	4.00–6.00	6.62–10.03
Quartzitic	6.0–7.0	N/A

3.1.5 NCB Cone Indenter Hardness Index

The cone indenter was designed at the Mining Research and Development Establishment (MRDE) of the previous National Coal Board (NCB) of England to determine the resistance of rock and coal to indentation by a tungsten carbide 60° cone (NCB 1977, Szlavin 1974). It is designed to determine the hardness of small fragments of rock by measuring its resistance to indentation by a hardened tungsten carbide cone. A typical example of an NCB cone indenter device is seen in Figure 3.12. A specimen about $12 \times 12 \times 6$ mm in size is placed on the steel strip and the cone is lowered by turning the micrometer under 40 N forces. Displacement between the first and the second advancement is

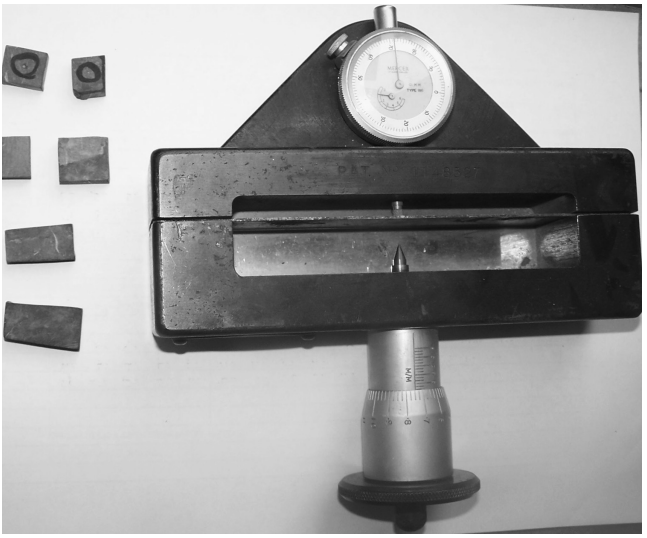

FIGURE 3.12
Typical NCB cone indenter device.

read ($M1$ and $M2$). The deflection of the thin spring bond is measured by the gauge and is directly related to the force on the specimen. The cone indenter hardness (CIH) is calculated as seen in Equation 3.5.

$$CIH = \frac{0.635}{(M1 - M2) - 0.635} \tag{3.5}$$

The correlation between the standard cone indenter number, CIH, and UCS has been determined by the NCB and is given in Equation 3.6.

$$\sigma_c = CIH \times 24.8 \text{ (MPa)} \tag{3.6}$$

3.1.6 Schmidt Hammer Rebound Hardness

The Schmidt hammer is a portable, small, and cost-effective instrument capable of estimating the rock surface hardness as an index value used in the laboratory and in situ. It was originally developed for estimating the in situ strength of concrete. Since then, a lot of research work has been carried out using Schmidt hammer to estimate the intact and rock mass properties, to characterize mine roof stability, to estimate the performance of roadheaders, and so on. The Schmidt hammer rebound value can be used as an index value or converted into unconfined compressive strength value based on the statistical relationships. Plasticity index can also be estimated using rebound values. The mechanism of operation is simple: a plunger released by a spring impacts against the rock surface and then the rebound distance of the plunger is read directly from the numerical scale changing from 10 to 100. Schmidt hammers are available in several different energy ranges, which include Types L, N, M having 0.735, 2.207, and 29.43 Nm impact energies, respectively. Hammer should be calibrated prior to testing. A core sample (block sample in any size larger than $20 \times 20 \times 20$ cm or an excavation face) can be used to apply the Schmidt hammer test. The rock surface should be flat and clean. The test is usually applied in a horizontal direction and correction should be applied for angled or vertical rebound readings (Bilgin et al. 2002). ASTM D5873 and ISRM describe the procedure for the testing of rock. A typical L-type Schmidt Rebound Hardness device is seen in Figure 3.13.

Schmidt hammer rebound values can be found through one of four procedures recommended by different investigators and explained below:

Procedure-1 (Poole and Farmer 1980): Taking the peak rebound value from five continuous impacts at a point and averaging the peaks of the three sets of tests conducted at three separate points.

Procedure-2 (Hucka 1965): Taking the peak rebound value from 10 continuous impacts at a point and averaging the peaks of the three sets of test conducted at three separate points.

FIGURE 3.13
Typical Schmidt rebound hardness device.

Procedure-3 (ISRM Standard, Brown 1981): Recording 20 rebound values from single impacts separated by at least a plunger diameter and averaging the highest 10 values.

Procedure-4 (ASTM 2013): Recording 10 rebound values from single impacts separated by at least the diameter of the piston. Only one test may be taken at any one point and discard readings differing from the average of 10 readings by more than 7 units and determine the average of the remaining readings.

3.1.7 Shore Scleroscope Hardness

Shore scleroscope hardness is one of the simplest methods given to determine the surface hardness of the tested material. It is determined by the rebound height of a diamond or tungsten-carbide tipped hammer dropped onto a horizontal smooth surface. In Shore scleroscope test, a diamond tip is dropped from a fixed height into the rock specimen. The hammer then rebounds, but not to its original height because some of the energy in the falling tip is dissipated in producing an indentation. The instrument used is supplied in two models designated Model C and Model D. Model C-2 consists of a vertically disposed barrel containing a glass tube which is graded from 0 to 140 as seen in Figure 3.14. A diamond tip is dropped from a specified height and rebounds within the glass tube. According to the suggested methods published by the International Society for Rock Mechanics (ISRM 2007), a test specimen having a minimum surface area of 10 cm^2 and

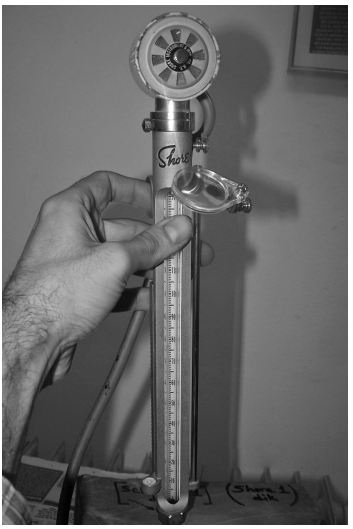

FIGURE 3.14
Typical shore scleroscope hardness device.

a minimum thickness of 1 cm is necessary. Measurement points should have at least 5 mm distance from each other and only one test must be carried out at the same spot. The minimum number of tests for each rock is recommended to be 20 for statistical reliability (ISRM 2007), explained in detail in Tumac et al. (2007) and Altindag and Guney (2006).

3.1.8 Density, Porosity, and Water Content

Density, porosity, and water content are common physical properties for rocks. Density is a measure of mass per unit of volume and generally changes between 2.2 and 2.8 kg/cm^3 for most rock types. Porosity is a measure of the void spaces in a rock. It is the ratio of the nonsolid volume to the total volume of material. Water content or moisture content of the rock is a measure indicating the amount of water that the rock material contains. It is the ratio of the volume of water to the bulk volume of the rock material.

Some physical and mechanical properties of rocks is given as a summary in Table 3.3.

3.2 Soils

Soil is an aggregate of mineral grains that can be separated by such gentle means as agitation in water. Soils can be classified into two categories such as cohesive (clays, silts, clayey silts, silty clays; particles bound together

TABLE 3.3

Some Physical and Mechanical Properties of Rocks

Rock Name	Density (g/cm^3)	Porosity (%)	*UCS* (MPa)	*BTS* (MPa)	*E* (GPa)	*CAI*
Granite	2.6–2.7	0.5–1.5	100–250	7–25	10–65	4–5.5
Andesite	2.4–2.8	0.15–8	60–300	4–20	8–60	2.3–4
Diorite	2.7–3	0.1–0.5	180–300	15–30	60–120	3.5–5.0
Dolerite	3–3.05	0.1–0.5	200–350	15–35	70–100	–
Gabbro	3–3.1	0.1–0.2	180–300	15–30	70–100	2.8–3.7
Basalt	2.22.9	0.1–1	140–350	10–30	50–100	1.5–3.5
Sandstone	2–2.6	5–25	20–175	4–20	5–100	1.5–4.5
Shale	2–2.4	10–30	10–100	2–10	10–35	0.5–1.5
Mudstone	1.8–2.75	–	10–150	5–25	20–50	1–2
Limestone	2.2–2.6	5–20	30–240	5–25	10–80	1–3
Dolomite	2.5–2.6	1–5	80–200	10–20	40–85	1.1–2
Coal	0.7–2.0	–	4–45	2–5	10–20	0.1–0.4
Quartzite	2.65	0.1–0.5	100–300	10–30	40–100	4–5.9
Gneiss	2.9–3.0	0.5–1.5	50–200	5–20	30–90	3–5.5
Marble	2.6–2.7	0.5–2	60–250	7–20	30–80	–
Slate	2.6–2.7	0.1–0.5	70–150	7–20	–	–
Copper ore	4.13	–	33	3.4	–	2.8
Harsburgite	2.65	–	58	5.5	2.1	0.8
Trona	2.13	–	30	2.2	–	–
Anhydrite	2.90	–	82	5.5	–	–

with clay minerals forces) and cohesionless soils (sands and gravel) loose particles without strong inter-particle. Grain shape, size, and clay minerals are important especially in the design and selection of mechanical miners. Grain size distribution or sieve analysis and the description of the clay minerals are the first soil properties that must be analyzed before selection of mechanical miners. The main parameters in the selection and designing of mechanical excavators for tunneling and mining in soft ground are given in Table 3.4. Those parameters are generally used for designing and prediction purposes on

- Surface settlement
- Face stability
- Earth pressure
- Slurry system
- Excavability
- Separation plant
- Sticky and swelling potential of clay minerals
- Muck disposal and transportation

TABLE 3.4

Soil Testing Methods and Standards for Mechanical Miners Selection

Test Name	AASHTO[a]	ASTM Standards	Other Recommended Methods
Physical and mechanical properties			
Cohesion	T 236	D 3080	
Angle of internal friction	T 236	D 3080	
Specific garvity	T 100	D 854	
Water content	T 265	D 4959	
Atterberg limits (liquid limit, plastic limit, and plasticity)	T 89	D 4318	
Standard penetration test	T 206	D 1586	
Unconfined compressive strength of cohesive	T 208	D 2166	
Triaxial strength	T 296, 297	D 2850, 4767	
Modulus of elasticity			USACE EM 1110-1-1904 (1990)
Direct shear strength	T 236	D 3080	
Petrografic and other properties			
Grain size distribution (sieve and hydrometer analysis)	T 88	D 422, D 2487, D1140	
Mineral contents (quartz content)			X-ray diffraction
Clay mineralogy			X-ray diffraction
pH		D 4972	
Groundwater conditions			
Sulfate content	T 290	D 4230	
Chloride content	T 291	D 512	
Abrasiveness (grain shape and hardness)		ASTM G75	SAT; Nilsen et al. (2006)
Swell potential of clays	T 256	D 4546	
Collapse potential of clays		D 5333	
Permeability for granular soil	T 215	D2434	
Permeability for all soil		D 5084	
Possible existence of boulders and cobbles: type, amount, sizes, strength, and abrasivity			

[a] American Association of State Highway and Transportation Officials.

Another soil classification was defined by Terzaghi (1950) for soft ground tunnels, which is called Tunnelman's Ground Classification as seen in Table 3.5 and it was modified by Heuer (1974).

3.2.1 Grain Size Distribution

Grain size distribution is widely used in classification of soils and defined by sieve analysis and hydrometer tests. The data obtained from grain size

TABLE 3.5

Tunnelman's Ground Classification for Soils

Classification		Behavior	Typical Soil Types
Firm		Heading can be advanced without initial support, and final lining can be constructed before ground starts to move.	Loess above water table; hard clay, marl, cemented sand and gravel when not highly overstressed.
Raveling	Slow raveling	Chunks or flakes of material begin to drop out of the arch or walls sometime after the ground has been exposed; due to loosening or to over-stress and "brittle" fracture (ground separates or breaks along distinct surfaces, opposed to squeezing ground). In fast raveling ground, the process starts within a few minutes, otherwise the ground is slow raveling.	Residual soils or sand with small amounts of binder may be fast raveling below the water table, slow raveling above. Stiff fissured clays may be slow or fast raveling depending upon degree of overstress.
	Fast raveling		
Squeezing		Ground squeezes or extrudes plastically into tunnel, without visible fracturing or loss of continuity, and without perceptible increase in water content. Ductile, plastic yield, and flow due to overstress.	Ground with low frictional strength. Rate of squeeze depends on degree of overstress. Occurs at shallow-to-medium depth in clay of very soft-to-medium consistency. Stiff-to-hard clay under high cover may move in combination of raveling at excavation surface and squeezing at depth behind surface.
Running	Cohesive-running	Granular materials without cohesion are unstable at a slope greater than their angle of repose (~30–35°). When exposed at steeper slopes they run like granulated sugar or dune sand until the slope flattens to the angle of repose.	Granular materials without cohesion are unstable at a slope greater than their angle of repose (~30–35°). When exposed at steeper slopes they run like granulated sugar or dune sand until the slope flattens to the angle of repose.
	Running		
Flowing		Clean, dry granular materials. Apparent cohesion in moist sand, or weak cementation in any granular soil, may allow the material to stand for a brief period of raveling before it breaks down and runs. Such behavior is cohesive-running.	A mixture of soil and water flows into the tunnel like a viscous fluid. The material can enter the tunnel from the invert as well as from the face, crown, and walls, and can flow for great distances, completely filling the tunnel in some cases.
Swelling		Ground absorbs water, increases in volume, and expands slowly into the tunnel.	Highly preconsolidated clay with plasticity index in excess of about 30, generally containing significant percentages of montmorillonite.

Source: Adapted from Hung, C.J. et al. 2009. *Technical Manual for Design and Construction of Road Tunnels Civil Elements*, U.S. Department of Transportation Federal Highway Administration, Publication No. FHWA-NHI-10-034, 704.

TABLE 3.6

Descriptive Terms for Soil Fractions from U.S. Standard Sieve

Material	Upper Limit 100% Passing	Lower Limit 100% Retained
Boulders	–	300 mm
Cobbles	300 mm	75 mm
Gravel		
Coarse	75 mm	19 mm
Fine	19 mm	4.75 mm
Sand		
Coarse	4.75	2 mm
Medium	2 mm	425 μm
Fine	425 μm	75 μm
Silt	75 μm low dry strength	
Clay	75 μm—moderate-to-high dry strength	

distribution curves is used in the selection of tunnel boring machines (TBMs) and to determine suitability of using different TBMs. The Standard grain size analysis test determines the relative proportions of different grain sizes as they are distributed among certain size ranges. The hydrometer test is used for sizes below 0.074 mm. The United States Classification System (USCS) is the most common soil classification system to describe soil properties for selection of mechanical miners. The method is standardized in ASTM D 2487 and D422. The definition of the grain size of soil particles according to their texture (particle size, shape, and gradation) is given in Table 3.6.

Selection criteria for earth pressure balance and slurry mix shield tunnel boring machines based on grain size distribution is seen in Figure 3.15.

3.2.2 Clay Minerals

It is very important to include clay minerals in tunnels excavated in soil or rock formation. Clay minerals can cause swelling and squeezing ground conditions. There are three main groups of clay minerals: kaolinite, illite, and montmorillonite. Water and moisture cause the swelling (expansion) of clay formations containing high swelling capacity clay minerals such as montmorillonite. In addition to size distribution, clay minerals can be defined by carrying out x-ray diffraction and mineralogical analysis. Clay grade, field description methods, and their range of UCSs can be found in Table 3.7.

3.2.3 Permeability

Permeability is commonly measured in terms of the rate of water flow through the soil in a given period of time. The coefficient of permeability

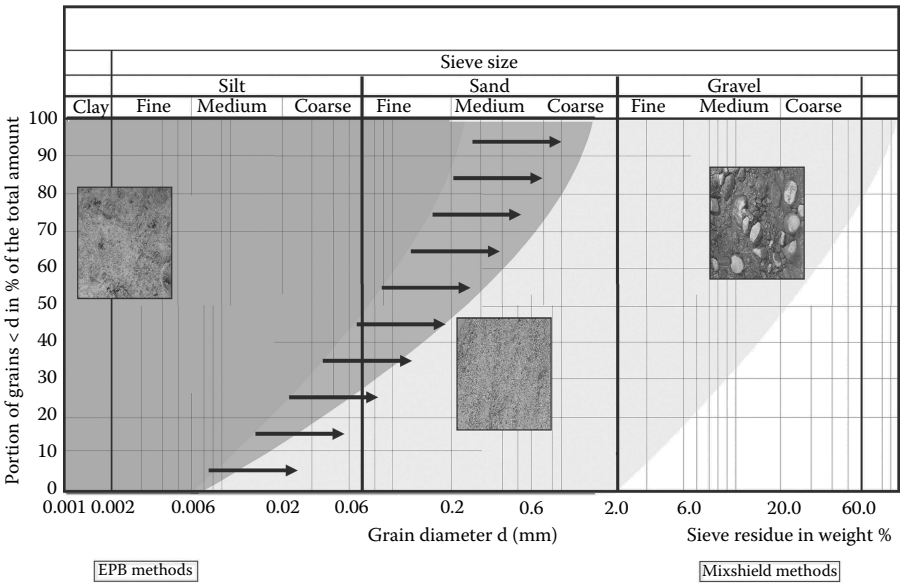

FIGURE 3.15
Selection criteria of grain size for earth pressure balance and slurry tunnel boring. (Adapted from Bäppler, K., 2007. *Tunnelling with Slurry TBMs (Mixshields)*, Tunneling Seminar, Herrenknecht AG, Germany, University of Texas at Austin. With permission.)

TABLE 3.7

Summary of Terms for Describing Clay

Grade	Description	Field Identification	Uniaxial Compressive Strength (kPa)
S1	Very soft clay	Easily penetrated several inches (cm) by fist	25
S2	Soft clay	S2 Easily penetrated several inches (cm) by thumb	25–50
S3	Firm clay	Can be penetrated several inches (cm) by thumb with moderate effort	50–100
S4	Stiff clay	Readily indented by thumb but penetrated only with great effort	100–250
S5	Very stiff clay	Readily indented by thumbnail	250–500
S6	Hard clay	Indented with difficulty by thumbnail	>500

Source: Adapted from Hung, C.J. et al. 2009. *Technical Manual for Design and Construction of Road Tunnels Civil Elements*, U.S. Department of Transportation Federal Highway Administration, Publication No. FHWA-NHI-10-034, 704.

Note: Grades S1–S6 apply to cohesive soils for example clays, silty clays, and combinations of silts and clays with sand, generally slow draining. If noncohesive fillings are identified, qualitatively identify, for example, fine sand.

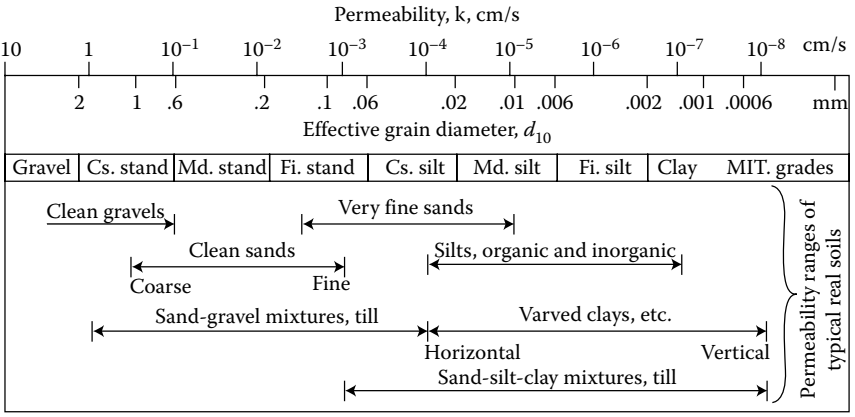

FIGURE 3.16
Soil types and permeability correlations. (Adapted from Schmidt, B., 1974. Exploration for soft ground tunnels-a new approach, in Subsurface exploration for underground excavation and heavy construction. *Proc. Specialty Conf. ASCE, American Society of Civil Engineers*, Geotech. Eng. Div., 84–96.)

is usually expressed as k in meters per second (m/s) or in centimeters per second (cm/s). Soil types and permeability correlations (Schmidt 1974) are given in Figure 3.16. The coefficient of permeability for soils is an important parameter in selecting mechanical miners, especially for earth pressure balance and slurry TBMs as seen in Figure 3.17.

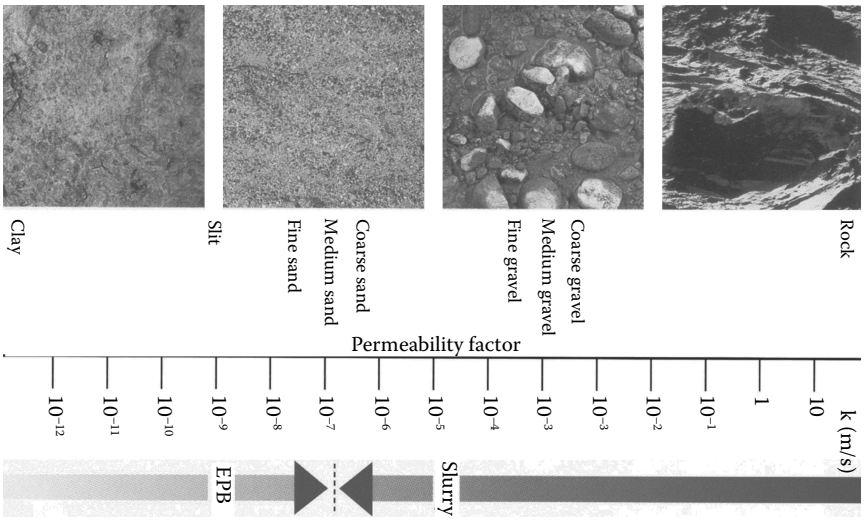

FIGURE 3.17
Selection criteria of permeability factor for earth pressure balance and slurry tunnel boring machines. (Adapted from Bäppler, K., 2007. *Tunnelling with Slurry TBMs (Mixshields)*, Tunneling Seminar, Herrenknecht AG, Germany, University of Texas at Austin. With permission.)

3.3 Coal

3.3.1 Compressive Strength of Coal

The *UCS* is a basic property in the classification of coal strength and in determining the cuttability of any geological formation. Coal is not a continuous solid material but contains various discontinuities, such as cracks, cleats, and bedding planes. Consequently, the strength of coal decreases with increasing specimen size. These aspects of the problem to determine coal strength are discussed in detail by different authors (Evans and Pomeroy 1966; Bieniawski 1968, 1984; Lama 1971; Peng 1978). Figure 3.18 is a typical example of the effect of cube specimen size on coal strength.

Although mechanical tests should preferably be carried out on large coal specimens, the difficulty, cost, and inefficiency of preparing such specimens, have always led researchers to use index tests and cube samples in sizes ranging from 2.5 to 5 cm. It is reported that the compressive strength ratio of 5 cm cubes to 2.5 cm cubes is around 1.36 (Bilgin et al. 1992).

3.3.2 Tensile Strength of Coal

Tensile strength breakage is an important factor in the mining of coal, so it is essential that tensile strength be determined in its own right (Evans and Pomeroy 1966). Due to this fact, straight pull, bending and Brazilian tests on different coal specimens were carefully examined by Evans and Pomeroy (1966). Tensile strength test is difficult to realize in coal samples and, although in disk testing the tensile stress is associated with an orthogonal compressive stress, it is always preferred by researchers for its simplicity

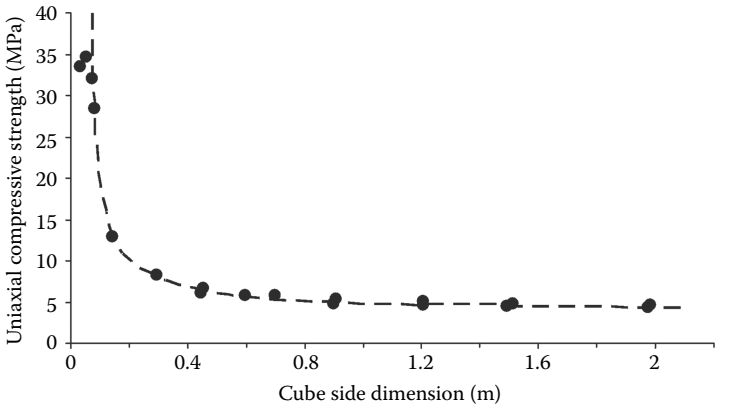

FIGURE 3.18
Variation of UCS of coal with cube size dimension. (Adapted from Bieniawski, Z.T., 1968. *International Journal of Rock Mechanics and Mineral Science*, 5:325–335.)

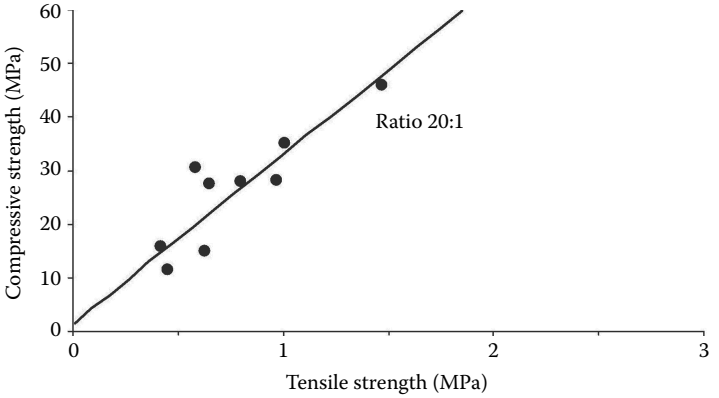

FIGURE 3.19
Ratio of UCS (perpendicular to bedding planes) to tensile strength (parallel to bedding planes). (Adapted from Evans, I., Pomeroy, C.D., 1966. *Strength Fracture and Workability of Coal*. London, Pergamon Press Ltd.)

and consistency. Evans and Pomeroy (1966) suggest using Figures 3.19 and 3.20 to estimate tensile strength from compressive strength values.

3.3.3 PL Strength of Coal

An attempt has been made to use the PL test on coal specimens in the Agean Lignite Mine (Bilgin et al. 1992). Cube specimens 5 cm in size were loaded perpendicular into the bedding planes with conical platens of standard geometry Special care was taken in performing and calculating $Is_{(50)}$ values as

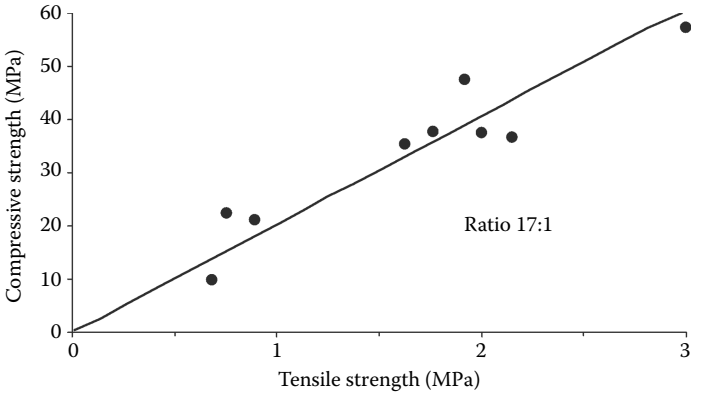

FIGURE 3.20
Ratio of uniaxial compressive strength (parallel to bedding planes) to tensile strength (perpendicular to bedding planes). (Adapted from Evans, I., Pomeroy, C.D., 1966. *Strength Fracture and Workability of Coal*. London, Pergamon Press Ltd.)

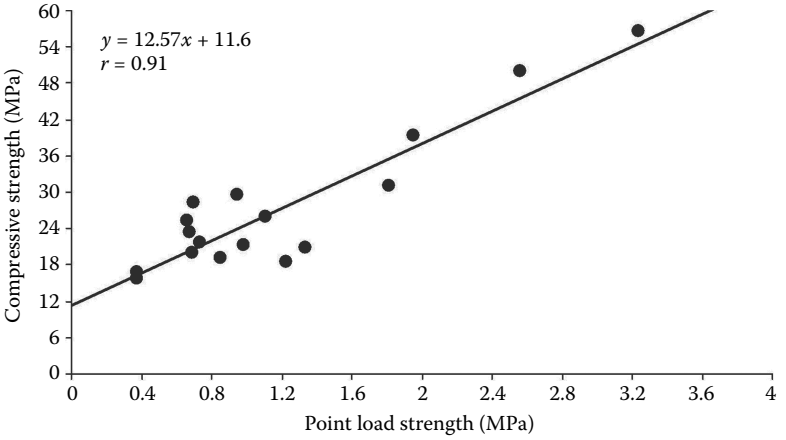

FIGURE 3.21
Relationship between uniaxial compressive strength and PL strength values of 5 cm cubes. (Adapted from Bilgin, N., Phillips, H.R., Yavuz, N., 1992. The cuttability classification of coal seams and an example to a mechanical plough application in Darkale Coal Mine. *The Eighth Coal Congress of Turkiye*, May, Zonguldak, Turkiye, in Turkish, 31–53.)

described by Brook (1977, 1985). A satisfactory correlation was found between UCS of coal (5 cm cubes) and PL strength values, as seen in Figure 3.21.

3.3.4 Schmidt Hammer Values of Coal

The Schmidt hammer was originally developed to estimate the in situ strength of concrete mass. Subsequently it has been used in a similar manner to estimate the strength of rocks and coal seams (Haramy and Demarco 1985; Sachpazis 1990). As can be expected, the relationship between in situ Schmidt hammer rebound values and the laboratory compressive strength of rocks or coal specimens exhibit a wide scatter due to the presence of joints, cleats, and the variation in the surface structure. The practical nature of in situ rebound values, reflecting both the strength and structural weakness properties of coal seams, makes the Schmidt hammer a useful device in any in situ strength classification. Variations of laboratory compressive strength with Schmidt hammer rebound values for Turkish and Indian coals are given in Figure 3.22 (Sheorey et al. 1984; Bilgin et al. 1992). To make the results more consistent, the compressive strength values of Indian coals are corrected to 50 mm cube specimen size by using the previously mentioned ratio of 1:36.

3.3.5 CIH of Coal

The cone indenter is a portable device that requires only small pieces of specimen not larger than $12 \times 12 \times 6$ mm. Figure 3.23 gives the relationship between the compressive strength of Aegean coal specimens and coal indenter hardness.

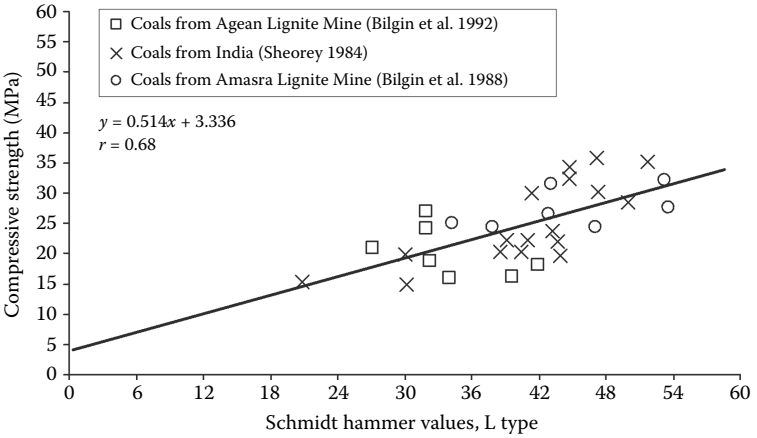

FIGURE 3.22
Relationship between uniaxial compressive strength (5 cm cubes) and Schmidt hammer rebound values. (Adapted from Bilgin, N., Phillips, H.R., Yavuz, N., 1992. The cuttability classification of coal seams and an example to a mechanical plough application in Darkale Coal Mine. *The Eighth Coal Congress of Turkiye*, May, Zonguldak, Turkiye, in Turkish, 31–53.)

3.3.6 Impact Strength Index of Coal

This test is described in detail by Evans and Pomeroy (1966). The apparatus consists of a vertical cylinder with 4.45 cm internal diameter. A steel plunger that weighs 1.8 kg, fits loosely inside the hollow cylinder. The coal specimen of 100 g in the 9.5–3.2 mm size range is poured into the cylinder, and

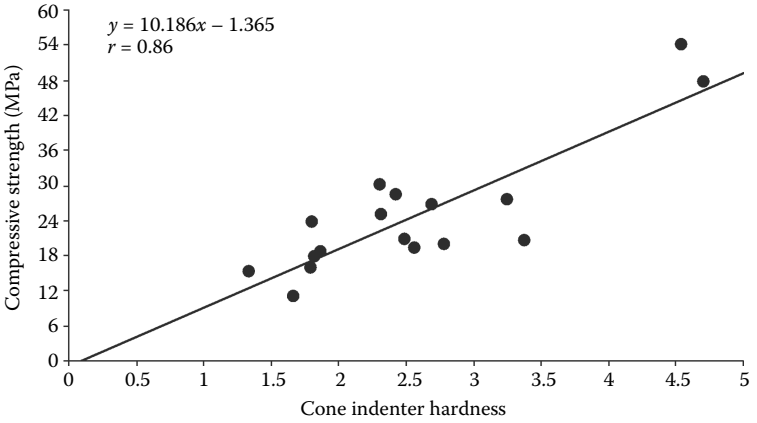

FIGURE 3.23
Relationship between CIH and uniaxial compressive strength of coal of 5 cm cubes in Agean Lignite Mine. (Adapted from Bilgin, N., Phillips, H.R., Yavuz, N., 1992. The cuttability classification of coal seams and an example to a mechanical plough application in Darkale Coal Mine. *The Eighth Coal Congress of Turkiye*, May, Zonguldak, Turkiye, in Turkish, 31–53.)

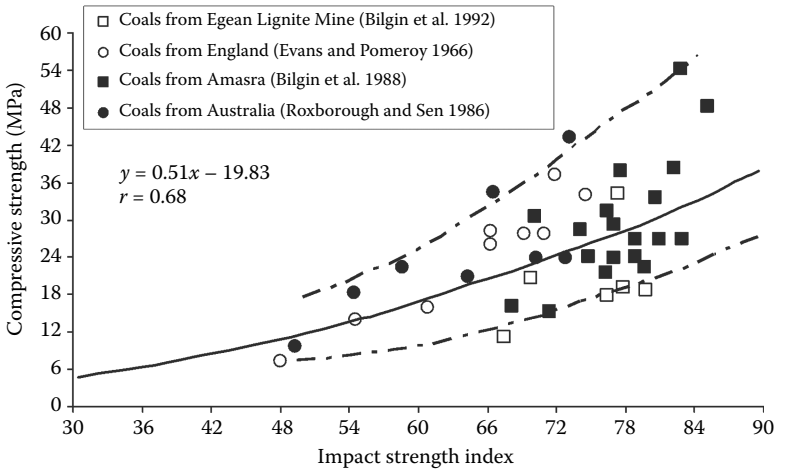

FIGURE 3.24
Relationship between impact strength index and uniaxial compressive strength values of coal from different provinces. (Adapted from Bilgin, N., Phillips, H.R., Yavuz, N., 1992. The cuttability classification of coal seams and an example to a mechanical plough application in Darkale Coal Mine. *The Eighth Coal Congress of Turkiye*, May, Zonguldak, Turkiye, in Turkish, 31–53.)

the plunger is dropped 20 times into the cylinder from a height of 30.5 cm. Finally the coal specimen is removed from the apparatus and sieved. The weight of coal in grams retained on the 9.5–3.2 mm sieve is defined as the impact strength index of the coal. As can be seen from Figure 3.24, the impact strength of the coal is related to compressive strength in an exponential function. In the evaluation of the test results for this relationship, a correction factor of 1:36, as explained previously, has been used to convert the compressive strength values of 2.5 cm into those of 5 cm cubes.

References

Altindag, R., Guney, A., 2006. ISRM suggested method for determining the shore hardness value of rock. *International Journal of Rock Mechanics and Mineral Science*, 43:19–22.

ASTM. 2013. American Society for Testing and Materials. Standard test method for unconfined compressive strength of intact rock core specimens. *Soil and Rock, Building Stones. Annual Book of ASTM Standards*, Vols. 4.08 and 4.09.1828.

Balci, C., 2004. Comparison of small scale and full scale rock cutting tests to select mechanized excavation machines. PhD thesis, Istanbul Technical University, 269.

Bamford, W.E., 1986. Cuttability and drillability of rock, Civil College Technical Report Engineers, Australia, July 11, 4.

Bäppler, K., 2007. *Tunnelling with Slurry TBMs (Mixshields)*, Tunneling Seminar, Herrenknecht AG, Germany, University of Texas at Austin.

Bieniawski, Z.T., 1968. The effect of specimen size on compressive strength of coal. *International Journal of Rock Mechanics and Mineral Science*, 5:325–335.

Bieniawski, Z.T., 1984. *Rock Mechanics Design in Mining and Tunneling*. Netherlands, Balkema Publications.

Bilgin, N., Akgun, S.I., Shahriar, K., 1988. The classification of coal seams in Amasra coalfield according to their mechanical strength. *The Sixth Coal Congress of Turkiye*, May, Zonguldak, Turkiye, in Turkish, 13–28.

Bilgin, N., Dincer, T., Copur, H., 2002. The performance prediction of impact hammers from Schmidt hammer rebound values in Istanbul metro tunnel drivages. *Tunnelling and Underground Space Technology*, 17: 237–247.

Bilgin, N., Phillips, H.R., Yavuz, N., 1992. The cuttability classification of coal seams and an example to a mechanical plough application in Darkale coal mine. *The Eighth Coal Congress of Turkiye*, May, Zonguldak, Turkiye, in Turkish, 31–53.

Broch, G., Franklin, J.A., 1972. The point load strength test. *International Journal of Rock Mechanics and Mineral Science and Geomechanics Abstracts*, 9:669–697.

Brook, N., 1977. The use of irregular specimens for rock strength tests. *International Journal of Rock Mechanics and Mineral Science and Geomechanics Abstracts*, 14: 193–202.

Brook, N., 1985. The equivalent core diameter method of size and shape correction in point load testing. *International Journal of Rock Mechanics and Mineral Science and Geomechanics Abstracts*, 22:61–70.

CSM. 1996. Test and model descriptions for performance and cost description of mechanical excavators for mining, underground construction and microtunnelling. EMI of Mining Engineering Department, 22.

Eskikaya, S., Bilgin, N., Ozdemir, L. et al. 2000. Development of rapid excavation technologies for the Turkish mining and Tunneling industries. NATO TU-Excavation SfS Programme Project Report. Istanbul Technical University, Mining Eng. Dept., Sept. 172.

Evans, I., Pomeroy, C.D., 1966. *Strength Fracture and Workability of Coal*. London, Pergamon Press Ltd.

Fowell, R.J., Mcfeat-Smith, I., 1976. Factors influencing the cutting performance of a selective tunnelling machine. *International Tunnelling '76 Symposium*, London, pp. 301–318.

Haramy, K.Y., Demarco, M.J., 1985. Use of the Schmidt hammer for rock and coal testing, *26th US Symposium on Rock Mechanics*, Rapid City, 549–555.

Heuer, R.E., 1974. Important ground parameters in soft ground tunneling. *Proceedings of Specialty Conference on Subsurface Exploration for Underground Excavation and Heavy Construction*, American Society of Civil Engineers (ASCE), NY, 41–55.

Howarth D.F., 1987. Mechanical rock excavation—Assessment of cuttability and boreability, In *Rapid Excavation and Tunneling Conference Proceedings*, ed. Society for Mining, Metallurgy, and Exploration, Inc., New York, Vol. 1, 145–164.

Hucka, V.A., 1965. A rapid method for determining the strength of rocks in-situ. *International Journal of Rock Mechanics and Mining*, 2: 127–134.

Hung, C.J., Monsees, J., Munfah, N., Wisniewski, J., 2009. Technical Manual for Design and Construction of Road Tunnels Civil Elements, U.S. Department of Transportation Federal Highway Administration, Publication No. FHWA-NHI-10-034, 704.

ISRM. 1981. Rock characterization testing and monitoring. In *ISRM Suggested Methods*, ed. Brown, E.T., Oxford, Pergamon Press, 211.

ISRM. 2007. The complete ISRM suggested methods for rock characterization, testing and monitoring 1974–2006. In eds. R. Ulusay and J.A. Hudson, Compilation arranged by the ISRM Turkish National Group, Ankara, 628.

Lama, R.D., 1971. *In-Situ and Laboratory Strength of Coal, Dynamic Rock Mechanics*. New York, SME, 265–300.

NCB. 1964. Methods of assessing rock cuttability; C.E.E. Report, No. 65(l).

NCB. 1977. NCB Cone indenter. MRDE Handbook No. 5. Staffordshire: Mining Research and Development Establishment, National Coal Board, UK, Bretby.

Nilsen, B., Ozdemir, L., 1999. Recommended laboratory rock testing for TBM projects. *American Underground Association (AUA) News,* 14(2): 21–35.

Nilsen, B., Dahl, F., Holzhäuser, J., Raleigh, P., 2006. SAT: NTNU's new soil abrasion test. *Tunnels & Tunneling International*, May 2006, 43–45.

Peng, S.S., 1978. *Coal Mine Ground Control*. New York, John Wiley & Sons, Inc., Press.

Poole, R.W., Farmer, I.W., 1980. Consistency and repeatability of Schmidt hammer rebound data during field-testing. *International Journal of Rock Mechanics and Mining Sciences & Geomechanics Abstracts*, 17: 167–171.

Roxborough, F.F., Sen, G.L., 1986. Breaking coal and rock, Australian coal mining practice. The Australian Institute of Mining and Metallurgy, 130–147.

Sachpazis, C.I., 1990. Correlating Schmidt hammer with compressive strength and Young's modulus of carbonate rocks. *Bulletin of the International Associate of Engineering Geology*, Paris, 42(1): 75–83.

Schimazek, J., Knatz, H., 1970. The influence of rock structures on the cutting speed and pick wear of heading machines (in German). *Gluckauf*, 106: 275–278.

Schmidt, B., 1974. Exploration for soft ground tunnels—A new approach, in Subsurface exploration for underground excavation and heavy construction. *Proc. Specialty Conf. ASCE, American Society of Civil Engineers*, Geotech. Eng. Div., 84–96.

Sheorey, P.R., Barat, D., Das, M.N., Mukherjee, K.P., Singh, B., 1984. Schmidt hammer rebound data for estimation of large scale insitu coal strength. *International Journal of Rock Mechanics and Mineral Science and Geomechanics, Abstracts*, 21(1): 39–42.

Szlavin, J., 1974. Relationships between some physical properties of rock determined by laboratory tests. *International Journal of Rock Mechanics and Mineral Science and Geomechanics, Abstracts*, 11: 57–66.

Tarkoy, P.J., 1979. Predicting raise and tunnel boring machine performance: State of the art. In *Rapid Excavation and Tunneling Conference Proceedings*, eds. Maevis, A.C., Hustrulid, W. New York, a Society of Mining Engineers of the American Institute of Mining, Metallurgical, and Petroleum Engineers, pp. 333–352.

Terzaghi, K., 1950. Geologic aspects of soft ground tunneling. In *Applied Sedimentation*, eds. Parker D., Task, R. New York, Wiley, pp. 193–209.

Tumac, D., Bilgin, N., Feridunoglu, C., Ergin, H., 2007. Estimation of rock cuttability from shore hardness and compressive strength properties rock mech. *Rock Engineering* 40(5): 477–490.

USACE EM 1110rr-1-1904, 1990. *Engineering and Design–Settlement Analysis*, Washington, DC, U.S. Army Corps of Engineers (USACE), 103.

Zare, S., Bruland, A., 2013. Applications of NTNU/SINTEF drillability indices in hard rock tunneling. *Rock Mechanics and Rock Engineering*, 46:179–187.

4

Rock-Cutting Tools and Theories

4.1 General

A student, a researcher, or a practicing engineer dealing with mechanical excavation should first understand the basic principles of rock-cutting mechanics affecting the efficiency of the rock-cutting process. The ability of excavation machines to operate and cut effectively in hard rock is limited by the system stiffness and the ability of cutting tools to withstand high forces. High forces may result in gross fracture damage to the tungsten carbide cutting tip or tool material and also damage to the machine components by exceeding the machine's torque and thrust capacities. Therefore, it is essential to understand the basic aspects of rock-cutting mechanics to minimize the large cost of a trial-and-error approach with an excavation machine in the field.

Within the frame of the concepts given above, different rock-cutting theories will be summarized first and some numerical examples will be given later in order to make the understanding of rock-cutting theories easier. Radial cutters (wedge or chisel cutters) and conical cutters are used in medium-strength rocks in machines such as roadheaders, continuous miners, coal ploughs, and shearers. However, disk cutters are mainly used in tunnel-boring machines (TBMs) from medium-strength to very hard rocks. The main types of these cutters are seen in Figures 4.1 and 4.2.

Simple chisel cutters are the first version of the radial- or complex-shaped cutters and are not used very much in practice. However, the majority of the cutting theories are developed for simple chisel cutters due to the simplicity of the geometrical parameters and the cutting theories are modified later by using correction factors for some geometrical parameters such as front ridge angle, bottom angle, and blunting.

4.2 Rock-Breakage Mechanism by Mechanical Tools

There are different theoretical explanations for rock-breakage mechanism induced by different cutting tools. Some of these theories are based on

FIGURE 4.1
Radial cutters (left), conical cutters (middle), and disk cutters (right).

tensile fracturing and some of them on shearing. In all of the cases, the mechanisms are similar in all of the tool geometries. Theoretical and experimental studies performed by different scientists indicate that both tensile and shear stresses play a role in the rock-breakage process; a crushed zone (pressure bulb) is created within the rock in front of and under the cutter or indenter due to the high compressive stress concentrations. This is a triaxial compression region that generates a tangential tensile (hoop) stress field and tensile fractures (Potts and Shuttleworth 1958; Evans 1962; Reichmuth 1963; Mishnaevsky 1995; Ozdemir 1995, 1997). A median (vent) crack starts and propagates into the rock until the tensile strain at the crack tip fell below that required for fracture development, and then the secondary (radial) tensile cracks develop and extend to the surface to form chips in rocks, behaving mostly elastic and/or brittle (Figure 4.3). A picture of the chipping process with a simple chisel (wedge) type of cutting tool is presented in Figure 4.4. The rock bridge between two cutting lines is removed if these fractures reach each other. If the stone behaves mostly plastic, then shear forces are

FIGURE 4.2
A disk cutter. (Courtesy of E-Berk.)

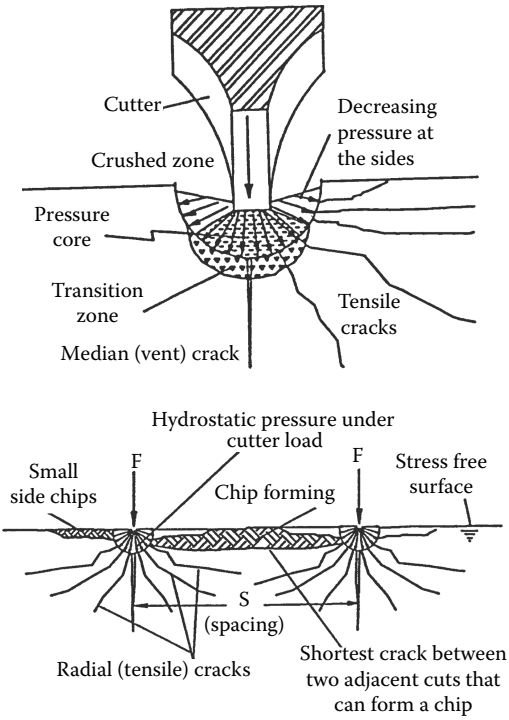

FIGURE 4.3
Idealized tensile breakage under CCS disk cutter. (Adapted from Rostami, J., Ozdemir, L., 1993. A new model for performance prediction of hard rock TBMs. *Proceedings of Rapid Excavation and Tunnelling Conference*, USA, pp. 794–809.)

more dominant than tensile forces acting within brittle rocks (Copur et al. 2003). The rock-breakage mechanism is complex in nature. Experimental and theoretical studies are still continuing for a better insight on many issues, such as brittleness and toughness in rock-cutting, fracture propagation modeling, and so on.

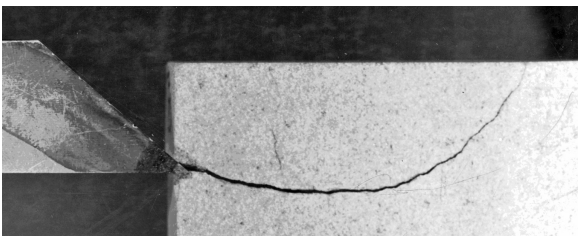

FIGURE 4.4
Tensile breakage by a wedge-type cutting tool. (From archive of N. Bilgin.)

4.3 Simple Chisel Cutters

The independent and dependent variables when cutting with chisel cutters are defined in Figure 4.5.

Basic independent variables are as follows:

d = Depth of cut
w = Width of tool
α = Rake angle
β = Clearence angle
s = Cutter sapacing

Basic dependent variables are as follows:

FC = Cutting force (force acting in the direction of cutting action)
FN = Normal force (force acting perpendicular to the direction of cutting action)
θ = Breakout angle
Q = Yield, the volume of material cut during a unit length of cut
SE = Specific energy which is defined as the energy spent to cut a unit volume of rock; it is found dividing FC by yield

The force acting on a cutting tool changes constantly in magnitude during the cutting process due to chipping and brittle nature of the rock. Averages of all of the force changes during the course of the cutting action give the mean cutter force; mean peak forces are averages of the peak forces for a given cutting condition. The ratio of peak forces to mean forces usually ranges between 1.5 and 3, generally being higher with brittle rocks. The ratio of cutting force to normal force is around 2 for sharp conditions of the tools. However, normal forces are affected by wear more than cutting forces and

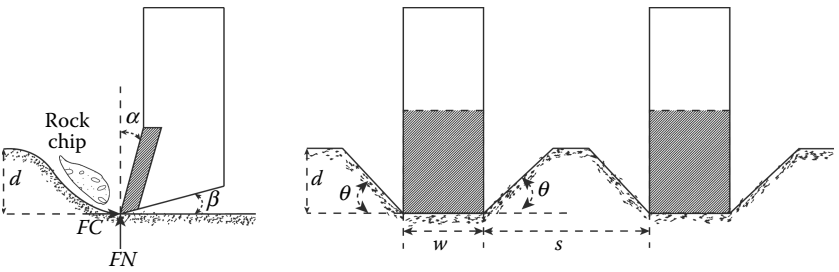

FIGURE 4.5
Dependent and independent variables when cutting with chisel cutters.

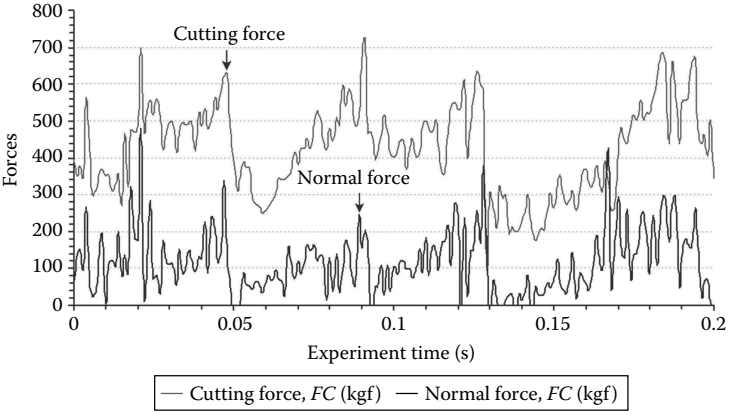

FIGURE 4.6
Typical recorded forces for chisel cutters when cutting.

increase rapidly with tool wear. Typically recorded cutter forces for chisel cutters in sharp condition are seen in Figure 4.6.

The work on coal-cutting mechanics performed by Evans (1962, 1972a,b, 1982, 1984a,b) and Evans and Pomeroy (1966) were used to establish the basic principles of coal cutting and these have been widely used in the efficient design of excavation machines such as shearers, continuous miners, and roadheaders. Evans demonstrated theoretically that tensile strength was the dominant rock property in rock cutting with chisel as formulated below in Equation 4.1:

$$F'C = \frac{2 \cdot \sigma_t \cdot d \cdot w \cdot \sin\frac{1}{2}\left(\frac{\pi}{2} - \alpha\right)}{1 - \sin\frac{1}{2}\left(\frac{\pi}{2} - \alpha\right)} \tag{4.1}$$

where d, w, and α are the parameters as defined in Figure 4.5, σ_t is the tensile strength, and $F'C$ is the peak cutting force.

He also formulated optimum spacing for chisel picks as three to four times the pick width. Roxborough (1973, 1985), Roxborough and Rispin (1973a,b), and Bilgin (1977) suggested that, to some extent the experimental forces for chisel picks were in good agreement with theoretical values using Equation 4.1.

Nishimatsu (1972) found that shear strength failure was dominant in cutting high-strength rocks, as formulated in Equation 4.2:

$$F'C = \frac{2 \cdot \sigma_S \cdot d \cdot w \cdot \cos(\psi - \alpha) \cdot \cos(i)}{(n+1) \cdot [1 - \sin(i + \psi - \alpha)]} \tag{4.2}$$

with the additional notations to Equation 4.1, σ_S is rock shear strength, i is rock internal friction angle, ψ is friction angle between rock and tool material, and n is stress factor, where $n = 12 - (\alpha/5)$.

TABLE 4.1

Friction Coefficient between Rock and Cutting Tool

Rock	Coefficient of Friction	Rock	Coefficient of Friction
Coal, Evans and Pomeroy (1966), dry condition, for steel	0.42–0.69	Greywacke, Bilgin (1977) for tungsten carbide and steel	0.44–0.2
Coal, Evans and Pomeroy (1966), wet condition, for steel	0.29–0.50	Harsburgite, Bilgin et al. (2006), for tungsten carbide	0.47
Gypsum, Bilgin (1977) for tungsten carbide and steel	0.96–0.90	Serpentinite, Bilgin et al. (2006), for tungsten carbide	0.53
Sandstone, Bilgin (1977) for tungsten carbide	0.32–0.45	Trona, Bilgin et al. (2006), for tungsten carbide	0.58
Sandstone, Bilgin (1977) for steel	0.17–0.18	Sandstone, Bilgin et al. (2006), for tungsten carbide	0.49–0.58
Anhydrite, Bilgin (1977) for tungsten carbide and steel	0.74–0.39	Limestone, Bilgin et al. (2006), for tungsten carbide	0.58
Limestone, Bilgin (1977) for tungsten carbide	0.63–0.43	Tuff, Bilgin et al. (2006), for tungsten carbide	0.51–0.62
Granite, Bilgin (1977) for tungsten carbide and steel	0.39–0.27	Copper, Bilgin et al. (2006) for tungsten carbide	0.6–0.78

The friction angle or friction coefficient between rock and cutting tool is sometimes difficult to determine, so, for a general interest, measured values by different authors are given in Table 4.1.

4.4 Radial Cutters and Complex-Shaped Pick Cutters

Radial, forward attack, and point attack tools are illustrated in Figure 4.7. Theoretical works were developed with many simplifications and assumptions, and usually for simple chisel cutters and unrelieved cutting mode. Therefore, the theoretical models must be modified for the different tool geometries and cutting conditions used in practice, including wear flat, front ridge angle, and v-bottom angle as defined in Figures 4.8 and 4.9.

As explained above, all theoretical works consider the unrelieved cutting mode, taking into account the cutters in isolated (unrelieved) mode without any interaction between grooves generated by another tool. However, in a rotary cutterhead of any mechanical miner, the cutting tools are placed in an array where there is always interaction between the groves, generating a relieved cutting condition. There is always an optimum ratio of cutter spacing to depth of cut (s/d) at which the specific energy is minimum. In that case, the energy spent to cut a unit volume of rock is minimum with

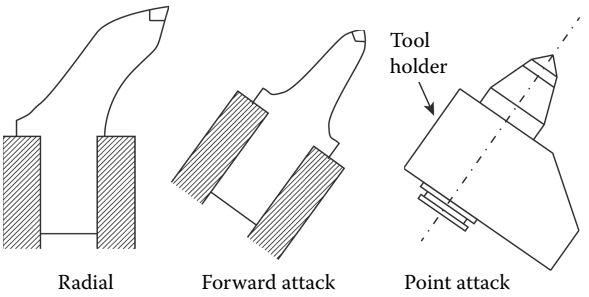

FIGURE 4.7
Radial, forward attack, and point attack tools.

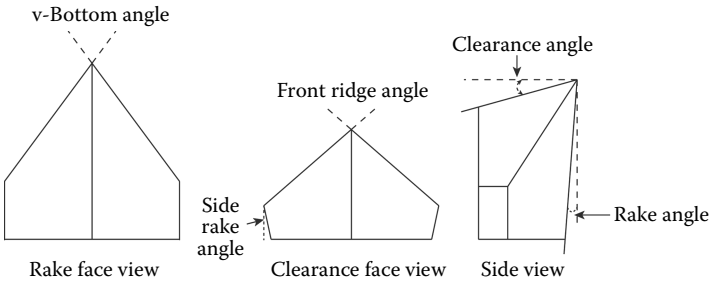

FIGURE 4.8
Definition of some basic tool parameters in a complex-shaped chisel cutter.

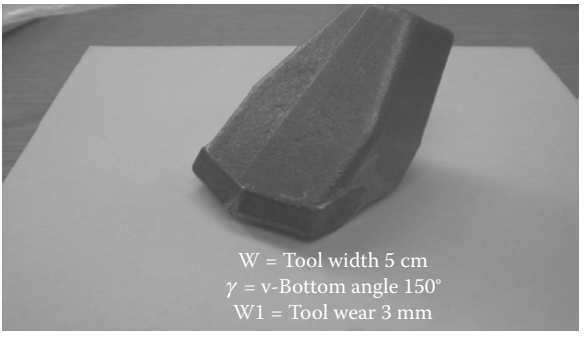

FIGURE 4.9
A complex-shaped chisel cutter used in TBMs. (From archive of N. Bilgin.)

minimum cutter consumptions (Roxborough 1973, Roxborough and Rispin 1973a,b). This also makes the tool forces approximately 10% lower than the tool forces obtained in unrelieved cutting mode at the same depth of cuts. Optimum (s/d) ratio is around 2 for chisel tools and conical cutters when cutting medium-strength rocks. The concept of relieved cutting with chisel cutters is illustrated in Figure 4.10.

Evans' cutting model, given in Equation 4.1 for chisel tools, was suggested to be modified by Bilgin et al. (2012) for complex-shaped cutters by using some experimental coefficients as in Equation 4.3:

$$F'C_W = k_1 \cdot k_2 \cdot k_3 \cdot k_4 \cdot \left[\frac{2 \cdot \sigma_t \cdot d \cdot w \cdot \sin \frac{1}{2}\left(\frac{\pi}{2} - \alpha\right)}{2 - \sin \frac{1}{2}\left(\frac{\pi}{2} - \alpha\right)} \right] \tag{4.3}$$

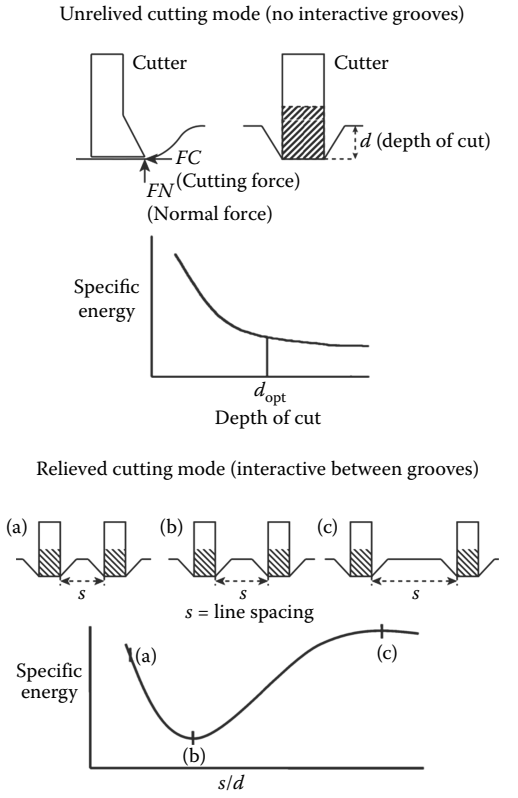

FIGURE 4.10
Relieved and unrelieved cutting mode with chisel cutters. (a) Too small spacing (overcrushing), (b) optimum spacing (chipping), and (c) too large spacing (ridge occurence-coring).

TABLE 4.2

Summary of the Effect of Wear Flat on Chisel Tool Forces

Wear Flat (mm)	$F'C_W/F'C_S = k_1$	$F'N_W/F'N_S$	$F'C_W/FC_W$	$F'N_W/FN_W$
0.5	1.27	1.74	2.20	1.74
1.0	1.55	2.41	2.13	1.67
1.5	1.83	3.09	2.06	1.61
2.0	2.11	3.76	1.99	1.54
2.5	2.39	4.43	1.92	1.48
3.0	2.67	5.10	1.85	1.41
3.5	2.95	5.78	1.78	1.35

Note: $F'C_S$, $F'C_W$, $F'N_S$, and $F'N_W$ values are the peak cutting and normal forces for sharp (indices s) and worn (indices w) state of the cutters, respectively; FC_W and FN_W values are the mean cutting and normal forces for worn (indices w) state of the cutters, respectively.

TABLE 4.3

Force Reduction Factors for Front Ridge and v-Bottom Angles to Be Used in Modification of Evans' Cutting Theory

Front ridge angle	–	90°	120°	150°	180°
Force reduction factor (k_2)	–	0.65	0.80	0.95	1.00
v-Bottom angle	60°	90°	120°	150°	180°
Force reduction factor (k_3)	0.50	0.65	0.80	0.90	1.00

where $F'C_W$ is the peak cutting force for a worn, complex-shaped chisel tool, $k_1 = (F'C_W/F'C_S)$ is a coefficient used for taking into account the effect of wear flat on tool force as defined in Table 4.2, k_2 is a coefficient used for taking into account the effect of front ridge angle, k_3 is a coefficient used for taking into account the effect of v-bottom angle as defined in Table 4.3, k_4 is a coefficient used for taking into account the effect of cutting in relieved mode (usually 0.9), and the other parameters are the same as for Equation 4.1.

4.5 Conical Cutters or Point Attack Tools

Evans (1984a,b) demonstrated theoretically that tensile strength and compressive strength were dominant rock properties in point attack tools as formulated below in Equation 4.4:

$$F'C = \frac{16 \cdot \pi \cdot d^2 \cdot \sigma_t^2}{\cos^2(\phi/2) \cdot \sigma_c} \tag{4.4}$$

where $F'C$ is the peak cutting force, d is the depth of cut, σ_t is the tensile strength, σ_c is the compressive strength and ϕ is the tip angle.

Goktan (1990) suggested a modification on Evans' cutting theory for point attack tools as indicated in Equation 4.5 and concluded that the force values obtained with this equation were close to previously published experimental values and could be of practical value, if confirmed by additional studies.

$$F'C = \frac{4\pi \cdot \sigma_t \cdot d^2 \cdot \sin^2(\phi/2 + \psi)}{\cos(\phi/2 + \psi)} \tag{4.5}$$

where ψ is the friction angle between cutting tool and rock and other parameters are as defined above for Equation 4.5.

Roxborough and Liu (1995) also suggested a modification of Evans' cutting theory for point attack tools as given in Equation 4.6. With all the parameters described above, they concluded that for Grindleford sandstone the predicted mean peak cutting force values are in good agreement with the modified cutting theory. However, the friction angle used was 16° using a steel block and a natural flat rock surface.

$$F'C = \frac{16\pi \cdot \sigma_c \cdot d^2 \cdot \sigma_t^2}{\left[2\sigma_t + (\sigma_c \cdot \cos(\phi/2)) \cdot \left(\frac{1 + \tan\psi}{\tan(\psi/2)}\right)\right]^2} \tag{4.6}$$

4.5.1 Estimation of Conical Cutter Forces and Specific Energy Empirically from Rock Properties

Twenty-two different rocks samples having compressive strength values ranging between 6 and 174 MPa were subjected to detailed laboratory mechanical and rock-cutting tests by the authors using conical cutters having a tip angle of 80° (Bilgin et al. 2006). Statistical analysis was carried out to estimate cutter forces and specific energy values from rock properties. The predictor equations are summarized in Table 4.4. The best correlations are obtained for uniaxial compressive and tensile strength values suggesting that these are the most important rock properties affecting the performance of conical picks. The third dominant rock property is found to be the Schmidt hammer rebound value obtained from an N-24-type hammer. The predictor equations given in Table 4.4 may enable any engineer to calculate tool forces from rock properties within acceptable statistical limits.

The published cutting theories for conical picks are only valid for estimating cutting forces in unrelieved cutting mode. Normal force controlling the depth of cut is a vital factor governing the efficiency of the cutting process, since cutting efficiency or specific energy is directly related to depth of cut. In an excavation process, each cut is affected by the adjacent relieving cut

TABLE 4.4

Prediction of Cutter Performance Based from Rock Properties

Unrelieved Cutting	R^2	Relieved Cutting (at Optimum s/d)	R^2
$FC/d = 0.826\ \sigma_c + 21.76$	0.810	$FC/d = 2.347\ \sigma_c^{0.785}$	0.808
$FC/d = 12.625\ \sigma_t + 8.78$	0.797	$FC/d = 16.794\ \sigma_t^{0.721}$	0.754
$FC/d = 4.542\ e^{0.058\ SH}$	0.772	$FC/d = 3.292\ e^{0.058\ SH}$	0.716
$FN/d = 1.217\ \sigma_c^{1.014}$	0.843	$FN/d = 0.752\ \sigma_c^{1.051}$	0.817
$FN/d = 15.74\ \sigma_t^{0.915}$	0.760	$FN/d = 10.687\ \sigma_t^{0.947}$	0.735
$FN/d = 1.723\ e^{0.079\ SH}$	0.784	$FN/d = 1.141\ e^{0.079\ SH}$	0.744
FC = mean cutting force in kgf		$SE_{opt} = 0.083\ \sigma_c + 1.424$	0.760
FN = mean normal force in kgf		$SE_{opt} = 1.259\ \sigma_t + 0.142$	0.743
d = depth of cut in mm		$SE_{opt} = 0.3912\ e^{0.058\ SH}$	0.757
SE_{opt} = specific energy at optimum cutting condition in kWh/m^3			
σ_c = uniaxial compressive strength in MPa			
σ_t = Brazilian tensile strength in MPa			
SH = N-24-Type Schmidt hammer			

as explained above. The tool forces in relieved cutting are lower than those in unrelieved cutting. Table 4.4 includes the predictor equations for specific energy, normal forces and cutting forces in relieved mode, which are not possible to estimate theoretically.

It should also be noted that the predictor equations given in Table 4.4 are valid for a cutter with 80° tip angle. If the tip angle is different from 80°, then a correction is required. Tip angles are usually manufactured between 60° (with softer rocks) and 90° (with stronger rocks) and 75°–80° are the most widely used tip angles. The relieved cuts in Table 4.4 are in single scroll cut pattern.

Designing or practicing engineers are also interested in the ratio of peak to mean forces since this ratio is an important factor affecting the vibration of a cutting head and the breakdown of the mechanical parts. The experimental results indicate that this ratio is not affected by the rock properties.

The ratio of peak cutting force to mean cutting force and the ratio of peak normal force to mean normal force are found to be 2.69 ± 0.32 Sd (standard deviation) and 2.39 ± 0.33 Sd for unrelieved cutting mode and 3.07 ± 0.55 Sd and 2.64 ± 0.49 Sd for relieved cutting mode, respectively. The values measured in relieved cutting mode are higher than those in unrelieved mode. This is expected, since larger chips are obtained in relieved cutting increasing peak forces.

The estimation of optimum specific energy is important in predicting cutting rates of excavation machines. Specific energy is best predicted from uniaxial compressive strength and tensile strength, verifying some of the previously published results (Copur et al. 2001). Moderate correlations are

obtained for Schmidt hammer rebound values of N-24-type and static and dynamic elasticity modulus.

Cutter spacing to depth of cut ratio (*s/d*) is the key factor in obtaining optimum specific energy; hence, the most efficient cutting conditions. Bearing in mind that cutter spacing on a cutting drum is fixed by the machine manufacturer, the only way to excavate in optimum condition is to apply the operational parameters, such as arcing or thrust force, giving the desired depth of cut. The optimum *s/d* ratio is found varying between 2 and 5 for the 22 rocks tested. However, a direct relationship between rock properties and optimum *s/d* ratio could not be found within the limits of the research program carried out by the authors. It is strongly recommended that this aspect of rock-cutting mechanics needs further research.

4.5.2 Relative Efficiency of Chisel Cutters against Conical Cutters

In sharp conditions, specific energy generated when cutting rocks with chisel or radial cutters is lower than obtained when cutting with conical cutters, since then they are mainly used in medium-strength nonabrasive rocks as explained above. Even with a moderate wear flat, tool forces and specific energy values increase considerably with chisel or radial cutters. However, conical cutters have a tendency to wear evenly; that is why they are preferred in comparatively abrasive and harder rocks.

4.6 V-Type Disk Cutters

Disk cutters are the main cutting tools of TBMs. The single disk cutter was the key innovation influencing the successful development of the modern TBMs. In 1956, the tunnel advance record of 35 m per day in the Toronto sewer tunnel was a breakthrough for TBMs. Since then, the disk cutter has proven to be the most effective tool for rock excavation. A typical V-type disk cutter is seen in Figures 4.11 and 4.12.

A typical disk cutter groove in the tunnel face and the effect of relieved cutting mode on specific energy is given in Figure 4.13.

The most used model among the researchers has been developed by Roxborough and Phillips (1975) and Roxborough (1978) in order to calculate the normal, rolling, and side forces acting on a V-type disk cutter. The model reflects the normal forces acting on a V-type disk cutter, assuming that the normal force equals the value of the compressive strength of the rock, multiplied by the projected area of disk contact area in the thrust direction. Normal force makes an action of penetration into the rock surface at a certain depth (p) for a disk cutter of edge angle of φ and diameter (D). While penetration increases, the chord length of contact (l) increases under the disk

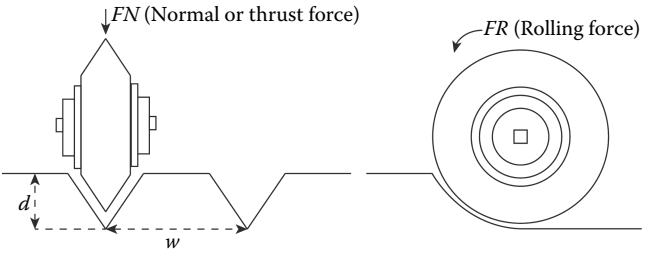

FIGURE 4.11
Sketch of a typical V-type disk cutter.

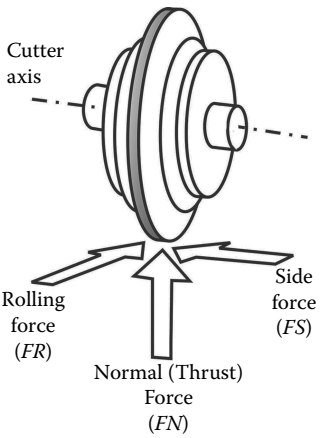

FIGURE 4.12
Sketch of a typical CCS disk cutter used in full-scale linear cutting machine.

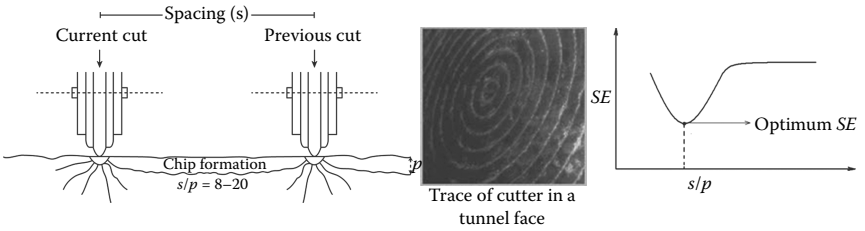

FIGURE 4.13
The effect of relieved cutting mode on specific energy (*SE*).

cutter. The chord length can be written using Equation 4.7. The contact area, between disk cutter and rock, may be given in Equation 4.8:

$$l = 2\sqrt{Dp - p^2} \tag{4.7}$$

$$A = 2 \cdot p \cdot l \cdot \tan\frac{\phi}{2} \tag{4.8}$$

The normal force, based on the assumption, may be written by following Equation 4.9. The rolling force acting on the disk is calculated by assuming that resultant forces pass through the center of the rotation. The relationship between *FN* and *FR* is expressed in Equation 4.10:

$$FN = 4 \cdot \sigma_c \cdot \tan\frac{\phi}{2}\sqrt{Dp^3 - p^4} \tag{4.9}$$

$$\frac{FN}{FR} = \sqrt{\frac{D-p}{p}} \tag{4.10}$$

The rolling force (Equation 4.11) can be obtained by putting Equation 4.9 into Equation 4.10.

$$FR = 4 \cdot \sigma_c \cdot p^2 \cdot \tan\frac{\varphi}{2} \tag{4.11}$$

Roxborough and Phillips (1975) formulated the optimum (*s/p*) ratio for V-shaped disk cutters as a function of the ratio of compressive to shear strength of the rocks; the results of which were in good agreement with the experimental values. The usual range for optimum (*s/p*) ratio is between 5 and 10.

Roxborough and Phillips (1975) developed their theory by not taking into account the edge radius of V-type disk cutters. Usually in practice, V-type disk cutters have a tip radius, changing from 1 mm to a few millimeters. In this case, predicted rock-cutting force values need to be corrected by taking into account the edge radius, since blunt disks give a different result to sharp disks. The following formulas (Equations 4.12 through 4.15) were developed by Bilgin (1977) and Phillips and Bilgin (1977, 1978) to correct the mean thrust and rolling forces when using theoretical disk cutter forces for sharp conditions.

$$FN_C = FN_{TS} \cdot e^{Ar} \tag{4.12}$$

$$FR_r = FR_{TS} \cdot e^{Br} \tag{4.13}$$

$$A = 0.0354 + \frac{0.6554}{p} \tag{4.14}$$

$$B = 0.06 + \frac{0.383}{p} \tag{4.15}$$

where FN_{TS}, FR_{TS} are the theoretical thrust (or normal) and rolling forces for a sharp disk; FT_r, FR_r are the forces for a disk with a tip radius of r, mm; and p is the disk penetration or depth of cut in mm.

4.7 Constant-Cross-Section Disk Cutters

Cutters with V cross sections are no longer used, except in special cases, due to uneven wear on the cutter tips, which progressively changes the contact area with the rock. They have been replaced with constant-cross-section (CCS) disk cutters, some of which have disk edge widths of a few millimeters.

In recent years, the CCS type of disk cutters, since taking higher cutter loads and efficiency, have a preferred diameter of 330–508 mm by manufacturer and contractor. Disk cutters having a diameter of 483 mm are the most widely used cutter type for TBMs (Rostami 2008). A typical CCS disk cutter is seen in Figure 4.12.

4.7.1 Model Proposed by Wijk

A mathematical model for the performance prediction and cutter life estimation of TBMs as formulated in Equations 4.16 and 4.17 is given by Wijk (1992). Two different types of cutters are considered, namely wedge-shaped tools and CCS disks. The stamp test, which was proposed originally for rock drillability classification by Wijk (1989, 1991), is used in the performance prediction model. Formulations by Wijk (1992) to predict the mean normal (thrust) force and rolling force acting on CCS disk cutters were dependent on the disk cutter tip width, compressive strength of rock, disk diameter, and cutting depth.

$$FN = 3 \cdot w \cdot \sigma_c \cdot \sqrt{Dd} \tag{4.16}$$

$$FR = 3 \cdot w \cdot \sigma_c \cdot d \tag{4.17}$$

where σ_c is the compressive strength; D is the disk diameter; d is the depth of cut; and w is the width of disk edge.

4.7.2 Model Proposed by Rostami–Ozdemir

Rostami and Ozdemir (1993) and Rostami et al. (1996) proposed a model based on the pressure distribution along the periphery of CCS disk cutters contacting with the rock. The equations derived for the mean normal (thrust) force and rolling force were dependent on the angle of contact between the rock and the disk cutter, radius of the disk cutter, width of the disk tip, line spacing between the disk cutters, uniaxial compressive strength of the rock, indirect (Brazilian) tensile strength of the rock, and penetration of the disks per revolution of the cutterhead. The equations developed by Rostami and Ozdemir are given in Equation 4.18.

$$\varphi = \cos^{-1}\left(\frac{R-p}{R}\right)$$

$$P_0 = C \cdot \sqrt[3]{\frac{s}{\varphi\sqrt{R \cdot T}} \cdot \sigma_c^2 \cdot \sigma_T} \quad \varphi \text{ is radian in this equation}$$

$$F_t = \frac{P_0 \cdot \varphi \cdot R \cdot T}{1+\phi} \quad \varphi \text{ is radian in this equation} \tag{4.18}$$

$$FN = F_t \cdot \cos(\varphi/2) \quad \varphi \text{ is degree in this equation}$$

$$FR = F_t \cdot \sin(\phi/2) \quad \varphi \text{ is degree in this equation}$$

where F_t is the total resultant force (kgf); R is the radius of cutter (cm); T is the width of disk (cm); φ is the constant for pressure distribution function (typically 0.2); ϕ is the angle of contact between the rock and disk cutter; p is the penetration per revolution (cm); P_0 is the pressure of crushed zone estimated from the rock strength and the cutting geometry as $P_0 = f(\sigma_c, \sigma_t, S, T, R, p)$, (kg/cm^2); σ_c is the uniaxial compressive strength of the rock (kg/cm^2); σ_t is the tensile strength of the rock (kg/cm^2); $c = 2.12$; and s is the spacing between the cuts (cm).

One important point in Rostami and Ozdemir equation is that it also covers the relieved cutting mode.

4.8 Efficiency of Chisel Cutters against Disk Cutters

Disk cutters are undoubtedly, inevitable cutting tools of TBMs. However, Roxborough and Rispin (1973a) and Bilgin (1977) reported that the pick cutters were 3–4 times more efficient than the disk cutters in medium-strength and nonabrasive rocks, verifying the theoretical findings of Evans (1972b).

This is true for short cutting lengths; after a certain length of cut, the pick cutters will deteriorate quickly in hard and abrasive rocks, making disk cutters to be the most popular cutting tools for hard and abrasive rocks. In soft clayey formations, the disks would not turn freely, resulting in local wearing, making the tunnel excavation quite inefficient. That is why pick cutters are preferred in special cases with soft grounds, which necessitate understanding their cutting mechanics in detail. Nowadays, in complex geologies that may cover a few kilometers of hard or medium-strength rocks, sometimes with frequent boulders, and few kilometers of soft ground, contractors use combination of disks (CCS- or V-type) and chisel cutters together. A good example for this type of geology and tunnel project is explained by Bilgin et al. (2012) for Beykoz–Istanbul sewerage tunnel. V-type disk cutters in a specific zone have proven to be the most effective tools for rock excavation with TBM for this project (Guclucan et al. 2007, 2008, 2009). The thrust of TBM was found to be inefficient (not to be enough) in excavating very hard and abrasive quartzite. CCS-type disk cutters were changed to the V-type disk cutter, although high cutter wear was expected, in order to get sufficient depth of cut per cutterhead revolution. Another important point for this project is that for a certain length of tunnel, the geologic formation changed from very soft to soft mudstone, siltstone. Disk cutters could not turn properly due to the lack of enough friction between the rock and disk cutter and heavy disk flat experienced during tunnel excavation. All disk cutters were changed to chisel cutters (Figure 4.9) giving the opportunity to compare the efficiency of chisel cutters against disk cutters in some specific conditions.

The efficiency of chisel tools in medium-strength rocks is clearly seen in Figure 4.14, which shows the relation between compressive strength of

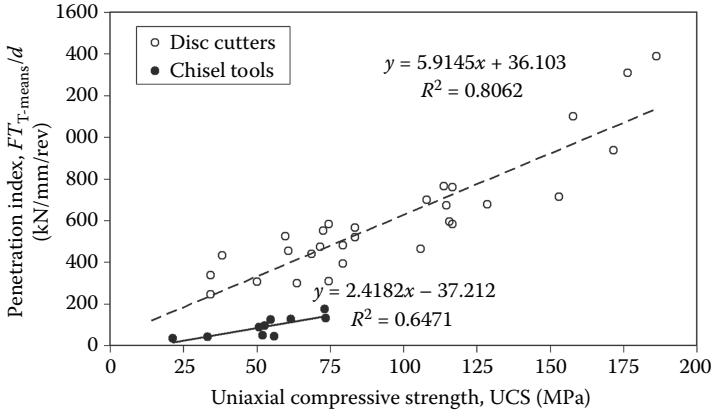

FIGURE 4.14
Relationship between uniaxial compressive strength of rocks and penetration index of TBM for chisel tools and disk cutters. (Adapted from Bilgin, N., Copur, H., Balci, C., 2012. *Tunnelling and Underground Space Technology*, 27, 41–51.)

rock and TBM penetration index (thrust force per unit cutting depth per revolution). It is also apparent in Figure 4.14 that the chisel tools demand around 3.5 times less thrust than the disk cutters for a given cutting depth. However, this advantage is not the same if the torque is considered for both cutters. As seen in Figure 4.15, the torque required for a unit depth of cut per revolution (torque index) is only around 1.4 times less for chisel tools compared to disk cutters. One of the most important factors determining the efficiency of an excavation process is the energy spent to excavate a unit volume of rock or specific energy. To estimate the specific energy, the cutting power of TBM is first calculated by using recorded torque values, and then, the cutting power is divided by the instantaneous production rate. Figure 4.16 shows clearly how the specific energy decreases with penetration for both chisel tools and disk cutters. Figure 4.16 reflects clearly the efficiency of chisel tools against disk cutters since they have better penetrability characteristics for a given thrust.

Roxborough and Rispin (1973a) reported that the pick cutters were 3–4 times more efficient than the disk cutters in medium-strength and nonabrasive rocks. The results of this study also support their findings. However, the results and comparison would be more detailed if the performances of chisel tools and disk cutters could be measured for the same type of rock.

It should be concluded that the disk cutters are unavoidable tools for cutting especially hard and abrasive rocks, since they have high thrust and wearing life capacity. However, it may be better to use chisel/ripper tools in relatively softer rocks in order to reduce the torque and thrust requirements of the TBMs, resulting in immediately higher production rates. The most important disadvantage of chisel tools is their limited durability and wearing life in relatively harder rocks.

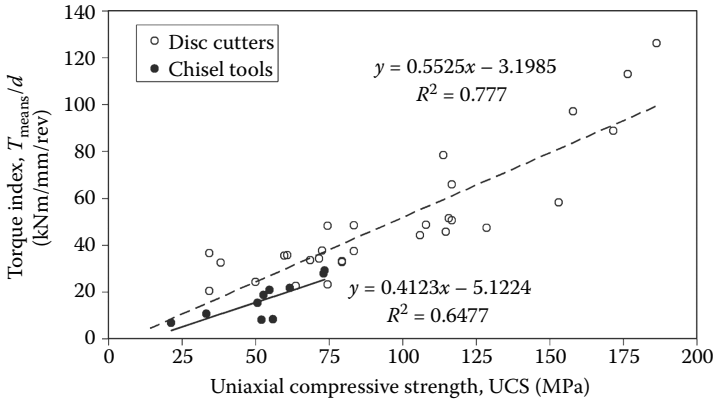

FIGURE 4.15
Relationship between uniaxial compressive strength of rocks and torque index (torque of TBM per unit depth of cut per revolution) of TBM for chisel tools and disk cutters. (Adapted from Bilgin, N., Copur, H., Balci, C., 2012. *Tunnelling and Underground Space Technology*, 27, 41–51.)

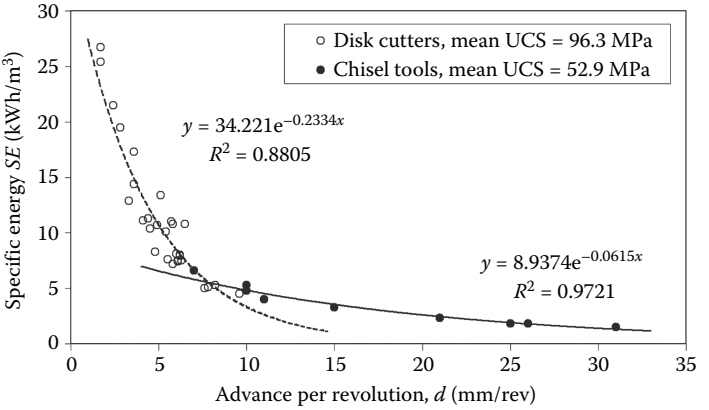

FIGURE 4.16
Relationship between advance per revolution of TBM cutterhead and consumed specific energy for chisel tools and disk cutters for mean values of compressive strength of rocks. (Adapted from Bilgin, N., Copur, H., Balci, C., 2012. *Tunnelling and Underground Space Technology*, 27, 41–51.)

4.9 Practical Considerations for an Efficient Rock-Cutting Process

One of the most important points in efficient cutting is the energy spent to excavate a unit volume of rock, or specific energy, *SE*. Figure 4.17 shows the variation of specific energy with penetration-depth of cut per revolution of a double shield TBM of 6 m diameter excavating in marl in Suruc

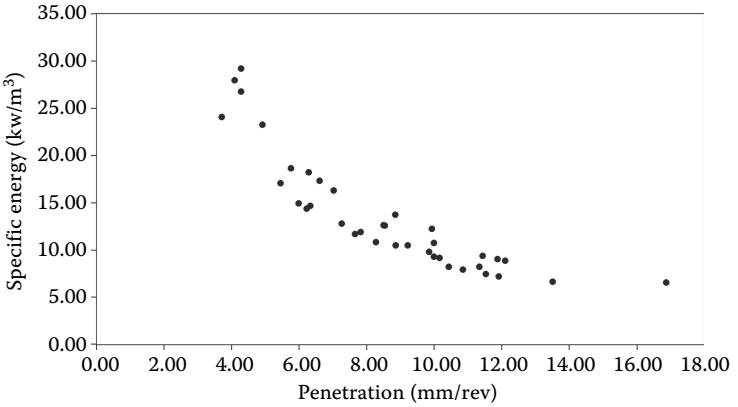

FIGURE 4.17
The variation of specific energy with penetration-depth of cut per revolution of a double shield TBM of 6 m diameter excavating in Marl in Suruc Tunnel-Turkey.

Tunnel-Turkey. As seen from this figure, for a penetration of 5 mm/revolution *SE* is around 30 kwh/m^3, it decreases down to an optimum value of 5 kwh/m^3 for a penetration of 10 mm/rev and it levels off thereafter. A practicing engineer should bear in mind that there is an optimum cutter spacing/penetration ratio given a minimum *SE*. For CCS disk cutters, this ratio ranges from 8 to 20, depending on the brittleness of the rock. Optimum *s/p* is estimated to be 9 for marl in the Suruc Tunnel and the cutter spacing is 8 cm, so theoretically optimum penetration should be 8/9 = 9 mm/rev as indicated in Figure 4.17 (Ilci et al. 2013).

4.10 Practical Examples of Using Cutting Theories for Prediction of Tool Forces, Specific Energy

4.10.1 Numerical Example 1

A mudstone sample with a compressive strength of 40 MPa and tensile strength of 3.5 MPa is cut with a chisel pick having a rake angle of 10°, chisel width of 1 cm with depth of cut 0.3, 0.6, and 0.9 cm. The breakout angle is observed to be constant for three different of cuts of 45°. The same rock sample is also cut with a conical bit having a tip angle of 70° and depth of cuts at 0.3, 0.6, and 0.9 cm. The breakout angle is found to be 45° for the depth of cut 0.3, 40° for the depth of cut 0.6, and 35° for the depth of cut 0.9 cm. The cutting parameters are given in Figure 4.18. Using Evans' theories, calculate and plot peak cutting forces for both cutters for different depth of cut. Discuss the results.

4.10.1.1 Solution

Cutting parameters of chisel picks and conical cutters are seen in Figure 4.5. In this figure, α is rake angle, d is depth of cut, w is width of tool, θ is breakout angle, *FC* is cutting force, *FN* is normal force, and $\varnothing$ is tip angle.

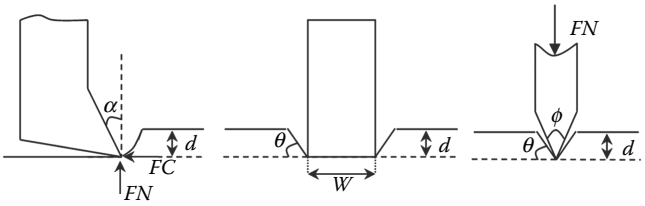

FIGURE 4.18
Cutting parameters of chisel picks and conical cutters.

4.10.1.2 For Chisel Picks

$$F'C = \frac{2 \cdot \sigma_t \cdot d \cdot w \cdot \sin \frac{1}{2}\left(\frac{\pi}{2} - \alpha\right)}{1 - \sin \frac{1}{2}\left(\frac{\pi}{2} - \alpha\right)} \tag{4.1}$$

For $d = 0.3$ cm; $\sigma_t = 35$ kg/cm^2; $w = 1$ cm; $\alpha = 10°$; $\pi/2 = 90°$

$$F'C = \frac{2 \cdot 35 \cdot 1 \cdot 0.3 \cdot 0.643}{1 - 0.643}$$

$FC = 37.8$ kgf or 0.38 kN
For $d = 0.6$ cm; $FC = 75.6$ kgf or 0.76 kN
For $d = 0.9$ cm; $FC = 113.4$ kgf or 1.13 kN

4.10.1.3 For Conical Cutters

$$F'C = \frac{16 \cdot \pi \cdot d^2 \cdot {\sigma_t}^2}{\cos^2(\phi/2) \cdot \sigma_c} \quad \text{given in Equation 4.4}$$

For $d = 0.3$ cm

$$F'C = \frac{16 \cdot \pi \cdot 0.3 \cdot 0.3 \cdot 35 \cdot 35}{0.671 \cdot 400}$$

$FC = 20.7$ kgf or 0.21 kN
For $d = 0.6$ cm; $FC = 82.7$ kgf or 0.83 kN
For $d = 0.9$ cm; $FC = 186.8$ kgf or 1.87 kN
The differences between the chisel and conical cutters cutting forces can be seen in Figure 4.21.

4.10.2 Numerical Example 2

Find the relation between the depth of cut and the specific energy (in MJ/m^3). Discuss the practical aspects of these relationships for both cutters. Discuss the relative efficiency of chisel picks against conical cutters.

$$SE = \frac{FC\,(\text{cutting force, kN})}{Q\,(\text{yield, m}^3/\text{km})} \tag{4.19}$$

SE = MJ/m^3.

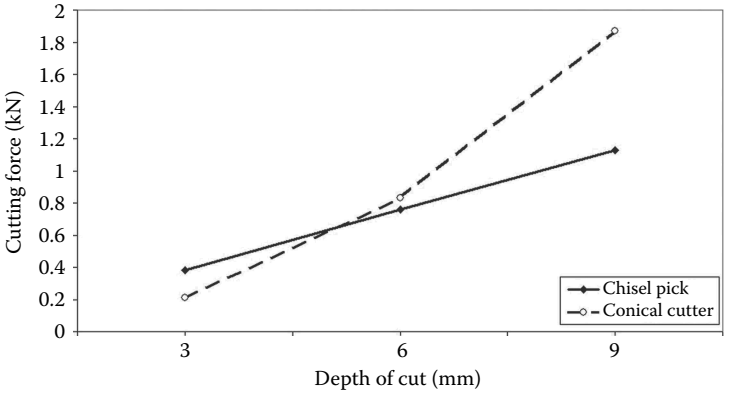

FIGURE 4.19
The theoretical relationship between peak cutting forces and depth of cut.

4.10.2.1 For Chisel Picks

Figures 4.19 and 4.20 show tool parameters for calculating specific energy.

$$\text{Yield} = \frac{\text{area of ABCD } (\text{m}^2) \cdot \text{m (for 1 m of cutting length)}}{\text{m (for 1 m of cutting length)}} = \frac{\text{m}^3}{\text{m}} \qquad (4.20)$$

$$F'C = \frac{16 \cdot \pi \cdot 0.3 \cdot 0.3 \cdot 35 \cdot 35}{0.671 \cdot 400}$$

$F'C$ = kgf
For d = 0.3 cm; Q = 0.039 m^3/km

$$SE = \frac{0.38\,\text{kN}}{0.039\,\text{m}^3/\text{km}} = 9.74\ \text{MJ/m}^3$$

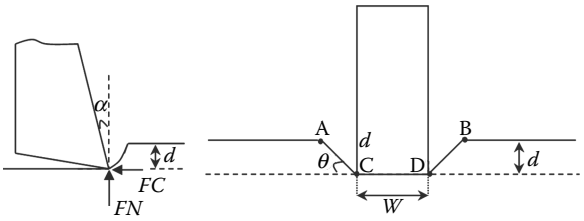

FIGURE 4.20
Basic tool parameters of calculation of specific energy.

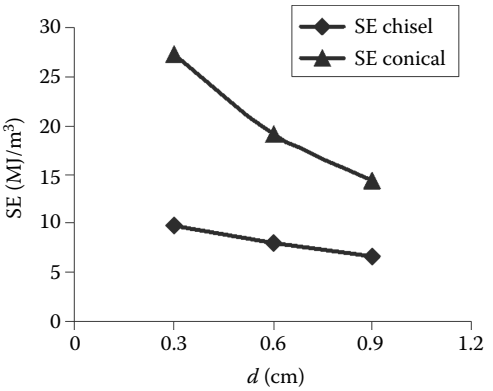

FIGURE 4.21
The relationship between depth of cut and specific energy.

$SE = 9.74$ MJ/m^3
For $d = 0.6$ cm; $Q = 0.096$ m^3/km; $SE = 0.756/0.096 = 7.9$ MJ/m^3
For $d = 0.9$ cm; $Q = 0.171$ m^3/km; $SE = 1.13/0.171 = 6.6$ MJ/m^3

4.10.2.2 For Conical Cutters

For $d = 0.3$ cm; $Q = 0.009$ m^3/km

$$SE = \frac{0.21\,\text{kN}}{0.009\,\text{m}^3/\text{km}}$$

$SE = 27.3$ MJ/m^3
For $d = 0.6$ cm; $Q = 0.0432$ m^3/km; $SE = 19.2$ MJ/m^3
For $d = 0.9$ cm; $Q = 0.129$ m^3/km; $SE = 14.4$ MJ/m^3
Figure 4.21 shows the relationship between the depth of cut and the specific energy.

4.10.2.3 Practical Implication

As seen from the above figure, *SE* decreases with the cutting depth. This is the main principle of rock-cutting mechanics. Chisel picks are more efficient than conical picks; however, chisel picks wear quickly and the efficiency of these types of cutters decreases rapidly in abrasive rocks. On the other hand, conical cutters rotate freely within the tool box causing a uniform wear pattern. After a certain cutting distance in abrasive rocks the conical cutters are more efficient than chisel picks.

4.10.3 Numerical Example 3

Compare peak cutting forces in relieved mode for both the simple chisel cutter and the complex-shaped chisel cutter when cutting a highly abrasive sandstone having *UCS* of 40 MPa and tensile strength of 3.5 MPa and the cutter parameters for simple chisel cutter are as follows: rake angle $\alpha = -10°$ and width of tool $w = 1.5$ cm. Cutter parameters for complex-shaped chisel cutters are as follows: rake angle $\alpha = -10°$, width of tool $w = 1.5$ cm, front ridge angle 120°, v-bottom angle 120°, and wear flat 2 mm. Compare peak cutter forces for both cutters at a depth of cut of 1 cm using Evans' cutting theory.

Modified Evans Equation 4.3 will be used to compare peak cutting forces.

$$F'C_W = k_1 \cdot k_2 \cdot k_3 \cdot k_4 \cdot \left[\frac{2 \cdot \sigma_t \cdot d \cdot w \cdot \sin \frac{1}{2}\left(\frac{\pi}{2} - \alpha\right)}{1 - \sin \frac{1}{2}\left(\frac{\pi}{2} - \alpha\right)} \right]$$

4.10.3.1 Solution

The peak cutting force for the simple chisel cutter is given in the second part of the equation and may be calculated as

$$F'C = 2 \cdot 35 \cdot 1 \cdot 1.5 \cdot \sin 0.5\,(90 + 10)/(1 - \sin 0.5(90 + 10))$$

In the above equation, σ_t is taken as in kg/cm^2.

$F'C = 343.72$ kgf

The first part of Equation 3.6 is the modification parameter for the complex-shaped chisel cutter.

k_1 is wear parameter, for 2 mm of wear flat, k_1 is 2.11, in Table 4.2.

k_2 is a parameter for front ridge angle, it is 0.8, in Table 4.3.

k_3 is a parameter for vee front angle, it is 0.8, in Table 4.3.

k_4 is relieved cutting parameter, for unrelieved cutting, it is taken as 1.

$k_1 \cdot k_2 \cdot k_3 \cdot k_4 = 1.35$

For the complex-shaped chisel cutter $F'C = 1.35 \cdot 343.72$ kgf or 464 kgf

Theoretical calculation shows that the peak cutting force for complex-shaped chisel cutters is 35% higher than peak cutting forces for simple chisel cutters, at a 1 cm depth of cut. However, simple chisel cutters deteriorate quickly in abrasive rocks so complex-shaped cutters are used in such rock formations.

4.10.4 Numerical Example 4

Compare theoretically thrust and rolling forces values for two different V-type disk cutters having edge angle of 90°, disk diameter of 35 cm, tip

radius values of $r = 0$ mm, and $r = 3$ mm for 0.8 cm depth of cut. Discuss the results. The cutters are supposed to cut a rock having uniaxial and tensile strength values of 120 and 11 MPa, respectively.

4.10.4.1 Solution

For a V-type disk cutter, having a tip radius of zero or sharp, the forces are found as follows:

Equation 4.9 gives $FN = 4 \cdot 0.8^2 \cdot 1200 \cdot 1 \cdot (35 \cdot 0.8 - 0.8^2)^{0.5}$

Normal or thrust force is found as 16,069 kgf

Equation 4.11 gives $FR = 4 \cdot 1200 \cdot 0.8^2 \cdot 1$

Rolling force is found as 3072 kgf

For a V-type disk cutter, having a radius of 3 mm or sharp, the forces are found as follows:

Equation 4.14 gives $A = 0.855$

Equation 4.15 gives $B = 0539$

Equation 4.12 gives $FN = 22{,}826$ kgf

Equation 4.13 gives $FR = 4247$ kgf

As seen from the calculations above, forces with a disk having a tip radius of 3 mm are around 40% higher compared to a sharp disk. The main reason for using disks having a tip radius is that they have a higher cutter life compared to sharp cutters.

4.10.5 Numerical Example 5

The same rock as in Section 4.10.4 is cut by a CCS disk cutter having a disk diameter of 48.3 cm with a tip width of 1.5 cm. Calculate the normal and rolling force.

4.10.5.1 Solution

$\sigma_c = 120$ MPa

$\sigma_t = 11$ MPa

$s = 8$ cm

$p = 0.8$ cm

FN and *FR* are calculated using Equation 4.18

FN is found as 219.3 kN

FR is found as 28.5 kN

References

Bilgin, N., 1977. Investigation into mechanical cutting characteristics of some medium and high strength rocks. PhD thesis, University of Newcastle Upon Tyne, UK, p. 332.

Bilgin, N., Copur, H., Balci, C., 2012. Effect of replacing disc cutters with chisel tools on performance of a TBM in difficult ground conditions. *Tunnelling and Underground Space Technology*, 27:41–51.

Bilgin, N., Demircin, M.A., Copur, H., Balci, C., Tuncdemir, H., Akcin, N., 2006. Dominant rock properties affecting the performance of conical picks and the comparison of some experimental and theoretical results. *International Journal of Rock Mechanics and Mining Sciences*, 43(1):139–156.

Copur, H., Bilgin, N., Tuncdemir, H., Balci, C., 2003. A set of indices based on indentation tests for assessment of rock cutting performance and rock properties. *Journal of South African Institute of Mining and Metallurgy*, November, 103(9):589–600.

Copur, H., Tuncdemir, H., Bilgin, N., Dincer, T., 2001. Specific energy as a criterion for the use of rapid excavation systems in Turkish Mines. *Transactions of the Institution of Mining and Metallurgy Section C—Mineral Processing and Extractive Metallurgy*, 110:A149–A157.

Evans, I., 1962. A theory of the basic mechanics of coal ploughing. *Proceedings of the International Symposium on Mining Research*, University of Missouri, Pergamon Press. V2: pp. 761–768.

Evans, I., 1972a. Line spacing of picks for efficient cutting. *International Journal of Rock Mechanics and Mining Sciences & Geomechanics*, 9:355–359.

Evans, I., 1972b. Relative efficiency of picks and discs for cutting rock. MRDE Report No. 41, National Coal Board, UK, p. 6.

Evans, I., 1982. Optimum line spacing for cutting picks. *The Mining Engineer*, January:433–434.

Evans, I., 1984a. A theory of the cutting force for point attack picks. *International Journal of Mining Engineering*, 2:63–71.

Evans, I., 1984b. Basic mechanics of the point attack pick. *Colliery Guardian*, May:189–193.

Evans, I., Pomeroy, C.D., 1966. *The Strength, Fracture and Workability of Coal*. Pergamon Press, Library of Congress Catalogue Card Nr. 66-14657. p. 277.

Goktan, M., 1990. Effect of cutter pick rake angle on the failure pattern of high strength rocks. *Mineral Science Technology*, 11:281–285.

Guclucan, Z., Meric, S., Gursoy, C., Algan, M., Bilgin, N., Balci, C., Tumac, D., 2007. The use of a TBM in difficult ground conditions. *Proceedings of the 2nd Symposium on Underground Excavations for Transportation*, Istanbul, Turkey, pp. 83–91 (in Turkish).

Guclucan, Z., Meric, S., Algan, M., Palakci, Y., Bilgin, N., Bilgin, A.R., Balci, C., Tumac, D., 2008. The use of a TBM in difficult ground conditions in Beykoz—Kavacik Sewerage Tunnel. *Proceedings of the World Tunnelling Congress, Underground Facilities for Better Environment and Safety*, Agra, India, pp. 1630–1638.

Guclucan, Z., Meric, S., Palakci, Y., Bilgin, N., Balci, C., Copur, H., Namli, M., Bilgin, A.R., Kandemir, E., 2009. The use of theoretical rock cutting concepts

in explaining the cutting performance of a TBM using different cutter types in different rock formations and some recommendations. *Proceedings of World Tunnelling Congress, Safe Tunnelling for the City and for the Environment*, Budapest, Hungary, pp. 487–489.

Ilci, N., Temel, M., Sezgin, S., Akpinar, T., Guarasio, S., Polat, C., Bilgin N., 2013. Clogging and squeezing effect of marl-clayey limestone on the performance of a hard rock TBM in Suruc Tunnel. *Turkey World Tunnel Congress*, Geneva.

Mishnaevsky, L.L., 1995. Physical mechanisms of hard rock fragmentation under mechanical loading: A review. *International Journal of Rock Mechanics and Mining Sciences*, 32:763–766.

Nishimatsu, Y., 1972. The mechanics of the rock cutting. *International Journal of Rock Mechanics and Mining Sciences*, 9:261–271.

Ozdemir, L., 1995. *Mechanical Mining Technologies. Short Course Notebook*. Colorado School of Mines, Mining Eng. Dept., Golden, Colorado.

Ozdemir, L., 1997. *Mechanical Mining. Short Course*. March 19–21, Colorado School of Mines, Golden, Colorado.

Phillips, H.R., Bilgin, N., 1977. Correlation of rock properties with the measured performance of disc cutters. *Proceedings of a Conference on Rock Engineering, University of Newcastle Upon Tyne*, UK, pp. 181–196.

Phillips, H.R., Bilgin, N., Price, D.L., 1978. The influence of tyre tip geometry on the design of disc cutter arrays. *Third Australian Tunnelling Conference, The Institutions of Engineers*, September 12–15, Sydney, pp. 48–52.

Potts, E.L.J., Shuttleworth, P., 1958. A study on the ploughability of coal, with special reference to the effects of blade shape, direction of planing to the cleat, planing speed and the influence of water infusion. *Transactions of the Institute of Min ing Engineers*, May, 117:519–553.

Reichmuth, D. R., 1963. Correlation of force-displacement data with physical properties of rock for percussive drilling systems. *Proceedings of the 5th US Rock Mechanics Symposium*, University of Minnesota, USA, ed. C. Fairhurst, Pergamon Press, pp. 33–59.

Rostami, J., 2008. Hard rock TBM cutterhead modeling for design and performance prediction. *Geomechanics and Tunnelling*, 1(1):18–28.

Rostami, J., Ozdemir, L., 1993. A new model for performance prediction of hard rock TBMs. *Proceedings of Rapid Excavation and Tunnelling Conference*, USA, pp. 794–809.

Rostami, J., Ozdemir, L., Nilsen, B., 1996. Comparison between CSM and NTH hard rock TBM performance prediction models. *Proceedings of Annual Technical Meeting of the Institute of Shaft Drilling and Technology (ISDT)*, Las Vegas, NV, pp. 11.

Roxborough, F.F., 1973. Cutting rock with picks. *The Mining Engineer*, June:445–454.

Roxborough, F.F., 1978. Fundamental studies on the mechanics of cutting rock with disc. *Third Australian Tunnelling Conference*, Sydney, pp. 43–47.

Roxborough, F.F., 1985. Research in mechanical excavation, progress and prospects. *Proceedings of Rapid Excavation and Tunnelling Conference*, Las Vegas, pp. 225–244.

Roxborough, F.F., Liu, Z.C., 1995. Theoretical considerations on pick shape in rock and coal cutting. *Proceedings of the 6th Underground Operator's Conference*, Kalgoorlie, WA, Australia, pp. 189–193.

Roxborough, F.F., Phillips, H.R., 1975. Rock excavation by disc cutter. *International Journal of Rock Mechanics and Mining Sciences & Geomechanics Abstracts*, 12:361–366.

Roxborough, F.F., Rispin, A., 1973a. The mechanical cutting characteristics of the lower chalk. *Tunnels Tunnelling*, 5:45–67.

Roxborough, F.F., Rispin, A., 1973b. A laboratory investigation into the application of picks for mechanized tunnel boring in the lower chalk. *The Mining Engineer*, May:1–13.

Wijk, G.A., 1989. The stamp test for rock drillability classification. *International Journal of Rock Mechanics and Mining Sciences & Geomechanics Abstracts*, 26:37–44.

Wijk, G.A., 1991. Rotary drilling prediction. *International Journal of Rock Mechanics and Mining Sciences & Geomechanics Abstracts*, 28:35–42.

Wijk, G.A., 1992. Model of tunnel boring machine performance. *Geotechnical and Geological Engineering*, 10:19–40.

5

Laboratory Rock-Cutting Tests

5.1 General Introduction on Performance Prediction Methods for Mechanical Miners

The prediction of the cutting/excavation/production performance of any mechanical miner for any mineral or rock formation is one of the main concerns in determining the economics of a mechanized excavation operation. Inaccurate performance predictions result in underestimation or overestimation of excavation costs. In the feasibility stage, this can drastically affect the decision-making process for project bidding, as well as the costing and scheduling of the entire project. The adverse affect of these mistakes might result in lower advance rates, higher machine maintenance, lower machine utilization, higher cutter changing rates and costs, sometimes changing excavation machine or method because of difficulties in excavation, and disputes between the parties involved (owner, designer, contractor, and other related parties). All these problems would increase the overall cost of excavation and sometimes make the project uneconomic or inapplicable.

If the parameters affecting an excavation system are well known, then it is easier to reach a high performance resulting in lower costs. Parameters affecting the performance of an excavation system can be classified into three general groups: geological–geotechnical, mechanical (machine related), and operational parameters, which are summarized in Table 5.1. Since it is not possible to change the geology after defining the alignment of an underground opening, a suitable machine should be selected/designed/matched for the geological conditions to be encountered. While the machine and geological parameters usually define the instantaneous (net) excavation rates (rate per cutting hour), operational parameters define the overall performance (machine utilization time (MUT) and daily advance rates) of the system.

Performance prediction generally includes the assessment of instantaneous cutting rates (ICRs), cutting tool consumption rates, MUT, and advance rates of drifts or tunnels for different geological units. Instantaneous (net) cutting rate (ICR) is the production rate for the realized cutting time (bank m^3 or ton/cutting hour); it is basically a function of mechanical and geological

TABLE 5.1

Summary of Parameters Affecting Performance of Mechanical Miners

Mechanical parameters	Machine type
	Machine weight and dimensions
	Thrust and torque capacities
	Cutterhead type
	Cutterhead power and RPM, lacing design
	Cutter type and dimensions, metallurgical properties of cutters
Geological–geotechnical parameters	Rock mass properties
	Rock quality designation (RQD)
	Bedding, foliation, fault zones
	Joint sets (orientation, spacing, filling, etc.)
	Hydrogeology (water table/water ingress)
	Adverse geology (squeezing, swelling, blocky grounds)
	Physical and mechanical (intact rock) properties
	Cuttability (cutter forces, specific energy, optimum cutting geometry—linear cutting tests)
	Strength (uniaxial compressive strength, Brazilian tensile strength, elasticity modulus, cohesion, etc.)
	Texture and abrasivity (hard mineral/quartz content and grain size, microfractures, grain interlocking, etc.)
	Others (brittleness, water content, swelling, etc.)
Operational parameters	Technical parameters
	Opening shape and dimensions
	Inclinations, cross-cuts
	Mining parameters
	Support (bolting, shotcrete, steel sets, etc.)
	Muck haulage (conveyor, locomotive, LHD, etc.)
	Utility lines (power, water, air supply) and surveying
	Ground treatment (drainage, grouting, freezing)
	Labor availability and quality

Source: Revised after Fowell, R.J., Johnson, S.T., 1982. Rock classification and assessment for rapid excavation. *Proceedings of the Symposium on Strata Mechanics*, pp. 241–244; Ozdemir, L., 1995. *Mechanical Mining Technologies. Short Course Notebook*. Colorado School of Mines, Mining Eng. Dept., Golden; Copur, H. et al. 1997. Studies on performance prediction of roadheaders. *Proceedings of the 4th International Symposium on Mine Mechanization and Automation*, Brisbane, Queensland, Australia, A4-1–A4-7; Copur, H., 1999. Theoretical and experimental studies of rock cutting with drag bits toward the development of a performance prediction model for roadheaders. PhD thesis, Colorado School of Mines, 361 p.

parameters, as well as technical operational parameters. Tool (cutter or bit) consumption rate (TCR) refers to the number of cutters changed per unit volume of excavated ground (cutters/bank m^3 or ton); it is basically a function of geological–geotechnical (especially abrasive mineral content) and mechanical parameters (especially cutter- and cutterhead-related parameters). MUT

is the net excavation time as a percentage of the total working (or shift) time, excluding all the stoppages (delays); it is usually estimated for specific projects since it depends on the delays (stoppages) caused by operational features of the projects, such as support system, muck pickup system, machine availability, and so on. Advance rate (AR) is the linear advance rate of the tunnel or drift excavation (m/shift, m/day, m/week, and m/month), and is a function of ICR, MUT, daily working hours, and cross-section area of the excavation face.

Delays of the excavation machine can be classified into two general groups: machine-related and nonmachine-related delays. Machine-related delays include cutter changes, unscheduled maintenance (unexpected machine breakdown), and scheduled maintenance. Nonmachine-related delays are caused by geological and operational parameters. Machine-related delays define the machine reliability as a percentage of machine-related delays over the total working (or shift) time. Machine availability is estimated as [(net excavation time + nonmachine-related stoppages)/shift time] or (100–reliability). The availability of modern mechanical miners reaches over 90–95%.

There are several methods for predicting the performance of mechanical miners, such as deterministic (semitheoretical) simulation, linear rock-cutting tests (full-scale or small-scale), empirical (statistical), probabilistic, in situ testing of a real-life machine, and laboratory testing of a prototype machine. It is strictly advisable to use more than one method to have more realistic/reliable results (Copur et al. 2001). A general classification and comparison of performance prediction methods are summarized in Table 5.2.

Empirical performance prediction models are mainly based on the past experience and the statistical interpretation of the previously recorded case histories; therefore, collection of field data becomes very important for developing empirical performance prediction models; the accuracy and reliability of these models depend on the quality and extent of the available data. Probabilistic methods are usually based on probabilistic evaluation of historical or experimental data for a given ground condition; also, there are some other probabilistic approaches implemented into a deterministic model (Dayanc 2011). The specific energy method is based on rock-cutting tests such as full-scale and small-scale linear. A general relationship between specific energy and ICR is used for preliminary cutting rate estimates; however, machine or cutterhead design possibilities are limited (medium). The rules of kinematics and dynamics are used for a general performance estimation in deterministic models by using the tool force estimates based on theoretical relationships, empirical relationships, and/or linear cutting experiments (full- or small-scale). A deterministic computer simulation requires results of the full-scale linear cutting tests for a complete simulation of the cutting action of a mechanical miner. It is possible to design a machine in detail with this method, given all the moments, detailed cutterhead design, and reaction forces acting on a machine or its cutterhead. Testing a prototype machine or its cutterhead in a laboratory is also a method used for performance

TABLE 5.2

General Classification and Comparison of Performance Prediction Methods

Prediction Model	Cost	Accuracy	Machine Design
Empirical			
• Based on small database	Low	Medium	Quite limited
• Based on very large database	High	High	Limited
Probabilistic	Low	Medium	Quite limited
Rock-cutting test (specific energy method)	Medium	High	Limited
Deterministic models (semitheoretical)			
• Based on theoretical tool forces	Medium	Low	Limited
• Based on empirically estimated tool forces (indentation tests, statistical relations between forces and rock mechanical properties)	Medium	Medium	Limited
• Based on tool forces obtained from rock cutting tests (full-scale, small-scale, portable, etc.)	Medium	High	Possible
Deterministic computer simulations (semitheoretical) based on tool forces obtained from cutting experiments (full-scale, small-scale, portable, etc.)	High	High	Possible
Testing a prototype machine in laboratory	Very high	Very high	Possible
On site testing of a real machine	Highest	Highest	Possible

Source: Revised after Rostami, J., Ozdemir, L., 1996. Computer modeling of mechanical excavators cutterhead. *Proceedings of the World Rock Boring Association Conference: Mechanical Excavation's Future Role in Mining*, September 17–19, Laurentian University, Sudbury, Ontario, Canada.

prediction; it is an expensive but precise method. Hiring and testing a used or new machine on site is a very expensive and time-consuming approach, but it is the most precise one, and this approach is usually suitable for small machines; if the hired machine yields a desired performance it could be bought.

It can be concluded that rock-cutting experiments are the best choice for performance prediction, since it is reliable and comparatively cheap, and gives the possibility of defining basic specifications of mechanical miners and designing/optimizing their cutterheads. A typical process for predicting the performance of mechanical excavation systems is presented in Figure 5.1.

5.2 Rock-Cutting Experiments

Selection, designing, and predicting the performance of mechanical miners became more important especially after the introduction of many new/modern mechanical miners such as coal ploughs, shearer loaders, roadheaders,

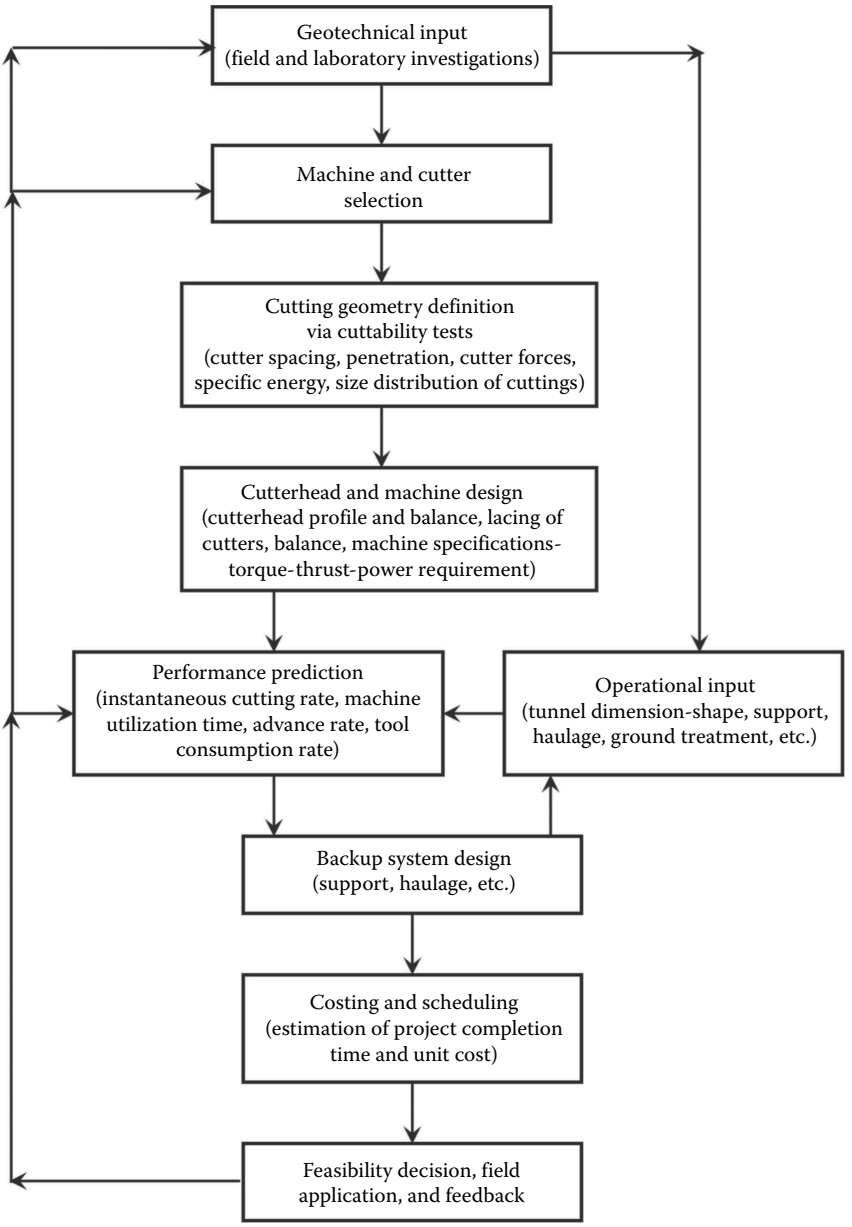

FIGURE 5.1
Generalized mechanical excavation system. (Modified after Copur, H., 1999. Theoretical and experimental studies of rock cutting with drag bits toward the development of a performance prediction model for roadheaders. PhD thesis, Colorado School of Mines, 361 p.)

and full-face TBMs during the 1950s. When Table 5.2 is analyzed, it shows that the rock-cutting experiments are the most reliable and economic solution for selection, designing, and predicting/optimizing the performance of mechanical miners. Many types of testing devices were developed for these purposes. Today, there are different rock-cutting devices used in the laboratories of universities, research institutes, and machine manufacturers.

The early rock-cutting devices were developed for in situ coal-cutting tests for assessing the ploughability of coals (Binns and Potts 1955). They were simple devices and usually using only one cutting tool; however, difficulties arose due to testing on site and the results were not convenient, since it was not possible to fully simulate the cutting action of a mechanical miner.

The early instrumented, laboratory-scale linear cutting devices were developed at the Mining Research Establishment of National Coal Board in England (Evans and Murrell 1958; Pomeroy 1958). However, since only small core or block samples and an index cutting tool were being used in these small-scale cutting tests, full-scale cutting devices using a real-life cutter for cutting a larger rock sample were required to simulate real cutting action of the mechanical miners.

One type of a full-scale rock-cutting device is a rotary-type device simulating a rotating cutterhead by using a single real-life cutter (Takaoka et al. 1974; Ozdemir et al. 1984). A constant vertical force was being applied to a single cutter by a hydraulic system. The penetration of the tool into the rock surface and the cutting or rolling force were being measured. The sample preparation and structural difficulties for applying this method probably forced the researchers to use linear rock-cutting devices. Studies indicated that the difference between rotary and linear cutting test results was only a small percent (Ozdemir, L. 1999. Personal communication). Therefore, a linear cutting device was/is dominantly preferred for full-scale rock-cutting tests.

Another version of a full-scale cutting device is horizontal drill rig (Ozdemir 1995, 1997; Kuzu and Balci 1998; Ergin et al. 2000), which provides testing of the real-life cutterheads of roadheaders, microtunnel boring machines, drum miners, and tricone or pdc bits. These devices are in use today and very useful also for the development of new cutting technologies (Ozdemir and Rostami 1995).

The third type of full-scale cutting device is a linear-cutting device using a real-life cutting tool for cutting a large block rock sample. This type of device is very reliable and commonly used today. It is successfully used for simulating the cutting action of mechanical miners in full scale by using a real-life cutter. Full-scale testing minimizes uncertainties. Some of the early versions of the full-scale linear cutting devices were designed to keep the normal (penetration) force constant (load controlled) while cutting and to measure cutting or rolling force (Rad and Schmidt 1973). The currently used linear-cutting devices are designed to keep the depth of cut constant (displacement controlled) and to measure normal, cutting, and sideways forces.

It usually is not possible or too expensive to obtain large block samples before starting the excavation project. The development for reliable portable or small-scale devices using small samples and small cutting tools is today a basic task for researchers working on rock-cutting mechanics; however, other types of testing cannot be as reliable as full-scale testing devices. One of the portable rock-cutting devices was developed in the Mining Engineering Department of Istanbul Technical University (Feridunoglu 2009; Bilgin et al. 2010). It is used for cutting small core samples or small block samples by a miniscale index disk cutter. Although this device is currently used for selection, design, and predicting the performance of different mechanical miners, a new generation of this device that provides for indexed (interactive) cutting is under development.

5.2.1 Small-Scale Linear Rock-Cutting Tests (Core-Cutting Tests)

The early instrumented, laboratory-scale linear cutting devices were developed at the Mining Research Establishment of National Coal Board in England (Pomeroy 1958; Evans and Murrell 1958). Then, a similar device was instrumented at University of Newcastle Upon Tyne, England, for cutting tests in unrelieved mode (noninteractive) (Roxborough 1969, 1973; Roxborough and Phillips 1974). The findings (specific energy values) of this device based on core cutting at 5 mm of depth of cut were then used for predicting the performance of roadheaders (McFeat-Smith and Fowell 1977, 1979) by using a standard chisel tool made of tungsten carbide, having a rake angle of (–5°) and clearance angle of (5°). Balci and Bilgin (2007) correlated the specific energy values obtained from small-scale linear cutting experiments with the specific energy obtained from full-scale linear cutting tests. Copur (2010) and Copur et al. (2011) used a small-scale linear cutting device for full-scale simulation of the cutting action of chain saw machines by using chain saw tools of the chisel type. The small-scale linear rock-cutting device used in the Mining Engineering Department of Istanbul Technical University is shown in Figure 5.2.

A shaping machine is used in this test to cut core samples or small block samples by a standard chisel-cutting tool or specially designed chain saw tools (Balci 2004, Balci and Bilgin 2007; Copur et al. 2007, 2011). The rig has a maximum cutting stroke of around 70 cm. Stone samples up to $15 \times 20 \times 25$ cm or core samples with a diameter of at least 50 mm is clamped on a vise mounted on the machine table, which can be raised, lowered, and laterally traversed with respect to cutting tool. The line spacing between the cuts is adjusted by lateral traversing. The rock sample is clamped with a certain dip angle, or parallel or perpendicular to the bedding planes in order to simulate the real cutting conditions of the sample.

The cutting tool is fixed with a tool holder directly to a load cell (dynamometer), equipped with strain gauge bridges, used for recording the forces acting on the tool. Tool-holder–dynamometer assembly can be raised or

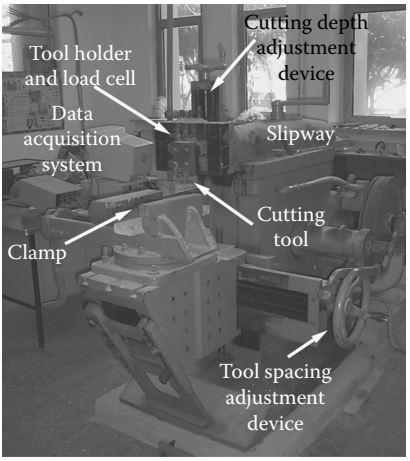

FIGURE 5.2
Small-scale linear cutting machine in ITU Laboratories.

lowered with a mechanical device to adjust the cutting depth. The tool has to be calibrated with the dynamometer prior to testing by applying different known loads with a hydraulic jack. A picture of the tools used with a small-scale linear cutting test device including standard chisel tool is presented in Figure 5.3.

The actuator of an electric motor triggers the tool-holder–dynamometer assembly, which is located in front of a slipway, through the fixed/clamped stone sample at a preset cutting depth, line spacing, and constant velocity of around 40 cm/s. During the cut, the dynamometer measures/records the normal, cutting and sideways forces (three orthogonal forces) acting on the tool. When using a small block sample, after each cut, the clamped stone sample can be moved sideways by a preset line spacing to duplicate the action of multiple tools on a miner. After a core sample is cut, then the sample is turned 90° to start a new cut. Four unrelieved (noninteractive) cuts can be achieved when using a core sample and relieved cuts (interaction between the cut grooves) cannot be performed in the sample. The plane of the sample

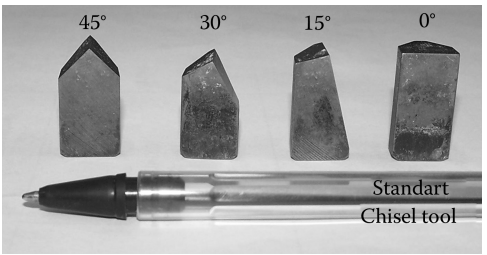

FIGURE 5.3
Cutting tools used with small-scale linear cutting machine.

surface should be leveled horizontally using a water level. The sample surface of uneven shape can be trimmed by the standard chisel tool to obtain a flat surface, or the surface can be conditioned by several passes (cutting levels) to obtain a surface with fractures perfectly developed, similar to a surface cut by a real-life machine.

In addition to tool forces, the cut material is weighed and used for an estimate of specific energy, which is defined as energy (work) required for cutting a unit volume or mass of rock (Pomeroy 1963, Roxborough 1973). The cut material can also be sieved to measure the size gradation, which gives information about the efficiency of the cutting process. Breakage mechanisms can also be analyzed by visual observations. The tests should be repeated at least 3 times for a specimen.

Data acquisition systems include a dynamometer (load cell), A/D card, signal conditioning amplifier, and personal computer. The data are recorded at a required gain and sampling rate by a commercial software. The data acquisition card should include at least three independent channels and monitors/measures/records data from the dynamometer. Excitation voltage of the amplifier should be 10 V. The data sampling rate should be at least 1000 Hz for cutting tests. The recorded data are evaluated using a custom-made spreadsheet macro program.

5.2.2 Full-Scale Linear Rock-Cutting Tests

The full-scale linear cutting tests measure full-scale forces acting on a real-life cutter of any type (single disk, conical, radial, and so on) while cutting a block of rock sample cast in a sample box. Full-scale testing minimizes the uncertainties of scaling and any unusual rock-cutting behavior not reflected in its physical properties. Results of this test can be used as input for selection, designing, and predicting/optimizing the costs and performance (excavation/production/cutting rate) of mechanical miners for feasibility purposes. This test along with deterministic computer simulation is accepted as the most reliable and economical method for these purposes.

The full-scale linear cutting machine features a large stiff reaction frame on which the cutter and load cell assembly are mounted. A block sample up to $0.6 \times 0.8 \times 1.0$ m in size is cast within a stiff (metal) sample box with a fast curing concrete at a certain dip angle or parallel or perpendicular to the bedding planes in order to simulate the real cutting conditions of the deposit. A servo-controlled hydraulic cylinder moves the sample within the box through the cutter at a preset depth of cut (penetration), width of spacing (line spacing of tool cutting tracks), and constant velocity. Cutting velocity, depth of cut, and line spacing of the tool can be adjusted by hydraulic cylinders as desired. A triaxial load cell located between the cutter and the frame monitors/measures/records the orthogonal forces (normal, drag–cutting–rolling, and sideways forces) acting on the tool. After each cut, the rock box is moved sideways by a desired spacing to duplicate the action of the

multiple cutters on the cutterhead of a mechanical excavator. After each cut, the cut length is measured; the cut materials are collected, weighed, and sieved. Sieve analysis is performed to measure the size gradation of the muck samples; this also gives information on the efficiency of the cutting. Each cut should be replicated at least 3 times; the results should be averaged and the cut surface should be photographed. A picture and a schematic drawing of the full-scale linear cutting machine found in the laboratories of the Mining Engineering Department of Istanbul Technical University are presented in Figures 5.4 and 5.5, respectively.

Data acquisition systems used with this testing system include a dynamometer (load cell), A/D card, signal conditioning amplifier, and personal computer. The data are recorded at required gain and sampling rate by a commercial software. The data acquisition card should include at least four independent channels for monitoring/measuring/recording data from the dynamometer. Excitation voltage of the amplifier should be 10 V. The data sampling rate should be a minimum of 1000 Hz. The recorded data can then be evaluated by using a custom-made spreadsheet macro program.

A schematic drawing of the orthogonal forces (normal, cutting, and sideways forces) acting on a conical tool, a chisel tool, and a disk cutter is presented in Figure 5.6. Cutting (drag or rolling) force, acting parallel to the surface being cut and tool travel (cutting) direction, is directly related to the torque requirement of a mechanical miner, and used to estimate specific energy, which is defined as energy (work) required to excavate a unit volume or mass of rock (Pomeroy 1963, Roxborough 1973). Normal (thrust) force, acting perpendicular to the surface being cut and tool travel direction, is used to estimate required effective mass and thrust of the excavator to keep the tool in a desired depth of cut (penetration). Sideways force, acting perpendicular

FIGURE 5.4
Full-scale linear cutting machine in ITU Laboratories.

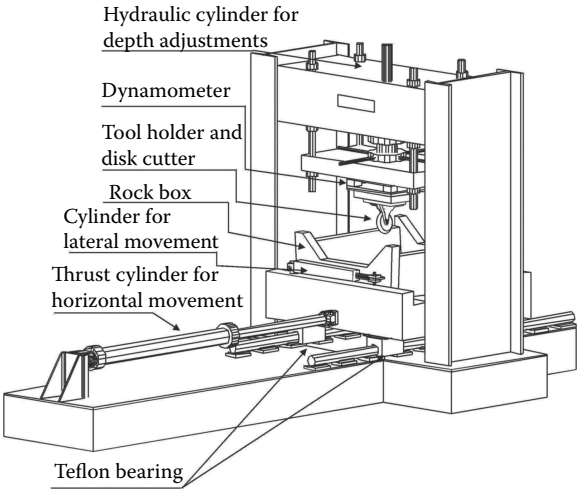

FIGURE 5.5
A schematic drawing of full-scale linear cutting machine.

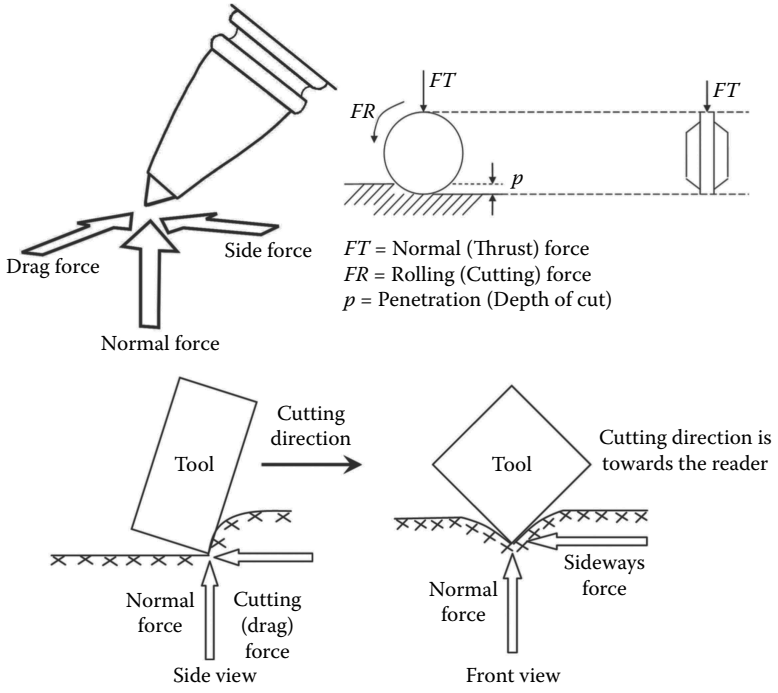

FIGURE 5.6
Forces acting on a conical, chisel, and disk cutter.

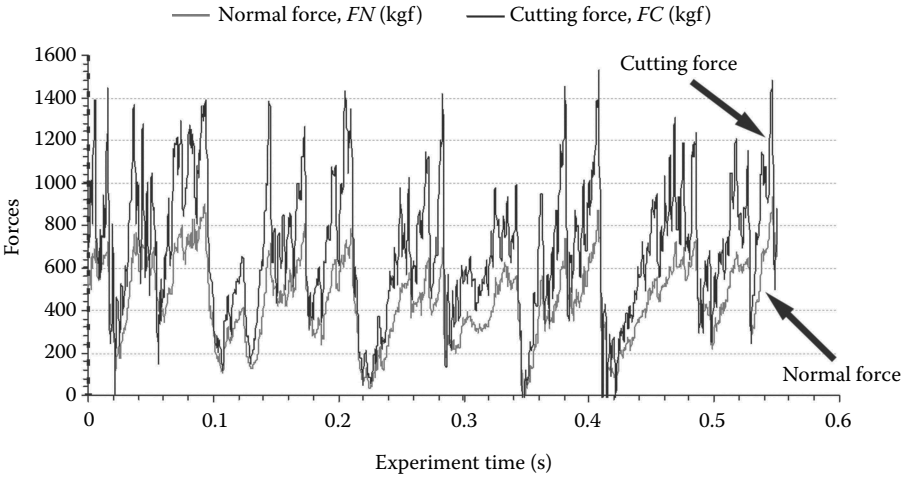

FIGURE 5.7
Typical force output after cutting a rock sample with a conical tool.

to the tool travel direction and the direction of normal and cutting forces, may be used along with normal and cutting forces to balance tool lacing for minimizing machine vibrations. An example showing the variation of forces acting on a tool while cutting is presented in Figure 5.7.

Tool forces alone are not enough to evaluate the efficiency of cutting systems. Specific energy is also used for estimation and comparison of cutting efficiency (production rates) of mechanized systems and one of the most important factors for defining their optimum cutting geometries (optimum ratio of depth of cut to line spacing) for a given rock sample. Specific energy is estimated as (Pomeroy 1963; Roxborough 1973)

$$SE = \frac{FC}{Q} \tag{5.1}$$

where SE is specific energy (MJ/m^3), FC is cutting force acting on the tool (kN), and Q is yield or rock volume cut in unit cutting length (m^3/km). The cutting power of a mechanical miner can be estimated by using specific energy. Achievable production rates can be estimated by using the specific energy for a machine with a known cutting power. Lower specific energy means that a mechanical miner with a known cutting power can achieve higher excavation rates or a smaller and cheaper excavation machine can be used for excavation.

The effects of line spacing and depth of cut on specific energy and cutting efficiency is explained in Figure 5.8. If the line spacing is too close (case a), specific energy becomes very high and the cutting is not efficient, since the rock is overcrushed. Tool wear is also high in this region due to the high

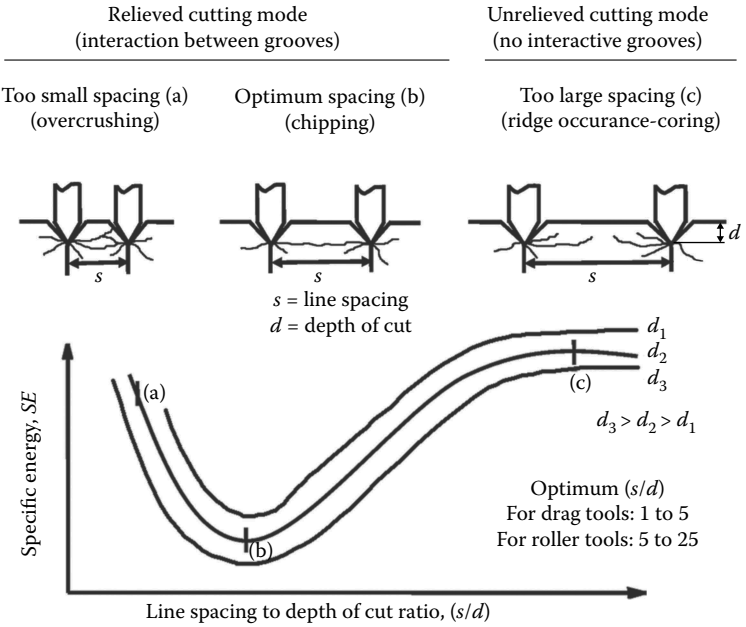

FIGURE 5.8
Effect of line spacing and depth of cut on specific energy and cutting efficiency.

friction between tool and rock. If the line spacing is too wide (case c), specific energy becomes very high again and the cutting is not efficient, since the cuts cannot generate relieved cuts (tensile fractures from adjacent cuts cannot reach each other to form a chip), creating a ridge or a groove-deepening (coring) situation, which might result in shock loads causing gross failures in cutting tools or stalling of the machine in some cases. The minimum specific energy is obtained with an optimum line spacing to depth of cut ratio as shown in case b, which indicates the most efficient cutting condition and the largest chips, as well as minimum tool wear.

Preliminary (rough) ICRs of a mechanical miner can be estimated by using Equation 5.2 (Rostami et al. 1994):

$$NCR = k \cdot \frac{P_{inst}}{SE_{opt}} \tag{5.2}$$

where NCR is net cutting rate (m^3/h), SE_{opt} is optimum specific energy (kWh/m^3) obtained from full-scale linear cutting experiments, P_{inst} is the installed cutting power of the mechanical miner (kW), and k is the coefficient related to transference of cutting power to the rock, depending on the mechanical miner type. This type of estimation does not take into consideration torque and thrust limitations of the mechanical miners. Therefore, a

deterministic simulation or a full computer simulation of the cutterhead is required for a more realistic estimate. Such computer simulations can also be used for designing cutterhead geometry, cutting tool allocation (layout), and cutterhead reaction forces and moments (Hurt and McAndrew 1981; Deliac 1993; Ozdemir 1995; Hekimoglu and Tiryaki 1998).

The individual cutters on a machine in the field always operate on a rock surface damaged from the previous cutting passes. This condition is duplicated in the laboratory by thoroughly conditioning the rock surface before testing begins. This is accomplished by making several passes before data are collected. The specific sequencing of cuts is used to simulate the different spirals (starts, scrolls, or flights) of cutters on a cutterhead. A schematic drawing showing the nomenclature is presented in Figure 5.9 for single and double spiral cutting patterns.

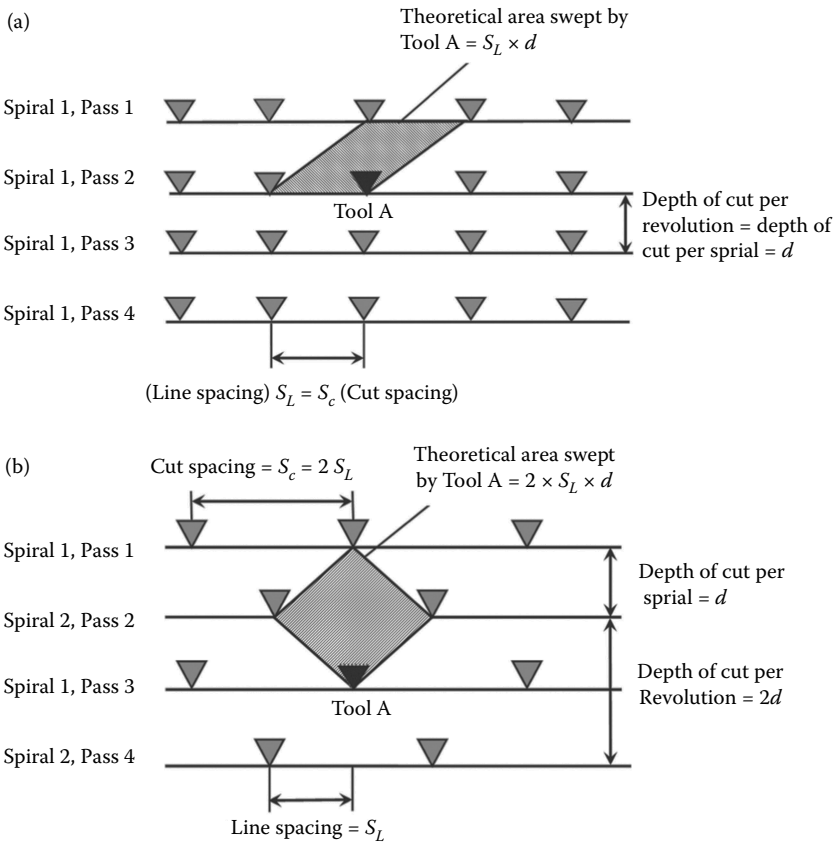

FIGURE 5.9
Nomenclature for single (a) and double (b) spiral cutting patterns on a block of rock sample.

Different cutting tools with different features can be tested for a specific rock sample for comparison of their efficiencies. The attack angle, skew angle, and tilt angle of the conical cutting tools can also be simulated in linear cutting experiments. The radial or chisel tools with different rake and clearance angles can also be tested in full-scale linear cutting experiments.

Breakage mechanisms can also be observed during the full-scale linear cutting tests. Both tensile and shear stresses play a role in a rock-breakage process (Mishnaevsky 1995). Tensile hoop stresses occurring in the crushed zone under a cutting tool generate radial tensile fractures in elastic rocks. The rock bridge between two cutting lines is removed if these fractures reach each other. If the stone behaves mostly plastic, then shear forces are more dominant than tensile forces.

5.2.3 Portable Linear Rock-Cutting Tests

One of the portable rock-cutting devices was developed in the Mining Engineering Department of Istanbul Technical University (Feridunoglu 2009; Bilgin et al. 2010). A groove is cut on the surface of a rock sample with a small disk cutter with 5 mm depth of cut. The table of the portable linear rock-cutting device is moved by a hydraulic cylinder. Block rock samples in $20 \times 20 \times 10$ cm in size or core samples split into two pieces (two halves) are attached to the table with a special mechanism or cast in a sample box with a flat surface on top to cut the rock with a minidisk having a diameter of 13 cm and tip angle of 70°. The forces acting on the cutter and specific energy values are measured using triaxial force transducer (dynamometer). Dynamometers equipped with strain gauges have been designed and developed for this special application, reaching a precision in the order of 1 kN and covering a range from 0 to 100 kN. The force dynamometer is calibrated with a hydraulic cylinder by applying known forces. The tests should be replicated at least 3 times for more reliable results in a given rock type. A developed cutting rig is seen in Figure 5.10. The results of the portable linear cutting tests were correlated with full-scale linear cutting test results for different real-life conical tools and disk cutters (Bilgin et al. 2010). The relationship between the tool forces of the portable linear cutting tests and full-scale linear cutting test for CCS disk cutters, with different tip widths and diameters, are presented in Figure 5.11 for thrust (normal) and rolling (cutting) forces.

5.2.4 Cutting Tests with a Horizontal Drill Rig

The horizontal drill rig found in the laboratories of the Mining Engineering Department of the Istanbul Technical University is introduced in this section. The rig can accommodate rock blocks up to $1.5 \times 1.0 \times 1.0$ m in size and has facilities to carry out drilling tests in the laboratory with real-life tricone and/or pdc drill bits and cutterheads of roadheaders, microtunnel boring machines, and drum miners (Figure 5.12). The machine has a power

FIGURE 5.10
Portable linear cutting machine in ITU Laboratories. (Adapted from Bilgin, N. et al. 2010a. Development of a portable rock cutting rig for rock cuttability determination. *Proceedings of the European Rock Mechanics Symposium (EUROCK 2010)*, eds. J. Zhao, V. Labiouse, J.P. Duth, J.F. Mathier, ISBN: 978-0-415-58654-2, June 15–18, Lausanne-Switzerland, CRC Press/Balkema, Taylor & Francis Group, pp. 405–408.)

of 135 kW and a torque capacity of 35 kNm with a varying thrust force of up to 500 kN, a rotational speed of up to 90 rpm, and a drilling rate of up to 60 m/h. It is also possible to move rock blocks horizontally with a lateral force of up to 250 kN and a speed of up to 15 m/h, which gives a unique opportunity to use the rig in simulating the lateral movement of cutterheads of roadheaders, microtunnel boring machines, and drum miners. The types of variables, such as thrust force, lateral force, rotational speed, torque, and drilling rate are controlled/measured/recorded with the aid of a data acquisition system similar to the one used with a full-scale linear cutting device, explained in a previous section of this chapter.

5.3 Numerical Examples

Two numerical examples are presented in this section to show how to use the results of rock-cutting experiments, one is for a surface miner, and the other is for a trench-cutter used for excavation of a slurry wall.

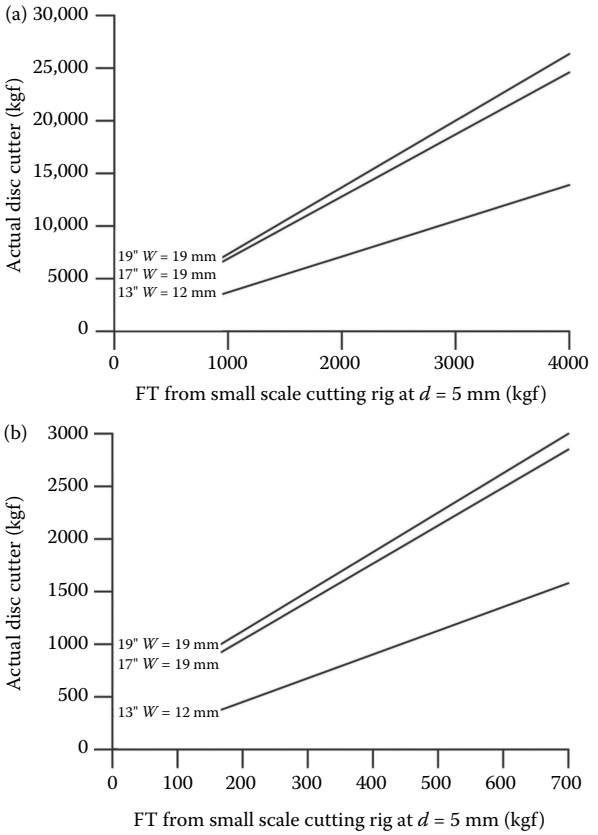

FIGURE 5.11
Relationships between the tool forces ((a) normal force and (b) rolling force) of the portable linear cutting tests and full-scale linear cutting tests for constant cross-section disk cutters with different tip width and diameters. (Adapted from Bilgin, N. et al. 2010a. Development of a portable rock cutting rig for rock cuttability determination. *Proceedings of the European Rock Mechanics Symposium (EUROCK 2010)*, eds. J. Zhao, V. Labiouse, J.P. Duth, J.F. Mathier, ISBN: 978-0-415-58654-2, June 15–18, Lausanne-Switzerland, CRC Press/Balkema, Taylor & Francis Group, pp. 405–408.)

5.3.1 Numerical Example for a Surface Miner

An open pit mine of Barite is considered to be excavated by a surface miner. Natural unit weight, uniaxial compressive strength, and Cerchar abrasivity index of Barite sample are 4.31 g/cm^3, 121 MPa, and 0.75, respectively. Specifications of two different surface miners (one small and one large machine) are summarized in Table 5.3. A summary of the results of full-scale linear cutting tests performed on Barite sample is presented in Table 5.4 for double scroll cutting pattern (at line spacing of 25 mm; cut spacing of 50 mm). Estimate the instantaneous (net) cutting rates of the selected surface miners for cutting Barite.

FIGURE 5.12
Horizontal drill rig in ITU laboratories.

TABLE 5.3

Some of the Technical Specifications of the Selected Surface Miners

Surface Miner	Wirtgen SM-2500	Wirtgen SM-4200
Installed drum power	783 kW	1194 kW
Maximum drum rotation speed	70 rpm	70 rpm
Drum width	2500 mm	4200 mm
Drum radius	700 mm	750 mm
Maximum milling depth	600 mm	650 mm
Maximum traverse speed	25 m/min	20 m/min
Machine weight	97 tons	202 tons

Source: Wirtgen, 2010. Product Catalogues.

TABLE 5.4

Summary of the Results of Relieved Double Scroll Cutting Experiments at Line Spacing of 25 mm

Ratio of Line Spacing to Depth of Cut	Depth of Cut (mm/scroll)	Average Normal Force (kgf)	Average Cutting Force (kgf)	Specific Energy (kWh/m^3)
8.3	3	474.1	366.4	5.3
5.0	5	488.0	392.8	4.4
3.6	7	551.4	534.3	4.5

5.3.1.1 Solution of Numerical Example 5.3.1

The model given in Equation 5.3 is used for predicting the net cutting (production) rate of a mechanical miner based on optimum specific energy obtained from linear cutting tests (Bilgin et al. 2010b, 2011b):

$$NCR = k\frac{P_{net}}{SE_{opt}} = k\frac{\eta P_{ins}}{SE_{opt}} \tag{5.3}$$

where

NCR = instantaneous (net) cutting rate (m^3/h)
P_{net} = net cutting power of the drum (cutterhead) (kW)
P_{ins} = installed cutting power of the drum (cutterhead) (kW)
k = coefficient related to a mechanical miner type and cutting geometry (usually between 0.8 and 0.9 for surface miners, can be taken as 0.8 for both SM-2500 and SM-4200)
SE_{opt} = optimum specific energy obtained from a linear cutting test (kWh/m^3)
η = mechanical efficiency factor (usually between 0.8 and 0.9 for electric motors, can be taken as 0.8 for SM-2500 and 0.9 for SM-4200)

Specific energy is the amount of energy required to excavate a unit volume of rock. The spacing and penetration values where specific energy reaches its lowest point define the most efficient cutting geometry. The specific energy values from linear cutting tests do not take into account the effects of the mechanical inefficiencies. These inefficiencies occur while transferring energy from the motors to the cutterhead (taken into account by η) or the changing penetration as the cutters rotate about a drum-type cutterhead (taken into account by k).

Linear cutting experiments presented in Table 3.2 indicate that the optimum cutting condition is obtained at the line spacing to depth of cut ratio of 5 and SE_{opt} is 4.4 MJ/m^3 at this cutting condition (line spacing of 25 mm, depth of cut of 5 mm/scroll). Based on the given parameters, the NCRs of SM-2500 and SM-4200 are estimated to be 114 m^3/h (490 tons/h) and 195 m^3/h (840 tons/h), respectively.

The cutting rate estimations based on this model should be checked for torque and thrust limitations. Thrust limitation estimates require detailed knowledge of mechanical miners and design features of the cutterhead. Therefore, thrust limitation is ignored in this study. A torque limitation criterion is given in Equation 5.4:

$$T_O < T_A \tag{5.4}$$

where T_O is the operational torque of the drum while cutting the rock and T_A is the allowable torque of the drum. T_O is estimated as in Equations 5.5 and 5.6:

$$T_O = N_C \cdot FC \cdot R \tag{5.5}$$

$$N_C = N_T \cdot \alpha_C = 1.05 \cdot (W/s_L) \cdot N_{CL} \cdot \text{acos}((R - MD)/R) \tag{5.6}$$

where

N_C = number of cutters in contact with the rock, which depend on drum contact angle α_C (in degrees), drum width (W, see Table 5.3), line

spacing (s_L, 25 mm in this case), cutter number per cutting line (N_{CL}, 1 cutter/line assumed in this case), drum radius (R, see Table 5.3), and milling depth (MD, in this case maximum for both of the surface miners, see Table 5.3). N_T is total number of cutters on drum.

FC = average cutting force acting on one cutter per revolution at optimum depth of cut, which is 5 mm/rev for Barite. At optimum conditions, FC is 393 kgf (~4 kN) for Barite as given in Table 5.4.

Allowable torque (T_A) values of these surface miners can be calculated by using Equation 5.7:

$$T_A = P_{NET}/2\pi \cdot N = \eta \cdot P_{INS}/(2\pi \cdot N) \tag{5.7}$$

where N is revolutions of cutterhead (drum) per second.

Based on the given parameters, the allowable torque values (T_A) of SM-2500 and SM-4200 are estimated to be 85 and 147 kNm, respectively. Similarly, the operational torque values (T_O) of SM-2500 and SM-4200 are estimated to be 84 and 123 kNm, respectively. Since, in both machine cases, the criterion given in Equation 5.4 is provided, the predicted NCRs for SM-2500 and SM-4200 (490 tons/h and 840 tons/h, respectively) are valid as preliminary estimations.

The results should also be checked for operational conditions of the surface miners. Advance (penetration) rate of a cutter is 5 mm/rev for optimum cutting conditions of Barite, assuming the 5 mm/rev penetration of the drum is average for the crescent shape (cissoid) of drum–rock contact per revolution. The average depth of cut of a drum is around 65% of the maximum depth of cut. Therefore, the maximum depth of cut (or advance of the drum per revolution) at middrum level is around 7.5 mm/rev. If the rotational speed of the drum is assumed to be 70 rpm for both surface miners, the traversing speed of the machine is obtained as $70 \times 7.5 = 525$ mm/min $= 525 \times 60 \cong 315$ 00 mm/h $\cong$ 31.5 m/h. If this advance rate is multiplied by the drum width and MD, volumetric net production rates are estimated, based on operational parameters, for Barite to be 47 m^3/h (200 tons/h) for SM-2500 and 86 m^3/h (370 tons/h) for SM-4200. Since these NCR values are smaller than the ones estimated by using Equation 5.3, the estimated values based on operational parameters should be used conservatively.

5.3.2 Numerical Example for a Trench-Cutter

A trench-cutter (double-drum) is going to be used for excavation and construction of a slurry wall (Figure 5.13). Some of the specifications of the machine are presented in Table 5.5. Results of core cutting tests performed by using small-scale linear cutting machine are summarized in Table 5.6 for four different samples having uniaxial compressive strength values varying

FIGURE 5.13
Trench-cutter. (Courtesy of Bauer.)

between 50 and 100 MPa to be excavated in the site. Small-scale linear cutting tests are performed by a standard chisel tool having a width of 12.7 mm in unrelieved cutting mode at 5 mm/rev of depth of cut, which is considered as the minimum economical depth of cut for pick cutters (chisel, radial, and conical cutters). Formations to be excavated can be considered as massive with high RQD values. Estimate the *NCR* of the trench-cutter to be used for excavation of the rocks.

TABLE 5.5

Specifications of the Bauer BC30 Trench-Cutter

Total Mass of the Trench-Cutter	**260 kN**
Cutting width	3200 mm (for two drums)
Diameter of a drum	1600 mm
Drum number	2 drums
Maximum rotational speed of drums	25 rpm
Torque capacity	81 kNm
Cutting tool type	Chisel
Total number of cutters	40×2
Width of a cutting tool	38 mm

TABLE 5.6

Summary of the Results of Small-Scale Linear Cutting Tests with a Standard Chisel Tool in Unrelieved Cutting Mode at a 5 mm/rev Depth of Cut

Station	Borehole	Core Depth (m)	*FN* (kgf)	*FN* (kN)	*FC* (kgf)	*FC* (kN)	*SE* (MJ/m³)	*SE* (kWh/m³)
Fahrettin Altay	SK-2	24.00–25.00	858	8.4	223	2.2	18.82	5.23
Poligon	SK-1	17.00–18.00	795	7.8	236	2.3	31.15	8.65
Poligon	SK-1	18.00–19.00	1064	10.4	339	3.3	50.04	13.90
Poligon	SK-2	18.00–19.00	1602	15.7	311	3.0	51.94	14.43

Source: Adapted from Bilgin, N. et al. 2011a. Cuttability of the formations to be encountered during excavation of slurry walls in construction of the 2nd Phase Izmir Light Rail System. Report submitted to Sigma-Borege Joint Venture. Istanbul Technical University, Faculty of Mines Foundation, Mining Engineering Department (in Turkish).

Note: *FN*, average of mean normal forces, *FC*, average of mean cutting force, *SE*, average of specific energies.

5.3.2.1 Solution of Numerical Example 5.3.2

Thrust requirement of the trench-cutter BC30 for excavation of the rocks tested can be estimated by using Equation 5.8:

$$\text{Thrust} = N_{CC} \cdot FN \cdot w_c \cdot r_c \tag{5.8}$$

where

Thrust = thrust requirement in kN.

N_{CC} = number of cutters in contact with rock during excavation. Since only half of a drum is in contact with the rock and there are two drums, N_{CC} is estimated to be 40.

FN = average mean normal force (in kN) obtained from small-scale linear cutting tests in unrelieved cutting mode at 5 mm/rev depth of cut.

w_c = tool width correction factor. Since the small-scale linear cutting tests are performed with a standard chisel tool having a width of 12.7 mm, *FN* (also *FC*) values should be corrected for cutter width of 38 mm used in trench-cutter by taking $w_c = 38/12.7 = 3$.

r_c = relieved cutting mode correction factor for a single scroll cutting pattern. Since the small-scale linear cutting tests are performed in unrelieved cutting mode, *FN* values should be corrected for relieved cutting modes. Experience indicates that the ratio between relieved tool forces and unrelieved tool forces for both *FN* and *FC* vary between 0.4 and 0.6 for soft and ductile rocks and 0.8 and 0.9 for hard and brittle rocks at optimum cutting conditions. Since the experimental observations and uniaxial compressive strength values indicate that the samples tested are hard and brittle, r_c value of 0.85 is taken for the samples tested.

The torque requirement of the trench-cutter BC30 for excavation of the rocks tested can be estimated by using Equation 5.9:

$$\text{Torque} = R_D \cdot N_{CC} \cdot FC \cdot w_c \cdot r_c \tag{5.9}$$

where

Torque = torque requirement (in kNm)
FC = average mean cutting force (in kN) obtained from small-scale linear cutting tests in unrelieved cutting mode at 5 mm/rev depth of cut
R_D = radius of the drums, which is taken to be 0.8 m (see Table 5.5)
w_c = tool width correction factor, which is taken to be 3
r_c = relieved cutting mode correction factor for single scroll cutting pattern, which is taken to be 0.85

Estimated thrust and torque requirements of a BC30 trench-cutter at 5 mm/rev depth of cut, which is considered as the minimum economical depth of cut for pick cutters, are summarized in Table 5.7.

As seen in Table 5.7, the estimated thrust and torque requirements of a BC30 trench-cutter are both higher than the thrust (260 kN provided by machine mass) and torque (81 kNm) capacities of the BC30 trench-cutter. Therefore, it can be concluded that the trench-cutter to be used cannot economically excavate the samples tested. The ratio of thrust requirement to thrust capacity (260 kN) varies between 3.1 and 6.2. The ratio of torque requirement to torque capacity (81 kNm) varies between 2.2 and 3.3. Therefore, the machine to be used can be considered as "thrust-limited" for the samples tested. The thrust capacity of the machine can only provide depth of cut values between 0.8 and 1.6 mm/rev for the samples tested. These depths of cut values cannot be considered as economical, since the machine would work in groove-deepening (unrelieved) mode, which would eventually cause machine stalling. Corrections for rake angle and tool wear are ignored in this example.

TABLE 5.7

Summary of the Results of Thrust and Torque Estimations

Station	Borehole	Core Depth (m)	Thrust Requirement (kN)	Torque Requirement (kNm)
Fahrettin Altay	SK-2	24.00–25.00	856	178
Poligon	SK-1	17.00–18.00	793	189
Poligon	SK-1	18.00–19.00	1061	271
Poligon	SK-2	18.00–19.00	1598	248

Source: Adapted from Bilgin, N. et al. 2011a. Cuttability of the formations to be encountered during excavation of slurry walls in construction of the 2nd Phase Izmir Light Rail System. Report submitted to Sigma-Borege Joint Venture. Istanbul Technical University, Faculty of Mines Foundation, Mining Engineering Department (in Turkish).

References

Balci, C., 2004. Comparison of small and full scale rock cutting test to select mechanized excavation machines. PhD thesis, Istanbul Technical University (in Turkish with English abstract). 269 p.

Balci, C., Bilgin, N., 2007. Correlative study of linear small and full-scale rock cutting tests to select mechanized excavation machines. *International Journal of Rock Mechanics and Mining Sciences*, 3:468–476.

Bauer. Product Catalogues.

Bilgin, N., Balci, C., Tumac, D., Feridunoglu, C., Copur, H., 2010a. Development of a portable rock cutting rig for rock cuttability determination. *Proceedings of the European Rock Mechanics Symposium (EUROCK 2010)*, eds. J. Zhao, V. Labiouse, J.P. Duth, J.F. Mathier, ISBN: 978-0-415-58654-2, June 15–18, Lausanne-Switzerland, CRC Press/Balkema, Taylor & Francis Group, pp. 405–408.

Bilgin, N., Copur, H., Balci, C., Tumac, D., 2010b. Cuttability characteristics of barite and andesite in Yenice Barite Mine for predicting performance and selection of a surface miner. Report submitted to Metal Maden AS, ITU Faculty of Mines Foundation Project, ITU Mining Engineering Department.

Bilgin, N., Copur, H., Balci, C., Tumac, D., 2011a. Cuttability of the formations to be encountered during excavation of slurry walls in construction of the 2nd Phase Izmir Light Rail System. Report submitted to Sigma-Borege Joint Venture. Istanbul Technical University, Faculty of Mines Foundation, Mining Engineering Department (in Turkish).

Bilgin, N., Copur, H., Balci, C., Tumac, D., Avunduk, E., 2011b. Selection criteria of surface continuous miners, an application to the Yenice –Sivas Barite. *The 3rd Mining Machinery Symposium of Turkey*, 5–6 May, Izmir.

Binns, P.D., Potts, E.L.J., 1955. The ploughability of coal seams. *King's College Mining Society Journal*, 2(1): 69–88.

Copur, H., 1999. Theoretical and experimental studies of rock cutting with drag bits toward the development of a performance prediction model for roadheaders. PhD thesis, Colorado School of Mines, 361 p.

Copur, H., 2010. Linear stone cutting tests with chisel tools for identification of cutting principles and predicting performance of chain saw machines. *International Journal of Rock Mechanics and Mining Sciences*, 47(1):104–120.

Copur, H., Balci, C., Bilgin, N., Tumac, D., Duzyol, I., 2007. Full-scale linear cutting tests towards performance prediction of chain saw machines. *Proceedings of the 20th International Mining Congress and Exhibition of Turkey—IMCET2007*, eds. C. Karpuz, M.A. Hindistan, E. Tercan, June 6–8, Ankara, pp. 161–169.

Copur, H., Balci, C., Tumac, D., Bilgin, N. 2011. Field and laboratory studies on natural stones leading to empirical performance prediction of chain saw machines. *International Journal of Rock Mechanics and Mining Sciences*, 48(2):269–282.

Copur, H., Rostami, J., Ozdemir, L., Bilgin, N. 1997. Studies on performance prediction of roadheaders. *Proceedings of the 4th International Symposium on Mine Mechanization and Automation*, Brisbane, Queensland, Australia, A4-1–A4-7.

Copur, H., Tuncdemir, H., Bilgin, N., Dincer, T., 2001. Specific energy as a criterion for the use of rapid excavation systems in Turkish mines. *The Institution of*

Mining and Metallurgy, Transactions Section—A Mining Technology, November–December, Vol. 110, pp. A149–A157.

Dayanc, C., 2011. Performance prediction of an EPB type TBM using Monte Carlo simulation. Master of Science Dissertation, Istanbul Technical University.

Deliac, E.P., 1993. Theoretical and practical rules for mechanical rock excavation. In *Comprehensive Rock Engineering*, ed. J.A. Hudson, Pergamon Press, Michigan University Vol. 4, Chapter 8, pp. 177–227.

Ergin, H., Kuzu, C., Balci, C., Bilgin, N., 2000. Optimum bit selection and operation for the rotary blasthole drilling through horizontal drilling rig (HDR)—A case study at KBI Murgul Copper Mine. *International Journal of Surface Mining and Reclamation*, 14:295–303.

Evans, I., Murrell, B.A., 1958. The forces required to penetrate a brittle material with a wedge-shaped tool. *Proceedings of the Congress on Mechanical Properties of Non-Metallic Brittle Materials*, ed. Walton, W.H. London, Butterworths Scientific Publications, pp. 432–449.

Feridunoglu, C., 2009. Development of a portable rock cutting rig for rock cuttability determination. PhD thesis, Istanbul Technical University (in Turkish with English abstract). 73 p.

Fowell, R.J., Johnson, S.T., 1982. Rock classification and assessment for rapid excavation. *Proceedings of the Symposium on Strata Mechanics*, Newcastle upon Tyne, pp. 241–244.

Hekimoglu, O.Z., Tiryaki, B., 1998. In-situ investigations on shearer drum design. *CIM Bulletin*, 91(1018):225–228.

Hurt, K.G., McAndrew, K.M., 1981. Designing roadheader cutting heads. *The Mining Engineer*, September, 167–170.

Kuzu, C., Balci, C., 1998. General layout of a horizontal drill rig designed for research studies and the data acquisition system of the rig. *ICAMC' 98—13th International Conference on Automation in Mining*, Kosice.

McFeat-Smith, I., Fowell, R.J., 1977. Correlation of rock properties and the cutting performance of tunnelling machines. *Proceedings of the Conference on Rock Engineering*, Newcastle upon Tyne, pp. 581–602.

McFeat-Smith, I., Fowell, R.J., 1979. The selection and application of roadheaders for rock tunnelling. *Proceedings of the Rapid Excavation and Tunnelling Conference*, Atlanta, Vol. 1, pp. 261–279.

Mishnaevsky, L.L., 1995. Physical mechanisms of hard rock fragmentation under mechanical loading: A review. *International Journal of Rock Mechanics and Mining Sciences*, 32:763–766.

Ozdemir, L., 1995. *Mechanical Mining Technologies. Short Course Notebook*. Colorado School of Mines, Mining Engineering Department, Golden, Colorado.

Ozdemir, L., 1997. *Mechanical Mining. Short Course*. March 19–21, Colorado School of Mines, Golden, Colorado.

Ozdemir, L., Evans, R.J., Miller, R.J., Sharp, W., 1984. Rotary cutting machine: Research capabilities and trials. *Tunnels and Tunnelling*, April:35–37.

Ozdemir, L., Rostami, J., 1995. Roadheader development for hard rock mining. *SME Annual Meeting*, March 6–9, Denver, Colorado, 8 p.

Pomeroy, C.D., 1958. The effect of lateral pressure on the cutting of coal by wedge shaped tools. *Proceedings of the Congress on Mechanical Properties of Non-Metallic Brittle Materials*, ed. Walton, W.H. London, Butterworths Scientific Publications, pp. 469–479.

Pomeroy, C.D., 1963. Breakage of coal by wedge action—Factors affecting breakage by any given shape of tool. *Colliery Guardian*, November 21, pp. 642–648; November 28, pp. 672–677.

Rad, P.F., Schmidt, R.L., 1973. Tunneling machine research—Development of an experimental full-scale research rock cutting device. U.S. Bureau of Mines, Report of Investigations-7787, 18 p.

Rostami, J., Ozdemir, L., 1996. Computer modeling of mechanical excavators cutterhead. *Proceedings of the World Rock Boring Association Conference: Mechanical Excavation's Future Role in Mining*, September 17–19, Laurentian University, Sudbury, Ontario, Canada.

Rostami, J., Ozdemir, L., Neil, D.M., 1994. Performance prediction: A key issue in mechanical hard rock mining. *Mining Engineering*, 11:1263–1267.

Roxborough, F.F., 1969. Rock cutting research for the design and operation of tunnelling machines. *Tunnels and Tunnelling*, September:125–128.

Roxborough, F.F., 1973. Cutting rocks with picks. *The Mining Engineer*, June:445–455.

Roxborough, F.F., Phillips, H.R., 1974. Experimental studies on the excavation of rock using picks. *Proceedings of the International 3rd ISRM Congress*, September 1–7, Denver, pp. 1407–1412.

Takaoka, S., Hayamizu, H., Misava, S., Kuriyagava, M., 1974. Mechanical fracture characteristics of rock with a cutter bit and disc cutter. *Proceedings of the International 3rd ISRM Congress*, September 1–7, Denver, pp. 1723–1729.

Wirtgen. 2010. Product Catalogues.

6

Wear of Cutting Tools

Wear properties of the rocks should be considered in any type of rock machineability investigation since they affect tool cutting performance dramatically. Rates of tool wear are very dependent on structure, composition, and properties of the excavated material. High-strength rocks give rise to high stress on the cutting edge, cracks are formed, and tool life is then reduced. Quartz has a great influence on the wear process, which in turn controls the economic success of rock machinery. Tool materials, design and operational variables, strength of the rock, shape, and content of quartz affect the life of cutting tools and makes the problem very complex indeed. Hence, this chapter should be considered in the light of such complexity.

The high hardness and wear resistance of tungsten carbide insert bits make them well suited as rock-cutting and drilling tools, and a large amount of hard metal produced annually is for the mining industry. It is vital to understand the wear mechanism of these cutting and drilling tools and the abrasivity of the rocks, since cutter cost is one of the most important factors in determining the success of mining or tunneling operations. In a roadheader application, typical examples for a medium-strength and abrasive sandstone are 5–7 $\$/m^3$ and for high-strength and very abrasive rock is 100 $\$/m^3$.

6.1 Metallurgical Properties of Tungsten Carbide Tools Affecting Wear Properties

Tungsten carbide is a hard metallic alloy produced by a high temperature and a carefully controlled sintering process. Grains of powdered tungsten carbide are mixed with small quantities of cobalt and compressed at a very high pressure to the required shape. Sintering is carried out at a temperature of around 1435°C, under continuous vacuum to minimize porosity, a factor that has a major affect on its quality. The primary manufacturing variables that affect the wear performance of mining-grade carbides are grain size, cobalt content (Co), carbon content, and porosity of drill and cutting bit. Two parameters that are usually used to compare grades are the transverse rupture strength (TRS; a measure of resistance to fracture) and the hardness. The procedure almost universally used to determine the TRS is the three-point load method. With increasing cobalt content, TRS increases to a maximum of 20% Co. In greater

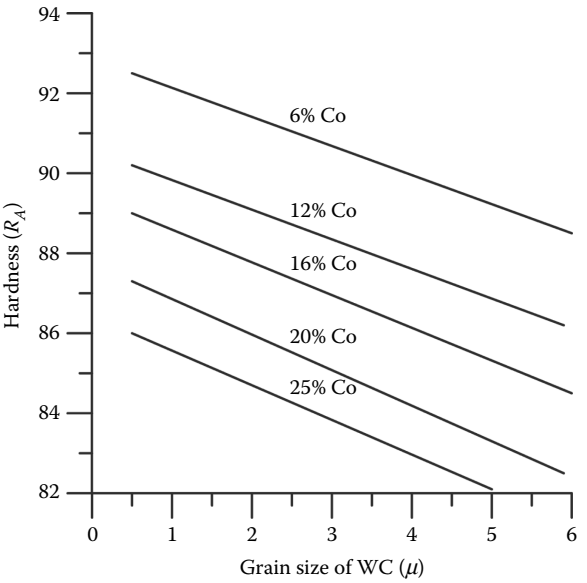

FIGURE 6.1
The variation of tungsten carbide bit hardness with grain size and cobalt content. (From Clark, G.B., 1982. Principles of rock drilling and bit wear. *Colorado School of Mines Quarterly*, 77(2).)

amounts, cobalt acts to separate the carbide grains. The relationship between hardness, cobalt content, and grain size is shown in Figure 6.1 (Clark 1982). For a given Co content, the larger the predominant grain size, the softer the alloy. Fine-grained compositions, particularly with a cobalt content of 4–10% are used where maximum abrasion resistance is required, but larger grain sizes are necessary for good shock resistance. The theoretical carbon content of pure tungsten carbure is 6.12%. If in the sintering process, free carbon content is introduced even in a very small quantity, the resistance to rupture markedly decreases. Porosity has a very important effect on the wear performance of tungsten carbide tools. It is examined and rated at a magnification of 200. The method of evaluating and classifying porosity is given in ASTM B276-05. The type of porosity is classified as A, B, or C. Type A designates porosity up to 10 μm diameter, and type B from 10 to 40 μm.

6.2 Some Theoretical Concepts on the Wear of Chisel Cutters and Point Attack Tools

The cohesive strength between the grains in most rocks is less than the strength of the grains themselves. Some minerals, such as quartz, rarely

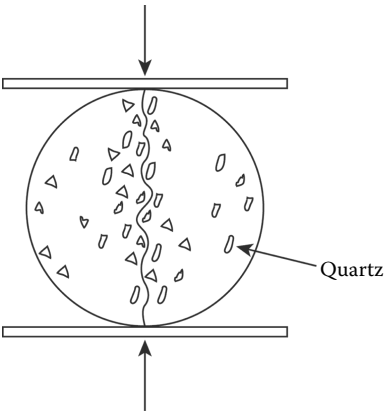

FIGURE 6.2
Failure of rock specimen between quartz grains.

have cleavage or other microscopic weakness, so that if a rock breaks, rupture will take place between the grains of such mineral. Figure 6.2 illustrates such a phenomenon.

If σ_{GB} is the strength of grain boundaries in rock, the tensile strength on the rock will probably be related to σ_{GB} as

$$\sigma_{\mathrm{GB}} = k \cdot \sigma_t \tag{6.1}$$

where k is rock texture or cementation index, which is different for each type of rock.

The force, F, to break one quartz grain from the rock matrix or rock texture can be calculated as illustrated in Figure 6.3.

$$F = \sigma_{GB} \cdot A$$

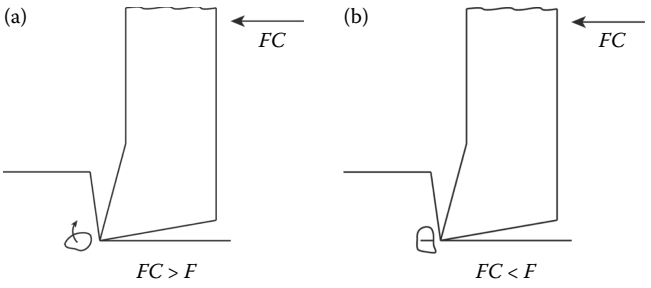

FIGURE 6.3
Theoretical consideration of cutting a quartz grain. (a) Quartz grain is broken from the rock matrix and (b) quartz grain is cut.

$$F = \sigma_{GB} \cdot k_1 \cdot \ell \tag{6.2}$$

where A is the surface area of a quartz grain, k_1 is quartz grain shape index, and ℓ is quartz grain size.

$$\sum F = k \cdot k_1 \cdot \sigma_t \cdot \ell \cdot Q_z\% \tag{6.3}$$

where Q_z% is percentage of quartz.

$$\text{If } FC < F, \quad \text{quartz grain is cut} \tag{6.4}$$

$$\text{If } FC > F, \quad \text{quartz grain is broken from the matrix} \tag{6.5}$$

Hence, it is obvious that the weight loss of the pick in the first case (Equation 6.4) will be more than in the second case (Equation 6.5). This clearly shows that F is related to wear.

In Chapter 4, it was shown that Evans' theory was in agreement with experimental results in trend and magnitude. When Equation 6.4 and the cutting forces obtained from Evans' theory are combined, the following relationships are obtained:

$$\text{For chisel cutters} \quad \frac{2 \cdot \sigma_t \cdot d \cdot \sin\frac{1}{2}\left(\frac{\pi}{2} - \alpha\right)}{1 - \sin\frac{1}{2}\left(\frac{\pi}{2} - \alpha\right)} < k \cdot k_1 \cdot \sigma_t \cdot \ell \cdot Q_z\% \tag{6.6}$$

$$\text{For conical cutters} \quad \frac{16 \cdot \pi \cdot \sigma_t^2 \cdot d^2}{\cos^2\frac{\varphi}{2} \cdot \sigma_c} < k \cdot k_1 \cdot \sigma_t \cdot \ell \cdot Q_z\% \tag{6.7}$$

For a given rock, the second part of Equations 6.6 and 6.7 will be a constant. If d increases, the weight loss of the tip should decrease, since the relation $FC < F$ will turn to be $FC > F$. With the same way of thinking, it can be concluded that tip weight loss increases with an increasing rake angle and the product of $k \cdot k_1 \cdot \ell \cdot Q_z$%. It is interesting to note that Equation 6.6 is independent of tensile strength. Hence, the following theoretical wear curves can be drawn for conical and chisel cutters as illustrated in Figures 6.4 and 6.5.

However, one should note that the above theoretical consideration does not take into account the wear mechanism that might occur in high-strength rocks, that is, chipping, gross failure, and so on. Considering the above

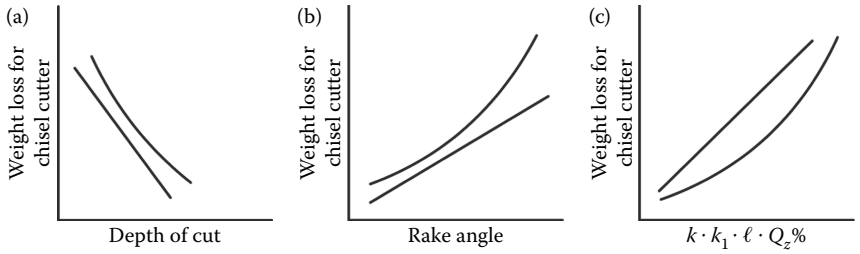

FIGURE 6.4
Theoretical wear curves for chisel cutters.

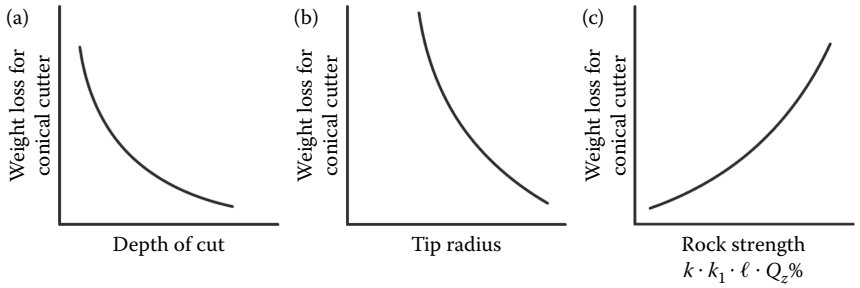

FIGURE 6.5
Theoretical wear curves for conical cutters.

theoretical figures, it may be concluded that for a chisel cutter, the wear is inversely proportional to the depth of cut, it is directly proportional to the rake angle, and it is the product of quartz content and quartz grain size. However, for the conical cutter, the wear is again inversely proportional to the depth of cut and the conical angle, and is directly proportional to the product of rock strength, quartz grain size, and content. Both figures emphasize the benefit that a deeper cut is less wear on cutting tools.

6.3 Laboratory Cutting Experiments with Chisel Cutters for Wear Studies

To emphasize the importance of the parameters mentioned above and to give a proposed quality control chart according to rock properties, a series of wear tests were carried out in Zonguldak Coalfield (Turkey) and at the University of Newcastle Upon Tyne, UK (Bilgin 1977, 1982).

Cutting conditions were: depth of cut 2.5 mm, cutting speed 0.2 m/s, tool width 10 cm, rake angle –5°, back clearance angle 5°, chisel insert, 10% cobalt by weight, and 3.5 μm nominal grain size. For rock-cutting experiments, seven different rocks having different strength and quartz content were tested with a standard rock-cutting tool under an instrumented rig.

In the process of rock cutting, there are wide fluctuations of forces. In a recorded trace, a peak force corresponds to a chip formation and a minimum force corresponds to the formation of a crushing zone. Specific energy, cutting, and normal force components acting on the cutting tool were recorded for each experimental rock. Pick forces and yield were recorded at various increments of cutting distance. For each increment of cutting distance, the tip was cleaned in an ultrasonic cleaner, weighed, and examined under a traveling microscope to measure weight loss and wear flat of the chisel insert. Each experimental rock was subjected to a broad range of physical and mechanical tests and the results are given in Table 6.1.

Test results: The tool forces and specific energy increased dramatically with a distance cut, with different rates in different rocks. Tool wear has a greater effect on the normal force than the cutting force. The ratio of mean peak to mean force is reduced when the tip starts getting blunt. Weight loss of the cutting bit is linearly related to cutting distance, suggesting that for a given bit and depth of cut, there is a constant wear rate for each type of rock (Figure 6.6). The relationship between wear flat and cutting distance is different than those for weight loss and cutting distance (Figure 6.7). As can be seen from Figure 6.8, specific energy is dramatically affected by wear flat. This figure shows clearly how the cost of an excavation system might be affected by tool wear and sometimes it might be as high as 100 $/m^3. From Figure 6.9 it can be concluded that the wear rate is a function of quartz grain size and quartz content in the rock; thus, these factors should be considered in any choice of rock-cutting tool.

TABLE 6.1

Some Properties of the Rock Subjected to Wear Tests

Rock	*UCS* (MPa)	σ_t (MPa)	σ_s (MPa)	E Modulus (10^4 MN/m^2)	μ	*SH*	Q_z%	$Q_z l$
Gypsum	45.0	2.3	4.5	5.0	0.96	34	0	0
D. Sandstone	55.8	3.1	11.0	1.2	0.43	60	76	0.2
M. Sandstone	71.3	4.4	11.0	5.3	0.32	54	14	0.2
Anhydrite	112.9	5.5	12.5	11.0	0.74	53	0	0
N. Limestone	127.3	7.5	20.0	6.0	0.63	77	0	0
Granite	179.1	10.8	30.0	6.8	0.39	88	38	1
Graywacke	183.9	16.5	34.0	6.1	0.44	70	32	0.05

Note: *UCS*, uniaxial compressive strength; σ_t, Brazilian tensile strength; σ_s, shear strength; μ, sliding friction between rock and tungsten carbide tool; *SH*, shore hardness; Q_z%, quartz percent; $Q_z l$, quartz grain size.

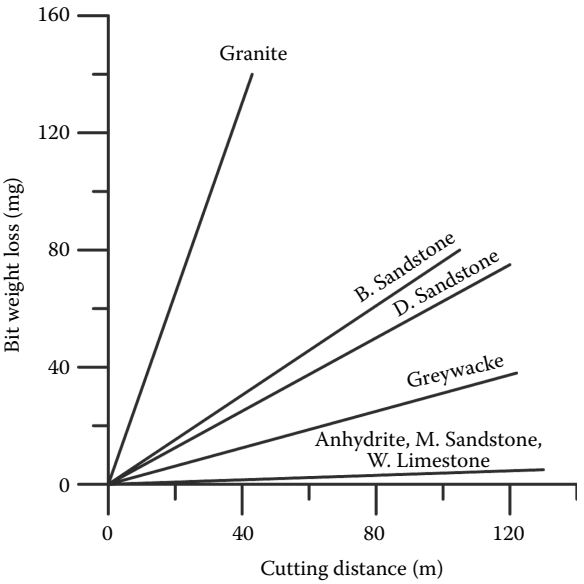

FIGURE 6.6
The relationship between cutting distance and bit weight loss.

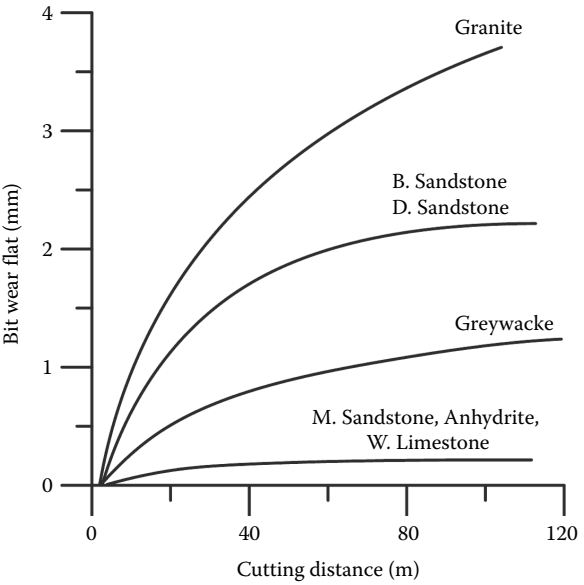

FIGURE 6.7
The relationship between cutting distance and bit wear flat.

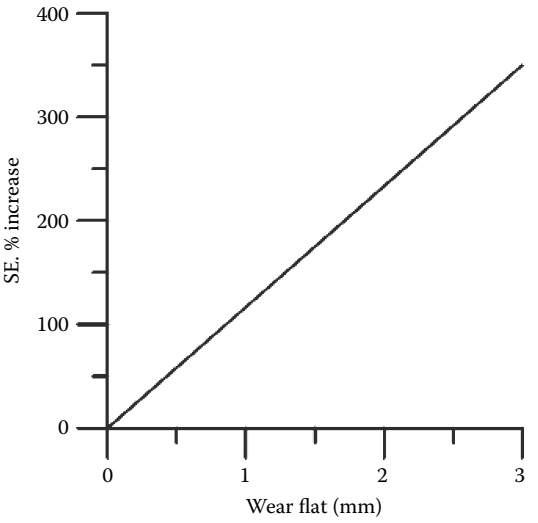

FIGURE 6.8
The relationship between wear flat and specific energy increase in percent.

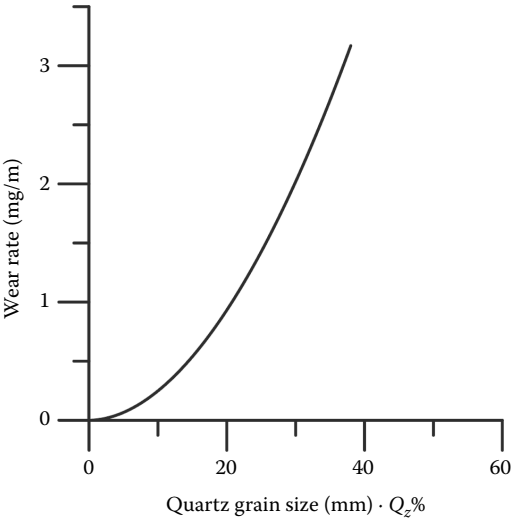

FIGURE 6.9
The variation of cutter wear rate with the product of quartz content and quartz grain size.

6.4 Field Studies for Drill Bit Wear

Bit wear in rock drilling is a major factor in determining the cost of drilling and may determine the drilling method for a given rock. Wear decreases penetration rates and increases drilling forces, which may also cause a major fracture of inserts. To better understanding the factors governing drill bit wear mechanism and to give new ideas to bit users about the quality control, some *in situ* drillability tests were carried out at Kozlu mine in the Zonguldak coalfield. The rock formation drilled was high-strength sandstone with a compressive strength of 900 kg/cm^2 and quartz content of 40%. The specifications of the percussive drill hammer used for *in situ* experiments were drill hammer weight 25 kg, operating pressure 45 kPa, blow frequency 3200 blows/min, piston diameter 80 mm, nominal stroke 40 mm, and a tungsten carbide drilling bit with a 110° edge angle. Two different drill bits with approximately the same Rockwell hardness (HRC) of 89, cobalt content of 7%, and grain size of 3–4 μm were used for these experiments. Bit wear radius (r) was continuously recorded during the tests, when it reached to $r = 3$ mm, the drill bit was resharpened and reused. The working life of the drill bit was concluded to be terminated when the drill bit diameter was reduced to 29 mm, which is the maximum allowable size for the cartridges used in the mine. Figure 6.10 shows the relationship between bit diameter and distance drilled. From this figure, it is clearly seen that the working life of drill bit 2 is twice that of drill bit 1. To understand the reason of this difference, the small samples were taken from each drill bit and were carefully

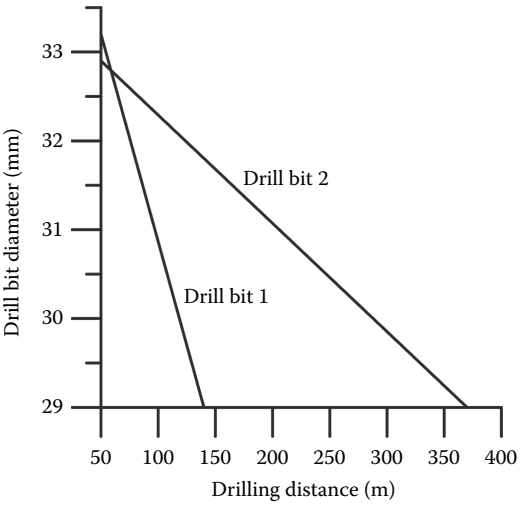

FIGURE 6.10
The variation of decrease in drill bit diameter with drilling distance due to wear characteristics of the drilled rock formations.

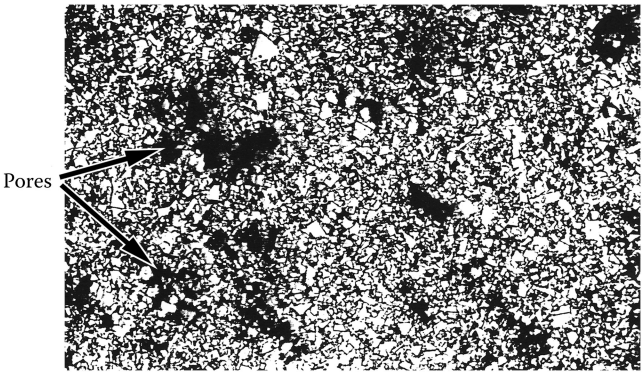

FIGURE 6.11
Microstructure (magnified 580 times) of drill bit 1.

examined under a microscope. Figures 6.11 and 6.12 show their microstructures. It is clearly evident that the abundance of pores in sample 1 caused the early failure of the first drill bit.

Some users of carbide check all incoming shipments of tools for hardness as a routine procedure and maintain control charts to show variations in production lots of carbides, classified as falling within a specific group. However, as previously shown, the hardness depends mainly on cobalt content and grain size. On the other hand, one should bear in mind that the porosity of drilling and cutting bits also plays a major factor in the bit wear mechanism. As a view of the author, porosity of rock bits should also be included in quality control programs of carbide bit users. Table 6.2 is suggested as a guide for the use of drilling and cutting bits suitable for different types of rock (Bilgin 1985).

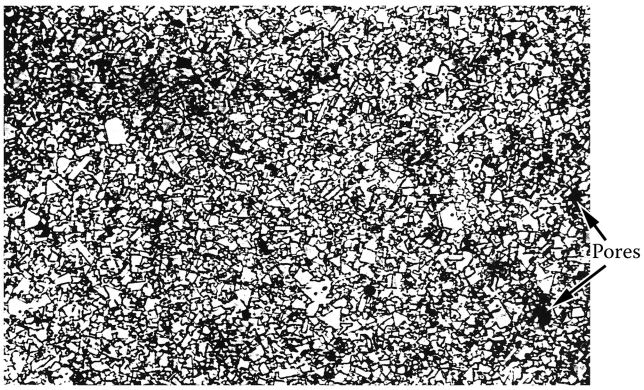

FIGURE 6.12
Microstructure (magnified 580 times) of drill bit 2.

TABLE 6.2

Guide to Quality Control for Rock Bit Users

Rock Material	Drilling Bits	Cutting Bits
Dolorite Diorite Gabro Basalt Quartize Granite	It is strictly recommended to control bit porosity according to ASTM B 276-54. Co content = 8–12% WC grain size = 5–6 μm	Cutting tools are not recommended.
Marble Dolomite Limestone Gneiss	It is strictly recommended to control bit porosity. Co content = 6–8% WC grain size = 3–4 μm	It is strictly recommended to control bit porosity. Co content = 8–12% WC grain size = 3–4 μm
Slate Sandstone Shale Coal measures	It is strictly recommended to control bit porosity. Co content = 4–6% WC grain size = 3–4 μm	Co content = 7–8% WC grain size = 3–4 μm

6.5 Abrasivity of Rocks Affecting Cutter Wear

There are several methods to define and measure the abrasivity of rocks (Deketh 1995; Verhoef 1997; Okubo et al. 2011). Some of the widely used abrasivity indexes will be defined below.

6.5.1 Schimazek Abrasivity Index

Schimazek observed that the wear of a pick increases with the percentage of quartz in the rock, with the grain size of quartz, and tensile strength of the rock. He proposed a wear coefficient F in kgf/cm as given below (Equation 6.8) and stated that a roadheader may efficiently cut a rock formation if F is less than 1 kgf/cm (Schimazek and Knatz 1970).

$$F = Q \cdot d \cdot \sigma_f \tag{6.8}$$

where Q is the equivalent quartz content by volume divided by 100, d is the average grain size of quartz in cm, and σ_f is the tensile strength of the rock in kgf/cm^2.

Equivalent quartz content may be calculated as 1 for quartz grain, 0.35 for feldspar, 0.03 for calcite, and 0.04 for clay minerals. Table 6.3 may be used for a rough estimation of conical cutter consumption from F values based on limited field data. Some roadheader manufacturers use F values exclusively to estimate cutter consumption.

TABLE 6.3

Conical Cutter Consumption Based on the Shimazek *F* Index

Schimazek *F* Value (N/mm)	Rock Abrasiveness	Cutter Consumption (m^3/cutter)
F less than 0.05	Nonabrasive	90–110
F = 0.05–0.07	Low abrasive	50–90
F = 0.07–1.0	Abrasive	30–50
F = 1.0–1.05	Very abrasive	10–30
F larger than 1.05	Very hard and abrasive	1–10

Schimazek also found that there is a critical speed that is greatly increased as the temperature for softening the hard metal is exceeded. The formulated critical speed V_{crit} is

$$V_{crit} = k/e^F \tag{6.9}$$

In the above equation V_{crit} is the critical speed of a cutting tool in m/s, k is a constant, depending on the cutter geometry and the critical temperature of the tip. Typical value of k is 8.4 (Schimazek and Knatz 1970; Hughes 1986).

6.5.2 Cerchar Abrasivity Index

Cerchar index was originally developed in the 1970s by the Cerchar Institute in France (Nizamoglu 1978). Thereafter, many research studies were carried out on the Cerchar abrasivity test (Atkinson et al., 1986; West 1989; Plinninger et al., 2003, 2004; Michalakopoulos 2006; Nilsen et al., 2006).

It basically constituted scratching a steel pin with a cone-shaped tip under a static load of 7 kg over the rock surface for a length of 10 mm. The diameter of the wear flat created by this action on the tip is the Cerchar index value when measured in 0.1 mm. The pin was made of steel with a tensile strength of 200 kg/mm^2 and an HRC of 54–56. The finished cone angle of the tip is 90°. The pin needs to be resurfaced after each test and examined under a microscope before being used again. A set of five pins are typically scratched over the sample and the diameter of wear flat is measured in two directions for one Cerchar test (10 measurements). However, Alber (2008) pointed out that Cherchar index is stress dependent and when excavating rock in depth, this characteristic should be taken into account.

One important point for the Cerchar abrasivity index (*CAI*) is that the method is universally accepted for estimation of cutter consumption for both conical cutters and disk cutters. Typical *CAI* values of different rocks are given in Table 6.4. It is reported by Plinninger (2004) that Figure 6.13 may be used to estimate pick cutter consumption after the *CAI* value.

Smith, in his article published in *Tunnelling Journal* in April/May 2012, emphasized that in some difficult conditions, the cost of disk cutters may

TABLE 6.4

Typical Cerchar Abrasivity Values of Different Rocks

Rock	Cerchar Abrasivity Values
Coal	0.5
Limestone, dolomite	1–2
Sandstone	1–3
Claystone	0–2.5
Marble	1–1.5
Andesite	2–4
Basalt	3–5
Granite	4–6
Quartzites	5.5–6

exceed even the cost of a TBM. However, wear of disk cutters in a TBM is a complex process; it does not just depend on the abrasivity of the rock. The tool material, the brittleness of the rock, geological discontinuities, the clogging effect of clayey material existing within the rock material also play an important role in disk wear process. Figure 6.14 shows the relationship between the *CAI* and wear coefficient. This figure, which is compiled by Bilgin based on different field experiences and the methodology described by Frenzel (2011), may be used for the estimation of disk cutter consumption.

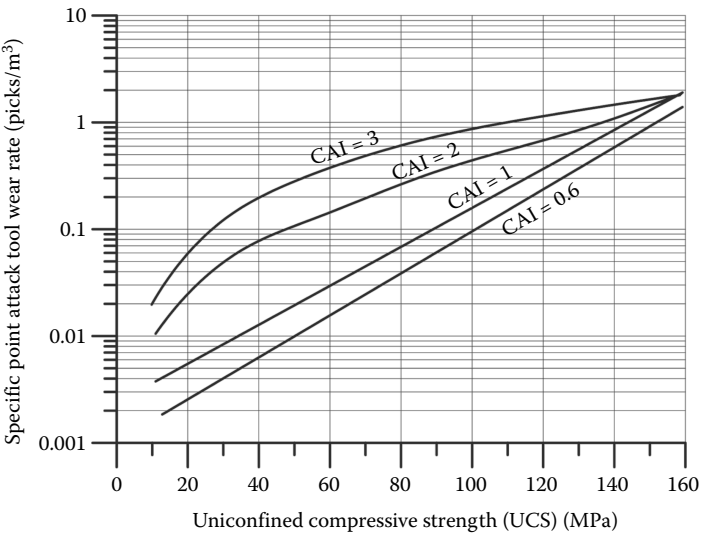

FIGURE 6.13
The relationship between uniaxial strength of rock and point attack tool wear for different Cerchar abrasivity values.

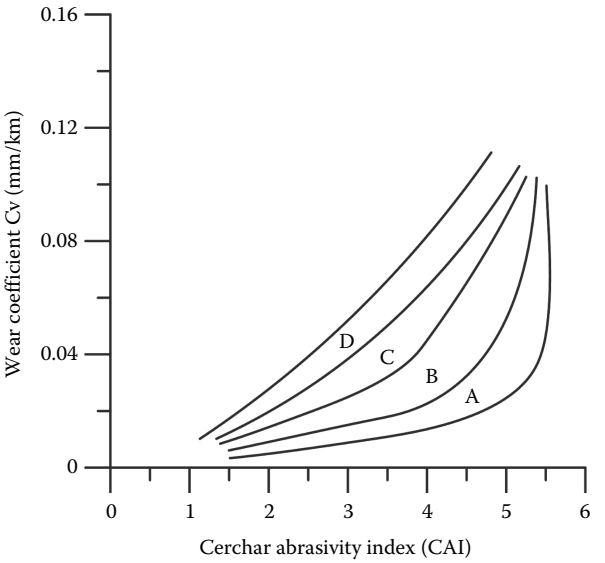

A—Medium brittle rock, coarse quartz grain, RMR = 1–2, UCS < 80 MPa

B—Medium brittle rock, fine quartz grain, RMR= 2–3, UCS = 80–200 MPa

C—Brittle rock, fine quartz grain, squeezing ground, RMR = 3–4

D—Very brittle rock, several foliations, fine quart grains, squeezing ground, RMR = 4–5

UCS = uniaxial compressive strength of the rock
RMR = rock mass rating

FIGURE 6.14
The relationship between Cerchar abrasivity index and wear coefficient, compiled by Bilgin based on different field experiences and the methodology described by Frenzel (2011). (Based on Frenzel, C., 2011. Disc cutter wear phenomenology and their implications on disc cutter consumption for TBM. *45th US Rock Mechanics/Geomechanics Symposium*, San Francisco, CA, June 26–29, ARMA 11-211.)

6.5.3 NTNU Abrasivity Index

Since the early 1980s, the test has been used mainly for predicting hard rock TBM wear performance according to the method developed by the Norwegian University of Science and Technology (NTNU) Department of Building and Construction Engineering (Bruland et al., 1995; Bruland, 2000).

The abrasion values AV/AVS represent time-dependent abrasion of tungsten carbide/cutter steel caused by crushed rock powder. The same test equipment for the AV is used to measure the AVS, but instead of the tungsten carbide test pieces used for AV, the AVS test uses pieces of steel taken from a cutter ring. This test is an indispensable element of hard rock TBM performance estimation for the NTNU method, which is universally accepted.

6.5.4 Methodology for Estimating the Abrasiveness of Soils for TBM Tunneling

Soft ground tunneling is increasing in urban areas and the estimating of soil abrasiveness for cutter consumption grew as well. Field-oriented research studies were initiated in this area; some of these studies will be summarized below.

6.5.4.1 New NTNU Soil Abrasion Test

The new NTNU soil abrasion test (SAT) described by Nilsen et al. (2007) is a further development of the existing abrasion tests for rock. Compared with the AVS test, only one detail has been changed: instead of crushed rock powder <1 mm, a sieved soil sample <4 mm is used in the SAT test. It is strictly advised to follow the standardized NTNU abrasion test procedures as closely as possible. This method shows a big potential in estimating soil abrasion for soft ground tunneling applications.

6.5.4.2 Soil Abrasivity Test Developed by Rostami et al. (2012)

Rostami et al. (2012) introduced a new test device designed to measure soil abrasion. The results of the initial testing at Pennsylvania State University were published. The testing system is configured to simulate the working condition of the cutting tools in an excavation chamber of pressurized face shields. This includes the high contact stresses between the tool and the soil, maintaining the original soil size distribution, field moisture conditions, and the possibility of applying high ambient pressures, as well as soil conditioners. However, it is believed that this method needs some further field studies to develop the nomograms for estimating cutter consumption for both pick and disk cutters.

6.6 Field Studies on the Wear of Conical Cutters and a Guide for Cutter Selection

The Kucuksu sewerage tunnel in Istanbul was chosen as a pilot tunnel to see the effect of physical, mechanical, and petrographical properties of the rocks on the cutter consumption, since this tunnel (as seen in Table 6.5) covers a variety of abrasive and high-strength rocks (Bilgin et al., 2005). Figure 6.15 gives the classification of cutter wear in the Kucuksu tunnel, emphasizing the percentage of symmetrical wear due to the high abrasive characteristics of sandstone, asymmetrical wear due to malfunction of the tool holder in siltstone and sandstone, breakage of the tungsten carbide tip due to small amounts of cobalt for high-strength andesite and limestone, and breakage of the tip shaft due to low-strength shaft material (Figures 6.16 through 6.19).

TABLE 6.5

Mean Compressive Strength of the Rock Formation Encountered during Tunnel Excavation with a Roadheader in the Kucuksu Tunnel

Rock	Compressive Strength ($kg/cm^2 \pm sd$)	Quartz (%)	Cutter Consumption ($cutter/m^3$)
Limestone	1118 ± 240	0	0.249
Sandstone	557 ± 57	35	0.143
Siltstone	833 ± 71	20	0.150
Andesite	1200 ± 449	40	0.890
Diabase[a]	770 ± 82	0[a]	0.438
Average along the tunnel route			0.330

[a] Highly rich in feldspars.

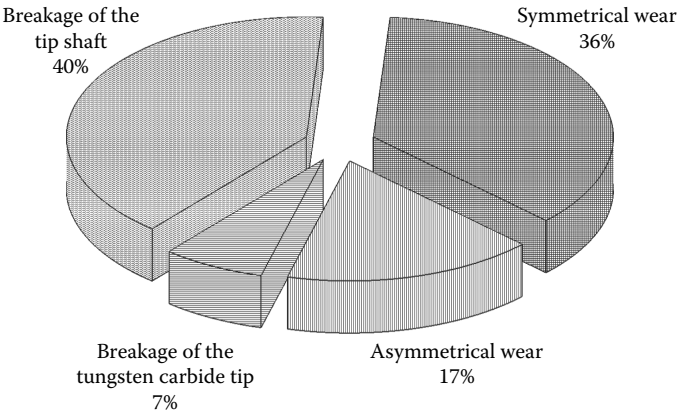

FIGURE 6.15
Classification of cutter wear in Kucuksu tunnel.

6.7 Numerical Examples

6.7.1 Numerical Example 1

Sandstone having a compressive strength of 40 MPa and tensile strength of 3 MPa will be excavated with a roadheader. Quartz content is 30% with grain size of 0.5 mm, feldspars of 20% with grain size of 0.4 mm, calcite of 20% with grain size of 0.1 mm, and clay minerals of 30% with grain size of 0.05 mm. The CAI is measured as 1.5. Calculate Schimazek F value, critical pick velocity, and pick consumption using both Schimazek and Cerchar abrasivity index values. Make a critique of the results.

FIGURE 6.16
Symmetrical wear due to high abrasive characteristic of sandstone.

FIGURE 6.17
Asymmetrical wear due to malfunction of tool holder in siltstone and sandstone.

FIGURE 6.18
Breakage of the tungsten carbide tip due to a small amount of cobalt in high-strength andesite and limestone.

FIGURE 6.19
Breakage of the tip shaft due to weakness of the low-strength steel of shaft material.

6.7.1.1 Solution

Equation 6.8 gives

$$F = \left[(30 \cdot 1 \cdot 0.5) + (20 \cdot 0.35 \cdot 0.4) + (20 \cdot 0.03 \cdot 0.1) + (30 \cdot 0.04 \cdot 0.05)\right] \cdot 3 / 100$$

F is calculated 0.538 N/mm.

From Table 6.3, the pick consumption is found as 30–50 m^3/pick cutter.

For a Cerchar abrasivity value of 1.5, Figure 6.14 gives a pick consumption of 40 m^3/pick cutter, which is in the same order of the calculated value for the Schimazek index. However, if *CAI* is taken as 2, pick consumption value drops to 13 m^3/pick cutter. This shows that Figure 6.14 is very sensitive to *CAI* values. One using the Schimazek and Cerchar abrasivity values should be careful since tool consumption is also related to metallurgical and geometric properties of cutting tools, cutting speed, and geological rock discontinuities. It may be concluded that there is not a universal abrasivity index to predict a definite tool consumption value. The abrasivity index values defined in this chapter are only a guide for project planning.

6.7.2 Numerical Example 2

Calculate disk consumption in the T26 Eskisehir-Kosekoy (Turkey) tunnel. A single-shield TBM is used with a diameter of 13.77 m. The main rock formation is graphitic schist with a Cerchar abrasivity of 3, RMR of 5, and of type class D (very brittle rock, fine quartz grain, squeezing ground). The average rotational speed of the TBM is 2 rpm.

6.7.2.1 Solution

Sr, which is the mean disk rolling distance in one revolution of the cutterhead

$$Sr = D_{\text{TBM}} \cdot 0.6 \cdot \pi/1000 \tag{6.10}$$

where *Sr* is in kilometers and D_{TBM} is the diameter of TBM in meters.

For Tunnel T26

$$Sr = 13.77 \cdot 0.6 \cdot \pi/1000$$

$$Sr = 0.026 \text{ km/revolution}$$

For 2 rpm, $Sr = 0.052$ km.

From Figure 6.14, for $CAI = 3$, $Cv = 0.04$–0.05 mm disk wear mm/km. 25 mm is wear limit of cutter tip.

For cutter replacement, *Uc*, which is the number of cutterhead revolution for disk replacement, is calculated as given below:

$$Uc = \frac{25}{Sr \cdot Cv} \tag{6.11}$$

$$Uc_1 = 25/0.052 \cdot 0.01; \quad Uc_1 = 48{,}076 \text{ revolution}$$

$$Uc_2 = 25/0.052 \cdot 0.06; \quad Uc_2 = 38{,}462 \text{ revolution}$$

The amount of rock excavated by one disk is calculated by multiplying disk rolling distance by cutter spacing (8.6 cm) and disk penetration per revolution (5 mm/rev):

$$\text{Average disk rolling distance } = 2 \cdot \pi \cdot D_{\text{TBM}}/4 \quad \text{or} \quad 21.6\,\text{m}$$

For a 48076 TBM cutter revolution, the volume of rock cut by disk cutter before replacement is

$$48076 \cdot 21.6 \cdot 0.005 \cdot 0.086 = 446\,\text{m}^3$$

Disk cutter consumption is 446 m^3/disk cutter.

For a 38462 TBM cutter revolution, the volume of rock cut by disk cutter before replacement is

$$38462 \cdot 21.6 \cdot 0.005 \cdot 0.086 = 356\ \text{m}^3$$

Disk cutter consumption is 356 m^3/disk cutter.

Mean disk cutter consumption is (446 + 356)/2 = 401 m^3/disk.

References

Alber, M., 2008. Stress dependency of the Cerchar abrasivity index (CAI) and its effects on wear of selected rock cutting tools. *Tunnelling and Underground Space Technology*, 23:351–359.

ASTM B276-5, 2010. Standard test method for apparent porosity in cemented carbides.

Atkinson, T., Cassapi, V.B., Singh, R.N., 1986. Assessment of abrasive wear resistance potential in rock excavation machinery. *International Journal of Mining and Geological Engineering*, 3:151–162.

Bilgin, N., 1977. Investigations into the mechanical cutting characteristics of some medium and high strength rocks, PhD thesis, The University of Newcastle Upon Tyne, England.

Bilgin, N., 1982. Drillability studies in Zonguldak coalfield, Turkish Scientific and Research Council, TUBITAK, MAG-548.

Bilgin, N., 1985. The role of quality control in tungsten carbide production for mining industries, *29th EOQL Conference*, Portugal, pp. 1–7.

Bilgin, N., Tumaç, D., Feridunoğlu, C., Karakas, A.R., Akgul, M., 2005. The performance of a roadheader in high strength rock formations in Kucuksu tunnel. *31st ITA-AITES World Tunnel Congress*, 7–13 May, Istanbul, eds. Erdem and Solak, ISBN 04 1537453 7/8, pp. 815–820.

Bruland, A., 2000, Hard rock tunnel boring, PhD thesis, Norwegian University of Science and Technology, Department of Building and Construction Engineering, 10 volumes.

Bruland, A., Dahl, T.S., Nilsen, B., 1995. Tunnelling performance estimation based on drillability testing. *ISRM Congress*, Tokyo, 1995, pp. 123–126.

Clark, G.B., 1982. Principles of rock drilling and bit wear. *Colorado School of Mines Quarterly*, 77(2), p. 91.

Deketh, H.J.R., 1995. *Wear of Rock Cutting Tools*. Balkema, Rotterdam, ISBN 90 5410 6204, p. 144.

Frenzel, C., 2011. Disc cutter wear phenomenology and their implications on disc cutter consumption for TBM. *45th US Rock Mechanics/Geomechanics Symposium*, San Francisco, CA, June 26–29, ARMA 11-211.

Hughes, H.M., 1986. Relative cuttability of coal seems. *Mining Science and Technology*, 3:95–104.

Michalakopoulos, T.N., Anagnostou, V.G., Bassanou, M.E., Panagiotou, G.N., 2006. The influence of steel styli hardness on Cerchar abrasiveness value. *International Journal of Rock Mechanics and Mining Sciences*, 43:321–332.

Nilsen, B., Dahl, F., Holzhäuser, J., Raleigh, P., 2006. Abrasivity testing for rock and soils. *Tunnels and Tunneling*, April:47–49.

Nilsen, B., Dahl, F., Holzhäuser, J., Raleigh, P., 2007. New test methodology for estimating the abrasiveness of soils for TBM tunnelling. *RETC Proceedings*, USA, pp. 104–116.

Nizamoglu, S., 1978. Study on the performance of TBM s and tool consumption. PhD thesis. Ecole Nationale Superieure de la Metallurgy et de L'industry des Mines de Nancy, p 139.

Okubo, S., Fukui, K., Nishimatsu, Y., 2011. Estimating abrasivity of rock by laboratory and *in situ* tests. *Rock Mechanics and Rock Engineering*, 44:231–244.

Plinninger, R.J., Kasling, H., Thuro, K., Spaun, G., 2003. Testing conditions and geomechanical properties influencing the Cerchar abrasiveness index (CAI) value. *International Journal of Rock Mechanics and Mining Sciences*, 40:259–263.

Plinninger, R.J., Kasling, H., Thuro, K., 2004. Wear prediction in hardrock excavation using the CERCHAR abrasiveness index (CAI). *EUROCK 2004 & 53rd Geomechanics Colloquium*, ed. Schubert, pp. 599–604.

Rostami, J., Gharahbagh, E.A., Palomino, A.M., Mosleh, M., 2012. Development of soil abrasivity testing for soft ground tunneling using shield machines. *Tunnelling and Underground Space Technology*, 28:245–256.

Schimazek, T., Knatz, H., 1970. The influence of rock structures on the cutting speed and pick wear of heading machines (in German), *Glücckauf*, March:275–278.

Smith, C., 2012. Getting a grip on TBM procurement. *Tunnelling Journal*, April/May:10–12.

Verhoef, P.N.W., 1997. *Wear of Rock Cutting Tools*, Balkema, Rotterdam, ISBN 90 5410 4341, p. 144.

West, G., 1989. Technical note–Rock abrasiveness testing for tunnelling. *International Journal of Rock Mechanics and Mining Sciences & Geomechanics Abstracts*, 26(2):151–160.

This page intentionally left blank

7

Roadheaders

7.1 General

Roadheaders were first developed for mechanical excavation of coal in the late 1940s in Europe (Kogelmann and Schenck 1982). Roadheaders are partial-face machines excavating only a portion of the face at once and a certain number of cutters are in contact with the face. The basic advantages of roadheaders over the other underground excavation machines are their mobility, flexibility, and selective mining ability (Ozdemir 1997). These advantages, in addition to general advantages of mechanical excavation, provide them for being used widely and having a very important and unique position in underground mining and tunneling operations, although they are also used in surface operations.

Typical roadheaders are presented in Figure 7.1. A cutterhead equipped with cutting tools and attached to a boom, which is movable in any direction, excavates the face. Excavated material (muck) falls down into a loading apron and is gathered and loaded into a chain conveyor located in the center of the loading apron by a continuous muck loading system such as gathering arm, star wheel, spinner disk, and scraper conveyor. The chain conveyor carries the loaded material through the roadheader body to the tail conveyor. From the tail conveyor, the material is transferred to any dry muck haulage (transportation) unit such as trucks, rail cars, belt conveyors, and shuttle cars.

7.2 Advantages, Application Areas, and Limits of Roadheaders

Ore/mineral and waste can be excavated selectively by roadheaders since they are partial-face machines. This situation results in less ore dilution and decreases the cost of ore processing. Separate excavation of hard and soft parts of a mixed face might ease the excavation process. Since the face is accessible, cutters can be inspected and changed easily.

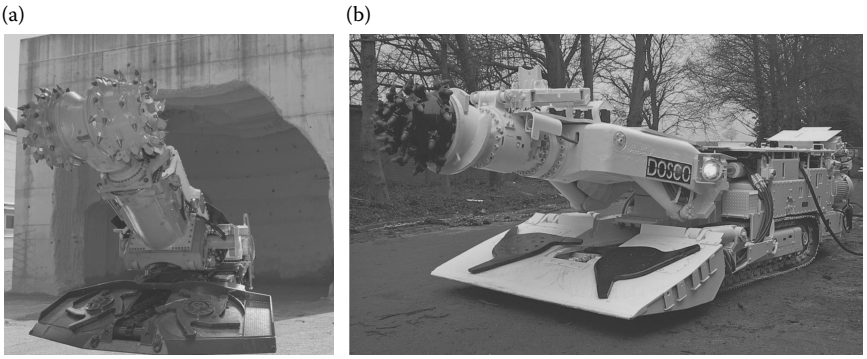

FIGURE 7.1
Transverse and axial types of roadheader cutterheads. (a) Trasverse cutterhead; (b) Axial cutterhead. (Courtesy of Dosco and Sandvik, formerly Voest Alpine.)

It is easy to relocate roadheaders from one face to another, which is frequently necessary in mining operations, since they are usually crawler mounted and their weight is lower compared to other underground excavation machines. They are mobile machines. They can be assembled or dissembled easily in less than a couple of days due to their modular structure. Since they are smaller and lighter compared to other underground excavation machines, they require relatively lower initial capital and operational costs.

Roadheaders are flexible machines; they can be adapted to any opening/profile shapes, such as horseshoe, rectangular, circular, and any other shape. This feature is especially important in mining operations due to flat floor requirements. They are adaptable to current/operating mine designs and can make sharp turns as much as 90°. They can work safely in gradients up to 15°; if bracing jacks are utilized, maybe openings with higher gradients up to 20–25° can be excavated, which are not suggested by manufacturers due to safety concerns.

Roadheaders are primarily limited to the excavation of massive rocks up to 100–120 MPa of UCS, depending on cutterhead power and weight of the roadheader and some structural characteristics of the rock mass (Copur et al. 1997, 1998a,b). If the rock mass is highly fractured–jointed–foliated, then they can excavate rocks up to 160 MPa UCS (Figure 7.2). These UCS values should be used cautiously, since they are not the only parameter for defining cuttability.

Water flow should be none or low for their effective use. However, it is known that water might have adverse effects on the performance when excavating sticky clayey formations (Bilgin et al. 2002). Sticking of clay onto cutterheads might cause a stop in the excavation and requires a cleaning job (Figure 7.3).

Roadheaders cannot excavate hard and abrasive rocks. They can only excavate up to moderately abrasive rocks. Their hard rock-cutting abilities

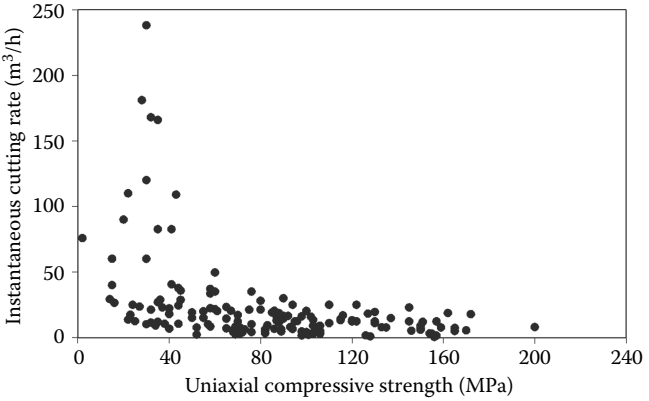

FIGURE 7.2
Variation of UCS with ICR for roadheaders. (Adapted from Copur, H., Ozdemir, L., Rostami, J., 1998a. *SME Annual Meeting*, Preprint No: 98-185, p. 5; Copur, H., Ozdemir, L., Rostami, J., 1998b. *Mining Engineering*, 50(3):38–42.)

are limited due to drag-type cutters; they are only utilized with drag-type cutters, mostly conical type. It is a known fact that when the cutter consumption rate exceeds 0.50 cutter/m^3, cutter breakages and wearing increase rapidly; forces on worn cutters increases tremendously (Copur et al. 1997, 1998a,b). This reduces the benefits of a project and may increase the unit cost of excavation; in many cases, mechanized excavation is left for another method of excavation (Figure 7.4). If the cutter consumption rates are between 0.2 and 0.5 cutter/m^3, the project cost is critical. If the excavation lengths are very short, then cutter consumption can be compromised and project costs should be reviewed. If the cutter consumption rate is lower than 0.20 cutter/m^3, there would not be any serious problem in excavation (Ocak and Bilgin 2010).

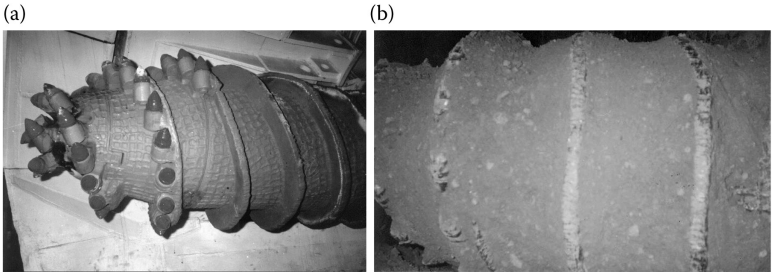

FIGURE 7.3
Clean roadheader cutterhead (a) and after clay sticking (b). (Adapted from Dincer, T. et al. 2005. *Proceedings of the Symposium on Geology of Istanbul*, December 16–18 (in Turkish).)

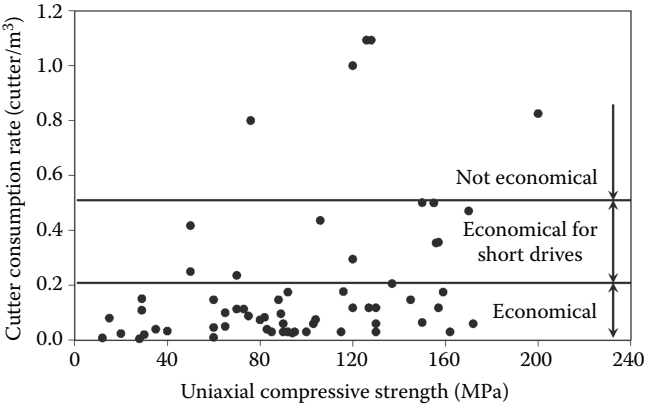

FIGURE 7.4
Variation of UCS with cutter consumption rate for roadheaders.

Roadheaders are usually used in underground mining operations for production and development operations, particularly in coal and evaporitic rock mining. They are also used for mining of metallic ores and other industrial minerals. They are used in room and pillar coal-mining applications, particularly for excavation of seams with strong inclusions. They are sometimes used in surface-mining operations. In the civil construction industry, they are used for excavation of tunnels (railway, roadway, sewer, water tunnels, etc.), as well as enlargement and rehabilitation of the tunnels, large shaft excavations, and foundation and channel excavations.

7.3 Basic Units and Mechanical Structure of Roadheaders

Basic units of roadheaders include a machine body and traveling (usually crawler) unit, cutting boom and cutterhead, loading apron and gathering arms, discharge (chain) and tail conveyors, electric and hydraulic power supply, and operator cabin and optional equipment such as water jets for dust suppression and cutter cooling purposes, bolting unit, steel set lifting unit, and explosion-proof equipment.

There are generally three types of traveling units used with roadheaders: crawler-mounted, rubber tire, and hydraulically pushed, shielded roadheaders. Crawler-mounted roadheaders are the most common ones. Rubber tire roadheaders are preferred for use with the applications of the New Austrian Tunneling Method (NATM), due to its fast-moving features. Shielded roadheaders move forward by the thrust of hydraulic push cylinders; they are used only with segmental lining-type supports since they get their thrust

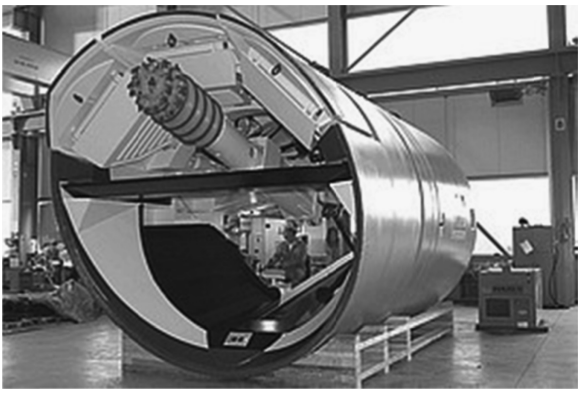

FIGURE 7.5
Shielded roadheader. (Courtesy of Sandvik, formerly Voest Alpine.)

from the linings. Shielded roadheaders are used for excavation of soft, weak, wet, or blocky formations (unstable rock conditions) to reduce collapse and rock-falling problems (Figure 7.5). If it is required, mechanical breasting faceplates can be used to provide for stability.

Booms of roadheaders can move in any direction (left, right, up, down, and diagonal) and a cutterhead equipped with cutting tools is attached to cut the face. Cutterhead motors, usually electrically driven, are located inside the boom. Booms are usually driven hydraulically. Hard-rock booms should be shorter than soft ground booms to reduce the machine vibrations.

Roadheaders usually have a single boom, although there are twin boom roadheaders (Figure 7.6), which are only used for excavation of soft rocks/minerals (such as coal, salt, potash, trona, etc.) with high production rates

FIGURE 7.6
Twin boom roadheader. (Courtesy of Dosco.)

up to 400–500 tons/h. The rotation of each cutterhead in a twin boom roadheader is in opposite directions to counterbalance the forces acting on the machine body.

There are different types of single booms: solid (nonextendable) boom, telescopic (extendable) boom, articulated boom, tilting boom, beam-supported (shielded) boom, and interchangeable (multipurpose) boom.

The advantage of utilizing telescopic boom (Figure 7.7) over nonextendable boom is that it allows the machine to sump the face and to smooth the gallery/tunnel wall by extending the boom without moving the whole machine forward. This reduces traveling (moving) time of the machine, as well as increases machine utilization time (MUT) and daily production rate.

Articulated booms (Figure 7.7) are used with the NATM in large cross sections. Their longer booms make it possible to excavate upper benches first and then lower benches in one excavation pass, saving excavation time. They are able to cut lower levels (pits) under their traveling levels. Since the longer boom generates more momentum on the machine, which affects machine stability, the articulated booms can only be used for soft rock excavations. An articulated boom allows the machine to sump the face and to smooth the gallery/tunnel wall by forwarding the boom without moving the whole machine, which increases MUT and daily advance rate.

Tilting booms (Figure 7.8) are used with transverse cutterhead roadheaders for obtaining better curvature by tilting the boom while excavating at the top portion of horseshoe-shaped openings. This provides better static condition for a steel arch support system.

In shielded roadheaders, the boom is attached to a stiff beam, which is attached to the shield of the machine (Figure 7.5).

Interchangeable or multipurpose booms (Figure 7.9) can be attached to any excavator chassis (carrier unit). They are suitable to use interchangeably with different attachments such as roadheader cutterhead, impact breaker, backhoe loader, ripper, and/or driller–bolter. An interchangeable boom provides more flexibility in variable geological conditions (Kogelmann 2008).

Mucking of the excavated material is provided by a loading apron. Muck falling down onto the loading apron is gathered by mechanical arms or

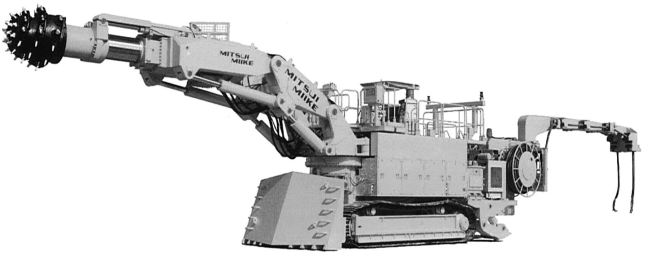

FIGURE 7.7
Telescopic and articulated boom roadheader. (Courtesy of Mitsui Miike.)

FIGURE 7.8
Tilting boom roadheader. (Courtesy of Schaeff.)

buckets and piled toward a chain conveyor located at the center of the apron. General types of gathering arms for different ground conditions are presented in Figure 7.10. Loading aprons of roadheaders can be manufactured as extendible providing for more mobility, flexibility, and a reduced

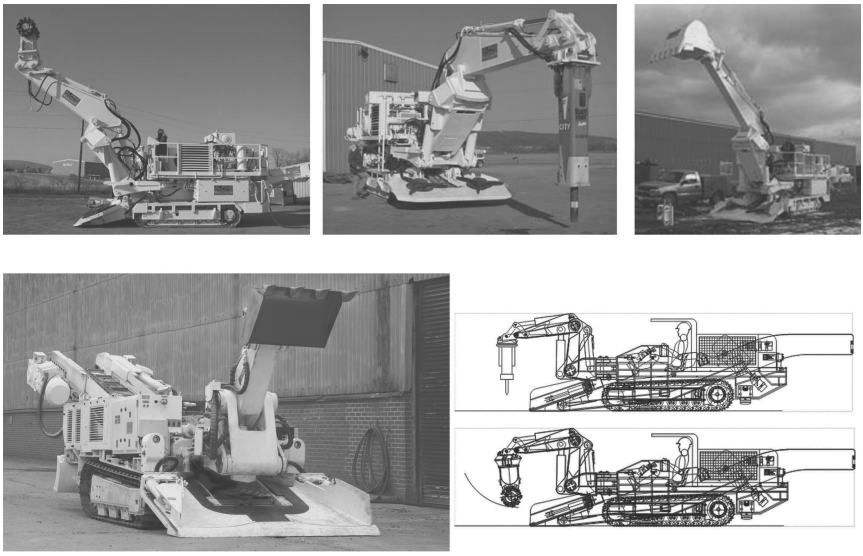

FIGURE 7.9
Interchangeable boom roadheader. (Courtesy of Dosco and Alpine Minor Kogelmann, W.J., 2008. Multi-tool miner for all rock conditions. *SME Annual Meeting*, February 24–27, Salt Lake City, Preprint No: 08-061, p. 4. With permission.)

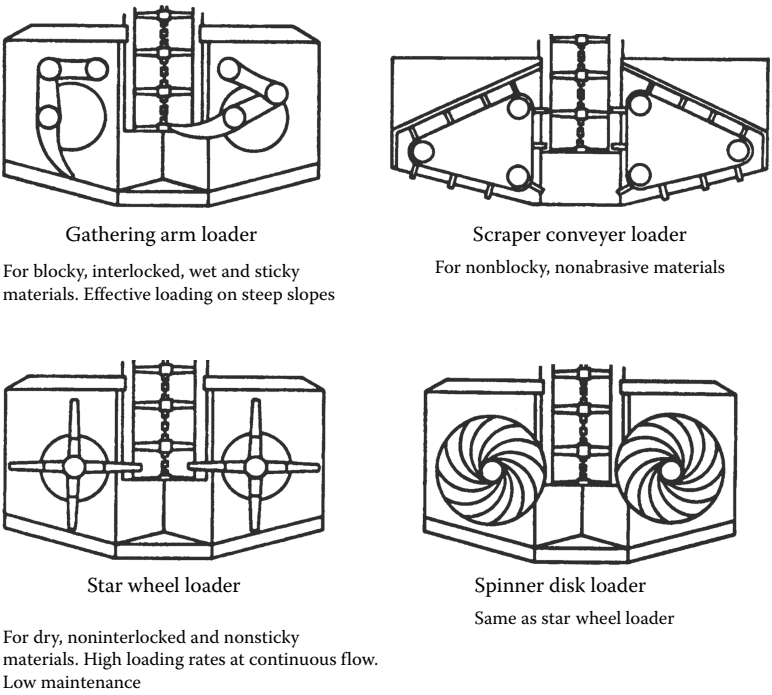

FIGURE 7.10
General types of gathering arms for different ground conditions. (Adapted from Kogelmann 1988 as quoted by Breeds C.D., Conway, J.J., 1992. *SME Mining Engineering Handbook*, Vol. 2, 2nd ed., Chapter 22.1, pp. 1871–1907.)

level of muck spillage problems. Muck transferred from a chain conveyor to a tail (belt) conveyor is loaded into any type of dry muck haulage system such as rail cars, belt conveyors, or shuttle cars. The tail conveyor is usually manufactured as a movable piece, thereby providing efficient loading.

Some roadheaders have rock-bolting equipment as attachments. Machines with rock-bolting attachments allow continuing the excavation job while bolting, which increases machine utilization (excavation) time. In the case of a roadheader without rock-bolting equipment, the roadheader and personnel should be retreated/withdrawn from the face for supporting the roof, which reduces MUT. Some roadheaders have a steel set lifting unit, which makes it easy to place/install the steel sets.

The roadheader performance is very sensitive to the operator's handling. They can have automated control systems such as laser-guided alignment control, computerized opening, profile control, and remote control. Automation provides reduced operator mistakes and increased efficiency.

7.4 Roadheader Cutterheads, Weights, and Technical Specifications

Roadheaders can be classified into two groups based on cutterhead types: axial (longitudinal, in-line, spiral, and milling) and transverse (ripping, drum) as seen in Figure 7.1. Their cutterhead shapes are generally cylindrical and conical with the nose section as semispherical or flat. A general comparison of axial and transverse cutterheads is summarized in Table 7.1.

Axial cutterheads consist of one drum and its rotation axis is parallel to the boom axis and perpendicular to the face. Shearing direction of the boom is perpendicular to the cutterhead rotation axis. The axial cutterhead roadheaders can excavate nonabrasive massive rocks having up to 60–80 MPa of UCS. If the conditions are favorable (i.e., fractured, foliated, bedded, or rock mass with low RQD), they can excavate rocks up to 80–100 MPa.

Transverse cutterheads consist of two symmetrical drums rotating along the same rotation axis that is perpendicular to the boom axis and parallel to the face. Shearing direction of the boom is parallel to the cutterhead rotation axis. Transverse cutterhead roadheaders can excavate nonabrasive or moderately abrasive massive rocks having up to 100–120 MPa of UCS. If the conditions are favorable, they can excavate rocks up to 160–180 MPa of UCS.

It should be noted that these strength ranges are valid for general cases. Rock strength values do not reflect cuttability of rocks in some cases (i.e., a soft rock with low compressive strength might be tough to cut). Therefore, it would be better to run cutting experiments for proper selection, design, and prediction of roadheaders.

In the case of a roadheader with an axial cutterhead, results of boom reaction forces usually act sideways, which forces the machine to slide on the floor. If any clay and water exist in the environment, this sliding becomes an obstacle for the excavation. The resultant boom reaction forces in the case of a roadheader with a transverse cutterhead usually act in a vertical direction, forcing the machine to lift up and is counterbalanced by most of the machine

TABLE 7.1

A General Comparison of Axial and Transverse Cutterheads

Comparison Criteria	Axial Cutterhead	Transverse Cutterhead
Profile smoothness	Favorable	Unfavorable
Machine stability	Unfavorable	Favorable
Muck loading efficiency	Unfavorable	Favorable
Application limits	Soft rocks (UCS <60–80 MPa), nonabrasive	Soft to medium-strength rocks (UCS <100–120 MPa), moderately abrasive
Production rate	Higher for UCS <40–60 MPa	Higher for UCS >60–80 MPa

Note: UCS, uniaxial compressive strength.

weight, which makes it more stable compared to roadheaders with an axial cutterhead (Kogelmann and Schenck 1982).

The throwing direction of muck, in the case of axial cutterhead, is usually sideways. This results in spillage of the cut material, which requires an extra effort to gather and place on the loading apron. Extendible loading apron designs reduce the spillage problem. In the case of a transverse cutterhead, the cut material is usually thrown directly to the loading apron (Kogelmann and Schenck 1982).

Profile smoothness affects support cost. Support installation in a smooth wall costs less than in a stepped (nonsmooth) wall. A transverse cutterhead generates an uneven (stepped) profile (Figure 7.11). However, this problem can be overcome by using a telescopic boom or by moving the machine forward and backward successively. An axial cutterhead can enable a smooth cutting profile by choosing a cutterhead cone angle convenient to the excavation face dimensions (Figure 7.11). This reduces the support cost. When cutting a relatively larger cross section, the smooth profile might not be achieved on the roof. However, it is possible to correct this profile by tracking the roadheader (a time-consuming operation) or by using a telescopic boom (more efficient).

Roadheader cutterhead powers have reached up to 400 kW, starting from around 30 to 40 kW, providing for higher torque capacities and production rates. Their weights have reached up to/over 135 tons, starting from 8 to 10 tons, providing for stability and less machine vibrations, resulting in higher production rates. The most important factors affecting the selection of the roadheader weight and cutterhead power for underground operations is the opening size and rock properties. Heavier machines require larger openings; however, as-small-as-possible openings are preferred in underground mining operations due to economical concerns. A heavier machine means less vibration and maintenance, with higher thrust capacities providing higher production rates. However, heavier machines

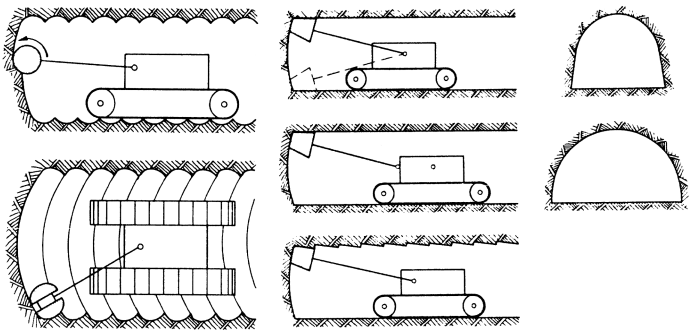

FIGURE 7.11
Profile smoothness on roadheaders with transverse (left) and axial (right) cutterheads. (Adapted from Menzel, W., Frenyo, P., 1981. *Glückauf*, 117(5):284–287.)

lose their mobility, as well. Increased cutterhead power requires heavier machines to withstand the higher boom reaction forces. Large and heavy machines have the ability to cut cross sections over 80 m^2 from a stationary point. Lighter roadheaders with an axial cutterhead usually face machine stability problems, which can be controlled by stabilizing jacks and/or grippers (bracing jacks).

Machine manufacturers usually follow a certain ratio of (cutterhead power/roadheader weight). The usual range of this ratio varies between 3 and 5 Hp/ton. Transverse cutterheads are usually set with the larger ratios within this range. Selecting a heavier and more powerful roadheader, as well as a larger cutterhead diameter, is usually advantageous. The disadvantages of using a larger cutterhead diameter in cutting harder rocks can be mostly overcome by reducing the sumping depth and rotational speed of the cutterhead.

A general classification of roadheaders based on weight and cutterhead power is presented in Table 7.2. Specifications of roadheaders manufactured by different companies are summarized in Table 7.3.

Roadheader cutterhead diameters are usually between about 70 and 140 cm for axial and transverse cutterheads. An empirical ratio of cutterhead diameter to cutterhead length is between 1.0 and 1.4. Longer cutterhead lengths are used with softer rocks. Shorter lengths and smaller diameters are used with stronger rocks. The usual tendency of the manufacturers is to manufacture larger-diameter cutterheads for heavier and more powerful roadheaders. Water sprays for dust suppression and cutter cooling purposes can be optionally used on cutterheads.

An electric motor, kept inside the boom, is used in most of the roadheader cutterheads to rotate/drive the cutterhead. Torque of the electric motor up to 400 kW is transmitted to input bevel gear of the transmission. Bevel gear is very expensive compared to hydraulic motors and very sensitive to shock loads, which is usual in roadheader applications (Kogelmann 2008), although it generates lower noise and heat during operation. The electric motors usually provide double-speed rotation. The lower speed is around 25–35 rpm and the higher speed is around 50–70 rpm, depending on the rock conditions. The

TABLE 7.2

General Classification of Roadheaders Based on Weight and Cutterhead Power

Roadheader Class	Roadheader Weight (ton)	Cutterhead Power (kW)	Maximum Cross-Section Area (m^2), Standard (Extended) Cutting Ranges	Maximum UCS (MPa), Standard (Extended) Cutting Ranges
Light	8–40	50–170	~25 (~40)	60–80 (20–40)
Medium	40–70	160–230	~30 (~60)	80–100 (40–60)
Heavy	70–110	250–300	~40 (~70)	100–120 (50–70)
Extra heavy	>100	350–400	~45 (~80)	120–140 (80–100)

Source: Adapted from Heiniö, M., 1999. *Rock Excavation Handbook*. Sandvik Tamrock Corp., p. 364.

TABLE 7.3

Specifications of Roadheaders Manufactured by Different Companies

Company (Web Address)	Model	Cutterhead Type	Weight (ton)	Cutterhead Power (kW)	Maximum Cutting Height (m)	Maximum Cutting Width (m)
Sandvik (mining.sandvik.com)	MT340	Transverse	56	200	4.87	7.45
	MR340	Transverse	62	200	4.87	7.45
	MR520	Transverse	102	325	5.3	8.3
	MR620	Transverse	128	300	5.9	8.9
	MT520	Transverse	115	315	5.3–8.0	5.5–10.8
	MH620	Transverse	120	300	5.3–5.8	8.0–8.8
	MH720	Transverse	135	300	6.6	9.1
SANYHE (sanyzz.com)	EBZ132	Axial	40	132/75	4.45	4.9
	EBZ160	Axial	48	160/100	4.8	5.5
	EBZ200	Axial	58	200/110	5.1	6.5
	EBZ200H	Axial	78	200/150	4.8	6.0
	EBZ260H	Axial	85	260/200	5.0	6.2
	EBZ318H	Axial	120	318	5.59	7.0
Dosco Overseas (dosco.co.uk)	SL320	Transverse/axial	40	134–246 Transverse 170–270 Axial	4.1 Transverse 3.9 Axial	5.1 Transverse 4.4 Axial
	LD 2000M (Backhoe M.)	(Multipurpose)	17	30 (Transverse)	3.0	4.2
	LH 1500	Axial	80	300	5.0	7.3
	Shielded	Axial/Transverse	2.2–11 m diameter			
Eickhoff (eickhoff-bochum.de)	ET 120	Transverse/axial	32	132	4.05 Transverse 4.6 Axial	5.5 Transverse 5.8 Axial
	ET 170	Transverse/axial	33	132	4.6 Transverse 4.9 Axial	6.1 Transverse 6.0 Axial

	ET 210	Transverse/axial	58 Transverse 56 Axial	200	4.7 Transverse 5.0 Axial	7.1 Transverse 6.8 Axial
	ET 250	Transverse/axial	58 Transverse 56 Axial	200	5.5 Transverse 5.8 Axial	7.5 Transverse 7.2 Axial
	ET 380	Transverse/axial	109 Transverse 107 Axial	200	7.1 Transverse 7.45 Axial	12.4 Transverse 12.4 Axial
	ET 410	Transverse/axial	104	300	5.5 Transverse 6.6 Axial	10.0 Transverse 10.0 Axial
	ET 450	Transverse/axial	110	300	7.3 Transverse 7.7 Axial	10.3 Transverse 10.4 Axial
	ET 480	Transverse/axial	114	300	7.9 Transverse 8.3 Axial	11.4 Transverse 11.5 Axial
IBS (ibstec.de)	SM100	Transverse	28	110	3.7	4.6
	SM130	Transverse	35	132	4.08	5.0
	SM160	Transverse	45	160	4.5	6.5
Mitsui Miike (mitsuimiike.co.jp)	MRH-S65	Axial	20	65	3.8	4.2
	MRH-S100	Axial	27	100/60	4.5	5.1
	MRH-S200	Axial	49	200/110	6.0	6.4
	MRH-S300	Axial	95	300/150	6.5	7.5
	SLB-300S	Axial	90	300/200	8.8	8.3
	SLB-350S	Axial	120	350/350	8.8	8.8
Aker Wirth (wirth-erkelenz.de)	T1.14	Axial/transverse	53–60	150–180	4.8	6.7
	T1.24	Axial/transverse	70–75	150–180	5.0	6.7
	T2.24	Axial/transverse	85–95	300–270	6.8	8.1
	T3.20	Axial/transverse	120–135	300	7.9	9.5

higher rpm values are used in average rock-cutting conditions and the lower rpm values are used in difficult rock-cutting conditions. Hydraulically driven motors are able to provide multispeed rotations, which mean the rotational speed can be arranged as desired. They are not sensitive to shock loads and are cheaper compared to electric motors, although their power transmission efficiency is lower.

7.5 Cutting Tools Used on Roadheaders

Drag (pick)-type cutters/cutting tools are used with roadheaders to break/cut/excavate rocks, where their cutting mechanism is dragging over the excavation face and generating tensile fractures between adjacent cutting grooves. They are more efficient than all other cutter types, since they break rocks in tension with lower force and energy. Mostly, conical tools are fitted on roadheaders, and rarely on radial tools (Figure 7.12). However, these cutters cannot cut hard and abrasive rocks due to their weak shape and dimension (sharp and pointed edges, small dimensions) and the type of their cutting action (dragging, friction). They require frequent stops for cutter replacement when cutting hard and abrasive rock. Therefore, the use of drag cutters is limited for the excavation of soft and medium-strength nonabrasive or medium-abrasive rocks. They are also used in many other types of underground and surface excavation machines such as continuous miners, surface miners, shearers, tunnel-boring machines, microtunneling machines, road planers, chain cutters, disk saws, and trenchers.

Radial cutters are generally able to cut rocks up to 40–60 MPa of UCS. They have a rectangular shank that stays fixed in the tool holder. Their bodies are

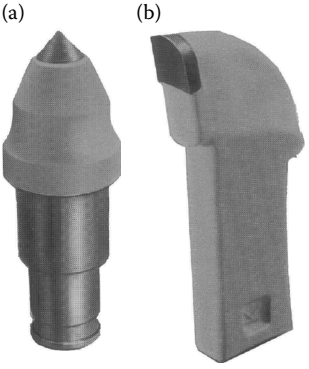

FIGURE 7.12
Cutting tools used on roadheaders: conical cutter (a) and radial cutter (b). (Courtesy of Kennametal, Product Catalogues. With permission.)

made of hardened steel and have a sharp tip made of tungsten carbide. They are more efficient than the conical cutters, since they have sharper edges and a large tool width that sweeps a larger area than conical cutters do. They cut the rocks with lower cutter forces and specific energy (SE), and produce less dust and fine particles. However, the radial cutters are very prone to blunting due to their very sharp tips and after a small amount of blunting, their cutter forces increase drastically.

Conical cutters are generally able to cut rocks up to 100–120 MPa of UCS. They have a circular shank, which is able to rotate in their tool holder, a conical body made of hardened steel, and a conical tip made of tungsten carbide at the very end of the body. Their shape allows them to wear out evenly, which results in a longer tool life compared to the radial cutters. Therefore, they are generally more common than radial tools, especially for excavation of stronger grounds. The larger tip diameters and shorter body lengths are preferred for relatively more difficult cutting conditions.

7.6 Some Operational Features of Roadheaders

The cutting action of roadheaders on the face in one cutting cycle can be divided into two general modes: sumping (penetration) and shearing (or slewing, traversing, and arcing).

Sumping is the beginning of a cutting cycle and a kind of preparatory operation for shearing. It is performed to open a hole on the face by pushing the machine or boom to the face. Sumping is a difficult cutting action, since there is almost no free surface to reduce the force requirement of the cutterhead. The sumping depth of the cutterheads should be arranged depending on the rock properties. If the rock is relatively soft, the sumping depth can be deeper. Deeper sumping depths give the advantage of more advances in one cycle. Sumping is easier for the roadheaders with telescopic booms, since only the boom has to be moved forward, not the whole machine.

Shearing is an enlargement of a sumping hole up to the wall perimeter. It includes all the actions of the boom in all directions on the face (up, down, left, right, and diagonal). The cutting action is relatively easier in shearing compared to sumping, since there is a free surface that reduces force requirement to cut the rock. The shearing action takes most of the excavation time in a cutting cycle compared to sumping. It is performed in a stationary position without moving the roadheader or boom forward to the face, unless it is necessary to move for a smooth finished wall.

Sumping with an axial cutterhead can be made at any point across the heading face in accordance with geological and mining requirements. In harder rocks, optimum results are usually achieved by keeping the boom horizontal in the direction of roadway axis. Cutting direction in shearing

with an axial cutterhead can be horizontal, vertical, or diagonal along the face. Undercutting mode is preferred to avoid impact loading and pick shattering. Therefore, the order of cutting during shearing is preferred in the direction of the cutterhead rotation. The cutting depth of the cutterhead during shearing can be selected from a few centimeters to the full diameter of the cutterhead, although the full diameter is usually used only for the initial cut after sumping. It is also possible to vary the sumping depth of the cutterhead in accordance with the geological conditions.

Sumping with a transverse cutterhead should preferably be started at the bottom of the face. The maximum sumping depth is two-thirds of the cutterhead diameter, although this can be achieved with several successive sequences of sumping, since the distance between cutter tip and gearbox block, which is located between the two halves of the cutterhead, does not allow deeper sumping depths at once. On the other hand, there are transverse cutterheads without gaps between the drums, as well (Kogelmann et al. 2003). The cutting direction in shearing can be horizontal, vertical, or diagonal along the face.

7.7 Roadheader Performance

Parameters affecting the roadheader performance can be divided into three general groups: mechanical, geological–geotechnical, and technical–operational parameters. A summary of these parameters is presented in Table 7.4.

Performance prediction generally means the assessment of an *ICR*, *TCR*, *MUT*, and *AR* for different geological units. Definitions of these parameters are given in Chapter 5 of this book. *ICR* is a function of mechanical and geological–geotechnical parameters, as well as technical–operational parameters. *TCR* is a function of geological (especially abrasive mineral content) and mechanical parameters (especially cutter and cutterhead-related parameters). *MUT* is usually estimated for specific projects, since it depends on the delays (stoppages) caused by operational features of the projects, such as support system, muck pickup system, machine availability, and so on. *MUT* shows the overall performance of an excavation system and is usually between 20% and 35% for roadheaders in mining operations requiring steel supports and between 30% and 50% in mining operations requiring rock bolts, shotcrete, and wire mesh. It would be higher if the opening requires no support.

A summary of the empirical models developed for predicting *ICR* of roadheaders is presented in Table 7.5. Prediction of cutting tool consumption is also an important factor affecting the economy of excavation projects. This subject is analyzed in Chapter 6 of this book.

TABLE 7.4

Summary of Parameters Affecting Roadheader Performance

Mechanical Parameters	Machine Type (Crawler Mounted, Shielded, Twin Boom, etc.) Machine Weight and Dimensions Boom Force Capacities (Shearing, Lifting, and Lowering) Cutterhead Type (Transverse, Axial) Cutterhead Power and RPM, Lacing Design Bit Type and Dimensions, Metallurgical Properties of Tip
Geological–geotechnical parameters	*Rock Mass Properties* RQD Bedding, foliation, and fault zones Joint sets (orientation, spacing, filling, etc.) Hydrogeology (water table/water ingress) Adverse geology (squeezing, swelling, and blocky grounds) *Physical and Mechanical (Intact Rock) Properties* Cuttability (cutter forces, SE, and optimum cutting geometry: linear cutting tests) Strength (UCS, BTS, elasticity modulus, cohesion, etc.) Texture and abrasivity (mineral/quartz content and grain size, microfractures, grain interlocking, etc.) Others (brittleness, water content, swelling, etc.)
Operational parameters	*Technical Parameters* Tunnel shape and dimensions Inclinations, crosscuts *Mining Parameters* Support (bolting, shotcrete, steel sets, etc.) Muck haulage (conveyor, locomotive, LHD, etc.) Utility lines (power, water, and air supply) and surveying Ground treatment (drainage, grouting, and freezing) Labor availability and quality

Source: Revised after Fowell, R.J., Johnson, S.T., 1982. *Proceedings of the Symposium on Strata Mechanics*, pp. 241–244; Ozdemir, L., 1997. *Mechanical Mining Short Course*. Section: "Roadheaders" by L. Ozdemir, March 19–21, Colorado School of Mines, Golden, Colorado; Copur, H. et al. 1997. *Proceedings of the 4th International Symposium on Mine Mechanization and Automation*, Brisbane, Queensland, Australia, pp. A4-1–A4-7; Copur, H., 1999. Theoretical and experimental studies of rock cutting with drag bits toward the development of a performance prediction model for roadheaders. PhD thesis, Colorado School of Mines, p. 361.

7.8 Numerical Examples on Predicting Performance of Roadheaders

7.8.1 Numerical Example on Roadheader Selection and Performance Prediction

A roadheader, which might be transverse or axial type, having 50 tons of weight and 200 kW of cutterhead power is considered for excavation of roadways in a cross-section area of 14 m^2 in a coal mine. Although the inclines (12°) and main roadways pass through all the strata types found in

TABLE 7.5

Summary of Empirical Roadheader Performance (ICR) Prediction Models

Author (Year)	Geological Parameters		Machine Parameters	Explanations
	Intact Rock	Rock Mass		
McFeat-Smith and Fowell (1977, 1979)	SE (or UCS, CC)	Not considered	P_{inst} (taken as ave.115 kW), W (two classes)	Developed for light (up to 40 tons) and medium-duty (up to 65 tons) axial roadheaders and massive coal measure strata. It needs correction for heavier and transverse roadheaders, and other rock masses.
Bilgin (1983)	Not considered	SE from drilling rate	Not considered	Developed for a light axial roadheader and coal measure strata. Standardization of drilling for SE calculation is difficult. It needs correction for heavier and transverse roadheaders, and other types of rock masses.
Sandbak (1985)	UCS	RMR	Not considered	Developed for only one type of roadheader (axial, light) and generally for quartz monzonite and dacite porphyry. It usually underestimates for RMR < 40. It needs correction for heavier and transverse roadheaders, other rock masses.
Farmer and Garrity (1987)	UCS, E	Not considered	P_{inst}, k	Developed for only two heavy-weight axial roadheaders and massive coal measure strata. Data are very scattered. The selection of energy transfer ratio is arbitrary. It needs correction for lighter and transverse roadheaders, and other rock masses.
Bilgin et al. (1988, 1990)	UCS	RQD	Not considered	Developed for a light, axial, and shielded roadheader and different rock types. It needs correction for nonshielded and heavier machine groups and transverse roadheaders.
Gehring (1989)	UCS	Not considered	Not considered	Developed for heavy-weight axial and transverse roadheaders and massive coal measure strata. It needs correction for lighter roadheaders and other rock masses. It also needs size correction for UCS values.
Natau et al. (1991)	UCS, BTS	Not considered	P_{inst}	Developed for transverse roadheaders in different power classes and different types of rocks. It needs correction for axial roadheaders.

Matsui and Shimada (1993, 1994)	RIHN	RQD	Not considered	Developed for only one type of medium-weight axial roadheader and coal measure strata. It needs correction for other weight classes of roadheaders and transverse roadheaders, and other rock masses.
Rostami et al. (1994)	SE_{opt}	Not considered	P_{inst}, k	Developed for axial and transverse roadheaders in different power and weight classes, and different types of rocks. The type of roadheader is not mentioned. Taking *k* value of 0.45 works for axial type and a value of 0.55 works for transverse type.
Bilgin et al. (1996)	UCS	RQD	P_{inst}	Developed for axial and transverse roadheaders in different power and weight classes, and different types of rock masses.
Copur et al. (1997, 1998a,b)	UCS	Not considered	P_{inst}, W	Developed for transverse roadheaders in different power and weight classes for excavation of especially evaporitic rocks (nonabrasive) up to 60 MPa.
Thuro and Plinninger (1999, 2003)	UCS (or Dw)	Not considered	Not considered	Developed for only one type of transverse roadheader and different types of rocks. It needs correction for other type and classes of roadheaders.
Bilgin et al. (2000)	SE_{opt}	Pf	P_{inst}, k	Developed for axial and transverse roadheaders in different power classes and different types of rocks. Considers the effect of overburden pressures.
Kirkbride (2000)	UCS, CI, CAI, CC, and Qc	Fs, Js, and RQD	P_{inst}, W (operational: A, Ps)	Developed for axial and transverse roadheaders in different power and weight classes, and different types of rock masses based on a classification system. Predicted values are given in a large range.
Copur et al. (2001)	UCS, BTS	Not considered	P_{inst}, k	Developed for different types of massive rocks. It works for transverse types of roadheaders.
Balci et al. (2004)	UCS, BTS	Not considered	P_{inst}, k	Developed for axial and transverse roadheaders in different, weight, power classes, and different types of rocks. Dynamic and static elasticity modulus, and Schmidt hammer can also be used in the model.
Bilgin et al. (2006)	UCS (or BTS)	Not considered	P_{inst}, k	Developed for axial and transverse roadheaders in different, weight, power classes, and different types of rocks. The type of roadheader is not mentioned. Dynamic and static elasticity modulus, and Schmidt hammer values can also be used in the model.

continued

TABLE 7.5 (continued)

Summary of Empirical Roadheader Performance (ICR) Prediction Models

Author (Year)	Geological Parameters		Machine Parameters	Explanations
	Intact Rock	Rock Mass		
Ocak et al. (2007); Ocak and Bilgin (2010)	UCS	Not considered	Not considered	Developed for only one type of transverse roadheader and different types of rocks. It needs correction for other type and classes of roadheaders.
Ebrahimabadi et al. (2011)	UCS, BTS	RQD	Not considered	Developed for only one type of light-weight axial roadheader and coal measure strata. It needs correction for other type, weight, and power classes of roadheaders, and other rock masses.

Source: Revised after Breeds, C.D., Conway, J.J., 1992. *SME Mining Engineering Handbook*, Vol. 2, 2nd ed., Chapter 22.1, pp. 1871–1907; Copur, H. et al. 1997. *Proceedings of the 4th International Symposium on Mine Mechanization and Automation*, Brisbane, Queensland, Australia, pp. A4-1–A4-7.

Note: SE, specific energy obtained from small-scale linear cutting experiments; SE_{opt}, optimum specific energy obtained from full-scale linear cutting experiments; UCS, uniaxial compressive strength; BTS, Brazilian tensile strength, E, deformation (Young's) modulus; Dw, destruction work; CAI, Cherchar abrasivity index; RIHN, rock impact hardness number; CC, cementation coefficient; CI, cone indenter hardness, Qc, quartz content; MF, microfractures; Pf, earth (overburden) pressure factor; RQD, rock quality designation; RMR, rock mass rating; Fs, fracture spacing; Js, joint distance; P_{inst}, installed cutterhead power; W, roadheader weight; k, energy transfer ratio; A, face cross-section area; Ps, face profile shape.

the site, with varying physical, mechanical, and rock mass properties (*UCS* of up to 100 MPa, *RQD* of up to 100%), most of the roadways pass through marl lithology found just under the coal layer and have an average *UCS* of 65 MPa, a *BTS* (indirect) of 4.0 MPa, an RQD of 40%, a *CAI* of 0.65, and an *SE* obtained from small-scale linear cutting experiments of 9.0 MJ/m^3 (2.5 kWh/m^3). Discuss the suitability of the selected roadheader and estimate the instantaneous cutting rate, daily advance rate, and cutter consumption rate by using different methods for both axial and transverse types of roadheaders.

7.8.1.1 Solution of Numerical Example 7.8.1

7.8.1.1.1 Suitability of the Selected Roadheader

Suitability of the selected axial-type roadheader can be controlled by the performance tables (Table 7.6 for roadheaders having weight between 20 and 40 tons and Table 7.7 for roadheaders having weight between 40 and 65 tons) given by McFeat-Smith and Fowell (1977, 1979) and the cutting rate graph (Figure 7.13) given by McFeat-Smith and Fowell (1977, 1979). As seen in these tables, an axial roadheader weighing 50 tons would operate without problem, with a cutting rate between 30 and 40 m^3/h in marl having SE of

TABLE 7.6

Performance Chart for Axial Roadheaders Having Weight between 20 and 40 Tons

SE (MJ/m^3)	Performance of Axial Roadheaders Having Weight between 20 and 40 Tons
20	Machines can only cut these rocks at economic rates if they occur in thin bands (<0.3 m). Short-term replacement of machine components may be required due to substantial cutting vibrations. Specialist advice should be obtained and modification for cutting hard rock may help.
15	Poor cutting performance. Excavation may have to be assisted by blasting of rock at the top end of scale. Shattered inserts should be expected. Regular replacement of slightly worn picks will improve energy requirements and reduce component wear. Point attack tools may be more beneficial. Having low-speed cutting motors and side steel will improve stability. Upper limit of weight stability.
12	Moderate–poor cutting performance. Shattered pick inserts can still be expected although they are less common. For abrasive rocks, picks must be inspected frequently as sharp picks will increase performance.
8	Moderate-to-good cutting performance with very low wear of machine components. Picks must be inspected and changed regularly particularly when excavating abrasive rocks. Drag picks are well adapted to these rocks if face geometry is suitable.
5	The machine is well suited to these rocks. Good advance rates can be anticipated. Mudstones in the lower end of the category may be ripped rather than cut and very high cutting rates can be achieved. Regular inspection and replacement of worn picks is still advantageous.

Source: Data from McFeat-Smith, I., Fowell, R.J., 1977. *Proceedings of the Conference on Rock Engineering*, April 4–7, Newcastle, UK, pp. 581–602; McFeat-Smith, I., Fowell, R.J., 1979. *Proceedings of the Rapid Excavation and Tunneling Conference*, Atlanta, Vol. 1, pp. 261–279.

TABLE 7.7

Performance Chart for Axial Roadheaders Having Weight between 40 and 65 Tons

SE (MJ/m³)	Performance of Axial Roadheaders Having Weight between 40 and 65 Tons
32	Machines can cut only thin bands of these rocks and tool wear will be exceptionally high. Short-term damage to the machine can be expected. Machines must be capable of adaption for hard rock-cutting conditions.
25	Poor cutting performance particularly in massive rocks. Pick wear is critical and cutting will improve by frequent inspection. Machines with modifications for cutting hard rock will reduce the risk of failure. Point attack picks are essential.
17	Moderate-to-good cutting performance at the bottom of the category. Picks should be inspected and changed regularly particularly when excavating abrasive rocks. Consistent cutting rates can be programmed for.
8	Machines are well suited to these rocks and rapid advance rates can be anticipated. Many mudstones in this category can be ripped rather than cut and progress rates will be enhanced by a large-capacity mucking system. Regular inspection and replacement of tools is still advantageous.

Source: Data from McFeat-Smith, I., Fowell, R.J., 1977. *Proceedings of the Conference on Rock Engineering*, April 4–7, Newcastle, UK, pp. 581–602; McFeat-Smith, I., Fowell, R.J., 1979. *Proceedings of the Rapid Excavation and Tunneling Conference*, Atlanta, Vol. 1, pp. 261–279.

9 MJ/m³. However, a lighter transverse cutterhead roadheader with a weight of around 40 tons would achieve at least a similar performance, since it is a more stable machine by using the whole machine weight. On the other hand, the cuttable excavation cross-section area (cutting height and width) should also be controlled by machine specifications.

7.8.1.1.2 Estimation of the ICR

The instantaneous (net) cutting rate of a mechanical miner is the excavation rate achieved only during excavation, excluding stoppages and including only the cutting hours. Instantaneous (net) cutting rates of roadheaders can be predicted by the model given below, which is based on full-scale linear cutting tests (Rostami et al. 1994)

$$ICR = k \cdot \frac{P_{\text{inst}}}{SE_{opt}} \tag{7.1}$$

where

ICR = instantaneous (net) cutting rate (m³/h)
P_{inst} = installed cutterhead power of the mechanical miner (kW)
SE_{opt} = optimum specific energy obtained from full-scale linear cutting tests (kWh/m³)
k = energy transfer coefficient, which is suggested as being between 0.45 and 0.55 for roadheaders

This approach does not give any suggestion for the type of roadheader; however, it can be generally said that the k value of 0.45 might work for

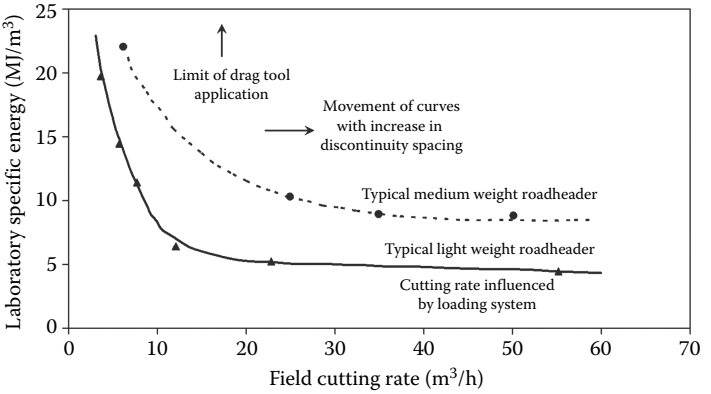

FIGURE 7.13
Cutting performance graph for axial-type roadheaders. (Modified from McFeat-Smith, I., Fowell, R.J., 1977. *Proceedings of the Conference on Rock Engineering*, April 4–7, Newcastle, UK, pp. 581–602; McFeat-Smith, I., Fowell, R.J., 1979. *Proceedings of the Rapid Excavation and Tunneling Conference*, Atlanta, Vol. 1, pp. 261–279.)

axial-type roadheaders, whereas the k value of 0.55 might work for transverse-type roadheaders. On the other hand, SE_{opt} values are not known for the rocks given in this problem. However, it should be known that there are some statistical relationships between SEopt and mechanical properties of the rocks in literature (Copur et al. 2001, Balci et al. 2004, Bilgin et al. 2006).

Gehring (1989) developed a model given below for *ICR* predictions of roadheaders having cutterhead powers of 230 kW (axial) and 250 kW (transverse) for massive formations:

$$ICR = (1739/UCS^{1.13}) \cdot t_1 \quad \text{for axial roadheader} \tag{7.2}$$

$$ICR = (719/UCS^{0.78}) \cdot t_2 \quad \text{for transverse roadheader} \tag{7.3}$$

where

t_1 = power correction factor (assuming the effect of power on performance is linear: 200/230 = 0.87) for axial roadheader

t_2 = power correction factor (assuming the effect of power on performance is linear: 200/250 = 0.80) for transverse roadheader

When the *UCS* value of 65 MPa is substituted in Equations 7.2 and 7.3

$$ICR = (1739/65^{1.13}) \cdot 0.87 = 13.5 \text{ m}^3/\text{h} \quad \text{for axial roadheader}$$

$$ICR = (719/65^{0.78}) \cdot 0.80 = 22.2 \text{ m}^3/\text{h} \quad \text{for transverse roadheader}$$

Bilgin et al. (1996) developed a model given below for predicting net cutting rates of axial-type roadheaders by considering the discontinuities of the formations:

$$ICR = 0.28 \cdot P_{\text{inst}} \cdot (0.974)^{RMCI} \tag{7.4}$$

$$RMCI = UCS \cdot (RQD/100)^{2/3} \tag{7.5}$$

where
$RMCI$ = rock mass cuttability index (MPa)
P_{inst} = installed cutterhead power (Hp)
UCS = uniaxial compressive strength of the rock (MPa)
RQD = rock quality designation of the rock mass (%)

ICR is estimated by substituting the values given in the problem into Equations 7.4 and 7.5:

$$RMCI = 65 \cdot (40/100)^{2/3} = 35.3 \text{ MPa}$$

$$ICR = 0.28 \cdot (200 \cdot 1.36) \cdot (0.974)^{35.3} = 30.0 \text{ m}^3/\text{h}$$

Thuro and Plinninger (1999) suggested a model given below for a transverse roadheader having cutterhead power of 132 kW:

$$ICR = (75.7 - 14.3 \cdot \ln(UCS)) \cdot t_3 \tag{7.6}$$

where t_3 is the power correction factor (assuming the effect of power on performance is linear: 200/132 = 1.52). By using this equation, ICR is estimated as

$$ICR = (75.7 - 14.3 \cdot \ln(65)) \cdot 1.52 = 24.3 \text{ m}^3/\text{h}$$

Since the roadheader will excavate through different strata with different rock mass properties, it would be helpful to develop a nomogram for the mine planners. It is possible to develop nomograms for all the ICR prediction models. However, the nomogram will be developed only for the model by Bilgin et al. (1996), since only the rock mass properties are taken into consideration by this model. The variation of ICR, estimated by using the model developed by Bilgin et al. (1996) is presented in Figure 7.14 for different UCS and RQD values. The engineers can use this figure for varying geological conditions and roadheader cutting power. The overall results of ICR predictions are presented in Table 7.8.

7.8.1.1.3 Estimation of the Daily Advance Rate

The daily advance rate (AR) can be estimated as follows:

$$AR = V_{\text{exc}}/A_{\text{face}} \tag{7.7}$$

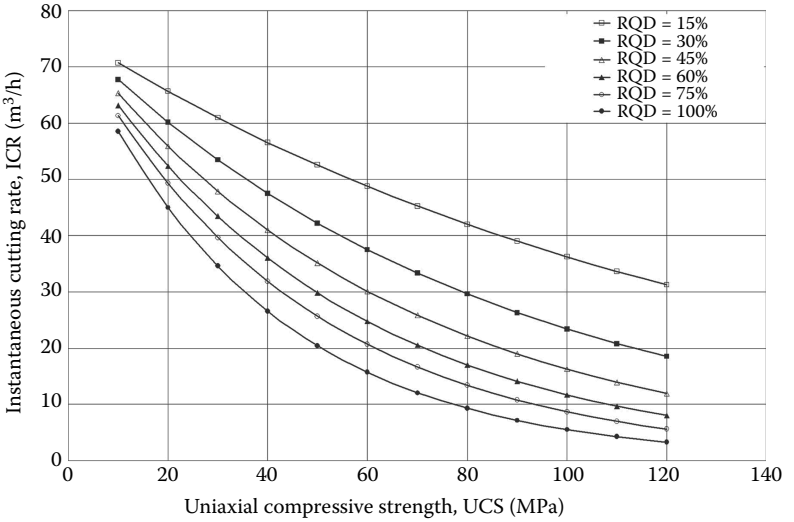

FIGURE 7.14
Variation of *ICR* estimated by using the model developed by Bilgin et al. (1996) for different *UCS* and *RQD* values. (From Bilgin, N., Yazici, S., Eskikaya, S., 1996. *Proceedings of the International Eurock '96 Symposium*, Torino, pp. 715–720.)

where
AR = daily advance rate (m/day)
V_{exc} = daily excavation volume (m³/day)
A_{face} = cross-section area of gallery (m²)

The daily excavation volume (V_{exc} in m³/day) can be estimated as follows:

$$V_{exc} = ICR \cdot MUT \cdot S_{day} \cdot H_{shift} \tag{7.8}$$

TABLE 7.8
Summary of *ICR* Predictions

	Roadheader Type	
Prediction Model	**Axial**	**Transverse**
McFeat-Smith and Fowell (1977, 1979)	30–40	—
Gehring (1989)	13.5	22.2
Bilgin et al. (1996)	30.0	—
Thuro and Plinninger (1999)	—	24.3

where
ICR = instantaneous cutting rate (m^3/h)
MUT = machine utilization time (%)
S_{day} = number of shifts in a day (shifts/day)
H_{shift} = shift time (hours/shift)

MUT determines the percentage of time used only for excavation (excluding stoppages) over in a whole shift (stoppages + excavation time). *MUT* depends on different operational, mining, and organizational parameters; it is usually between 25% and 40% for gallery excavation with steel set supports. In the remaining times, there would be some stoppages due to support, muck transportation, water drainage, machine breakdowns, and other similar reasons.

Variation of the daily *AR* with *MUT* is presented with a 14 m^2 of cross-section area in Figure 7.15 for the given conditions: a working pattern of 8 h/shift—3 shifts/day, *UCS* of 65 MPa, *RQD* of 40%, axial roadheader with a weight of 50 tons, and cutterhead power of 200 kW (average *ICR* of 30 m^3/h based on the model by Bilgin et al. (1996)). According to this figure, 15–24 m/day advance rates are possible in the field. The advance rates may be higher for transverse-type roadheaders.

Assuming an average 30% of *MUT*, V_{exc} is estimated by using Equation 7.8:

$$V_{exc} = 30 \cdot 0.30 \cdot 3 \cdot 8 = 216 \text{ m}^3/\text{day}$$

By using Equation 7.7, *AR* is estimated as

$$AR = 216/14 = 15.4 \text{ m/day}$$

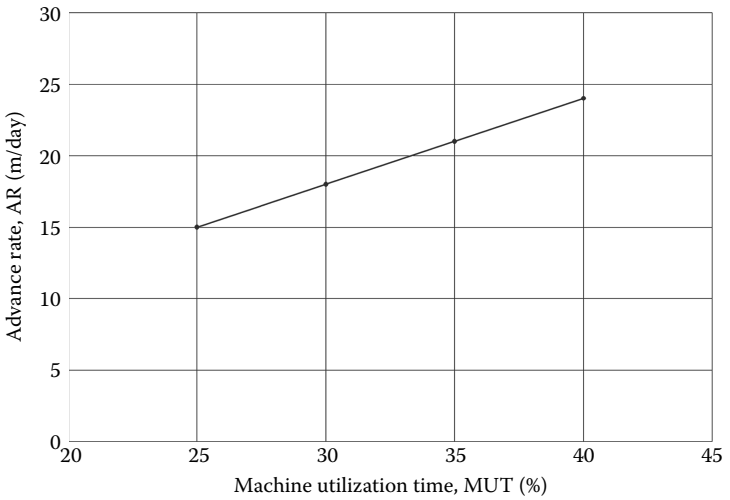

FIGURE 7.15
Variation of daily *AR* with *MUT* for 14 m^2 of cross-section area.

7.8.1.1.4 Estimation of Cutter (Tool) Consumption Rate (TCR)

Not only the excavation rates and discontinuities, but also tool consumption rates (TCRs) determine the excavation performance and costs. To judge precisely the cuttability of formation, TCRs should also be predicted. TCR for any type of drag-type tool (conical or radial) can be estimated as follows (Ozdemir 1998):

$$TCR = K_1 \cdot K_2 \cdot CAI/4 \tag{7.9}$$

where

TCR = tool consumption rate for excavation of unit volume of rock (tools/m^3)
CAI = Cerchar abrasivity index of rock
K_1 = coefficient varying between 1 and 1.2 related to cutterhead rotation velocity (can be taken as 1 for fast rotations)
K_2 = coefficient varying between 1 and 0.85 related to water spraying for toll cooling or dust suppression (can be taken as 0.85 for water utilization)

CAI of the marl is 0.65. Assuming that the cutterhead is usually rotating in fast mode and water spraying is used, TCR is estimated as follows:

$$TCR = 1.0 \cdot 0.85 \cdot 0.65/4 = 0.138 \text{ tools/m}^3$$

Copur et al. (1997, 1998a,b) developed a model of predicting TCR for transverse roadheaders equipped with conical tools excavating soft rocks of basically evaporitic origin having UCS values lower than 60 MPa as follows:

$$TCR = 897 \cdot RCI^2 + 6.18 \cdot RCI \tag{7.10}$$

$$RCI = UCS/(P_{\text{inst}} \cdot W \cdot CHD) \tag{7.11}$$

where

TCR = tool consumption rate for excavation of unit volume of rock (tools/m^3)
RCI = roadheader tool consumption index (MPa/[kW × tons × m])
UCS = uniaxial compressive strength of the rock (MPa)
P_{inst} = installed cutterhead power (kW)
CHD = cutterhead diameter (m)

Assuming that the cutterhead diameter is 1.0 m, TCR is estimated as follows:

$$RCI = 65/(200 \cdot 50 \cdot 1) = 0.0065 \quad (\text{MPa}/[\text{kW} \times \text{tons} \times \text{m}])$$

$$TCR = 897 \cdot 0.0065^2 + 6.18 \cdot 0.0065 = 0.078 \text{ tools/m}^3$$

Ocak et al. (2007) developed a model of predicting conical TCRs for a transverse roadheader with weight of 74 tons and cutterhead power of 170 kW as follows:

$$TCR = 0.001 \cdot UCS^{0.9765} \tag{7.12}$$

Using this equation, *TCR* is estimated as being 0.059 tools/m^3.

It is a known fact that when the *TCR* exceeds 0.5 tools/m^3, tool breakages and tool wear increases rapidly; tool forces on worn tools increase tremendously (Copur et al. 1997, 1998a,b; Copur 1999). This reduces the benefits of the project or increases the cost per cubic meter of excavation; in many cases, mechanized excavation is left in favor of another method of excavation. If the TCRs are between 0.2 and 0.5 tools/m^3, the project cost is critical. If the excavation lengths are very short, then this much tool consumption can be compromised and project costs should be reviewed. If the *TCR* is lower than 0.2 tools/m^3, many times, there would be no problem in excavation.

7.8.2 Numerical Example on Predicting Performance of a Transverse Roadheader Excavating Evaporitic Rocks

A roadheader with a transverse cutterhead having 50 tons of weight, 200 kW of cutterhead power, and 1.0 m of cutterhead diameter is considered for excavation of trona mineral. The average *UCS* of trona is 30 MPa. Estimate the *ICR* and cutter consumption rate by using the methods developed by Copur et al. (1997, 1998a,b).

7.8.2.1 Solution of Numerical Example 7.8.2

Copur et al. (1997, 1998a,b) developed a model for predicting net cutting rates of transverse-type roadheaders excavating evaporitic minerals:

$$ICR = 27.511 \cdot e^{0.0023 \cdot RPI} \tag{7.13}$$

$$RPI = P_{inst} \cdot W / UCS \tag{7.14}$$

where

ICR = instantaneous cutting rate (m^3/h)
RPI = roadheader penetration index (kW · tons/MPa)
P_{inst} = installed cutterhead power (kW)
W = roadheader weight (tons)
UCS = uniaxial compressive strength of the rock (MPa)

ICR is estimated as 59 m^3/h by substituting the given values into Equations 7.13 and 7.14:

$$RPI = (200 \cdot 50)/30 = 333 \text{ (kW} \times \text{tons/MPa)}$$

$$ICR = 27.511 \cdot e^{0.0023 \cdot 333} = 59 \text{ m}^3/\text{h}$$

Copur et al. (1997, 1998a,b) developed a model for predicting *TCR* for transverse roadheaders equipped with conical tools. These roadheaders excavate soft rock of basically evaporitic origin having *UCS* values lower than 60 MPa, as given in the previous numerical examples in Equations 7.10 and 7.11:

$$RCI = 30/(200 \cdot 50 \cdot 1.0) = 0.003 \text{ (MPa/[kW} \times \text{tons} \times \text{m])}$$

$$TCR = 897 \cdot 0.003^2 + 6.18 \cdot 0.003 = 0.027 \text{ tools/m}^3$$

References

Aker-Wirth. Product catalogues.

Balci, C., Demircin, M.A., Copur, H., Tuncdemir, H., 2004. Estimation of optimum specific energy based on rock properties for assessment of roadheader performance. *Journal of the South African Institute of Mining and Metallurgy*, 104(11):633–642.

Bilgin, N., 1983. Prediction of roadheader performance from penetration rates of percussive drills: Some applications to Turkish coalfields. *Proceedings of the Eurotunnel '83 Conference*, June 22–24, Basel, Switzerland, pp. 111–114.

Bilgin, N., Demircin, M.A., Copur, H., Balci, C., Tuncdemir, H., Akcin, N., 2006. Dominant rock properties affecting the performance of conical cutters and the comparison of some experimental and theoretical results. *International Journal of Rock Mechanics and Mining Science*, 43(1):139–156.

Bilgin, N., Dincer, T., Copur, H., 2002. The performance prediction of impact hammers from Schmidt hammer rebound values in Istanbul metro tunnel drivages. *Tunnelling and Underground Space Technology*, 17(3):237–247.

Bilgin, N., Kuzu, C., Eskikaya, S., Ozdemir, L., 1997. Cutting performance of jack hammers and roadheaders in Istanbul metro drivages. *Proceedings of World Tunnel Congress 97*, April 12–17, Vienna, Austria, pp. 455–460.

Bilgin, N., Seyrek, T., Shahriar, K., 1988. Golden horn clean-up contributes valuable data. *Tunnels and Tunnelling*, June:41–44.

Bilgin, N., Seyrek, T., Shahriar, K., 1990. Roadheaders glean valuable tips for Istanbul metro. *Tunnels and Tunnelling*, October:29–32.

Bilgin, N., Tuncdemir, H., Balci, C., Copur, H., Eskikaya, S., 2000. A model to predict the performance of tunneling machines under stressed conditions. *Proceedings of AITES-ITA 2000 World Tunnel Congress*, May 13–18, Johannesburg, pp. 47–53.

Bilgin, N., Yazici, S., Eskikaya, S., 1996. A model to predict the performance of roadheaders and impact hammers in tunnel drivages. *Proceedings of the International Eurock '96 Symposium*, Torino, pp. 715–720.

Breeds, C.D., Conway, J.J., 1992. Rapid excavation. *SME Mining Engineering Handbook*, ed. Hartman, H.L. Vol. 2, 2nd ed., Chapter 22.1, pp. 1871–1907.

Copur, H., 1999. Theoretical and experimental studies of rock cutting with drag bits toward the development of a performance prediction model for roadheaders. PhD thesis, Colorado School of Mines, p. 361 .

Copur, H., Ozdemir, L., Rostami, J., 1998a. Roadheader applications in mining and tunneling industries. *SME Annual Meeting*, Preprint No: 98-185, p. 5.

Copur, H., Ozdemir, L., Rostami, J., 1998b. Roadheader applications in mining and tunneling. *Mining Engineering*, 50(3):38–42.

Copur, H., Rostami, J., Ozdemir, L., Bilgin, N., 1997. Studies on performance prediction of roadheaders. *Proceedings of the 4th International Symposium on Mine Mechanization and Automation*, Brisbane, Queensland, Australia, pp. A4-1–A4-7.

Copur, H., Tuncdemir, H., Bilgin, N., Dincer, T., 2001. Specific energy as a criterion for the use of rapid excavation systems in Turkish mines. *The Institution of Mining and Metallurgy, Transactions Section-A Mining Technology*, 110:A149–A157.

Dincer, T., Bilgin, N., Copur, H., Erdogan, M., Eyuboglu, R., 2005. Effect of geological factors on performance of a roadheader in a tunnel excavation. *Proceedings of the Symposium on Geology of Istanbul*, December 16–18, Istanbul (in Turkish).

Dosco. Product catalogues.

Ebrahimabadi, A., Goshtasbi, K., Shahriar, K., Seifabad, M.C., 2011. A model to predict the performance of roadheaders based on the rock mass brittleness index. *Journal of the Southern African Institute of Mining and Metallurgy*, 111:355–364.

Eickhoff. Product catalogues.

Farmer, I.W., Garrity, P., 1987. Prediction of roadheader cutting performance from fracture toughness considerations. *Proceedings of the 6th International Congress on Rock Mechanics*, Montreal, Canada, Vol. 1, pp. 621–624.

Fowell, R.J., Johnson, S.T., 1982. Rock classification and assessment for rapid excavation. *Proceedings of the Symposium on Strata Mechanics*, Newcastle upon Tyne, pp. 241–244.

Gehring, K.H., 1989. A cutting comparison. *Tunnels and Tunnelling*, November:27–30.

Heiniö, M., 1999. *Rock Excavation Handbook*. Sandvik Tamrock Corp., p. 364.

IBS. Product catalogues.

Kennametal. Product catalogues.

Kirkbride, M.A., 2000. Prediction of roadheader performance: A geological assessment scheme. *Proceedings of Mine Planning and Equipment Selection*, eds. Panagiotou, G., Michalakopoulos, T. Athens, pp. 607–612.

Kogelmann, W.J., 2008. Multi-tool miner for all rock conditions. *SME Annual Meeting*, February 24–27, Salt Lake City, Preprint No: 08-061, p. 4.

Kogelmann, W.J., Jaeger, M., Dietrich, W., Greinacher, J., Ertmer, K., 2003. New and safe European tunneling techniques. *Proceedings of the Rapid Excavation and Tunneling Conference*, New Orleans, LA, pp. 1197–1211.

Kogelmann, W.J., Schenck, G.K., 1982. Recent North American advances in boom-type tunnelling machines. *Proceedings of Tunnelling 82*, London, pp. A155–A165.

Matsui, K., Shimada, H., 1993. Rock impact hardness index for predicting cuttability of roadheader. *Proceedings of Mine Planning and Equipment Selection*, October 18–20, Istanbul, Turkey, pp. 509–514.

Matsui, K., Shimada, H., 1994. Prediction of machine performance in mine tunnel drivage. *Proceedings of the 2nd International Symposium on Mine Mechanization and Automation*, June 7–10, Lulea, Sweden, pp. 265–270.

McFeat-Smith, I., Fowell, R.J., 1977. Correlation of rock properties and the cutting performance of tunneling machines. *Proceedings of the Conference on Rock Engineering*, ed. Attawell, P.B. April 4–7, Newcastle, UK, pp. 581–602.

McFeat-Smith, I., Fowell, R.J., 1979. The selection and application of roadheaders for rock tunnelling. *Proceedings of the Rapid Excavation and Tunneling Conference*, Atlanta, Vol. 1, pp. 261–279.

Menzel, W., Frenyo, P., 1981. Teilschnitt-Vortriebsmaschinen mit Langs—und mit Querschneidkopf (Partial-face excavation machines with longitudinal and transverse cutting head). *Glückauf*, 117(5):284–287.

Mitsui Miike. Product catalogues.

Natau, O., Mutschler, T.H., Lempp, C.H., 1991. Estimation of the cutting rate and the bit wear of partial-face tunnelling machines. *Proceedings of the 7th ISRM Congress*, September 16–20, Aachen, pp. 1591–1595.

Ocak, I., Bilgin, N., 2010. Comparative studies on the performance of a roadheader, impact hammer and drilling and blasting method in the excavation of metro station tunnels in Istanbul. *Tunneling and Underground Space Technology*, 25:181–187.

Ocak, I., Eyigun, Y., Cinar, M., Nahya, T., 2007. Investigation into roadheader excavation performance and pick consumption used in Kadikoy–Kartal metro tunnels. *Proceedings of the 2nd Symposium on Underground Excavations for Transportation*, Turkish Chamber of Mines, Istanbul, Turkey, pp. 199–206.

Ozdemir, L., 1997. *Mechanical Mining Short Course*. Section: "Roadheaders" by L. Ozdemir, March 19–21, Colorado School of Mines, Golden, Colorado.

Ozdemir, L., 1998. *Mechanical Tunneling, Raise Boring and Shaft Drilling. Short Course*. February 21–22, Colorado School of Mines, Golden, Colorado.

Rostami, J., Ozdemir, L., Neil, D.M., 1994. Performance prediction: A key issue in mechanical hard rock mining. *Mining Engineering*, 11:1263–1267.

Sandbak, L.A., 1985. Roadheader drift excavation and geomechanical rock classification at San Manuel, Arizona. *Proceedings of the Rapid Excavation and Tunneling Conference*, New York, Vol. 2, pp. 902–916.

Sandvik. Product catalogues.

Sanyhe. Product catalogues.

Schaeff. Product catalogues.

Thuro, K., Plinninger, R.J., 1999. Roadheader excavation performance—Geological and geotechnical influences. *Proceedings of the 9th ISRM Congress*, Paris, August 25–28, 1999, pp. 1241–1244.

Thuro, K., Plinninger, R.J., 2003. Hard rock tunnel boring, cutting, drilling and blasting: Rock parameters for excavatability. *Proceedings of ISRM 2003*, pp. 1227–1233.

This page intentionally left blank

8

Impact Hammers

8.1 Background

Hydraulic impact hammers have been used widely in mining industry and civil engineering applications since 1960 (Rodford 1974; Pelizza et al. 1994). Almost 20 km of metro tunnels were driven in Istanbul with impact hammers, since the initial capital investment was relatively lower and rock formations were highly fractured in some zones; rock quality designation (RQD) values ranging from 0 to 80. The impact hammers may be mounted in any type of excavator and operated easily. A typical impact hammer working in a tunnel is seen in Figure 8.1.

8.2 Working Principles and Operational Features

It is a well-known fact that mechanical impact offers several advantages over other continuous methods of excavation. These advantages are enhanced when the impact energy is increased to very high levels. The working principle of a modern hydraulic hammer is simple. There is a piston moving up and down and striking against the tool end. To produce big energy pulses during downwards strokes, the hammer is equipped with an accumulator that is able to supply needed oil volume in a very short time. The accumulator is charged continuously by a hydraulic pump. Different research works demonstrated that specific energy, defined as the energy to break the unit volume of the rock, is inversely proportional to below energy (Wayment and GrantMyre 1976). Since then, continuous works have being done to increase piston speed and piston weight, or hammer operating weight, to have higher blow energies. The relationships between impact energy, specific energy, piston weight, and velocity are given in Equations 8.1 and 8.2 (Hughes 1974).

$$SE = k/\sqrt{E_i} \tag{8.1}$$

FIGURE 8.1
An impact hammer working in a tunnel excavation.

$$E_i = MV^2/2 \tag{8.2}$$

where
SE = specific energy
E_i = impact or blow energy
M = weight of piston
V = piston velocity
k = a constant

Hydraulic impact hammers may be mounted on many different types of excavators and are, thus, also connected into many different hydraulic systems. It is very important for safe and efficient operations to match the size of the carrier/excavator to the weight and power of the hammer. The excavator/carrier is a more costly unit than the breaker and that is why the manufacturers of the hydraulic hammers build hammers that have high blow energies relative to their weights (Wyllie 1985).

The first comprehensive work on the theoretical performance prediction of the hydraulic hammers was done by Evans (1974). He pointed out that the susceptibility of the rock to impact breakage was a function not only of compressive strength but of tensile strength also. Compressive strength alone was found to be a misleading criterion. Formulae were given for calculating the size of "below" required for breaking a piece of rock.

Hughes (1974) reported that compared with pneumatic hammers, hydraulic jackhammers have a relatively heavier hammer, working at a relatively slower speed. Pneumatic hammers are the noisiest equipment in the mine, around 80% of the noise deriving from its exhaust. Hydraulic hammers have no exhaust and are less noisy.

FIGURE 8.2
An impact hammer breaking oversized boulders.

Hydraulic impact hammers can be used in several phases of mining, such as breaking oversized boulders in quarries and open pit mines and trenching when the ground is too hard to be removed with an excavator. An impact hammer used for breaking oversized boulders is seen in Figure 8.2. Driving tunnels or roadways in fractured zones is also very frequent and goes back to the 1970s in the European Coal Mines (Gaskell and Phillips 1974; Levetus and Cagnioncle 1974; Rodford 1974). Since then, the use of hydraulic impact hammers has gained worldwide acceptance both in mining and civil engineering applications. This technical process makes available, very highly powered machines with impact energy values of up to more than 12 kJ/blow (Pelizza et al. 1994). Pelizza reported that hydraulic hammers were widely used in Italy in the construction industry, mainly due to the stringed Italian regulations on the use and transportation of explosives. Support for selecting hydraulic impact hammers in Italian tunneling operations were cited as: the tunnels were usually driven in heavily altered and geologically disturbed zones, the geomechanical characteristics of the rock could remarkably vary along the tunnel axis, and tunnel boring machines (TBMs) and roadheaders might have discontinuous and uneconomical performance.

There is no standard that may be used to compare the performance of hydraulic hammers. The technical data in sales literature are inconsistent and sometimes even misleading. However, if the basic information of different hammers is analyzed in the same way, quite competent comparisons can be made. The ratio of output power to input power is the hammer efficiency and may be used to compare the efficiency of hydraulic hammers. The relevance is shown in Equations 8.3 through 8.5 below (Tuncdemir 2008).

$$Pinput = Q \cdot p \tag{8.3}$$

$$Poutput = n \cdot Ei \tag{8.4}$$

$$\eta = Poutput/Pinput \tag{8.5}$$

where
$Pinput$ = input power, kW
Q = oil flow, m^3/s
p = oil pressure, kN/m^2
$Poutput$ = output power, kW
Ei = single blow energy, kN m
n = blow frequency, blow/s
η = Hammer efficiency

8.3 Classification and Technical Features

Major manufacturers of impact hammers with upper and lower operating parameters are given in Table 8.1.

Tuncdemir (2007) analyzed statistically the data of 600 impact hammers available in the industry, and found the following equations which are very useful in proper selection of impact hammers in special applications as will be seen in numerical example (Section 8.4).

$$Ei = 2.4718 \cdot Wham - 27.774 \tag{8.6}$$

$$EWmax = 0.015 \cdot Wham + 3.2343 \tag{8.7}$$

$$EWmin = 0.0094 \cdot Wham + 1.3485 \tag{8.8}$$

$$Poutput = 0.0187 \cdot Wham + 7.1016 \tag{8.9}$$

$$Pinput = 0.0187 \cdot Wham + 11.837 \tag{8.10}$$

where
Ei = single blow energy, J
$Wham$ = operational weight of impact hammer, kg
$EWmax$ = maximum recommended weight of excavator, t
$EWmin$ = minimum recommended weight of excavator, t
$Poutput$ = output power, kW
$Pinput$ = input power, kW

TABLE 8.1

Major Manufacturer of Impact Hammers with, Upper and Low Operating Parameters

Company	Model No.	Hammer Weight (kg)	Carrier Weight (t)	Oil Flow (L/min)	Maximum Blow Frequency (bpm)	Impact Energy (J)	Maximum Operating Pressure (bar)
Atlas Copco	SBC 60	30	0.4–0.7	11–14	1500	60	150
	HBC 4000HD	2470	25–40	110–200	480	4000	160
BTI	TB135ME	110	1–4	20–35	1150	230	147
	TB2080X	3660	34–68	240–320	510	7306	190
Caterpillar	H45	130	1–3	20–50	2200	137	115
	H180s	3800	40–80	220–300	470	5906	160
Continental	RH100	100	1–3	25	–	–	100
	RH8200	8200	80–100	480	270	–	180
Daemo	DMB S150-V	170	1–4	25–40	1000	490	100
	DMB S5000-V	3700	40–55	250–320	320	10,780	180
Dainong	K20-II	140	1–3	15–20	1300	280	120
	T180	3900	40–80	240–350	430	11,000	155
Dehaco	DHB 35	35	0.3–0.9	8–16	1600	–	100
	DHB 5205	4500	44–60	250–320	520	–	180
Euroram	RM45	88	–	13–33	1300	185	115
	RM215	7425	57–110	330–425	425	15,250	160
FRD-Furukawa	F1	66	1–2	9–20	1250	160	140
	HB100GLN	6800	65–100	280–390	350	15,690	180
Huskie	HH100	75	1–2	26	1300	135	110
	HH8000	3000	31–58	290	370	11,000	190
Hy-Ram	690	75	1–2	30	1350	–	110
	805CS	3975	34–68	320	750	–	180
Indeco	MES 121W	80	1–3	12–30	1350	180	115
	MES12000HD-W	7150	45–120	325–420	420	14,000	160
Italdem	GK20 (hand)	19	–	15–20	1600	70	145
	GK3400	3300	40–50	280–300	600	8000	190
JCB	HM 70	72	0.6–1	15–28	2200	91	120
	HM 2950	2950	35–55	210–310	600	6000	150
Kent	KF2	93	2–3	16–30	1200	132	140
	KF70Qt	4670	45–75	250–340	320	7130	180
Komatsu	JKHB50	68	1–3	15–20	1000	–	120
	JKHB2000	2600	30–40	150–200	1000	–	180
Korota	K-5	50	1–2	15–25	1100	170	100
	K-300	4000	35–48	210–230	450	–	180
Krupp	HM 60	75	1–3	15–35	1700	–	120
	HM4000/V	6900	65–120	300–480	460	–	190
Montabert	30 (Metro-Sil.)	85	0.7–2	12–28	1530	165	135
	V5 5 (Metro-Sil.)	3170	32–55	240–320	1045	8500	165

continued

TABLE 8.1 (continued)

Major Manufacturer of Impact Hammers with, Upper and Low Operating Parameters

Company	Model No.	Hammer Weight (kg)	Carrier Weight (t)	Oil Flow (L/min)	Maximum Blow Frequency (bpm)	Impact Energy (J)	Maximum Operating Pressure (bar)
NPK	E-102	39	0.5–0.5	10–12	1100	–	150
	E-260A	7700	80–110	300–400	330	–	210
Okada	OKB300	77	1–3	15–25	1200	–	150
	OKB330	5400	45–50	280–380	340	–	180
Rammer	Piccolo City	80	1–2	15–25	1600	130	100
	G130 City	6600	60–100	300–400	400	12,500	140
Soosan	SB-40	250	3–10	30–45	750	1085	130
	SB-150	3850	40–70	210–250	320	13,558	180
Stanley	MB156	79	1–2	15–38	1200	237	144
	MB100EXS	3991	40–65	208–302	320	16,272	186
Tabe	AGB 75	80	–	18–20	1200	–	120
	AGB 30	3300	–	205–245	550	–	190
Taeshin	TB 30G	170	3–4	24–40	1100	680	130
	TB 550G	4050	35–55	220–310	450	16,320	180
Tramac	30	85	0.7–2	12–28	1530	165	135
	V65	5800	45–75	380–420	950	–	165

8.4 Performance Prediction and Practical Examples for Impact Hammers

A contractor is always interested in predicting the machine performance prior to starting a tunnel project that will definitely define the tunnel's drivage economy. A research team of several staff and students collected data in Istanbul metro tunnels from 1994 to present days (Dincer 1999). A detailed work study was realized and analyzed to make some recommendations to increase tunneling efficiency. Tunneling performance data collected by many research students, during seven years of in situ site investigations in Istanbul Metro were analyzed statistically and a model to predict the net breaking rate in m^3/h was developed. In that study, detailed in situ studies and accumulated data led to a statistical model for the prediction of instantaneous or net breaking rate of the hydraulic impact hammers and the following prediction equation was driven (Bilgin et al. 1996, 1997, 2002).

$$IBR = 4.24 \cdot P \cdot (RMCI)^{-0.567} \tag{8.11}$$

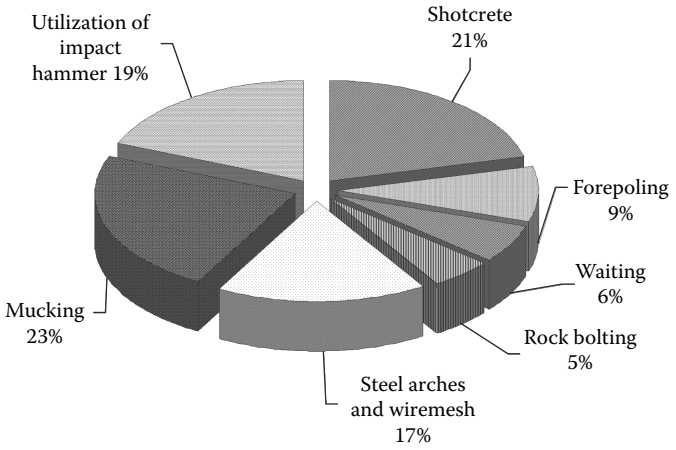

FIGURE 8.3
Overall performances of tunnel drivages in metro tunnels phase 2.

$$RMCI = \sigma_c \cdot (RQD/100)^{2/3} \tag{8.12}$$

where
IBR = instantaneous or net breaking rate, m^3/h
P = cutting or breaking power of the hydraulic impact hammer, HP
RMCI = rock mass cuttability index, MPa
σ_c = uniaxial compressive strength, MPa
RQD = rock quality designation, %

A typical work study diagram for impact hammers is seen in Figure 8.3 for NATM applications in Istanbul Metro drivages. As noted from this figure, impact utilization is lower, as 19% is due to time spent for mucking. That is why impact hammers usually are used with gathering arms to ease mucking.

Further studies into applications of impact hammers were carried out by Tuncdemir (2008) and Aksoy (2009). Tuncdemir correlated RMR (rock mass rating) and Aksoy developed a model to predict the instantaneous breaking rate for weak rocks from block punch index.

8.4.1 A Numerical Example to Calculate Hammer Efficiency

Calculate output power, input power, and hammer efficiency for impact hammer, the technical characteristics are given below.

Impact rate = 500 impact/min (8.3 impacts/s)

Impact energy = 3500 J (3.5 kN m)

Oil supply required = 160 L/min (2.66×10^{-3} m^3/s)

Operating pressure = 140 bar (14,000 kN/m^2)

8.4.1.1 Solution

$Pinput = Q \cdot p$
$Pinput = 2.66 \times 10^{-3} \times 14{,}000$
$Pinput = 37.3$ kW
$Poutput = n \cdot Ei$
$Poutput = 8.3 \cdot 3.5$
$Poutput = 29.2$ kW
$\eta = Poutput/Pinput$
$\eta = 29.3/37.3$
$\eta = 78\%$

8.4.2 A Numerical Example to Calculate Impact Hammer Performance

A tunnel having a length of 1200 m and cross section of 14 m^2 will be excavated in a mudstone formation, having compressive strength of 80 MPa and RQD value of 40%. The job organization will be arranged to have two shifts of 10 h/day. The Montabert BRH 250 having an output power of 33 HP will be used with a suitable excavator.

1. Calculate net cutting rate of the impact hammer.
2. Calculate in how many days the tunnel may be excavated.
3. Discuss the possibility of increasing the excavation efficiency.

8.4.2.1 Solution

1. Instantaneous or net cutting rate may be calculated as in Equations 8.11 and 8.12

   $IBR = 4.24 \cdot P \cdot (RMCI)^{-0.567}$
   $RMCI = \sigma_c \cdot (RQD/100)^{2/3}$
   $RMCI = 80 \cdot (40/100)^{2/3}$
   $RMCI = 40$ MPa
   $IBR = 4.24 \cdot 33 \cdot (43.4)^{-0.567}$
   $IBR = 17$ m^3/h

2. The job duration in (m) may be calculated, as in Equations 8.13 and 8.14.

$$J_D = T_L/(IBR \cdot H_T/T_A) \tag{8.13}$$

$$H_T = M_{UT} \cdot S_H \tag{8.14}$$

In these equations
J_D = job duration, days
T_L = tunnel length, 1000 m
IBR = instantaneous breaking rate, 17 m^3/h
T_A = tunnel cross-section area, 14 m^2
M_{UT} = machine utilization time, 20%
S_H = daily shift hour, 20 h
H_T = daily hammering time, 20 × 0.2 h or 4 h/day

$$J_D = 1000/(17.4/14)$$

$$J_D = 206 \text{ days}$$

The excavation of the tunnel is calculated to be finished in 206 days.

3. Possibility of increasing the excavation efficiency.

As seen in Figure 8.3 time spent for muck transportation is 23%. Which means that if an impact hammer has a gathering arm, impact hammer utilization time may be doubled, meaning that time spent for tunnel excavation may decrease to around 100 days.

8.4.3 A Numerical Example to Select a Proper Hydraulic Hammer and Excavator for a Specific Job

A collector tunnel will be constructed under the TEM highway in Istanbul. A tunnel cross section is very small as seen in Figure 8.4, with excavation dimensions of 2.5 × 2.6 m and final dimensions of 1.95 × 1.8 m. A hydraulic hammer is recommended to be used due to safety regulations. A proper hydraulic hammer with a suitable excavator needs to be selected and calculations of daily advance rates. The rock formation has σ_c = 20 MPa and RQD values of 20% (Bilgin et al. 2010).

8.4.3.1 Solution

The main restriction for this application is the size of excavator to be fitted inside of the tunnel. A Bobcat 425 Excavator having maximum height of 2.4 m and width of 1.9 m is chosen for this reason.

The excavator chosen has a weight of 3 t. For excavator stability as determined in Equation 8.8 optimum operational weight of the impact hammer should be 176 kg. The manufacturer claims that the Bobcat 425 may be used with hammers having weight up to 335 kg. Equation 8.9 gives the hammer output power of 13.37 kW or 17.9 HP.

Using Equations 8.12 and 8.11, *RMCI* and *IBR* values are computed as 17.3 MPa and 15.6 m^3/h. If hammer utilization time is 20% and the daily

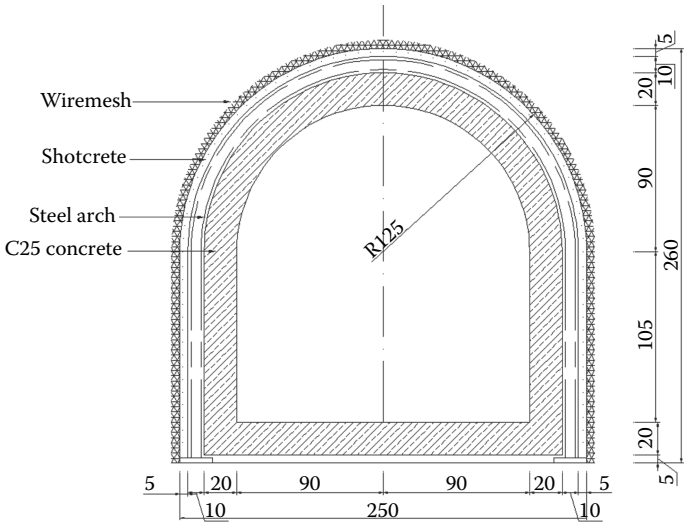

FIGURE 8.4
Cross section of TEM tunnel.

excavation time is 10 h, a daily net hammering time of 2 h is calculated which makes a daily production rate of $13.6 \times 2 = 31.2$ m^3/day. The cross-section area of the tunnel is 5.83 m^3. The daily advance rate is calculated as 31.2/5.83 = 5.4 m/day.

8.4.4 A Numerical Example to Select a Proper Hydraulic Hammer and Excavator for a Specific Job

A tunnel will be excavated having a cross-section area of 150.11 m^2, in a rock formation with σ_c of 63.1 MPa and *RQD* of 100%. The tunnel will be excavated in two sections. Dimensions of the crown and invert are given in Figure 8.5. The contractor wants to have 5 m of daily advance rate. Select the proper excavator and impact hammer.

8.4.4.1 Solution

For different weights of excavators, maximum and minimum operating weights of impact hammers are calculated using Equations 8.7 and 8.8. The output power of impact hammers are found using Equation 8.9. The net or instantaneous breaking rates are calculated using Equations 8.11 and 8.12 for part 1, or the invert which has a bigger cross section than the crown or part 2. All the calculated values are tabulated in Table 8.2. As seen for this table, two excavators having weights changing between 50 and 78t; hammers with an operational weight of 5 t or having output of 101 kW is necessary for upper and lower sections of the tunnel.

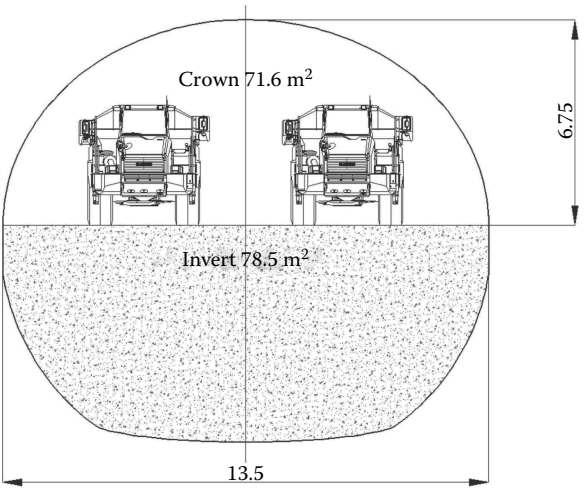

FIGURE 8.5
Cross section of the power tunnel.

TABLE 8.2

Calculated Values for Relevant Impact Hammer Application Problem 8.4.3

Hammer Weight (tons)	Excavator Weight (t)		Hammer Output Power (kW)	Net Breaking Rate (m^3/h)	Estimated Daily Advance Rate (m/day) 8 h of Net Daily Hammer Time for Invert
	Max.	Min.			
3	49	30	64	34.7	3.7
4	64	40	82	44.3	4.7
5	78	50	101	54.5	5.8
6	94	60	128	69.1	7.4

References

Aksoy, C.O. 2009. Performance prediction of impact hammers by block punch index for weak rock masses, *Int. J. Rock Mech. Min. Sci.*, 46:1383–1388.

Bilgin, N., Çopur, H., Balcı, C. 2010, Study for Eze–Foy construction company on tunnel excavation techiques for a collector tunnel to be constructed under TEM highway in Istanbul, ITU, 41.

Bilgin, N., Dinçer, T., Çopur, H. 2002. The performance prediction of impact hammers from Schmidt hammer rebund values in Istanbul metro tunnel drivages. *Tunnel. Underground Space Technol.*, 17:237–247.

Bilgin, N., Kuzu, C., Eskikaya, S. 1997. Cutting performance of rock hammers and roadheaders in Istanbul Metro drivages. *Proceedings, Word Tunnel Congress'97, Tunnels for People*, Balkema, pp. 455–460.

Bilgin, N., Yazıcı, S., Eskikaya, S. 1996. A model to predict the performance of roadheaders and impact hammers in tunnel drivages. *Proceedings, Eurock '96*, Balkema, pp. 715–720.

Dincer, T. 1999. The effect of some rock properties on performance of roadheaders and impact hammers. PhD thesis, Istanbul Technical University, p. 108.

Evans, I. 1974. Energy requirements for impact breakage of rocks. *Proceedings, Fluid Power Equipment in Mining, Quarrying and Tunnelling*, IMM, London, pp. 1–8.

Gaskell, J., Phillips, R. A. 1974. The Gullick Dobson impact ripper. *Proceedings, Fluid Power Equipment in Mining, Quarrying and Tunneling*, IMM, London, pp. 73–82.

Hughes, H. M. 1974. The hydraulic hammer in coal mining. *Proceedings, Fluid Power Equipment in Mining, Quarrying and Tunnelling*, IMM, London, pp. 83–88.

Levetus, F. B., Cagnioncle, G. 1974. Completely hydraulic rotary-percussive rock drills. *Proceedings, Fluid Power Equipment in Mining, Quarrying and Tunnelling*, IMM, London, pp. 67–78.

Pelizza, S., Patrucco, M., Benedetto, G. 1994. Workplace environmental conditions and innovative Tunnel driving techniques. *Proceedings, Tunneling and Ground Conditions*, Balkema, pp. 617–623.

Rodford, I. G. 1974. Experience with impact units. *Proceedings, Fluid Power Equipment in Mining, Quarrying and Tunnellin*g, IMM, London, pp. 57–66.

Tuncdemir, H. 2008. Impact hammer applications in Istanbul metro applications. *Tunnel. Underground Space Technol.*, 23:264–272.

Wayment, W., Grantmyre, I. 1976. Development of high blow energy hydraulic impactor. *Proceedings, Rapid Excavation and Tunnelling Conference*, pp. 611–626.

Wyllie, B. 1985. Hydraulic breakers. *Int. Mining*, March:18–24.

9

Hard Rock TBMs

9.1 Classification, Working Principles, and Operational Features

Tunnel boring in hard rock has increased continuously since the 1950s, reaching several tens of meters of daily advance rates in competent rock. However, the success of mechanized tunneling is based on a continuous improvement of mechanical excavation during many years of engineering innovations. Pioneering works leading to the construction of modern TBMs include the work done by a Belgian engineer Joseph Maus in 1846 for Mount Cenis Tunnel; the work done by Charles Wilson in 1851 on using disk cutters was patented by Wilson in 1847; a TBM was designed by Beumound for the Chanel Tunnel; TBMs built by Wittaker for the Chanel Tunnel reached daily advance rates of 2.7 m in lower chalk near Folkestone; and a breakthrough by a TBM was designed by James S. Robbins in 1950, reaching daily advance rates of 30 m in limestone in the Humber Sewer Tunnel (Stack 1995; Maidl et al. 2008).

Hard rock TBMs may be classified as open type (open gripper, Kelly beam, or main beam), single shield, and double shield, with TBMs working in open and closed modes (EPB) in some special cases. The basic working principles of each type will be explained below.

9.1.1 Open-Type (Open Gripper, Kelly Beam, or Main Beam) TBMs

Open-type TBMs are often called gripper or main beam-type TBMs and are mainly suitable for competent rock or geological formations having little amount of geological discontinuities and water ingress. A general view of an open-type TBM is given in Figure 9.1 The cutterhead (2) of the TBM is equipped with disks pushed against the tunnel with hydraulic thrust cylinders. The transfer of this high thrust through the disk cutters creates fractures in the rock, causing chips to break away from the tunnel face. Typical views of the grooves opened by disk cutters are seen in Figure 9.2. A gripper system (1) pushes on the sidewalls of the tunnel and is locked in place whereas the thrust cylinders extend, allowing the advance of the TBM. After

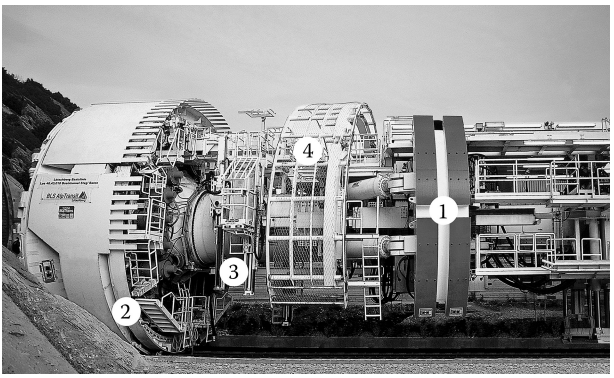

FIGURE 9.1
General view of an open-type TBM. (With the courtesy of Herrenknecht.)

completion of a boring stroke, the boring process is stopped and the machine is moved forward, with the TBM being stabilized by an additional support system. The excavated rock is collected through the openings (buckets) of the cutterhead and is discharged into the conveyor belt by special chutes located in the cutterhead. The belt conveyor transports the muck along the length of the TBM to the transfer conveyor between the TBM and the backup area. At the end of a stroke, the rear legs of the machine are lowered, the grippers and propel cylinders are retracted, which enables repositioning the gripper assembly for the next boring cycle. The grippers are extended, the rear legs are lifted, and boring begins again.

FIGURE 9.2
Grooves opened by disk cutters in a tunnel face. (Adapted from Eskikaya, Ş., Bilgin, N., 2000. Development of rapid excavation technologies for the Turkish mining and tunnelling industries. *NATO TU-Excavation Project Sponsored by SfS Programme*, Istanbul Technical University, p. 171.)

The tunneling performance of an open-type TBM essentially depends on the time required to install rock-supporting systems via ring erectors (4), rock bolts using drilling devices (3), meshes, shotcrete, steel arch, or any type of transfer support.

9.1.2 Single-Shield TBMs

Single-shield TBMs are used in hard rocks where geological discontinuities are frequent. As seen in Figure 9.3, the TBM is equipped with a shield (1) to protect personnel and machine from falling on rock until the tunnel lining or segments can be safely installed. The TBM is advanced by hydraulic thrust cylinders (2) pushing the cutterhead (4) toward the tunnel face. The transfer of high thrust forces through the rolling disk cutters creates fractures in the rock, causing chips to break away from the face. Only segment lining can be used with single-shield TBMs as tunnel support. The shield is supported by hydraulic thrust cylinders (2) on the last segment ring installed (3). The body of the machine is enclosed in a shield that is marginally smaller than the excavation diameter of the tunnel. The cutter head (4) is fitted with free rolling disk cutters. Muck bucket lips (5), which are positioned at some distance behind the disks, carry the extracted rock behind the cutting wheel. The excavated material can be brought to the surface by conveyers (6). As the cutterhead turns, a ring of hydraulic cylinders provides forward thrust through shoes that push against the tunnel lining. Boring and lining installation are performed sequentially.

9.1.3 Double-Shield TBMs

This type of machine is suited for boring long tunnels in hard rock where geological fault and shear zones exist.

A double-shield TBM consists of a rotating cutterhead, a sliding telescopic shield within the larger outer shield, a gripper shield, and a tail shield (Figure 9.4). In normal double-shield mode, the gripper shoes push against the

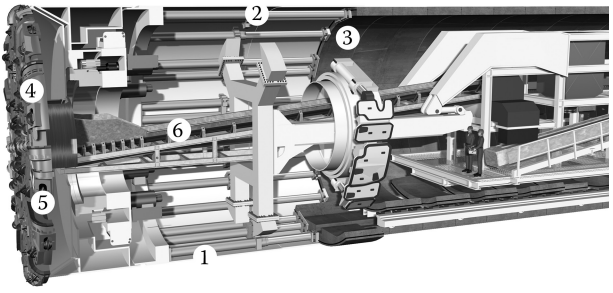

FIGURE 9.3
General view of a single-shield TBM. (With the courtesy of Herrenknecht.)

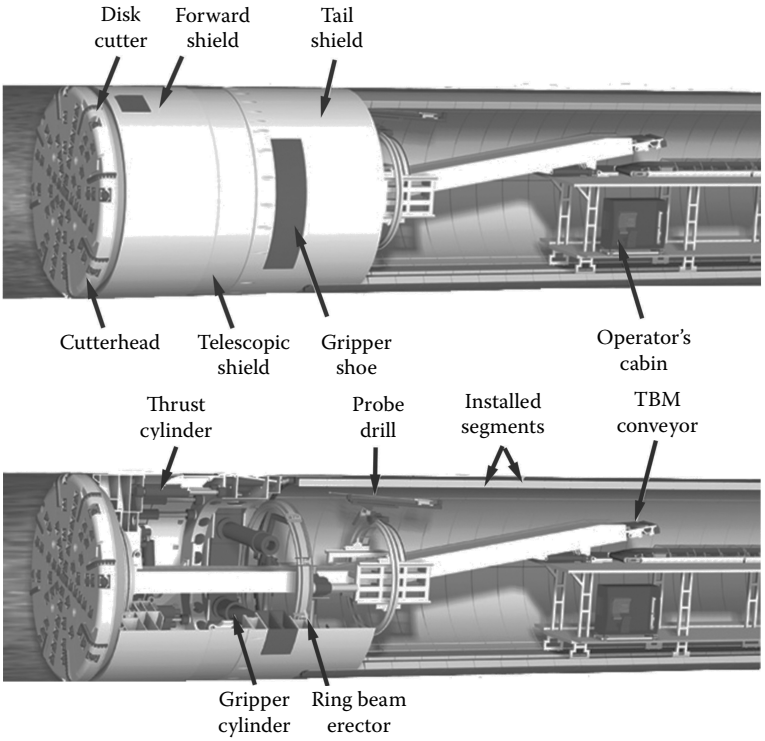

FIGURE 9.4
General view of a double-shield TBM. (With the courtesy of Robbins)

tunnel walls and thrust cylinders are then extended to push the cutterhead forward. The rotating cutterhead cuts the rock. The telescopic shield extends as the machine advances protecting the TBM from the ground surrounding it. The gripper shield remains stationary during boring. Any type of support can be used with double-shield TBMs, but mostly, segmental lining is used. A segment erector is fixed to the gripper shield allowing precast segments to be erected while the machine is boring. On completion of a thrust stroke, the gripper shoes are retracted and the rear section of the machine is pushed against the front shield by the auxiliary thrust cylinders. This changeover phase lasts only for a few minutes and then the next section of the tunnel can be excavated, increasing machine utilization time (*MUT*) of the TBM.

If the ground becomes too weak to support the gripper shoe pressure, the machine is operated in "single-shield mode." Auxiliary thrust cylinders are located in the gripper shield. In single-shield mode, they transfer the thrust from the gripper shield to the tunnel lining. Since the thrust is transferred to the tunnel lining, it is not possible to erect the lining simultaneously with boring. In the single-shield mode, tunnel boring and tunnel lining erection are sequential operations.

9.1.4 Single-Shield TBMs Working in Open and Closed Modes (EPB Mode)

Earth pressure balance (EPB) TBMs are mainly soft ground machines and they are dealt in detail in Section 10.5 of this book. However, in some cases where unstable tunnel face conditions exist only in some parts of the tunnel route, they are designed to work in closed (EPB) mode or in open mode as a single shield in the area where the rock is competent.

In unstable geological conditions, losses in stability of the tunnel face or surface settlements are prevented by creating a support pressure. The rock excavated by the cutters (1) falls through the openings of the cutting wheel into the pressure chambers (2) where soil conditioning is realized in this area (Figure 9.5). Thrust on the cutterhead is realized by hydraulic cylinders (4) and the material within the pressure chamber is transported out by means of a screw conveyor (5). The pressure within the chamber is controlled by changing the discharge speed of the screw conveyor. The gap or void between the segments' outer side and the rock should be continuously filled with grouting material to control the behavior of the surrounding geological formation.

9.2 Technical Characteristics of Hard Rock TBMs

In a recent study carried out by Ates (2013), a database of 263 TBMs manufactured after 1985 and having a diameter greater than 4 m, was created and statistical analysis was performed by the authors of this chapter for the selection and performance prediction of TBMs. The relationships between diameters of TBMs and other characteristics of different types of TBMs are given in Figures 9.6 through 9.14. Statistically derived equations are summarized

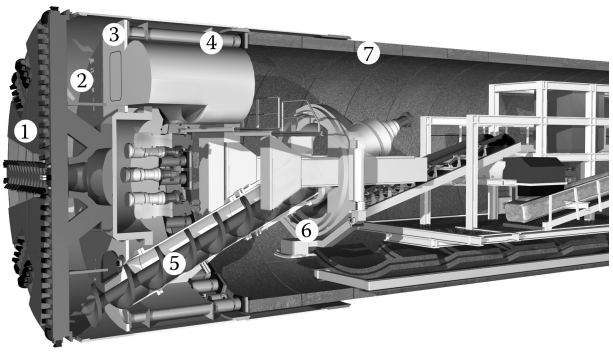

FIGURE 9.5
General view of an EPB TBM. (With the courtesy of Herrenknecht.)

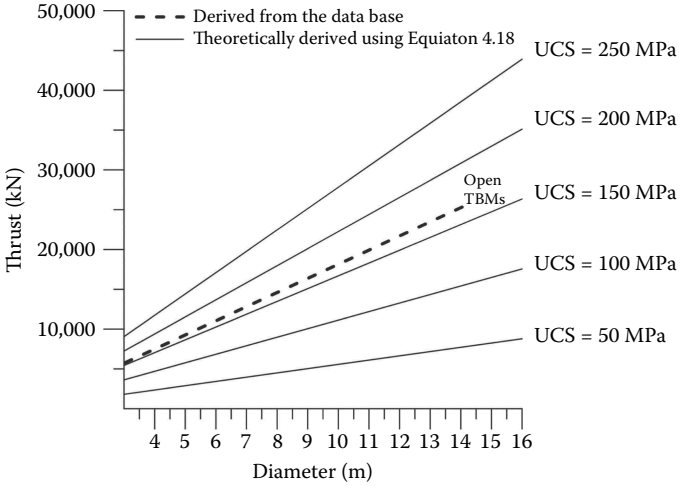

FIGURE 9.6
Relationship between diameter and thrust for open-type TBMs for different rock compressive strength.

in Table 9.1 for different hard rock TBMs with upper and lower limits of predicted values corresponding to different geological conditions. The equations given in Table 9.1 will serve a basis for performance prediction of different hard rock TBMs and some numerical examples will be given at the end of the chapter to clarify the prediction methodology. As clearly shown

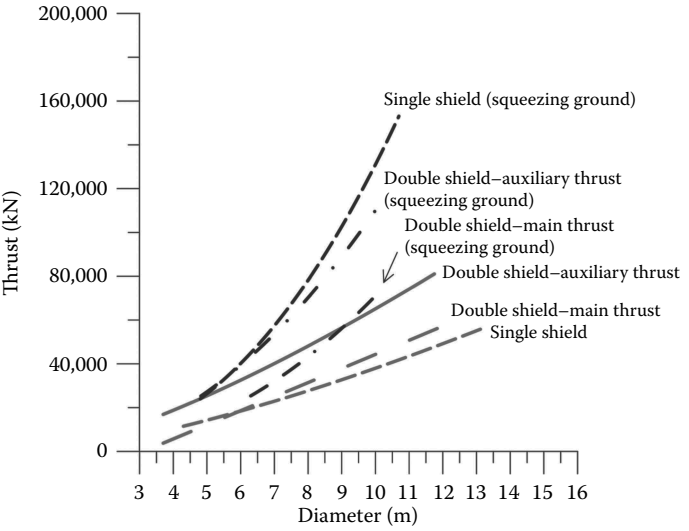

FIGURE 9.7
Relationship between diameter and thrust for single- and double-shield-type TBMs.

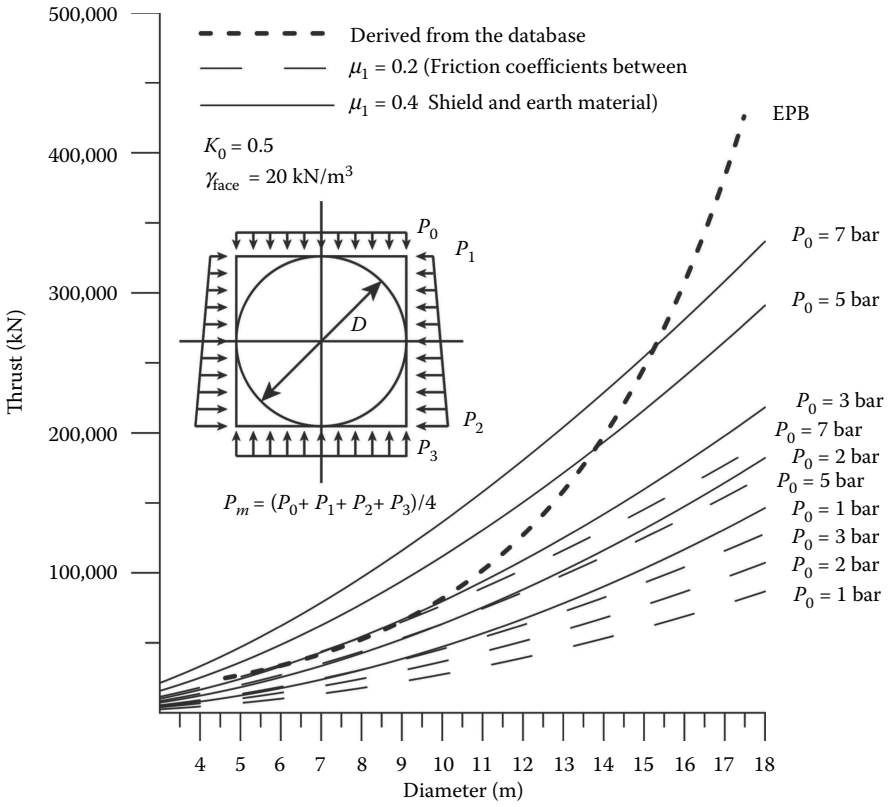

FIGURE 9.8
Relationship between diameter and thrust for EPB-type TBMs.

inthese figures, open-type TBMs demand less torque and thrust force for a given TBM diameter; they are also less heavier than the other TBM types. These diagrams calculate thrust and torque demands of single- and double-shield TBMs in squeezing ground conditions.

Figures 9.6 and 9.9 give the relationship between diameter, installed thrust force, and cutterhead torque values for open-type TBMs for different rock compressive strength. The dotted line is for a statistically derived relationship and continuous lines are for theoretically derived relationships, using Rostami and Ozdemir (1993) equations as explained in Chapter 4. It is interesting to note that the dotted line corresponds to a rock compressive strength of 150 MPa.

The relationships between diameters, installed thrust, and torque values for single- and double-shield-type TBMs are given in Figures 9.7 and 9.10 with the opportunity to calculate thrust force values in squeezing ground conditions as well. In these figures, two different lines are given for double-shield TBMs corresponding to the main and auxiliary trust values.

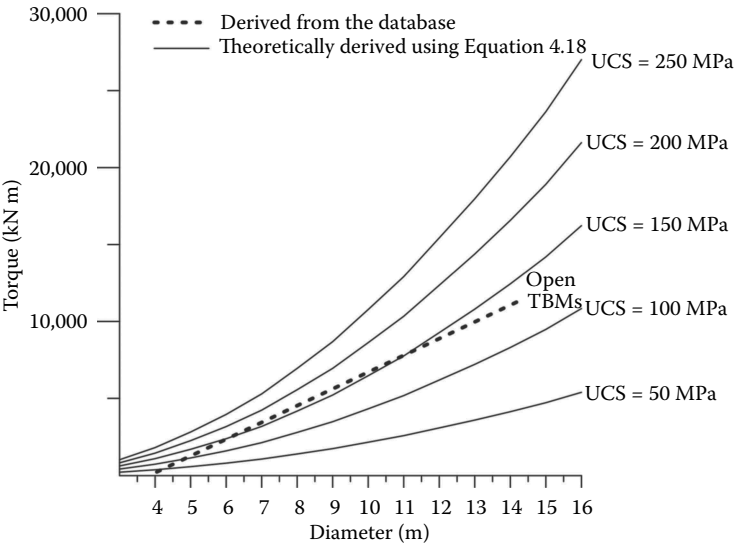

FIGURE 9.9
Relationship between TBM diameter and torque for open-type TBMs.

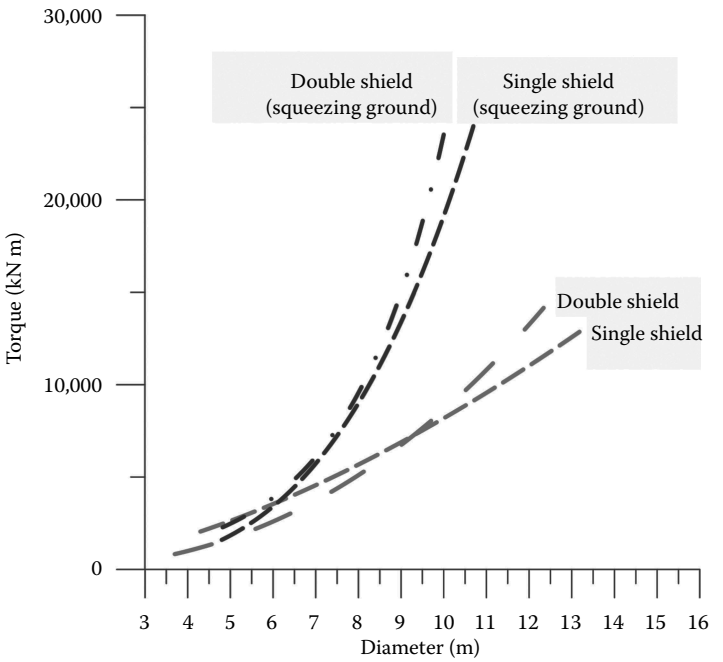

FIGURE 9.10
Relationship between TBM diameter and torque for single- and double-type TBMs.

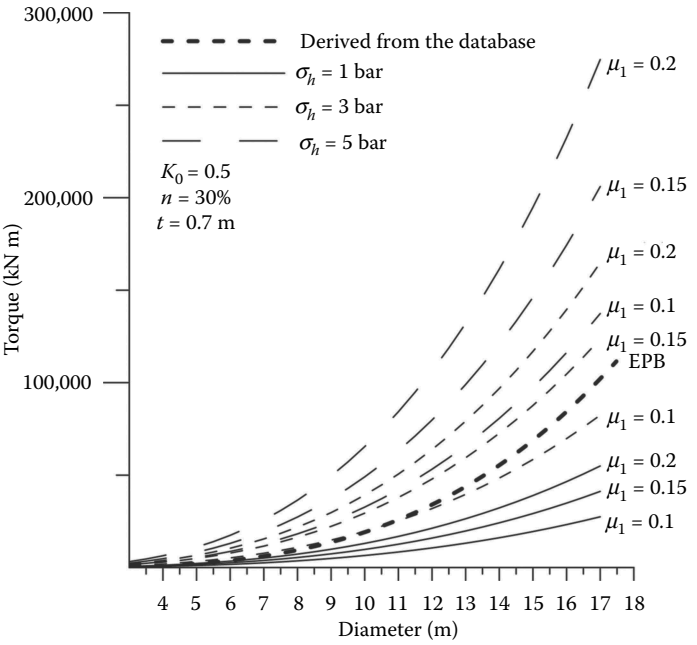

FIGURE 9.11
Relationship between TBM diameter and torque for open EPB TBMs.

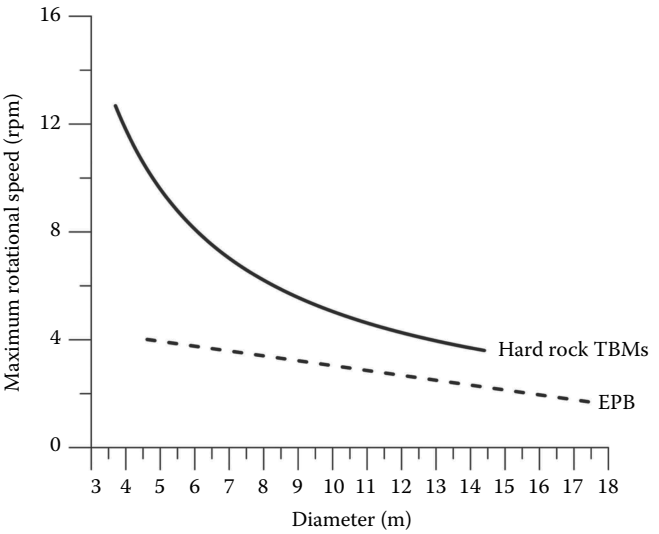

FIGURE 9.12
Relationship between TBM diameter and rotational speed for all types of TBM.

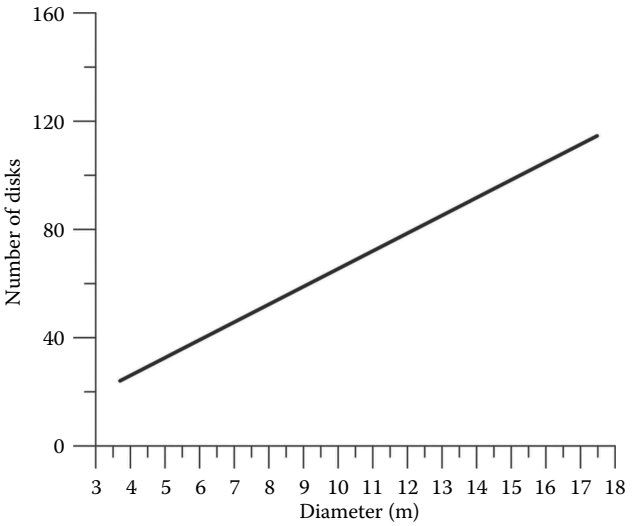

FIGURE 9.13
Relationship between TBM diameter and number of disks for all types of TBMs.

Hard rock TBMs working in open and closed EPB modes are used in complex geologies such as in some metro and water tunnels in Turkey (Bilgin et al. 2009). It is possible to use these types of TBMs in open mode in competent rock formation and in closed mode in fractured and weak zones within the same tunnel route. Figures 9.8 and 9.11 give the relationship between TBM diameters, thrust, and torque values for the machine working in EPB mode. Dotted bold lines are for statistically derived equations and other lines

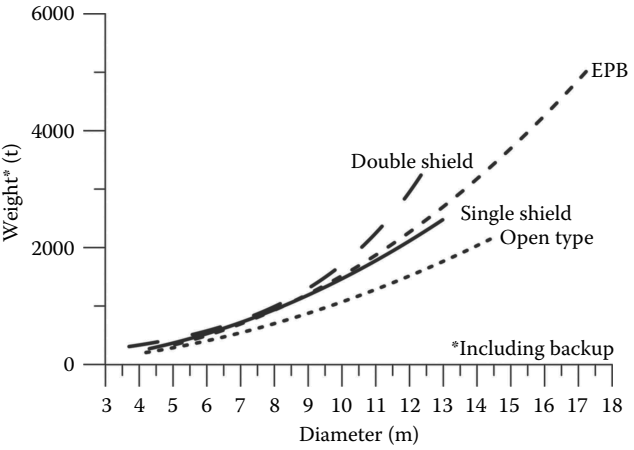

FIGURE 9.14
Relationship between TBM diameter and weight for different types of TBMs.

TABLE 9.1

Statistically Driven Equations to Predict TBM Parameters by Using Cutterhead Diameter (x) as Predictor

TBM Type	Thrust (kN)	Torque (kN m)	Total Weight (t)	Rotational Speed (rpm)	Number of Disks
Gripper	$FN = 1777.1x + 377.7$ $R^2 = 0.40$ $n = 72$ Lower limit –37% Upper limit +48%	$T = 1089.3x - 4188.8$ $R^2 = 0.63$ $n = 72$ Lower limit –53% Upper limit +47%	$W = 13.242x^{1.9076}$ $R^2 = 0.73$ $n = 34$	$rpm = 42.58x^{-0.9259}$ $R^2 = 0.78$ $n = 52$	$NC = 6.5698x - 0.2500$ $R^2 = 0.82$ $n = 96$
Single shield	$FN = 1459.8x^{1.4156}$ $R^2 = 0.42$ $n = 18$ Lower limit –62% Upper limit +54%	$T = 187.7x^{1.6390}$ $R^2 = 0.66$ $n = 18$ Lower limit –45% Upper limit +59%	$W = 14.482x^{2.0056}$ $R^2 = 0.92$ $n = 14$		
Double shield	$FN = 6435.1x - 20{,}032$ $R^2 = 0.63$ $n = 32$ Lower limit –64% Upper limit +71% [a]$FN = 2862.8x^{1.3569}$ $R^2 = 0.97$ $n = 7$ Lower limit –34% Upper limit +22%	$T = 38.12x^{2.3546}$ $R^2 = 0.79$ $n = 32$ Lower limit –38% Upper limit +48%	$W = 113.55e^{0.2752x}$ $R^2 = 0.71$ $n = 23$		
Single-shield TBM in squeezing and fractured zone	$FN = 635.83x^{2.3139}$ $R^2 = 0.87$ $n = 6$ Lower limit –18% Upper limit +23%	$T = 7.99x^{3.3784}$ $R^2 = 0.93$ $n = 6$ Lower limit –32% Upper limit +26%	—		

continued

TABLE 9.1 (continued)

Statistically Driven Equations to Predict TBM Parameters by Using Cutterhead Diameter (x) as Predictor

TBM Type	Thrust (kN)	Torque (kN m)	Total Weight (t)	Rotational Speed (rpm)	Number of Disks
Double-shield TBM in squeezing and fractured zone	FN = $422.6x^{2.2254}$ $R^2 = 0.79$ $n = 4$ Lower limit −20% Upper limit +23% [a]FN = $1066.4x^{2.0136}$ $R^2 = 0.94$ $n = 10$ Lower limit −24% Upper limit +21%	$T = 260.27e^{0.4504x}$ $R^2 = 0.98$ $n = 11$ Lower limit −28% Upper limit +11%	—		
EPB	FN = $8972.6e^{0.2208x}$ $R^2 = 0.79$ $n = 86$ Lower limit −40% Upper limit +47%	$T = 13.438x^{3.154}$ $R^2 = 0.85$ $n = 86$ Lower limit −63% Upper limit +55%	$W = 9.673x^{2.1956}$ $R^2 = 0.87$ $n = 31$	rpm = $-0.180x + 4.846$ $R^2 = 0.17$ $n = 46$	

Source: From Ates, U., 2013. A comparative study on the relationships between design parameters of TBMs with two current examples of large section TBMs. MSc thesis, Istanbul Technical University, Graduate School of Science, Engineering and Technology, pp. 105. With permission.

[a] Auxiliary thrust.

are for those calculated theoretically for different earth pressure and the friction coefficient between shield and the geological formation to be excavated.

Figures 9.12 through 9.14 correspond to the variation of rotational speed, number of cutters, and weights of TBMs with machine diameter.

9.3 Performance Predictions for Hard Rock TBMs and Practical Examples

9.3.1 Colorado School of Mines Method

The background data of the model is a large database of linear cutting tests performed on nonfractured rock samples in the CSM–Earth Mechanics Laboratory under the leadership of Dr. Levent Ozdemir. The CSM model is to estimate the necessary cutter forces for a given penetration (mm/rev). The cutter force equations may be solved with regard to penetration or one may use iteration to find the maximum obtainable penetration for a given set of machine specifications in a given rock. An important part of the CSM models has been the machine design (i.e., the cutter and cutterhead design) and all the other parameters for the TBM performance prediction (Rostami and Ozdemir 1993; Rostami et al. 1996).

It is reported that CSM method to estimate daily advance rates of the TBM are in good agreement with field data (Eskikaya and Bilgin 2000).

9.3.2 Model Developed by Ernst Buchi

Buchi (1984) presented a prediction model for net penetration rate on the influence of geological parameters affecting advance rates of a TBM. The model uses the cutter force obtained in a full-scale linear cutting machine as in the Colorado School of Mines (CSM) and then makes corrections for rock anisotropy and rock mass fracturing. The background data of the model are from tunneling projects covering approximately 38 km of bored tunnels. Büchi emphasized on schistosity in his model to modify CSM method. He pointed out that an angle of 90° between the tunnel axis and the orientation of the anisotropy increased penetration rate around 30%.

9.3.3 NTNU (Trondheim Norwegian University of Science and Technology) Method

This method is used to estimate the performance of open-type TBMs and gained worldwide acceptance for hard rock formations. The method is purely empirical, based on a very large database on field studies and statistical analysis of data from 35-tunnel TBM tunneling projects of more than 250 km of tunnels mainly excavated in Norway. The model consists

of estimating the net penetration rate in m/h, cutter life in h/cutter, mean advance rate expressed by time consumption as h/km, and excavation costs in NOK/m (Bruland 2000).

The input parameters to predict the penetration in mm/rev are obtained from geological and machine parameters such as fracturing, frequency and orientation of geological discontinuities, drilling rate index (DRI), porosity, gross average cutter thrust, average cutter spacing, and cutter diameter. The input parameters to predict the cutter life in h/cutter are rock mass parameters, cutter life index (CLI), rock quartz content (%), number of cutters on the cutterhead, cutter diameter, TBM diameter, and cutterhead RPM. The CLI gives the abrasion properties of crushed rock powder representing the tunnel face. The CLI is composed of the AVS of crushed rock powder and of the rock surface hardness measured by Sievers' *J*-value.

It should be emphasized that this method is only valid for open-type TBMs working in hard rock formations where the geology, rock discontinuities, and index values such as DRI and CLI are well defined.

9.3.4 Model Based on SE Concept

Different TBM performance prediction methods are used in the past as explained above (Bilgin et al. 2012a,b; Namli et al. 2013). However, none of them is applicable in the area where the complexity of the geology is dominant. In this section, a model based on past experiences, obtained in mixed faces of Istanbul with TBM excavations, will be mentioned. The TBM data collected from different tunnels in Istanbul were used to develop the model described below. The methodology is based on using the energy spent to excavate a unit volume of rock (*SE*), which is one of the most important factors in determining the efficiency of rock excavation. It may be used to estimate the net or instantaneous production rate of TBMs, roadheaders, and so on. Optimum *SE* values may be determined experimentally using a full-scale laboratory cutting rig as explained in Chapter 5 or in the field as given in Equation 9.1. One of the most important points is that optimum SE may be used to calculate the net production rate of any mechanical excavator as given in Equation 9.2

$$SE_f = 2 \cdot \pi \cdot N \cdot T / PR_f \tag{9.1}$$

where N is rotational speed in revolutions per second of the cutterhead and T is the TBM torque in (kN m) that is directly obtained from the data-acquisition system of TBM. The part $(2 \cdot \pi \cdot N \cdot T)$ of Equation 9.1 is the power (in kW) spent during excavation for a given torque and rotational speed, PR_f is the field value of the penetration rate in (m^3/h), and SE_f is field *SE* in (kW h/m^3).

$$NPR = k \cdot P / SE_{opt} \tag{9.2}$$

where *NPR* is the mean net instantaneous production rate in (m^3/h), *k* is energy transfer ratio from the cutting head to the tunnel face (it is usually 0.8 for TBMs), *P* is power spent to excavate the rock, and SE_{opt} is optimum specific energy in kW h/m^3 obtained from full-scale laboratory cutting experiments. However, a correction related to *RQD* should be made for net production rate values.

The concept will be clarified by using numerical examples at the end of this chapter.

Equations 9.1 and 9.2 clearly indicate that if field *SE* and the power spent during excavation are predicted, net production rate of a TBM may be calculated.

Figure 9.15 gives the relationship between uniaxial compressive strength and optimum *SE* for different rock samples tested in full-scale linear cutting rig by using CCS disk cutters. However, it should be noted that the equation given in this figure should be used for massive rocks having grain size not higher than 4 mm. The upper line should be used for rocks having coarser grain sizes and the lower line should be used for rocks having intern fractures such as limestone found in Istanbul.

Typical relationships obtained between field *SE* values and advance per revolution for some tunnels in Istanbul are given in Figures 9.16 and 9.17. It is clearly seen from these figures that field *SE* levels off and stay constant after a certain value of advance per revolution or penetration. This optimum value of *SE* may be taken into consideration for predicting net production rates of TBMs. For the model described in this section, the project description of each tunnel is taken into consideration, with mean compressive strength of the geological formation obtained from borehole samples, including field

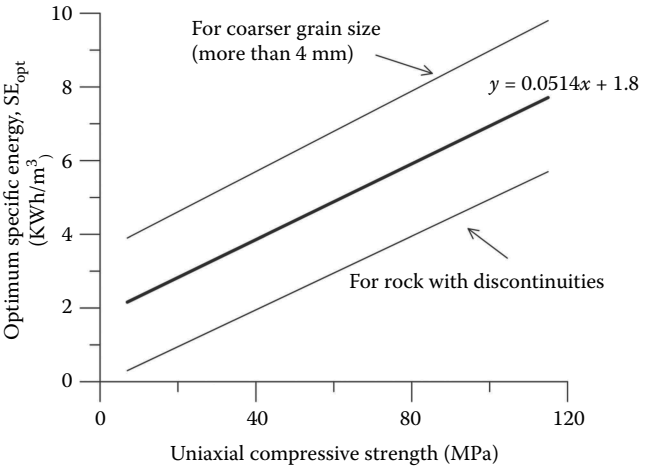

FIGURE 9.15
Variation of optimum SE values with uniaxial compressive strength.

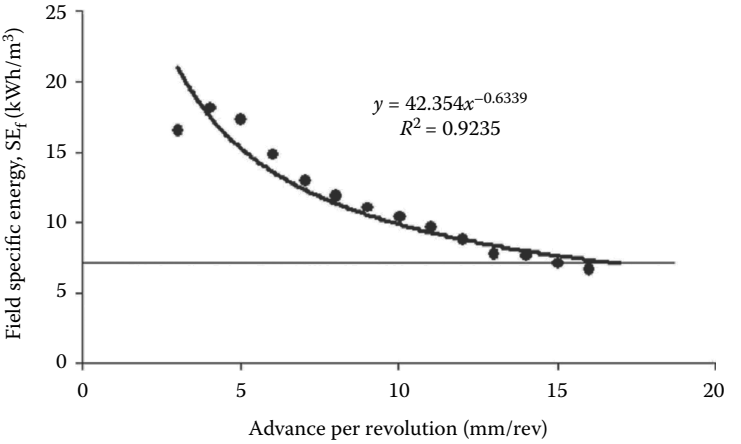

FIGURE 9.16
Relationship between advance per revolution and field SE in Kadikoy–Kartal Metro Tunnel for Kartal Dolayoba limestone, siltstone, and carbonated shale with mean compressive strength of 50 MPa. (Adapted from Bilgin, N. et al., 2012b. Rock mechanics aspects related to cutting efficiency of mechanical excavators, 25 years of experience in Istanbul, *EUROCK 2012*, Stockholm.)

SE and predicted *SE* values using the equation given in Figure 9.15 that is tabulated in Table 9.2. However, one important point is that sedimentary formations found in Istanbul region are cut by dikes, making the geological formation highly fractured in some areas. Owing to this fact, hard rock TBMs in some of Istanbul's metro tunnels are used in semi-EPB mode with some parts of the chamber full with muck to stop face collapses in front of TBMs,

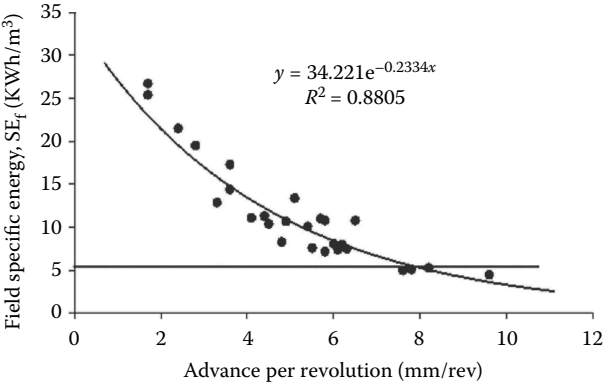

FIGURE 9.17
Relationship between advance per revolution and field SE in Beykoz Tunnel for limestone, sandstone, and carbonated shale with mean compressive strength of 100 MP. (Adapted from Bilgin, N., Copur, H., Balci, C., 2012a. *Tunnelling and Underground Space Technology*, 27, 41–51.)

TABLE 9.2

Description of Tunnel Projects with Field and Predicted SE Values

Project	Geology	D (m)	UCS (MPa)	SE_F (kW h/m³)	SE_P (kW h/m³)	SE_F/SE_P	NPR_F (m³/h)
Hard Rock TBMs							
Beykoz Utility Tunnel	Limestone, sandstone, and carbonated shale	3.2	96.3	5	6.75	0.75	14.2
Cayirbasi Water Tunnel	Interbedded, sandstone, limestone, and mudstone	3.1	119.3	9.5	7.93	1.20	16.5
Uluabat Power Tunnel	Akçakoyun limestone	5.1	52.0	5	4.5	1.10	96
Uluabat Power Tunnel	Karakaya metasandstone, mudstone, and graphitic shist	5.1	25.0	3	3.1	0.97	135
Hard Rock TBMs Working in Semi-EPB Mode							
Kartal–Kadkoy Metro Tunnel	Kartal–Dolayoba limestone, siltstone, and carbonated shale	6.6	45.8	7	6.75	1.03	100
Pendik–Kaynarca Metro Tunnel	Kartal formation, limestone, shale, and mudstone	6.5	42.0	6	6.2	0.97	105
Pendik–Kaynarca Metro Tunnel	Dolayoba formation and limestone	6.5	32.0	7	6.8	1.03	100

Note: Uniaxial compressive strength (*UCS*) is the mean value and for Beykoz and Cayirbasi Tunnels, it is obtained from the rock samples obtained from the tunnel face; for the other projects, *UCS* is the mean value obtained from core samples. SE_P values are obtained using the relation given in Figure 9.15; for EPB mode, the values are multiplied by 1.8 as explained in the text.

D, tunnel diameter; *UCS*, uniaxial compressive strength; SE_F, field specific energy; SE_P, predicted field specific energy; NPR_F, field net production rate.

increasing the *SE* 1.8 times higher than the open mode. The TBM in Uluabat (Bursa) power tunnel worked in many cases in open mode. As clearly seen in Table 9.2, the predicted optimum *SE* values are in good agreement with the field *SE* values.

In Table 9.2, the TBMs are equipped with disks, chisel cutters, or rippers in the tunnels having mixed conditions (hard and soft ground). Careful analysis of the field data showed that in such conditions, the normalized cutterhead power/cutterhead diameter ratio for TBMs using disk and ripper cutters is 118.8 kW/m, for the rocks having a mean compressive strength value ranging between 30 and 100 MPa. However, this ratio is found to be 80 kW/m in hard rock TBMs using only disk cutters in rock formations having compressive strength values between 100 and 120 MPa. Cutting power of

TBM working in optimum *SE* conditions in rocks up to 100 MPa compressive strength may be calculated empirically as given below

$$P_{\text{Cutting–semi-EPB}} = 118.8 \cdot D \tag{9.3}$$

$$P_{\text{Cutting hard rock}} = 80 \cdot D \tag{9.4}$$

where $P_{\text{Cutting–semi-EPB}}$ is cutting power in kW for TBMs working in semi-EPB mode in difficult conditions when half of the pressure chamber is filled with muck and D is cutterhead diameter in m.

Machine Utilization Time *(MUT)* as defined in Table 9.3 is a summary of accumulated data from 30 different tunneling projects in Turkey and this

TABLE 9.3

Steps to Calculate M_{UT} for TBMs

	Stoppage Type	Stoppage Duration (%) of One-Day Shift Time
Adverse ground	Contact zones between formations	A few days to 1 week
	Dikes	
	Faults	A few days to 2 weeks
	Water	A few days to 1 week
TBM breakdown	New TBM (experienced crew)	2–4%
	New TBM (inexperienced crew)	4–6%
	Refurbished TBM (experienced crew)	4–6%
	Refurbished TBM (inexperienced crew)	6–8%
Cutter replacement	Quartz content of 0–20%	5%
	Quartz content greater than 20%, weak and blocky ground	5–10%
	Quartz content greater than 20%, hard rock	10%
Muck transportation	By train: Transportation distance of 0–3 km	7%
	By train: Transportation distance greater than 3 km	10%
	By belt conveyor: Transportation distance of 0–3 km	5%
	By belt conveyor: Transportation distance greater than 3 km	7%
Maintenance	Experienced contractor and crew	10%
	Moderately experienced contractor and crew	15%
Setting the segments		20–25%
TBM mobilization at stations		2–3 weeks
Other stoppages		10–15%
Machine utilization		22–43%

Source: Adapted from Namli, M. et al. 2013. A methodology of using past experiences in the performance prediction of a TBM in a complex geology and risk analysis. *World Tunnel Congress*, Geneva.

table may be used as a first approximate to calculate *MUT* and mean daily advance rates. However, it should be mentioned here that the work done by Farrokh and Rostami (2012) is more comprehensive covering accumulated data from 89 projects worldwide, 66 data from open-type TBMs, seven data from single-shield TBMs, and 16 from double-shield TBMs.

9.3.5 Model Based on Accumulated Data and Statistically Derived Equations

The following steps may be taken for performance predictions:

1. Use Table 9.4 to estimate the maximum cutter penetration for different rock and disk cutter properties. One important point when using this table is that optimum *SE* is obtained for spacing to penetration ratio changing between 8 and 14, even more in special cases. Bearing in mind that mean cutter spacing in TBMs is around 8 cm for optimum conditions, cutter penetration per revolution should never pass 1 cm. However, this is a difficult process to control during the excavation and the penetration may go up to 1.6 cm in the geological formations where the geological discontinuities are abundant.
2. Use Figure 9.12 to estimate rotational speed.
3. Use rotational speed, cutter penetration, daily shift time, and *MUT* (Table 9.3) to estimate daily advance rates.
4. Use predictor equations given in Table 9.1 to estimate disk cutter numbers, TBM thrust, and cutterhead torque values taken into consideration for the upper and lower limits, which are directly related to the geological conditions.

A numerical example will be given at the end of this chapter to clarify the methodology explained in this section.

TABLE 9.4

Estimation of Disk Cutter Penetrations for Different Disk Diameter, Tip Width, and Different Rock Properties

	Disk Diameter 432 mm, Tip Width 15.9 mm, and Maximum Load 220 kN			**Disk Diameter 483 mm, Tip Width 1.9 mm, and Maximum Load 310 kN**		
σ_c (MPa)	**$\sigma_c/\sigma_t = 10$ p (cm/rev)**	**$\sigma_c/\sigma_t = 15$ p (cm/rev)**	**$\sigma_c/\sigma_t = 20$ p (cm/rev)**	**$\sigma_c/\sigma_t = 10$ p (cm/rev)**	**$\sigma_c/\sigma_t = 15$ p (cm/rev)**	**$\sigma_c/\sigma_t = 20$ p (cm/rev)**
200	0.3	0.4	0.5	0.4	0.6	0.8
150	0.6	0.8	1.0	0.8	1.2	1.6
125	1.0	1.2	1.6			

Note: In this table, σ_c is compressive strength of the rock, σ_t is tensile strength, and p is penetration per revolution.

9.4 Tunneling in Difficult Ground with Hard Rock TBMs

The main problems with hard rock TBMs are mixed faces, boulders, weak contact zones between two different geological formations, highly fractured rock formations, sedimentary rocks cut by magmatic inclusion (dikes), and uneven distribution of the strength of rock formations. A typical example of this problem is seen in the Kozyatagi–Kadikoy Metro Tunnels. Two identical single-shield TBMs working in open and closed modes were selected for this project. Some of the basic parameters of these TBMs are given in Table 9.5 (Bilgin et al. 2009).

The excavation data were carefully collected during tunnel drivages. At the beginning, it was observed that the contact zones between dikes and the main rock formation were highly fractured, and in some areas, big rock blocks having sizes up to $30 \times 40 \times 50$ cm were ripped off by the disk cutters from the fractured zones, passing from the openings of the cutterhead and causing several problems such as collapses of the tunnel face. Such big blocks are seen in Figure 9.18 and face collapse is seen in Figure 9.19. Face collapses dramatically decreased daily advance rates to around 2.5 m/day. After several technical discussions between project management staff and the TBM manufacturer, it was decided to install some grill bars to limit the big rock blocks passing from the openings of the cutterhead. Figure 9.20 shows TBM before and after installing grill bars. The daily advance rate increased up to 6 m/day after the modification of the cutterhead as seen in Figure 9.21 and Table 9.6. This figure also gives the changes of the TBM (Guclucan et al. 2008, 2009) after transition to EPB mode, in soft and fractured ground indicating a significant increase in daily advance rates.

However, it should be mentioned here that in the other two tunneling projects in Istanbul, grill bars were also added to other TBMs; one in the

TABLE 9.5

Basic Technical Specifications of the TBM Used in Kozyatagi–Kadikoy Metro Tunnel

Machine diameter	6.57 m
Number of cutters	26 single + 6 double (12) = 38
Maximum contact pressure per disk	267 kN
Maximum thrust capacity of the main bearing	20,000 kN static
Cutterhead drive	Electric motors
Cutterhead power	1260 kW (4×315)
Cutterhead rotational speed	1.6–5.5 rpm
Cutterhead torque	5200 kN m at 1.6 rpm
	1515 kN m at 5.5 rpm
Maximum working pressure of the thrust cylinders	42,575 kN at 350 bar
Thrust cylinder stroke	1.5 m

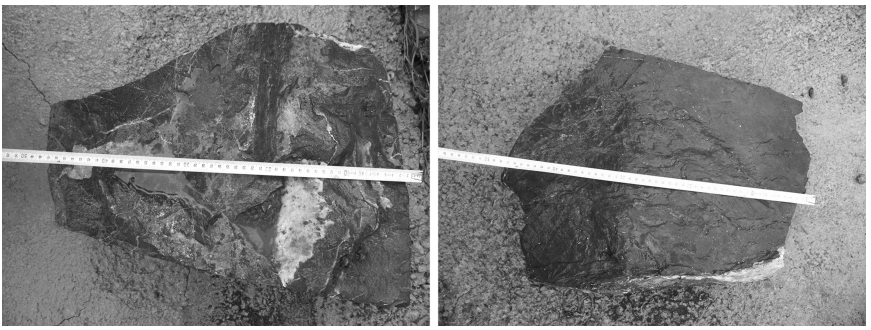

FIGURE 9.18
Big rock blocks coming from the tunnel face. (From archive of N. Bilgin.)

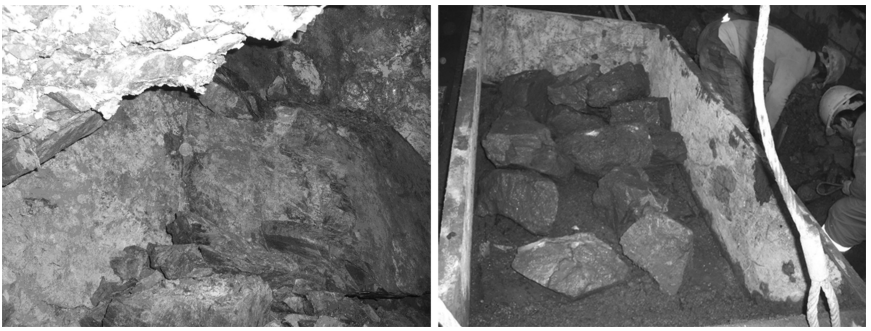

FIGURE 9.19
Collapse in front of the cutterhead on the left figure and big rock blocks on the right figure. (From archive of N. Bilgin.)

FIGURE 9.20
TBM S-360, cutter head with grill bars on the right and cutter head before modification on the left in Kozyatagi–Kadikoy (Istanbul) Metro Tunnel. (From archive of N. Bilgin.)

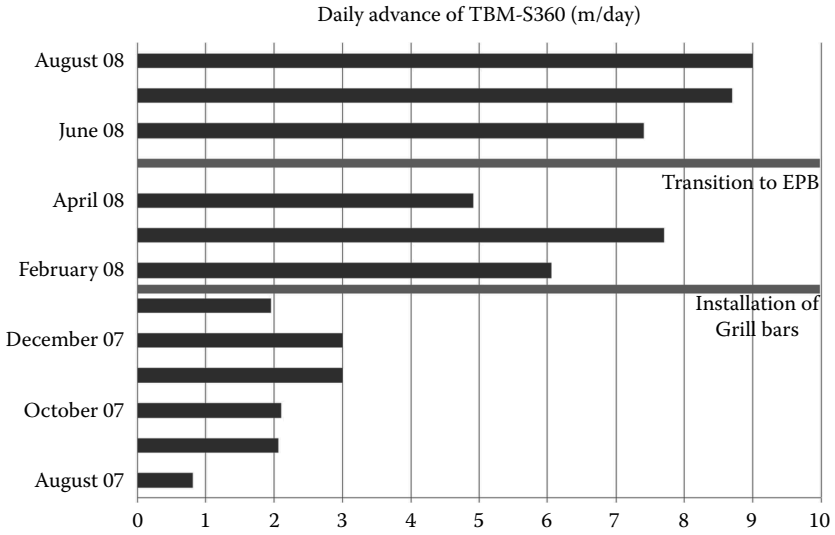

FIGURE 9.21
Daily advance rates of TBM S-360 in line 1. (From archive of N. Bilgin.)

Beykoz Tunnel in a hard rock TBM and one in Marmaray Project, in a slurry machine, where thereafter, face collapse stopped and TBM utilization time increased considerably. Figure 9.22 shows tunnel face collapse due to weak contact zone of an andezite dike and Figure 9.23 shows the gallery opened to rescue the jammed cutterhead due to face collapse.

One of the most important parameters affecting the excavation efficiency in mixed ground and in complex geology is excessive disk consumption. Big loose rock blocks or boulders in the tunnel face may block the rolling cutters and cause cutter deterioration; if such cutters do not change immediately, the cutterhead may be damaged that may cause several weeks of cutterhead repair (Figure 9.24).

Tungsten carbide-studded disk cutters should be never used in mixed ground having abrasive characteristics. In such cases, steel material of disk cutter gets worn out more quickly than tungsten carbide as seen in Figures 9.25 and 9.26; as a result, uneven destruction of disk cutters may cause cutterhead vibration and cutterhead damage.

In complex geology where the ground may have sludgy characteristics in some parts of the tunnel route, a disk cutter may not be turned freely due to a lack of friction between the ground and disk material. Very uneven and excessive wear may be encountered as seen in Figure 9.27. In such cases, the problem may be solved by changing disk cutters with chisel cutters, as seen in Figure 9.28 (Bilgin et al. 2012a).

TABLE 9.6

Daily Advance Rates of TBM–S360 in Line 1

August 2007	September 2007	October 2007	November 2007	December 2007	January 2008	February 2008	March 2008	April 2008	May 2008	June 2008	July 2008	August 2008
	TBM Working in Open Mode					Installation of Grill Bars			TBM Working in EPB Mode			
0.7 (m/d)	2.1	2.1	3	3	1.9	6.1	7.7	4.9	0	7.4	8.8	9

Source: From Archive of N. Bilgin.

FIGURE 9.22
Tunnel face collapse in Beykoz Tunnel due to weakness planes between sedimentary rocks and andezite dikes (magmatic intrusions). (From archive of N. Bilgin.)

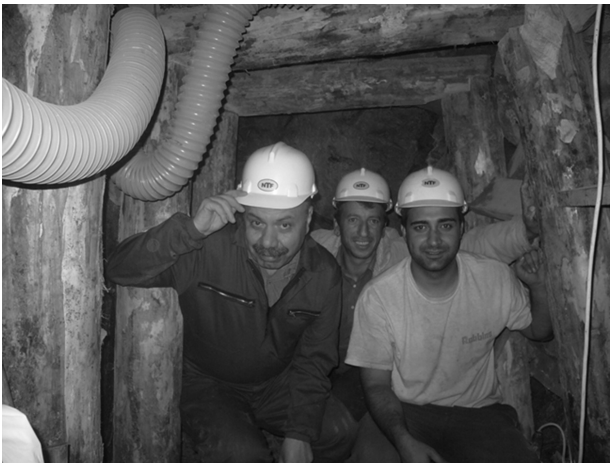

FIGURE 9.23
Gallery excavated to rescue the jammed TBM. (From archive of N. Bilgin.)

9.5 Numerical Examples

9.5.1 A Numerical Example on Using Statistically Derived Equation for TBM Performance Prediction

A tunnel of 3 km in length will be opened in a rock formation having compressive strength of 150 MPa and a tensile strength of 7.5 MPa, with a

FIGURE 9.24
Deterioration of disk cutter due to disk blockage in Kozyatagi–Kadikoy Metro Tunnel. (From archive of N. Bilgin.)

single-shield TBM of 8 m diameter. 432 mm CCS disk cutters with 15.9 mm of tool width will be used.

Although the rock is competent and the average mean RQD is 80%, some geological discontinuities exist within the tunnel route, limiting the net advance rate and the average *MUT* is expected to be 40%. The daily tunneling time will be carried out with two shifts of 10 h each.

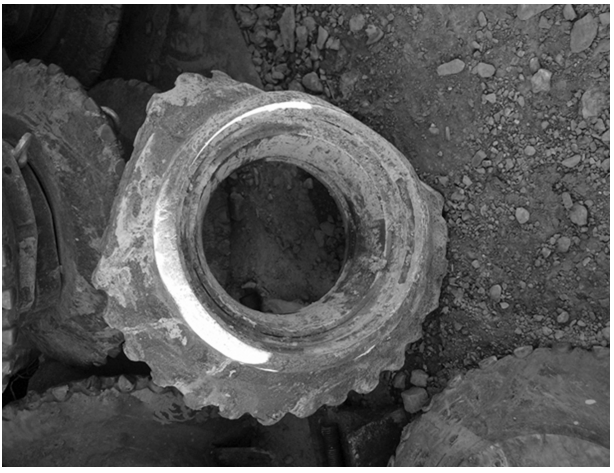

FIGURE 9.25
Uneven disk wear in mixed faces. (From archive of N. Bilgin.)

FIGURE 9.26
Wear problems of disk cutters in very abrasive rock formations. (From archive of N. Bilgin.)

Calculate

1. Maximum penetration/rev
2. Mean rotational speed of the machine
3. Net production rate
4. Mean daily advance rate
5. Number of disk cutters in the cutterhead
6. Thrust and torque of the machine

FIGURE 9.27
Sludgy formation encountered in Beykoz Tunnel route and disk wear within this formation. (Adapted from Bilgin, N., Copur, H., Balci, C., 2012a. *Tunnelling and Underground Space Technology*, 27, 41–51; Guclucan, Z. et al., 2008. The use of a TBM in difficult ground conditions in Istanbul (Beykoz–Kavacik) sewerage. *World Tunnel Congress*, September 22–24, Agra, India, pp. 1630–1638; Guclucan, Z. et al., 2009. The use of theoretical rock cutting concepts in explaining the cutting performance of a TBM using different cutter types in different rock formations and some recommendations. *ITA, AITES World Tunnel Congress*, May 23–28, Budapest, Hungary, p. 10.)

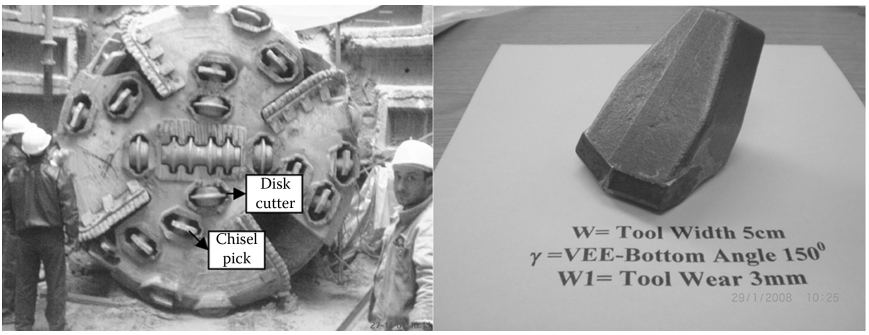

FIGURE 9.28
Use of disk cutters and chisel picks in soft formation on the left and pick cutter used on the right in Beykoz Tunnel. (Adapted from Bilgin, N., Copur, H., Balci, C., 2012a. *Tunnelling and Underground Space Technology*, 27, 41–51; Guclucan, Z. et al., 2008. The use of a TBM in difficult ground conditions in Istanbul (Beykoz–Kavacik) sewerage. *World Tunnel Congress*, September 22–24, Agra, India, pp. 1630–1638; Guclucan, Z. et al., 2009. The use of theoretical rock cutting concepts in explaining the cutting performance of a TBM using different cutter types in different rock formations and some recommendations. *ITA, AITES World Tunnel Congress*, May 23–28, Budapest, Hungary, p. 10.)

9.5.1.1 Solution

1. From Table 9.4 in optimum conditions, a penetration of 1 cm/rev is found.
2. From Figure 9.12 and Table 9.1, maximum rotational speed of 6 rpm is found; to be safe, a mean rotational speed of 4 rpm is selected.
3. Net production rate per day is calculated and given below.

$$NPR = \text{Penetration} \cdot \text{ rotational speed} \cdot \text{ daily working hours} \cdot MUT \cdot \text{ tunnel area} \tag{9.5}$$

$$NPR = 0.01\,(\text{m/rev}) \cdot (4 \cdot 60)(\text{rev/h}) \cdot 20\ \text{h} \cdot 0.4 \cdot 50.3\ \text{m}^2$$

$$NPR = 965.8\ \text{m}^3/\text{day}$$

4. Mean daily advance rate is found dividing the daily net production rate by the area of the tunnel face as 19.2 m/day.
5. Number of disks is 52 using Figure 9.3 and Table 9.1.
6. Average thrust and torque values are calculated using predictor equations given in Table 9.1 as

   Thrust = $1459.8 \cdot 8^{1.4156} = 27{,}715$ kN

   Predicted minimum thrust = $27{,}715 \cdot 0.38 = 10{,}532$ kN

   Predicted maximum thrust = $27{,}715 \cdot 1.54 = 42{,}681$ kN

Torque= $187.7 \cdot 8^{1.6390} = 5670$ kN m

Predicted minimum torque = $5670 \cdot 0.55 = 3119$ kN m

Predicted maximum torque = $5670 \cdot 1.59 = 9015$ kN m

9.5.2 A Numerical Example on Using Statistically Derived Equation for TBM Performance Prediction for Squeezing Ground

A tunnel of 3 km in length will be opened in a rock formation having compressive strength of 150 MPa with a single-shield TBM of 8 m diameter. 432 mm CCS disk cutters with 15.9 mm of tool width will be used. The geological formation is cut in several places with graphitic schist having a squeezing characteristic. *MUT* is expected to be 30% due to geological difficulties. The daily tunneling time will be carried out with two shifts of 10 h each.

Calculate

1. Maximum penetration/rev
2. Mean rotational speed of the machine
3. Net daily advance rate
4. Mean daily advance rate
5. Number of disk cutters in the cutterhead
6. Thrust and torque of the machine

9.5.2.1 Solution

The values asked in a,b, and e are the same as calculated above.

1. Net production rate per day is calculated as given in Equation 9.5.

$$NPR = 0.01\,(\text{m/rev}) \cdot (4 \cdot 60)(\text{rev/h}) \cdot 20\ \text{h} \cdot 0.3 \cdot 50.3\ \text{m}^2$$

$$NPR = 724.3\ \text{m}^3/\text{day}$$

2. The mean daily advance rate is found dividing the daily net production rate by the area of the tunnel face as 14.4 m/day.
3. Thrust and torque values of TBM in squeezing ground are found using the equations given in Table 9.1 as

   Thrust = $635.83 \cdot 8^{2.3139} = 78{,}163$ kN

   Predicted minimum thrust = $78{,}163 \cdot 0.82 = 64{,}034$ kN

   Predicted maximum thrust = $78{,}163 \cdot 1.23 = 96{,}141$ kN

   Torque = $7.99 \cdot 8^{3.3784} = 8986$ kN m

   Predicted minimum torque = $8986 \cdot 0.68 = 6111$ kN m

   Predicted maximum torque = $8986 \cdot 1.26 = 11{,}322$ kN m

9.5.3 A Numerical Example on Using SE Concept for TBM Performance Prediction

Find the daily advance rate of TBM having a diameter of 6.6 m in chainage 5 + 250 given in Figure 9.29 when passing the conglomerate having uniaxial compressive strength of 70 MPa and *RQD* of 45%.

9.5.3.1 Solution

SE is found using the equation given in Figure 9.15 as 5.4 kW h/m^3. Conglomerate is a coarse-grained rock; so, *SE* should be corrected, resulting in 7.3 kW h/m^3. Since EPB TBM is used, *SE* is again corrected by multiplying with 1.8, resulting in 13.14 kW h/m^3.

The cutting power of EPB TBM is estimated by using Equation 9.3 resulting in 784 kW. The net production rate is estimated by using Equation 9.2 resulting in 47.7 m^3/h.

A working pattern is 20 h/day. Referring Table 9.3, stoppage due to a TBM breakdown is 7%, stoppage due to muck transportation by belt conveyor is 5%, stoppage due to maintenance is 10%, stoppage due to cutter replacement is 10%, stoppage due to the replacement of the segments is 20%, and stoppage due to other reasons is 8%. This sums up a total of 60% of stoppages.

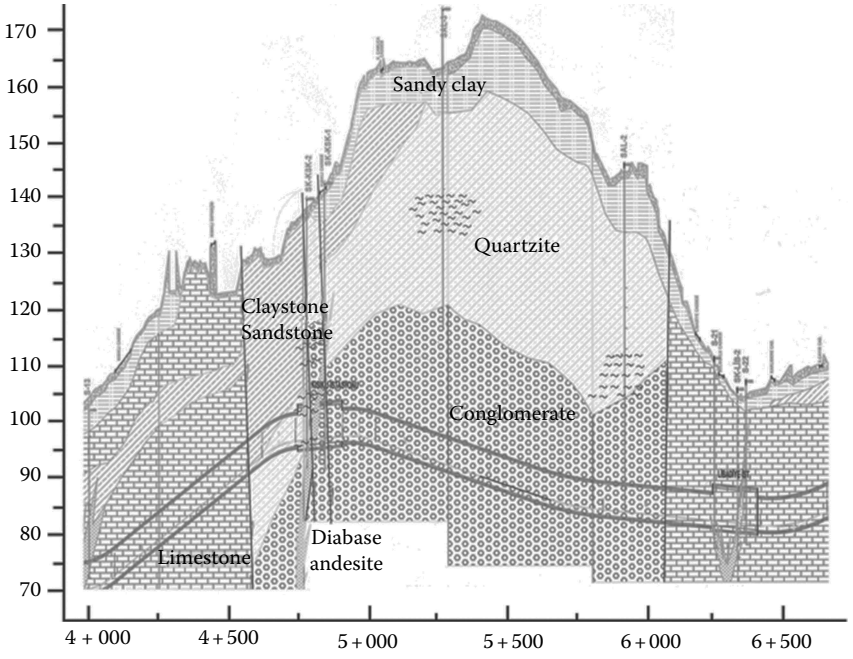

FIGURE 9.29
Geological cross section relevant to the numerical example.

Therefore, machine utilization is estimated as 40%. However, downtime analysis developed by Farrokh and Rostami (2012) advises it to be used in open-type TBMs.

Knowing the tunnel cross-section area of 34.2 m^2, the daily advance rate is estimated as

$$\text{Daily advance rate} = \frac{47.7 \cdot 20 \cdot 0.4}{34.2} \cong 11 \text{ m/day}$$

However, this number should be used cautiously since the experience obtained with an EPB TBM in conglomerate in Istanbul is very limited. The largest portion of conglomerate is composed of quartzite indicating severe wear problems.

9.5.3.2 Solution for the Same Problem Given in Section 9.5.3 If the TBM Is Worked in Open Mode

In this case, *SE* should be taken as 7.3 kW h/m^3. The power spent when cutting the rock is calculated using Equation 9.4 and is found as 528 kW.

Hence, a net production rate is calculated using Equation 9.2 as 57.9 m^3/h and daily advance rate as 13.5 m/day.

9.5.4 Numerical Example on Using Full-Scale Rock-Cutting Tests to Calculate Daily Advance Rates of TBM

A rock formation sample having representative compressive strength of 58 MPa and tensile strength of 3.6 MPa will be excavated with a double-shield TBM having the design parameters given in Table 9.7 (Bilgin et al. 1999). Full-scale cutting tests are carried out with a CCS disk cutter to predict cutting performance of the TBM. An optimum SE value of 2.1 kW h/m^3 is obtained for *s/p* (cutter spacing/penetration) of 10, with the cutting parameter given in Table 9.8 as mean and peak thrust forces (*FN*, *FN'*) and

TABLE 9.7

Specification of Double-Shield TBM

Machine diameter	5.0 m
Number of cutters	36
Cutter spacing	7.5 cm
Rotational speed	6 rpm
Normal thrust force	471 tons
Maximum thrust force	785 tons
Cutting head power	600 HP
Power of the miscellaneous pumps, and so on	285 HP

TABLE 9.8

Cutting Parameters Obtained in Laboratory Cutting Tests

Type of Cutters	CCS Type
FN (kN/mm)	5.21
FN' (kN/mm)	8.34
FR (kN/mm)	0.64
FR' (kN/mm)	1.09

mean and peak rolling forces (*FR*, *FR'*) per revolution. Calculate the daily advance rate of TBM.

9.5.4.1 Solution

For $s/p = 10$, $p = 7.5/10 = 0.8$ cm

From Table 9.8 for CCS cutter type, $FN' = 8.34$ kN/mm
For $p = 10$ mm, total machine thrust is $36 \cdot 10 \cdot 8.34 = 3000$ kN
Total machine thrust is 3000 kN
Torque of the machine is estimated by Equation 9.6.

$$\text{Torque} = \sum_{i=1}^{i=n} r_i \cdot FR \tag{9.6}$$

In this equation, n is number of cutters, r_i is distance from the cutter to the center of the cutting head, and FR is mean rolling force obtained from Table 9.8, for a cutting depth of 10 mm.

Torque for the cutting head for $p = 10$ mm; $36 \cdot 1.375 \cdot 10 \cdot 0.64 = 317$ kN m.

Power of the machine is estimated by using Equation 9.7.

$$P = 2 \cdot \pi \cdot N \cdot T \tag{9.7}$$

In this equation, the cutterhead power P is in kW, N is cutterhead rotation in rotations per second, and T is torque in kN · m.

The expected cutting power of the machine for a cutting depth of 10 mm is

$$P = 2 \cdot \pi \cdot 6 \cdot 317/60 = 199 \text{ kW}$$

Using Equation 9.2, the net excavation rate is found as 76 m^3/h.

In competent rock, an average *MUT* of 30% and 16 h working time per day will result in a daily advance rate of

$$\text{Daily advance rate} = \frac{16 \text{ h} \cdot 76 \text{ m}^3 \cdot 0.3}{\text{h} \cdot \pi \cdot 25/4 \text{ m}^2} \cong 18.5 \text{ m/day}$$

TABLE 9.9

Comparison of Predicted and Measured TBM Performance Values

Tunnel (km)	Disk Cutting Depth (mm)	Measured *FN′* (kN/disk)	Predicted *FN′* (kN/disk)	Measured Net Cutting Rate (m^3/h)	Predicted Net Cutting Rate (m^3/h)
172.7	11	73.9	91.3	71	80
175.3	7	69.8	58.1	49	53
190.2	8	69.9	66.4	57	61
194.0	9	72.3	75.1	64	60
225.6	7	59.3	58.1	49	53
227.9	10	117.2	83.0	71	70
251.3	8	111.2	66.4	57	61
272.1	11	123.7	91.3	71	80
275.4	9	89.0	75.1	64	60
275.4	13	126.2	107.8	92	74
284.5	8	96.0	66.4	57	61

FN′, Peak thrust force.

The predicted excavation rate given above is for competent rock. It is obvious that the geological discontinuities will increase the net excavation rate to a certain level and a high amount of *RQD* or water income in rock formation with high amount of clay will decrease the daily advance rate due to regional collapses, face instability, clogging the cutters, and so on. These factors tremendously affect the advance rate of the TBM during Tuzla–Dragos tunnel drivages.

Eleven different zones were chosen for in situ observation of the TBM performance in the Tuzla–Dragos tunnel. Special attention is paid to the fact that the rock formation in selected zones should have similar mechanical properties with those tested in a full-scale cutting rig. Measured and predicted values are compared in Table 9.9. As it is seen from this table, predicted and measured TBM performance values are very close to each other. Also, please consult the paper by Bilgin et al. (2008) to see the validity of laboratory cutting tests to predict the daily advance rates of TBMs.

References

Ates, U., 2013. A comparative study on the relationships between design parameters of TBMs with two current examples of large section TBMs. MSc thesis, Istanbul Technical University, Graduate School of Science, Engineering and Technology, pp. 105.

Bilgin, N., Balci, C. et al. 1999. The performance prediction of a TBM in Tuzla–Dragos sewerage tunnel. *The World Tunnel Congress'99*, Oslo, 31 May–3 June, Balkema, Rotterdam, pp. 817–822, ISBN 90 5809 0639.

Bilgin, N., Copur, H., Balci, C., Tumac, D., Akgul, M., Yuksel, A., 2008. The selection of a TBM using full scale laboratory tests and comparison of measured and predicted performance values in Istanbul Kozyatagi–Kadikoy metro tunnels. *World Tunnel Congress*, September 22–24, Agra, India, pp. 1509–1517.

Bilgin, N., Ozbayir, T, Sozak, N., Eyigun, Y., 2009. Factors affecting the economy and the efficiency of metro tunnel drivage with two TBMs in Istanbul in very fractured rock. *ITA AITES World Tunnel Congress*, Budapest, Hungary, May 23–28, p. 10 .

Bilgin, N., Copur, H., Balci, C., 2012a. Effect of replacing disc cutters with chisel tools on performance of a TBM in difficult ground conditions. *Tunnelling and Underground Space Technology*, 27, 41–51.

Bilgin, N., Balci, C., Copur, H., Tumac, D., Avunduk, E., 2012b. Rock mechanics aspects related to cutting efficiency of mechanical excavators, 25 years of experience in Istanbul, *EUROCK 2012*, Stockholm.

Bruland, A., 2000. Hard rock tunnel boring, PhD thesis, Norwegian University of Science and Technology Department of Building and Construction Engineering, Vol. 10

Buchi, E., 1984. Einfluss geologischer Parameter auf die Vortriebsleistung einer Tunnelbohrmaschine, PhD dissertation, Bern.

Eskikaya, Ş., Bilgin, N., 2000. Development of rapid excavation technologies for the Turkish mining and tunnelling industries. *NATO TU-Excavation Project Sponsored by SfS Programme*, Istanbul Technical University, Istanbul, p. 171.

Farrokh, E., Rostami, J., 2012. Downtime analysis. *North American Tunnelling Journal*, January, 15–18.

Guclucan, Z., Meric, S., Palakci, Y., Bilgin, N., Balci, C., Tumac, D., Algan, M., Namli, M., Bilgin, A.R., 2008. The use of a TBM in difficult ground conditions in Istanbul (Beykoz–Kavacik) sewerage. *World Tunnel Congress*, September 22–24, Agra, India, pp. 1630–1638.

Guclucan, Z., Meric, S., Palakci, Y., Bilgin, N., Balci, C., Copur, H., Namli, M., Bilgin, A.R., Kandemir, E. 2009. The use of theoretical rock cutting concepts in explaining the cutting performance of a TBM using different cutter types in different rock formations and some recommendations. *ITA, AITES World Tunnel Congress*, May 23–28, Budapest, Hungary, p. 10.

Maidl, B., Schmid, L., Ritz, W., Herrenknecht, M. 2008. *Hardrock Tunnel Boring Machines*. Ernst and Son, Germany, p. 343.

Namli, M., Cakmak, O., Pakis, I.H., Tuysuz, L., Talu, T., Dumlu, M., Balci, C., Copur, H., Bilgin, N. 2013. A methodology of using past experiences in the performance prediction of a TBM in a complex geology and risk analysis. *World Tunnel Congress,* Geneva.

Rostami, J., Ozdemir, L., 1993. A new model for performance prediction of hard rock TBMs. *Proceedings of the Rapid Excavation and Tunnelling Conference* 1993, Boston, pp. 793–809.

Rostami, J., Ozdemir, L., Nilsen, B., 1996. Comparison between CSM and NTH hard rock TBM performance prediction models. *Proceedings of Annual Technical Meeting of the Institute of Shaft Drilling Technology*, Las Vegas.

Stack, B., 1995. *Encyclopaedia of Tunnelling, Mining and Drilling Equipment*, Hobart, Tasmania, Muden Pub. Co. Vol. 3. ISBN 0 9587711 1 1.

This page intentionally left blank

10

Soft Ground Tunnel Boring Machines

10.1 General Classification of Soft Ground TBMs

Demand on tunneling through soft ground has been increasing in parallel to urbanization, since most of the urban areas are on soft ground and most of the infrastructure systems are constructed in shallow depths where soft grounds/soils below underground water are dominant. Very weak and weathered rocks are also considered as soft ground in addition to soils. Therefore, the most important tunneling problems arise in stability of the excavated environment such as roof or face collapse and surface settlement. Accordingly, the shielded and face pressurized soft ground tunnel boring machines (TBMs) have been developed to minimize the stability and safety problems for the last 3–4 decades (Maidl et al. 1996).

A general classification of TBMs used for excavation of soft grounds are presented in Table 10.1 based on face support types, muck haulage systems, and working modes. The most widely used soft ground TBMs are earth pressure balance (EPB) and slurry pressure balance (SPB). Both of these TBM types can work in closed (with face pressure in unstable grounds) and open (without face pressure in stable grounds) working modes to minimize the stability problems.

A rigid (usually) circular steel shield protects the equipment and personnel in the tunnel. Shields generally consist of two telescopic sections to ease the excavation of curved alignments: front and rear shields (front and rear skins/cans) connected to each other by articulation jacks (hydraulic cylinders).

The cutterhead is located in front of the shield system. The excavation diameter is slightly larger than the shield diameter to reduce the frictional forces between the shield and ground and provide easier excavation of the curves. This is provided by usually a few gauge (corner) cutters placed on the most outer portion of the cutterhead. The circumferential speed of the gauge cutters in soft ground TBMs is usually arranged between 15 and 25 m/min depending on planned advance rate and soil properties, and might be increased for accelerated constructions (JSCE 2007).

The most common cutting tools used in EPB and SPB TBM cutterheads are scraper (ripper, blade, knife, teeth) tools. Conical picks and disk cutters

TABLE 10.1

General Classification of Soft Ground TBMs

Machine Type	Face Support	Muck Haulage	Mode
Earth pressure balance TBMs (EPB TBMs, auger TBMs)	Pressured muck + one or more of water, foam, polymer, bentonite (processed muck)	Dry muck haulage (rail, conveyor belt, truck)	Closed, open
Slurry pressure balance TBMs (SPB TBMs, hydroshields, bentonite shields)	Pressured water or water + bentonite (or + polymers)	Hydraulic muck haulage (steel pipe)	Closed, open
Compressed air shields (mostly partial face excavation)	Pressured air (against only water ingress, not against earth pressure)	Dry muck haulage (rail, conveyor belt, truck)	Closed, open
Polyshields (Mixshields)	Combination of two or more of the above methods	Combined muck haulage (dry and/or hydraulic)	Closed, open
Blind (extrusion) shields, shields with pressure relieving gate	Mechanical plates	Dry muck haulage (rail, conveyor belt, truck)	Partly open

Source: Adapted from Copur, H., 2012. Mechanical excavation and mechanization in soft ground. Graduate Class Notes. Istanbul Technical University, Mining Engineering Department.

used for excavation of mixed grounds having hard rocks or boulders in addition to soft ground can be used in case of a mixshield TBM. The disk cutters are installed around 4–5 cm in front of the ripper tools; in soft ground they sink and the ripper tools start working/scraping. By the cutting tools attached on the cutterhead the excavated materials enter the excavation/pressure chamber through slits (openings). Size and geometry of the slits depend usually on the allowable maximum boulder size and the properties of soil to be excavated. Allowable boulder size usually depends on the type and diameter of the screw conveyor used in EPB TBMs, as well as the type and geometry of the crusher used in SPB TBMs. The opening ratio of the cutterhead should be designed based on ground and machine features, and is usually between 10–30% for SPB and 30–40% for EPB TBMs (JSCE 2007). It is generally increased for excavation of highly cohesive soils to prevent sticking and clogging problems.

Pressure bulkhead, being a rigid steel plate, separates the excavation/pressure chamber (including the cutterhead wheel) and the shield section in atmospheric pressure. It should generally withstand the earth pressure (usually up to ~5 bar for EPB and ~10 bar for SPB) in the chamber, which is the space between the bulkhead and the cutterhead, and pressure of the thrust cylinders. Most of the inlets to the excavation chamber, such as for slurry, conditioning agents, foam, man lock, are usually located on the upper part of the bulkhead, while the outlets of the muck discharge pipe line or screw conveyor are located on the bottom part. Man lock is required for pressure

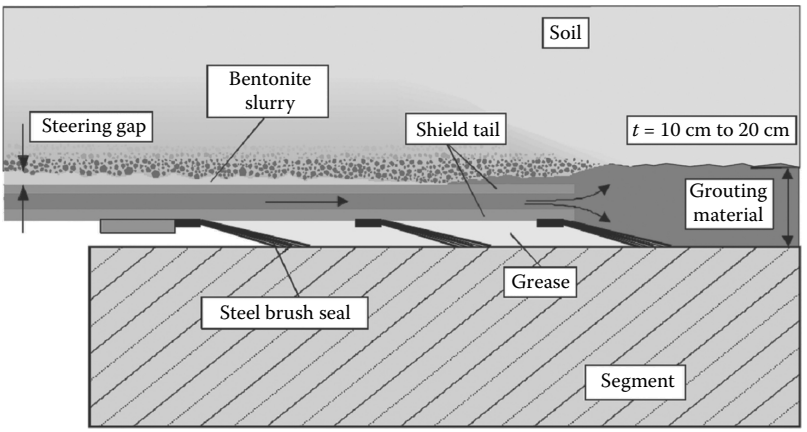

FIGURE 10.1
Wire brush tail seals used between segmental rings and tail shield. (Adapted from Babandererde, S., 1999. *Tunnels and Tunneling International*, 11:48–49.)

adjustment of the personnel who need to enter into the excavation chamber for any job, such as maintenance and cutter replacement under pressure.

The tunnel lining should be segmental rings in soft ground TBMs, since these machines get their thrust force for advancement from the segments. Since their shields are a single shield design, excavation stops during segment erection, although there are some possibilities in especially large diameters for continuing excavation during segment erection.

Tail seals located at the far most rear end of the tail shield is used between the segmental rings and the tail shield of the soft ground TBMs and is necessary to prevent the entry of water into the shield. Although there are different sealing systems and materials, wirebrush-type seals are the most common ones. Pressurized grease is filled into the place between each line/bunch of the tail seals (Figure 10.1). The seals must be flexible to absorb misalignment of the shield relative to the segment, occupy as little radial space as possible, be long wearing, and be replaceable in case of damage.

The pressure bulkhead, seals between shield tubes, seals between rear shield and segmental linings, and seals between segment pieces provide a totally distinguished underground opening with no connection to the ground in soft ground TBMs.

10.2 Compressed Air Shields

Compressed air shields are used in a decreasing number of cases due to health and safety problems (requiring strict regulations), as well as some operational aspects. They can be applied with hand shields, partly or fully

mechanized shields with an additional compressed air and lock installation (Maidl et al. 1996). Only water (hydrostatic) pressure should be balanced by the compressed air face support. They are normally used in sandy formations having permeability values lower than 10^{-4} m/s (Maidl et al. 1996). The compressed air must not be used to counteract earth pressure; earth pressure has to be balanced additionally by natural or mechanical support. The air pressure in the cutterhead chamber should be set to water pressure in the invert of tunnel. If there is no underground water, the system can be used in open mode (without face pressure). Increased soil permeability above 10^{-4} m/s (which is an upper limit) makes use of this method more difficult, since the air would escape. Minimum depth of cover above the crown should be single or double the tunnel diameter (depending on ground type) to avoid blow-outs. The air pressure is usually limited to a maximum pressure of 4 bar (3 bar excess pressure) for personnel entering the pressure chamber (Maidl et al. 1996).

Tunneling with compressed air shields reduces staff performance due to the danger of Caisson's disease (compressed air disease), it reduces work time due to compression and decompression of staff, and increases the danger of fire and smoke (respiratory–visibility considerations). It also requires a large compressed air generation system on the surface. However, compressed air use becomes a common practice with SPB and EPB TBMs as being mixshield, which provides additional means to face support especially for conditions of staff working in excavation/pressure chamber and of face pressure regulations.

10.3 Partly Open Face (Blind) Shields

The utilization of blind shields, also called extruding or manual shields, is also quite limited since they are used only for very special soil conditions. Blind shields are used in very short tunnels for excavation of very homogeneous plastic clays having a standard penetration test number (N) of less than 5 (Maidl et al. 1996), where no soil conditioning is required. The earth pressure is balanced by hydraulic jacks used for machine advancement and face plate. Also, an adjustable door system helps face/muck control. There are no cutting tools for excavation; the soil at face is just extruded/squeezed by pushing/thrusting the shield forward. The extruded ground falls into the transportation system located behind the shield. It is very difficult to enter the front side of the shield to see the ground or to remove any obstacle.

10.4 Slurry Pressure Balance TBMs and Slurry Conditioning

The earth pressures in unstable/loose grounds with or without ground water can be easily counterbalanced by the face pressures given by a special

bentonite–water mixture (if it is required, some other admixtures can be used) in slurry pressure balance (SPB) TBMs. The pressure chamber should be full with slurry and muck mixture for an efficient pressurization. The slurry feeding from the slurry conditioning/treatment/preparation system to the excavation chamber and transportation of the mixture of slurry and muck from the chamber to the slurry separation system are performed by means of hydraulic transportation through two separate metal pipe lines using speed-controlled pumps: feeding line and discharging line. Flexible pipes are normally used for passing the mixture from the chamber to the tunnel or the slurry from tunnel to the chamber. Telescopic pipes are normally used for adaptation to moving backup system of the TBM. The slurry system works in a closed circuit providing reuse of the slurry after reprocessing.

In stable ground and hard rock conditions, SPB TBMs can be used in open mode without giving any face pressure. They are normally used for excavation of gravel, coarse and medium size sands, and silty and/or clayey sands having hydraulic conductivity between 10^{-8} and 10^{-2} m/s (Efnarc 2005). The best applicable soil range including conditioning suggestions for SPB and EPB TBMs is presented in Figure 10.2.

One of the most important developments with SPB TBMs realized in Germany is the utilization of a submerged wall in the pressure chamber, which divides the chamber into two separate portions in the upper part. The upper part of the rear chamber portion should be pressurized by compressed air while the lower part should be full of slurry and muck mixture. The front chamber portion should be filled completely with slurry and muck mixture. The face support pressure is regulated in the rear chamber by an air cushion acting also as a dumping unit for sudden pressure changes (Maidl et al. 1996). The rise and fall of the interface between the slurry and air cushion/pocket, as cutterhead pressure varies, is detected and the discharge pump is altered to suit the pressure. This type of face pressure control makes possible to respond quickly to any pressure changes in the chamber, resulting in better settlement control. These types of SPB TBMs are more common today and they are called Hydroshield or Bentonite Shield in German literature and can be considered as a mixshield (polyshield) type of TBMs combining different face pressure methods. A typical schematic view of SPB TBMs is presented in Figure 10.3.

The cutting tools excavate the ground, the excavated material enters to the pressure/excavation chamber through slits or openings and mixes in the chamber with the pressurized slurry pumped through feeding line, and then, the mixture is pumped to the surface through the discharging line. There is a mixing mechanism inside the working chamber in front of the discharging line for improved transportation without clogging or settling of the mixture in the line. The slurry feeding line enters the chamber in the upper or middle part and the mixture of slurry and excavated material exits in the lower part, in front of which there is a grill for blocking any large pieces of stones entering to the line. Also, there is a stone crusher usually located in front of the

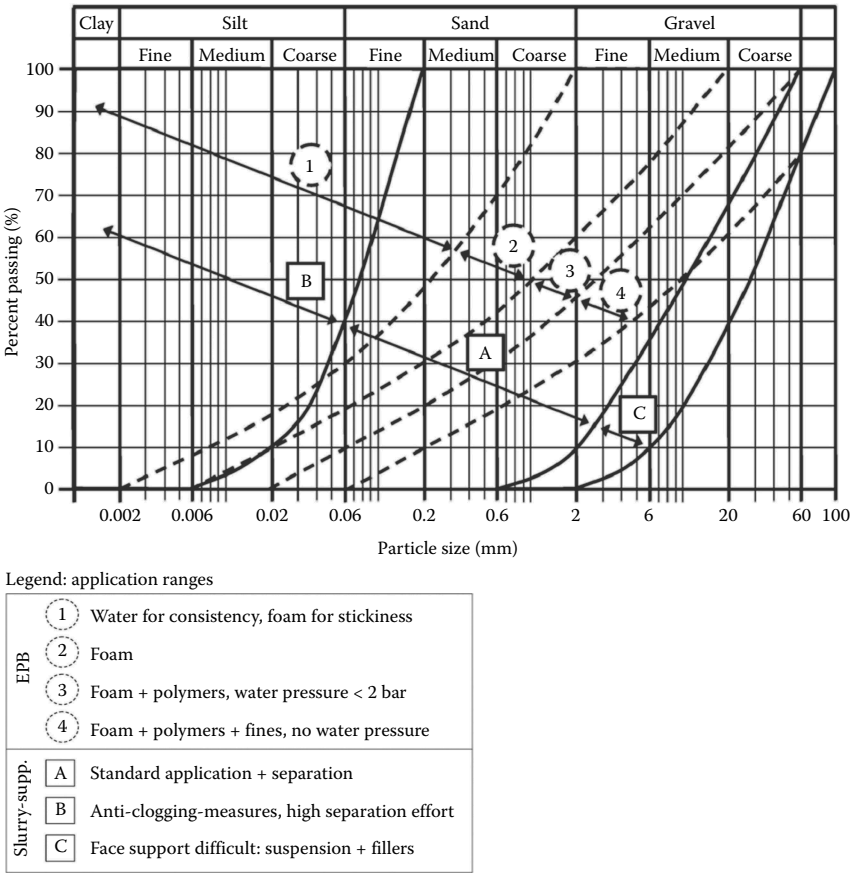

FIGURE 10.2
Applicable soil ranges for SPB and EPB TBMs. (Adapted from Thewes, M., 2007. *Proc. the 2nd Symposium on Underground Excavation for Transportation*, November 15–17, Istanbul, pp. 49–56; Thewes, M., Budach, C., 2010. *Geomechanics and Tunnelling*, 3(3):256–267.)

discharging line intake to reduce the size of boulders and any stones, which prevents any clogging within the discharging line and enables easy transportation. Different types of stone crushers such as jaw, roller, and box types can be used, of which the jaw crusher type is the most common one.

An air lock system is usually incorporated in these machines behind the cutterhead. When personnel are required inside the working chamber, the fluid inside the head can be displaced by pumping in compressed air for maintaining the face support and preventing the ingress of water. Then, the worker goes into the air lock before entering the chamber, so that they get used to pressure increase to protect against Caisson's disease, which is a very time consuming process.

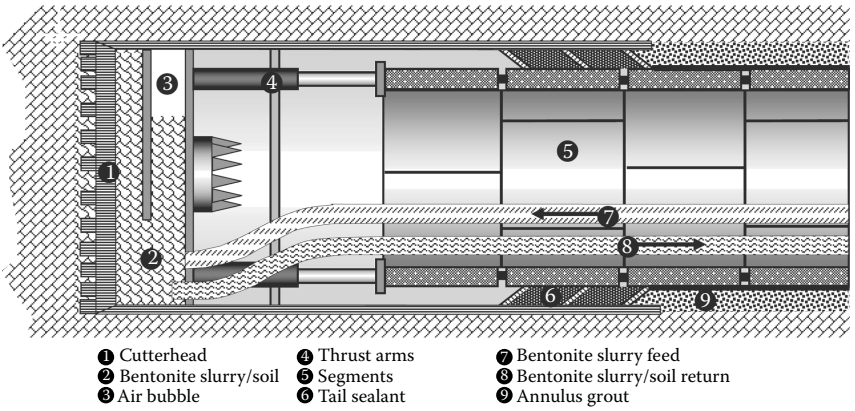

FIGURE 10.3
Typical schematic view of a SPB TBM. (Adapted from Efnarc, 2005. Specification and guidelines for the use of specialist products for mechanized tunnelling (TBM) in soft ground and hard rock. European Federation Dedicated to Specialist Construction Chemicals and Concrete Systems.)

A separation plant is required on the surface, sometimes in back up (inside the tunnel), for solid–liquid separation of the discharged muck, which requires extra space and cost. The design of separation plant is important in terms of functioning and TBM performance. Also, a slurry preparation system is required. The key rheological, physical, and chemical test parameters for water + bentonite slurry are density, solids contents, pH, plastic viscosity, apparent viscosity, yield value, gel strength, and filter water (filterability) (Aftes 2005). Tests for these characteristics are described in EN ISO 13500 (1998). The properties of the water used for slurry preparation and underground water should be carefully handled for a better control of the rheological properties of the mixture. After a certain amount of utilization, it may be necessary to totally refresh the slurry. Before using a fresh slurry, well stirred with a centrifuge mixer, it is better to first store it in a tank where hydration of bentonite can continue 12–24 more hours. Chemical agents or polymers may be required to disperse the bentonite more efficiently and faster.

There are some basic functions of the slurry (Aftes 2005):

1. It supports an unstable face by applying pressure opposed to the combination of soil and hydrostatic forces and a filter cake occurs on the face.
2. It provides a transportation medium to carry away the excavated material by hydraulic (steel pipe) transportation.
3. It lubricates and cools the cutterhead and reduces the abrasive wear of cutters and the cutterhead.

There are generally three models for filtration of slurry into the ground: caking (in cohesive soils), penetration (in gravelly soils), and combined (caking + filtration) in sandy soils (Kirchebauer 1977 as quoted by Kanayasu et al. 1995). In especially sandy cohesive conditions, the bentonite penetrates the face and produces a semi-impermeable membrane (cake, caking, filter cake) or film effect, creating structural resistance to a face collapse and an obstacle for slurry loss into the ground.

The specific gravity of the fresh slurry (water + sodium bentonite powder) entering to the pressure chamber should be around 1.02–1.03 (Guglielmetti et al. 2008). This requires around 4–5% bentonite added to the water by weight. Enough time in a tank, usually around 12–24 hours, should be given to the fresh-mixed slurry for proper hydration and rheological properties. Generally the discharge side density should be of an average of 1.25 (~400 kg/m^3 solids) and densities up to 1.50 can be handled, depending on the properties of the excavated material (Maidl et al. 1996). It is possible to improve the rheological properties of the slurry by adding some polymers. Polymers with long-chain molecules behave usually as reinforcement fibers. The ratio of slurry feeding volume to in situ volume of the soil excavated varies depending on the ground properties. Typical slurry feed/discharge pipe sizes are presented in Table 10.2.

There should be a lower (critical) limit of the carrier fluid velocity in the pipe line to prevent settling (sedimentation) of the solids along the line, and an upper limit based on head (frictional) losses and wear of the pipes and pumps (Maidl et al. 1996; Guglielmetti et al. 2008). The speed of the transported material should not be slower than 0.5–0.7 m/s; and the separation plant should be designed for a speed higher than 1.0 m/s (Guglielmetti et al. 2008). Sedimentation of the particles conveyed through pipe lines can be avoided if the conveying speed is greater than the critical velocity or at least 17 times of the settling (sedimentation) rate of the particles (Abulnaga 2002). In heterogeneous suspensions, the critical velocity depends on the settling rate, density, concentration and grain size of the solids conveyed, and the

TABLE 10.2

Typical Slurry Feed/Discharge Pipe Sizes

Excavation Diameter of SPB TBM (m)	Discharge Pipe Diameter (mm)	Feed Pipe Diameter (mm)
2–4	100–250	100–200
4–6	150–300	150–300
6–8	200–300	200–300
8–10	200–350	200–300
10–14	300–350	300–350

Source: Adapted from JSCE, Japan Society of Civil Engineers, 2007. *Standard Specification for Tunnelling-2006: Shield Tunnels*. ISBN: 978-4-8106-0568-6, 270 p.

pipe diameter. In case of any interruption in the excavation process, a bypass valve system is used for continuation of slurry or mixture circulation to prevent any clogging or sedimentation on the lines, which means system failure and downtime.

In clay soils, addition of bentonite may not be necessary, as the face is not permeable, and the clay would naturally disperse within the water; only water can be used as a carrier fluid. Water escapes when working in nonplastic soils above underground water level and if the water feeding pressure exceeds the underground water pressure. The water loss is generally low in silty and fine-grained sand. In uniform coarse gravel, it is necessary to use special suspensions which are based on polymers or which contain cellulose-based additives.

10.5 Earth Pressure Balance TBMs and Soil/Ground/Muck Conditioning

The earth/ground and water pressures in unstable (nonself-supporting) cohesive soils, with or without ground water, is counterbalanced with the face pressure given by thrust cylinders to the excavated material (muck, earth) filled fully on the chamber and processed usually by different foaming agents and polymers in earth pressure balance (EPB) TBMs. Processed (conditioned) muck/ground/soil is transported from the excavation chamber to the tail conveyor behind the TBM by a rotating screw conveyor. The rotational speed of the screw conveyor and the opening of screw conveyor discharging gate/door can be adjusted to control face (excavation chamber) pressure. In this way, excessive muck removal leading to face instability and settlement, and over pressures leading to compression and heaving of the ground, as well as high cutterhead torques are all avoided. The muck discharge rate and rotational speed of the screw conveyor should be equivalent to the advance (excavation) rate of the machine, adjusted by thrust cylinders, for proper face pressure control without hazardous stability problems. The amount of excavated material should be controlled by either a weighing or a laser scanning system.

EPB TBMs are normally used for excavation of fine sand, silt, and clay having low permeability. They are not very effective in soils having fine material less than 10% (Guglielmetti et al. 2008) and water heads over 4 bar. They can also be used for hard rock excavations if their cutterheads and muck transportation units are suitable, of which these types can be considered as mixshields (polyshields).

Any dry/mechanical muck haulage system such as conveyor belts, rails, and trucks can be used from the tail conveyor of TBM to the shaft bottom or surface. In self-supporting low permeable stable soils and hard rock

conditions without water income, they can be used in open mode without giving face pressure. In self-supporting stable soils with moderate water income, they can be used in transition mode, being half-filled with conditioned muck without giving any face pressure, and may be giving pressure only by compressed air to stop water ingress. A schematic view of an EPB TBM system is presented in Figure 10.4. Different working modes of EPB TBMs are presented in Figure 10.5. A general comparison of EPB and SPB TBMs is presented in Table 10.3 based on Babandererde (1991), Maidl (2005), Copur (2012), and Lovat (2007).

There are generally two types of screw conveyors: shaft and ribbon (without shaft) (Figure 10.6). The type of the screw conveyor is usually defined based on the expected sizes of the boulders in the tunnel alignment. Ribbon-type screws can carry larger boulders, while shaft-type screws require less maintenance. The screw conveyor is located at an angle to the tunnel axis to generate a pressure gradient between pressurized chamber and atmospheric conditions. In very large diameters, two or three screw conveyors can be used spontaneously for enabling enough transportation capacity such as in Madrid's M-30 highway (Herrenknecht 2013). Especially where the water pressure is critical, the angled screw conveyor can be extended by a horizontal section (Figure 10.7) allowing for working up to 10 bar face pressures, which is a recent development (Herrenknecht et al. 2011; Gonzales and Magro 2012).

Since the excavated materials are usually inhomogeneous and highly permeable, it is not possible to generate such things as uniform face pressure, impermeable plugs within the chamber, screw conveyors for preventing water entering the tunnel, and pulpy (in gel form)—plastic—low internal friction—low permeability—low cohesion (easy to transport) muck, without

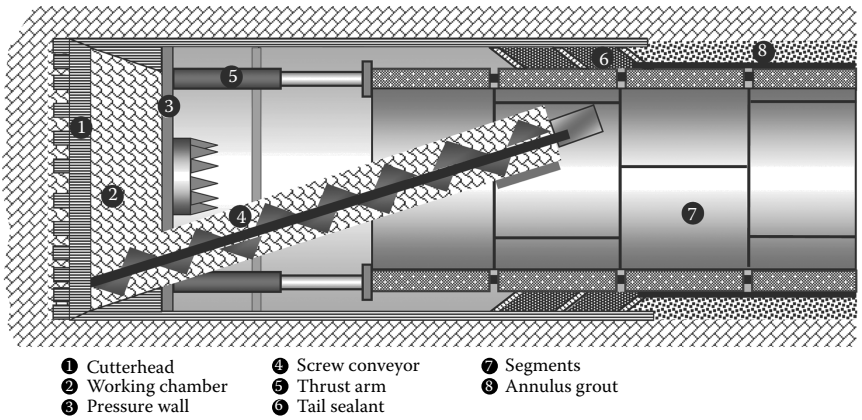

FIGURE 10.4
Schematic of an EPB TBM System. (Adapted from Efnarc, 2005. Specification and guidelines for the use of specialist products for mechanized tunnelling (TBM) in soft ground and hard rock. European Federation Dedicated to Specialist Construction Chemicals and Concrete Systems.)

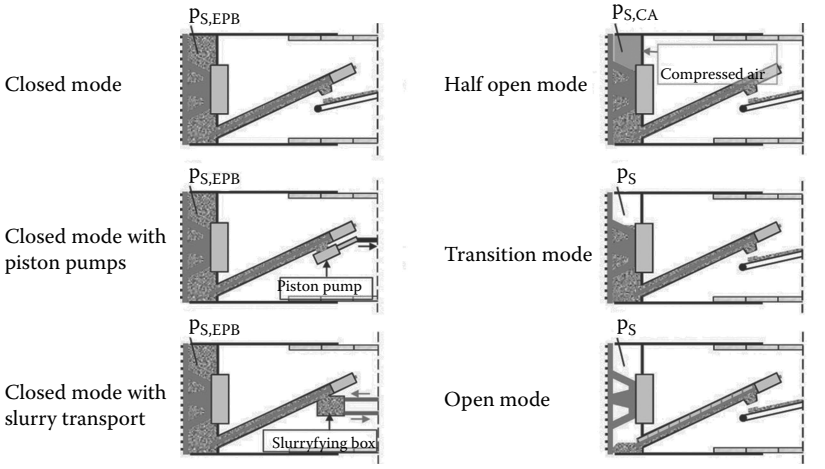

P_S : No support pressure, $p_{S,EPB}$: support pressure in closed mode, $p_{S,CA}$: support pressure of compressed air)

FIGURE 10.5
Working modes of EPB TBMs. (Adapted from Herrenknecht, M., Thewes, M., Budach, C., 2011. *Geomechanics and Tunnelling*, 4:1:11–35. With permission.)

TABLE 10.3

A General Comparison of EPB and SPB TBMs

Criterion	Slurry TBMs	EPB TBMs
Cutterhead torque requirement	Requires lesser torque	Requires more torque
Handling boulders	Handles easily the stones and boulders using crusher units	Stones and boulders endanger the mud stirring bars and screw conveyor
Adaptability to varying geology	More tolerant/adaptable	Lesser tolerant/adaptable
Applicable geology	Best applicable to sandy soils under water table	Best applicable to clayey soils under water table
Excavation rate	Best in the applicable geology	Best in the applicable geology
Muck haulage	Hydraulic transportation	Dry muck haulage
Muck separation plant	Requires (on surface or in tunnel), resulting in extra cost and space	No need for muck separation plant
Face support	Water + bentonite slurry	Conditioned muck
Face pressure control	More elaborate (faster control)	Simpler (slower control)
Face pressure limit	4–4.5 bar (up to 8 bar recently)	8–9 bar (up to 15 bar recently)
Surface settlement	Lower	Higher
Slurry loss into ground	Easier	More difficult

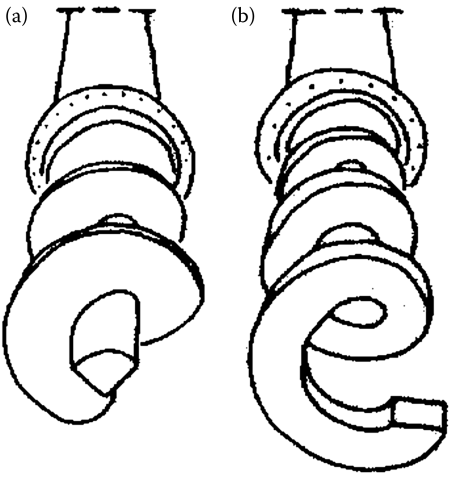

FIGURE 10.6
Shaft-type (a) and ribbon-type (b) screws. (Adapted from Maidl, B., Herrenknecht, M., Anheuser, L., 1996. *Mechanized Shield Tunnelling*. Ernst and Sohn, ISBN: 3-433-01292-X, 427 p. With permission.)

conditioning the excavated material. Therefore, EPB-TBMs require additional injection and mixing units for suitable (homogeneous) conditioning of excavated ground (soil/earth/ground/muck conditioning). Mixing bars (mixing blades) fixed on the pressure bulkhead and attached on the cutterhead wheel are used to properly mix the additives with the excavated ground. The usual additives are foaming agents (surfactants), polymers, water, and air. In grounds having fine materials less than 10%, fillers such as fine sand or

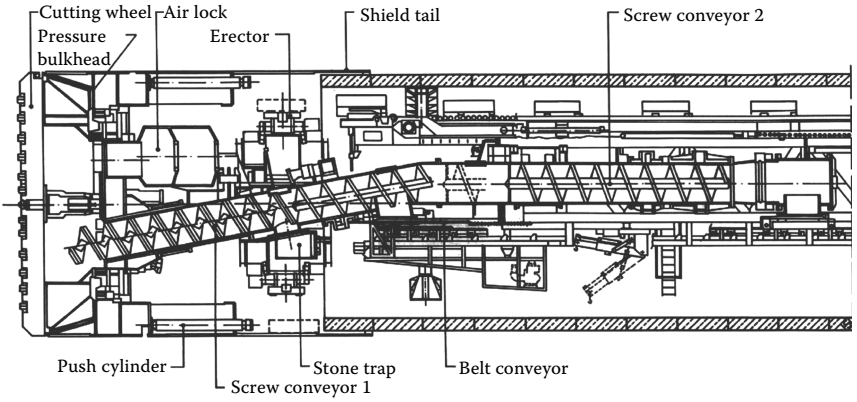

FIGURE 10.7
Extended screw conveyor of EPB TBMs. (Adapted from Herrenknecht, M., Thewes, M., Budach, C., 2011. *Geomechanics and Tunnelling*, 4:1:11–35. With permission.)

fine crushed limestone can be added to provide suitable working of the foam (Efnarc 2005). Additives are injected on the cutterhead face, in the excavation chamber, and through the screw conveyor.

The first step of a successful conditioning operation is to define the basic characteristics of the soil or ground to be excavated. The second step is to characterize the conditioning agents (chemicals, additives), which are usually surfactants and/or polymers. The third and last step is to apply the tests to identify the interaction between the ground sample and conditioning agents. Knowing the results of these tests, some suggestions can be set for the given ground conditions to obtain an optimum and safe performance of EPB TBM operation.

Some parameters, such as foam expansion ratio (FER), foam injection ratio (FIR), and surfactant (foam) concentration (C_F) determine the success of a conditioning process. A solution is prepared by mixing water and surfactant usually in concentrations between 0.5% and 5% (Efnarc 2005). This solution is mixed with compressed air to generate foam; the amount of air within the foam determines FER, which is usually between 5 and 30 (Efnarc 2005). The amount of foam injected to the excavated material determines FIR, which is usually between 10% and 80% (Efnarc 2005).

10.6 Surface Settlements on Soft Grounds

Many surface and subsurface structures around shallow, soft ground tunneling in urbanized areas, make underground construction work very delicate due to ground deformation influence, which should definitely be controlled to acceptable levels. The short- and long-term surface and subsurface ground deformations should be predicted and precautions against any damage to existing structures should be planned prior to construction of any underground structure.

The basic parameters that affect ground deformations are ground conditions, technical and/or environmental parameters, and tunneling and/or construction methods (O'Reilly and New 1982; Arioglu 1992; Karakus and Fowell 2003; Tan and Ranjit 2003; Minguez et al. 2005; Suwansawat and Einstein 2006). A thorough site investigation should be performed to find out the ground conditions; especially the stiffness of soft ground, which is important in terms of deformations. Technical and environmental parameters affecting ground deformations include tunnel depth and geometry, tunnel diameter–line–grade, single or double track lines, and neighboring structures. The construction method is selected based on site characteristics and technical project constraints (safety and economy) and should be planned so that ground movements are limited to an acceptable level. Excavation method, face support pressure, advance (excavation) rate,

stiffness of support system, excavation sequence, and ground treatment (improvement) have dramatic effects on the ground deformations occurring due to tunneling operations.

The primary reason of ground movements (surface settlements) is convergence of the ground into the tunnel after excavation. This changes in situ stress states of the ground and results in a stress relief. Convergence of the ground is also known as ground loss or volume loss. The volume of the settled ground on the surface is usually assumed to be equal to the ground (volume) loss inside the tunnel (O'Reilly and New 1982).

Ground loss can be classified as radial loss around the tunnel periphery and axial (face) loss at the excavation face (Attewell et al. 1986; Schmidt 1974). It is possible to minimize the face loss in full-face (closed face) mechanized excavations by means of applying a face pressure. The ground loss is usually more in granular soils than in cohesive soils for similar construction conditions. The width of the settlement trough on both sides of the tunnel axis is wider in the case of cohesive soils, which means a lower maximum settlement for the same amount of ground loss.

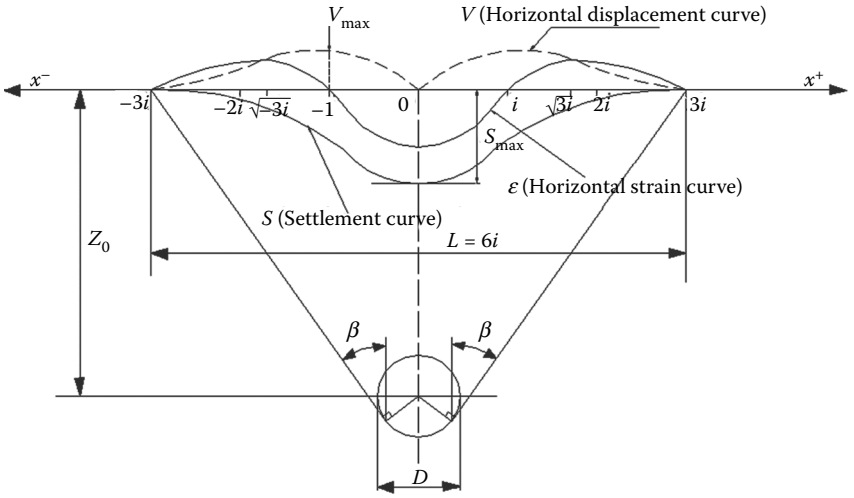

S = Theoretical settlement curve (gauss error function, normal probability curve),
S_{max} = Initial maximum settlement (immediate, short term, undrained),
s = Transverse horizontal distance from the tunnel center line,
i = Point of inflexion of the settlement curve,
Z_0 = Depth to tunnel axis,
D = Tunnel excavation diameter (D_{TBM}) or equivalent tunnel diameter,

FIGURE 10.8
Surface settlement parameters. (Adapted from Copur, H., Ercelebi, S.G., Bilgin, N., 2007. *Proc. 2. Symposium on Underground Excavationd for Transportation*, pp. 443–454 (in Turkish); Ercelebi, S., Copur, H. Ocak, I., 2011. *Environmental Earth Sciences*, 62:357–365.)

Short-term settlements occur during or after a few days (mostly a few weeks) of excavation, since undrained soil conditions are dominant. Long-term settlements are mostly due to creep, stress redistribution, and consolidation of soil after drainage of the underground water and elimination of pore water pressure inside the soil; it may take a few months to a few years to reach a stabilized level (Attewell et al. 1986). The long-term settlements may be considered as very limited in dry soil conditions.

There are mainly three settlement prediction approaches for mechanized tunnel excavations: (a) numerical analysis such as finite element method, (b) analytical method, and (c) semi-theoretical method. It is generally suggested to apply more than one method to predict the surface settlements. The results of all methods should be used carefully by an experienced field engineer in the designing stage of an excavation project. Based on the predictions, risk levels, and required precautions (action plans) to minimize the risks are identified.

Surface settlement parameters are presented in Figure 10.8. As seen, the shape of the settlement curve is very similar to Gaussian probability (error) curve and the maximum surface settlement occurs over the axis (centerline) of tunnel.

10.7 Numerical Examples Related to Soft Ground TBMs

10.7.1 A Numerical Example on Estimation of Global Face Stability

A closed-face TBM with a diameter of 6.5 m is used for excavation of a dry sandy silt formation. The tunnel depth to the crown is 15 m. The length of the shield is 8 m. The surcharge pressure is 30 kPa. The average soil bulk unit weight, undrained cohesion, and internal friction angle are 18 kN/m^3, 40 kPa, and 12°, respectively. Analyze the global stability of the face. Estimate the face pressure based on limit face pressures.

10.7.1.1 Solution of Numerical Example 10.7.1

According to Broms and Bennermark (1967), if the stability ratio (N) given in Equation 10.1 for a cohesive soil is smaller or equal to 4, the face is stabile:

$$N = \left[\frac{\sigma_{\text{Sur}} + \gamma_b \cdot (h + D_{\text{TBM}}/2) - \sigma_T}{C_U} \right] \tag{10.1}$$

where

N = stability ratio (overload factor)
σ_{Sur} = surface surcharge pressure (kPa)
σ_T = face pressure (kPa)

γ_b = bulk unit weight of soil (kN/m^3)
h = depth of cover to crown (m)
D_{TBM} = diameter of tunnel (or excavation diameter of TBM) (m)
C_U = undrained shear strength (cohesion) of soil (kPa)

Assuming the shield length and face pressure is 0, the stability ratio becomes

$$N = \left[\frac{30 + 18 \cdot (15 + 6.5/2)}{40}\right] = 9.0$$

Since the estimated stability ratio of 9.0 is greater than the threshold stability ratio value of 4.0, the face is not stable.

Another method to check the global face stability is based on critical undrained cohesion ($C_{Ucritical}$) (Mair and Taylor 1997):

$$C_{Ucritical} = \frac{\sigma_{Sur} + \gamma_b \cdot (h + D_{TBM}/2)}{N_{Cri}} \tag{10.2}$$

where N_{Cri} is the critical stability ratio and it can be found from the graph given in Figure 10.9. If the critical undrained cohesion is smaller than the undrained cohesion of the ground, then, the face is stabile. Since, the ratio of overburden over the crown (h) to TBM diameter (D_{TBM}) is around 2.3 and the ratio of shield length (L) to TBM diameter (D_{TBM}) is around 1.2, the critical load factor (N_{Cri}) is found to be around 6. Then,

$$C_{Ucritical} = \frac{30 + 18 \cdot (15 + 6.5/2)}{6} = 60\,\text{kPa}$$

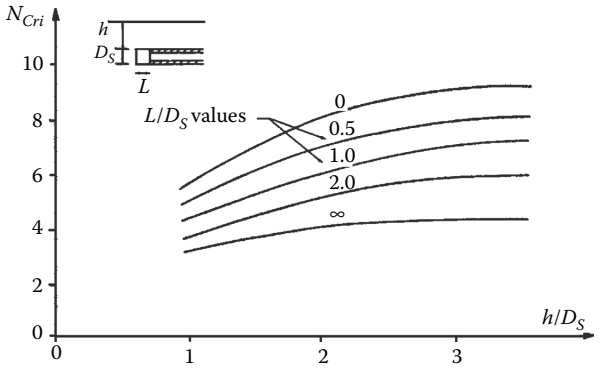

FIGURE 10.9
Estimation of critical load factor. (Adapted from Mair, R.J., Taylor, R.N., 1997. *Proc. the 14th Int. Conference on Soil Mechanic and Foundation Engineering*, Hamburg, Balkema, Vol. 4, pp. 2353–2385.)

Since the critical undrained cohesion (60 kPa) is greater than the undrained cohesion of the ground (40 kPa), the face is not stable. Then, a face pressure should be applied.

The upper and lower limit face pressures are estimated by (Thomson 1995):

$$\sigma_{T-\min} \geq \sigma_{\text{Sur}} + \gamma_b \cdot (h + D_{\text{TBM}}/2) - N_C \cdot C_U \text{ (against collapse)} \quad (10.3)$$

$$\sigma_{T-\max} \leq \sigma_{\text{Sur}} + \gamma_b \cdot (h + D_{\text{TBM}}/2) + N_C \cdot C_U \text{ (against blow – out)} \quad (10.4)$$

$$\sigma_{T-\min} \geq 30 + 18 \cdot (15 + 6.5/2) - 6 \cdot 40 \approx 120 \text{ kPa}$$

$$\sigma_{T-\max} \leq 30 + 18 \cdot (15 + 6.5/2) + 6 \cdot 40 \approx 600 \text{ kPa}$$

The face pressure (σ_T) can be estimated by dividing the undrained cohesion by a safety factor of 1.5–2.0 (as suggested by PJA 1995):

$$\sigma_T \approx 30 + 18 \cdot (15 + 6.5/2) - 6 \cdot 40/2 \approx 240 \text{ kPa}$$

10.7.2 Numerical Example on Estimation of Theoretical Earth Pressures

Estimate the vertical and horizontal earth pressures theoretically using the suggested method by ITA (2000) for the same parameters given in Problem 10.7.1.

10.7.2.1 Solution of Numerical Example 10.7.2

The International Tunneling Association (ITA) suggests that if the depth of cover (overburden) to crown is greater than $2D_{TBM}$, arching height (h_0) should be considered for estimating vertical (σ_v) and horizontal (σ_h) earth pressures (ITA 2000). The arching height for dry formations is estimated as follows (ITA 2000):

$$h_0 = \frac{\left\{ b_S \cdot \left(\gamma_b - \frac{C_U}{b_S} \right) \cdot \left[\frac{1 - e^{-K_0 \cdot \tan(\delta) \cdot (h/b_S)}}{K_0 \cdot \tan(\delta)} \right] + \sigma_{\text{Sur}} \cdot e^{-K_0 \cdot \tan(\delta) \cdot (h/b_S)} \right\}}{\gamma_b} \quad (10.5)$$

$$b_S = \frac{D_{\text{TBM}}}{2} \cdot \cot\left(\frac{\pi}{8} - \frac{\phi}{4} \right) \quad (10.6)$$

where

b_S = half-width of arching soil prism (m)

γ_b = bulk unit weight of soil (kN/m^3)

C_U = undrained cohesion of soil (kPa)
K_0 = lateral earth pressure at rest (it is suggested as 1.0 by ITA 2000)
σ_{Sur} = surface surcharge pressure (kPa)
δ = angle of wall friction of arching prism (°), (suggested as equal to ϕ by ITA 2000)
h = depth of cover to crown (m)
D_{TBM} = diameter of tunnel (or excavation diameter of TBM) (m)
ϕ = undrained internal friction angle of ground (°)

$$b_S = \frac{6.5}{2} \cdot \cot\left(\frac{\pi}{8} - \frac{12}{4}\right) = 9.2 \text{ m}$$

$$h_0 = \frac{\left\{9.2 \cdot \left(18 - \frac{40}{9.2}\right) \cdot \left[\frac{1 - e^{-\tan(12)\cdot(15/9.2)}}{\tan(12)}\right] + 30 \cdot e^{-\tan(12)\cdot(15/9.2)}\right\}}{18} = 10.8 \text{ m}$$

ITA (2000) suggests that the vertical (σ_v) earth pressure at tunnel crown and horizontal (σ_h) earth pressure at tunnel springline are estimated by selecting the maximum one of (h_0) and ($2D_{TBM}$) as follows:

$$\sigma_v = \max(\gamma_b \cdot h_0, \gamma_b \cdot 2 \cdot D_{TBM}) \tag{10.7}$$

$$\sigma_h = K_0 \cdot [\sigma_v + \gamma_b \cdot (D_{TBM}/2)] \tag{10.8}$$

Since ($2D_{TBM}$ = 13 m) is greater than (h_0 = 10.8 m),

$$\sigma_v = 18 \cdot \ 2 \cdot \ 6.5 = 234 \text{ kPa}$$

$$\sigma_h = 234 + 18 \cdot (6.5/2) = 293 \text{ kPa}$$

The face pressure (σ_T) that should be applied in the working chamber of the TBM can be estimated by adding a safety margin (may be around 20 kPa) to the horizontal earth pressure (σ_h) as being 313 kPa.

When the tunnel is under ground water level, instead of bulk unit weight of the soil, buoyant weight of soil is used and hydrostatic pressure is added to the earth pressures. Another approach may be using total pressure (saturated unit weight of the soil) instead of effective pressure (JSCE 2007).

10.7.3 Numerical Example on Estimation of Excavation Performance

A closed face TBM with an excavation diameter of 13.25 m is used for excavation of a tunnel with a length of 4000 m in silty sand formation. The excavation job should be completed in 400 days. The working pattern is arranged as 2 of 10 hour-shifts per day and 7 days per week.

1. Estimate instantaneous penetration rate for 40% of machine utilization time.
2. Estimate rotational speed (*RPM*) of the cutterhead based on maximum corner cutter speed of 45 m/min.
3. Estimate penetration per revolution.
4. Estimate mean cutting force and mean normal force per cutter (wedge type) in cutting the soil by using Labanov and Joanknecht (1980) model for the estimated penetration per revolution value above and taking cutter width of 10 cm, rake angle of 30°, clearance angle of 10°, internal friction angle of ground of 25°, friction angle between cutter and ground of 30°, and shear strength (cohesion) of ground of 100 kPa.
5. Estimate thrust, torque, and power requirement of the machine for just cutting the ground (without considering face pressure) by using the cutter forces estimated above. Assume that the center cutter has the same cutters and the TBM cutterhead has six spokes.

10.7.3.1 Solution of Numerical Example 10.7.3

10.7.3.1.1 Estimation of Instantaneous Penetration Rate

$$IPR = \frac{L_{\text{tunnel}}}{D_{\text{total}} \cdot S_{\text{day}} \cdot H_{\text{shift}} \cdot MUT} \tag{10.9}$$

$$IPR = \frac{4000}{400 \cdot 2 \cdot 10 \cdot 0.40} = 1.25 \text{ m/h}$$

where
L_{tunnel} = total tunnel length (m)
D_{total} = total days to complete the tunnel excavation (days)
S_{day} = shift number per day (shift/day)
H_{shift} = working hours per shift (h/shift)
MUT = machine utilization time (%)

10.7.3.1.2 Estimation of Revolution of Cutterhead per Minute

$$RPM = \frac{CS_{\text{MAX}}}{D_{\text{TBM}} \cdot \pi} \tag{10.10}$$

$$RPM = \frac{45}{13.25 \cdot \pi} = 1.1 \text{ rpm}$$

where
CS_{MAX} = maximum corner cutter speed (m/min)
D_{TBM} = excavation diameter of TBM (m)

10.7.3.1.3 Estimation of Penetration per Revolution (p)

$$p = \frac{IPR}{RPM} \tag{10.11}$$

$$p = \frac{IPR}{RPM} = \frac{1.25 \cdot 1000/60}{1.1} = 19.3 \text{ mm/rev}$$

10.7.3.1.4 Estimation of Mean Cutting Force and Mean Normal Force

Labanov and Joanknecht (1980) developed a theoretical model for estimation of cutting force acting on a sharp wedge-type cutter of dredging machines under hydrostatic pressure as follows:

$$FC = k \cdot (1 + \cot(90 - \alpha) \cdot \tan\delta) \cdot p \cdot W \cdot \frac{1 - \sin\phi \cdot \cos 2\xi}{1 + \sin\phi \cdot \cos 2\xi} \cdot c \cdot \cos\phi \tag{10.12}$$

$$\xi = 2\pi - 2\alpha - \delta - \arcsin(\sin\phi \cdot \sin\delta) \tag{10.13}$$

where

k = an experimental constant for different cutting conditions (it can be taken as 2.5 for a closed face TBM)
δ = angle of friction between cutter and ground (30°)
p = penetration per revolution (0.0193 m/rev)
W = width of the cutter (0.10 m)
ϕ = internal friction angle of the ground (25°)
c = shear strength (cohesion) of the ground (100 kPa)
α = tool rake angle (30°)

This model is valid for the rake angles (α) between 20° and 70°. Based on the given parameters:

$$\xi = 2\pi - 2\alpha - \delta - \arcsin(\sin\phi \cdot \sin\delta)$$

$$= 360 - 2 \cdot 30 - 30 - \arcsin(\sin(25) \cdot \sin(30)) = 258°$$

$$FC = 2.5 \cdot (1 + \cot(90 - 30) \cdot \tan(30)) \cdot 0.0193 \cdot 0.10 \cdot \frac{1 - \sin(25)\cos(2 \cdot 258)}{1 + \sin(25)\cos(2 \cdot 258)}$$

$$\cdot 100 \cdot \cos(25)$$

$$FC \approx 1.3 \text{ kN/cutter}$$

In fact, the estimated (FC) is the theoretical maximum cutting force. This can be assumed to be the average cutting force for soils (Copur 2012), since there would be no brittle chipping in soil cutting (Copur et al. 2003).

Therefore, it can also be assumed that normal (thrust) force acting on a cutter (*FN*) is equal to the cutting force (*FC*) (Copur 2012). Then, for soils:

$$FC \approx FN \tag{10.14}$$

$$FN \approx 1.3 \text{ kN/cutter}$$

These cutter forces are estimated for wedge-type tools in sharp condition. Since the cutters are manufactured with a pre-blunting to prevent premature breakages, the effect of blunting should be taken into consideration. Bilgin et al. (2012) indicated that the peak cutting forces in worn conditions increased up to 3 times more than sharp condition. It was also indicated that the peak normal forces in worn conditions increased up to 6 times more than sharp condition. Assuming the same increase values are valid for average tool forces, the average increase on cutting and normal forces can be assumed to be 2 and 3.5 times, respectively. Thus, the average cutting and normal forces acting on a tool with an average wear flat are:

$$FC \approx 1.3 \times 2 \approx 2.6 \text{ kN/cutter}$$

$$FN \approx 1.3 \times 3.5 \approx 4.6 \text{ kN/cutter}$$

10.7.3.1.5 Estimation of Thrust, Torque, and Power Requirement of the TBM for Just Cutting the Ground

Torque requirement of the cutterhead for just cutting the ground (Tq_1) can be estimated as follows (Bilgin et al. 2008):

$$Tq_1 = \sum_{i=1}^{N_C} r_i \cdot FC \cdot f \approx FC \cdot N_C \cdot f \cdot \frac{r}{2} \tag{10.15}$$

where

r_i = distance of the (ith) cutting tool to the center of the cutterhead (m)
r = radius of the cutterhead ($D_{TBM}/2$) (m)
N_C = total number of cutters on the cutterhead
f = a constant for frictional loses and can be taken as 1.2 for rocks (Bilgin et al. 2008). It is assumed in this study that f is 1.2 for soft grounds, as well

Assuming the same cutters are also placed on the center cutter and optimum ratio of line spacing to penetration (s/p) is 0 for soils, the total number of cutters on the cutterhead (N_C) can be estimated by

$$N_C = \frac{(D_{TBM}/2)}{W} + Sn \tag{10.16}$$

where *Sn* is the number of spokes or corner cutting tools, which is 6 in this case.

$$N_C = \frac{(1325/2)}{10} + 6 = 72 \text{ cutters}$$

Then, the torque requirement of the cutterhead for just cutting the ground (Tq_1 in kN m) can be estimated as

$$Tq_1 = 2.6 \cdot 72 \cdot 1.2 \cdot \frac{(13.25/2)}{2} = 745 \text{ kN m}$$

Thrust requirement of the TBM for just cutting the ground (ΣFN or F_6 in kN) can be estimated as

$$\sum FN = F_6 = FN \cdot N_{\text{Cutter}} \cdot f \tag{10.17}$$

$$\sum FN = F_6 = 4.6 \cdot 72 \cdot 1.2 \approx 397 \text{ kN}$$

The net power requirement of the TBM for just cutting the ground ($P_{\text{cutting-net}}$ in kW) can be estimated as (Bilgin et al. 2008)

$$P_{\text{cutting-net}} = 2\pi \cdot Tq_1 \cdot RPM \tag{10.18}$$

where

Tq_1 = cutterhead torque requirement for just cutting the ground (kN m)
RPM = cutterhead rotational speed (rpm) and can be estimated by using Equation 10.10

Then, the net power requirement of the TBM for just cutting the ground ($P_{\text{cutting-net}}$) is estimated as

$$P_{\text{cutting-net}} = \frac{2\pi \cdot 745 \cdot 1.1}{60} = 87 \text{ kW}$$

10.7.4 A Numerical Example on Estimations of TBM Thrust, Cutterhead Torque, and Power

Estimate the total TBM thrust (*Th*), cutterhead torque (*Tq*), and power ($P_{\text{cutterhead}}$) requirement for the given parameters in Problem 10.7.3.

10.7.4.1 Solution of Numerical Example 10.7.4

10.7.4.1.1 Estimation of Thrust Requirement of Soft Ground TBMs

Total thrust requirement of the soft ground TBMs is suggested as the sum of five thrust components by Japan Society of Civil Engineers (JSCE 2007):

$$Th = F_1 + F_2 + F_3 + F_4 + F_5 \tag{10.19}$$

where

Th = total thrust (normal) force requirement of the soft ground TBMs
F_1 = thrust force required to overcome friction (adhesion) between shield and ground due to earth pressure
F_2 = thrust force required to overcome the chamber pressure acting on bulkhead
F_3 = thrust force required to overcome the drive force caused by direction changes in curved alignments (If the tunnel is straight; (F_3) is taken to be 0.)
F_4 = thrust force required to overcome the frictional force acting between the segments and the tail seals
F_5 = thrust force required to overcome the hauling force of trailing (backup) units (If the backup is self-propelled; (F_5) is taken to be 0.)

This estimation ignores the thrust force required to overcome the penetration (normal) force of cutting tools into the ground (let us say F_6), which can also be included in Equation 10.19 for completeness of theoretical considerations (Copur 2012), although it might be very low for soil cutting. If F_6 is also added to the thrust requirement of the TBM:

$$Th = F_1 + F_2 + F_3 + F_4 + F_5 + F_6 \tag{10.20}$$

where F_6 is thrust force required to overcome the penetration (normal) force of cutting tools into the ground.

F_1 is estimated by (JSCE 2007)

$$F_1 = \mu_1 \cdot [\pi \cdot D_{\text{TBM}} \cdot L_S \cdot P_M + W_S] \quad \text{for sandy soils} \tag{10.21}$$

$$F_1 = C_A \cdot \pi \cdot D_{\text{TBM}} \cdot L_S \quad \text{for clayey soils} \tag{10.22}$$

where

μ_1 = coefficient of friction between steel (shield) and soil
D_{TBM} = excavation diameter of TBM (m)
L_S = shield length (m)
P_M = average earth pressures acting on shield (kPa)
W_S = weight of shield machine (kN)
C_A = adhesion pressure (between shield and cohesive soil) (kPa)

Equation 10.21 is used and Equation 10.22 is ignored in this study assuming there is no adhesion and only the frictional forces are in effect. The suggested values of (μ_1) are presented in Table 10.4 and it is assumed to be 0.35 in this study for sand containing silt.

TABLE 10.4

Frictional Coefficient (μ_1) between Steel Surface and Soil

Soil Type	Frictional Coefficient (μ_1)
Gravel	0.55
Sand	0.45
Loam, marl	0.35
Low-grade clay (soft alluvial clay)	0.30
Clay	0.20

Source: Adapted from Herzog 1985 as quoted by PJA, Pipe Jacking Association, 1995. *Guide to Best Practice for the Installation of Pipe Jacks and Microtunnels*. London.

The shield length (L_S) can be assigned as a function of (D_{TBM}) by assuming that (L_S/D_{TBM}) ratio varies linearly between 2 (for D_{TBM} of 3 m) and 1 (for $D_{TBM} \geq 13$ m). Therefore, L_S can be assumed to be 13.25 m for this study.

The weight of the shield machine (W_S) can be estimated as a function of (D_{TBM}) for both EPB and SPB TBMs as follows (Ates 2013):

$$W_S = 883.65 \cdot e^{0.2207 \cdot D_{TBM}} \tag{10.23}$$

$$W_S = 883.65 \cdot e^{0.2207 \cdot 13.25} = 16{,}454 \text{ kN}$$

The average earth pressures acting on shield (P_M) is the same as averages of four components of vertical and horizontal earth pressures at rest (soil and water pressures) on crown and invert levels by JSCE (2007). In this study, P_M is assumed to be averages of uniformly distributed vertical earth pressure, acting on crown and horizontal earth pressure, acting on tunnel springline, as suggested for microtunneling applications by PJA (1995):

$$P_M = \frac{\sigma_v + \sigma_h}{2} \tag{10.24}$$

where

σ_v = vertical earth pressure at rest acting on crown (kPa)

σ_h = horizontal earth pressure at rest acting on tunnel springline (kPa)

The earth pressures can be estimated based on ITA (2000) suggestions by selecting the maximum of arcing height (h_0) or ($2D_{TBM}$). In this study, ($2D_{TBM}$) is used for estimation of earth pressures without considering the arcing height, assuming that the tunnel depth is greater than ($2D_{TBM}$). It is also assumed that the total pressure approach (groundwater pressure being included with the soil pressure) is valid and estimated by using bulk unit weight instead of buoyant unit weight of the soil. Therefore, the vertical

earth pressure at rest (σ_v) at the crown and the horizontal earth pressure (σ_h) at the tunnel springline are estimated as a function of (D_{TBM}) as follows:

$$\sigma_v = 2 \cdot D_{\text{TBM}} \cdot \gamma_b \tag{10.25}$$

$$\sigma_h = K_0 \cdot (\sigma_v + \gamma_b \cdot D_{\text{TBM}}/2) \tag{10.26}$$

where

γ_b = bulk unit weight of soil (kN/m^3)
K_0 = coefficient of lateral earth pressure at rest

The bulk unit weight of the soil (γ_b) is assumed to be 17 kN/m^3 in this study. The coefficient of lateral earth pressure at rest (K_0) is usually suggested to be either 1.0 or 0.5 in different standards and assumed to be 0.75 in this study.

On the basis of these considerations and assumptions F_1 is estimated as follows:

$$\sigma_v = 2 \cdot 13.25 \cdot 17 = 451 \text{ kPa}$$

$$\sigma_h = 0.75 \cdot (451 + 17 \cdot 13.25/2) = 423 \text{ kPa}$$

$$P_M = \frac{451 + 423}{2} = 437 \text{ kPa}$$

$$F_1 = 0.35 \cdot \left[\pi \cdot 13.25 \cdot 13.25 \cdot 437 + 16{,}454\right] = 90{,}118 \text{ kN}$$

F_2, F_3, F_4, and F_5 can be estimated by suggestions of JSCE (2007):

$$F_2 = \sigma_T \cdot \frac{\pi \cdot D_{\text{TBM}}^2}{4} \tag{10.27}$$

$$F_3 = \mu_1 \cdot D_{\text{TBM}} \cdot \frac{L_S}{2} \cdot \frac{q}{2} \tag{10.28}$$

$$F_4 = \mu_2 \cdot \pi \cdot D_0 \cdot L_{SC} \cdot P_M \tag{10.29}$$

$$F_5 = \mu_3 \cdot G \tag{10.30}$$

where

σ_T = face pressure acting on the excavation chamber if the face is not stable, can be estimated by adding 20 kPa to (σ_h) (Kanayasu et al. 1995) for both EPB and SPB TBMs (kPa)

q = pressure imposed by direction change of the shielded TBM and can be assumed to be equal to (σ_h) as a maximum
μ_2 = coefficient of friction between seals and segments (usually between 0.2 and 0.3, assumed to be 0.25 in this study)
μ_3 = coefficient of friction between wheel and rail (in fact, it can be considered as rolling resistance of wheels which is assumed to be 0.15 in this study)
D_0 = outer diameter of segments which is assumed to be (D_{TBM}–0.25 m = 13.0 m) in this study
L_{SC} = length of contact between segment and tail seal which is assumed to be 0.30 m as an average in this study
G = weight of trailing gears (backup) (kN)

The weight of the trailing gears G can be estimated as a function of (D_{TBM}) for both EPB and SPB TBMs (Ates 2013):

$$G = 868.82 \cdot e^{0.1713 \cdot D_{TBM}} \tag{10.31}$$

$$G = 868.82 \cdot e^{0.1713 \cdot 13.25} = 8407 \text{ kN}$$

Then,

$$F_2 = (423 + 20) \cdot \frac{\pi \cdot 13.25^2}{4} = 61{,}084 \text{ kN}$$

$$F_3 = 0.35 \cdot 13.25 \cdot \frac{13.25}{2} \cdot \frac{423}{2} = 6498 \text{ kN}$$

$$F_4 = 0.25 \cdot \pi \cdot 13 \cdot 0.3 \cdot 437 = 1339 \text{ kN}$$

$$F_5 = 0.15 \cdot 8407 = 1261 \text{ kN}$$

F_6 has already been estimated theoretically in solution of Problem 10.7.3 (e) as follows:

$$F_6 = \Sigma FN = FN \times N_C \cdot f = 4.6 \cdot 72 \cdot 1.2 \approx 397 \text{ kN}$$

Then, the total thrust requirement of the TBM is

$$Th = 90{,}118 + 61{,}084 + 6498 + 1339 + 1261 + 397 = 160{,}697 \text{ kN}$$

Installed thrust requirement (Th_{inst}) can be estimated by

$$Th_{inst} = \Sigma Th \cdot \text{safety factor} \tag{10.32}$$

The safety factors vary depending on the machine manufacturer and expected geological conditions. If it is assumed to be 1.5 for this study, then the installed thrust capacity of the TBM should be around 240,000 kN.

According to JSCE (2007), the thrust factor (α) varies usually between 1000 and 1500 kN/m^2 for both EPB and SPB TBMs, based on a database of manufactured soft ground TBMs. The thrust factor (α) is estimated by

$$\alpha = Th_{\text{inst}}/A_{\text{face}} \tag{10.33}$$

where

α = thrust factor (kN/m^2)

A_{face} = cutterhead or tunnel cross-section area (m^2)

For this case study, the thrust factor (α) is estimated as 1740 kN/m^2, which is slightly higher than the range of 1000–1500 kN/m^2.

Jancsecz et al. (1999) suggested an average installed total thrust force as

$$Th_{\text{inst}} = 850 \cdot D_{\text{TBM}}^2 \tag{10.34}$$

However, they also pointed out that the installed thrust force was not enough in some projects of soft ground tunneling. Based on this empirical approach, Th_{inst} is estimated as 149,230 kN, which is around 60% of the estimate above (240,000 kN) based on JSCE (2007).

10.7.4.1.2 Estimation of Cutterhead Torque Requirement of Soft Ground TBMs

The estimates of cutterhead torque requirements for soft ground TBMs require knowing many detailed TBM properties/specifications, which are usually unknown during machine selection stage before the manufacturing process. It is possible, however, to estimate the basic torque components such as torque requirement to overcome face/earth pressure in the excavation chamber and the cutterhead face. The cutterhead torque estimations for soft ground TBMs is suggested as a sum of six basic torque components by the JSCE (2007):

$$Tq = Tq_1 + Tq_2 + Tq_3 + Tq_4 + Tq_5 + Tq_6 \tag{10.35}$$

where

Tq = total (installed) cutterhead torque requirement of the soft ground TBMs

Tq_1 = torque required to overcome the cutting resistance of the soil

Tq_2 = torque required to overcome the frictional resistance of the soil

Tq_3 = torque required to overcome the resistance of the soil mixing and stirring

Tq_4 = torque required to overcome the resistance of the main bearing

Tq_5 = torque required to overcome the frictional resistance of the bearing seals
Tq_6 = torque required to overcome mechanical losses in the reduction gears

As seen, the Tq value suggested by JSCE (2007) is the installed torque of the cutterhead, since it includes mechanical loses in the reduction gears.

The JSCE (2007) also suggested an empirical model to estimate cutterhead torque requirements (Tq in kN m) as follows:

$$Tq = \alpha \cdot D_{\text{TBM}}^3 \tag{10.36}$$

where
α = torque factor (it is suggested between 10 and 25 for EPB TBMs, and 8 and 20 for SPB TBMs by JSCE 2007)
D_{TBM} = cutterhead or excavation diameter of TBM (m)

The rule of thumb torque requirement of an EPB or SPB TBM with diameter of 13.25 m can be estimated by assuming a torque factor of 20 as follows:

$$Tq = 20 \cdot 13.25^3 = 46{,}525 \text{ kN m}$$

Jancsecz et al. (1999) pointed out that an average torque factor was around 20 in most projects.

The installed cutterhead power requirements ($P_{\text{cutterhead-inst}}$) of any TBM can be estimated by

$$P_{\text{cutterhead-inst}} = 2\pi \cdot Tq \cdot \text{RPM} \tag{10.37}$$

where
$P_{\text{cutterhead-inst}}$ = installed cutterhead power requirement of TBMs (kW)
Tq = total (installed) cutterhead torque requirement of TBMs (kN m)
RPM = cutterhead rotational speed (rpm) estimated by using Equation 10.10

Then, the installed power requirement of the TBM ($P_{\text{cutterhead-inst}}$) is estimated as

$$P_{\text{cutterhead-inst}} = \frac{2\pi \cdot 46{,}525 \cdot 1.1}{60} = 5360 \text{ kW}$$

The net power that can be generated by the TBM ($P_{\text{cutterhead-net}}$) is a function of efficiency for the cutterhead motors (η), which depend on several factors. For this study, the efficiency factor (η) is taken as 0.75, and the net power is estimated around 4000 kW:

$$P_{\text{cutterhead-net}} = \eta \cdot P_{\text{cutterhead-inst}} \tag{10.38}$$

$$P_{\text{cutterhead-net}} = 0.75 \cdot 5360 \approx 4000 \text{ kW}$$

10.7.5 A Numerical Example on Slurry Conditioning for SPB TBMs

A SPB TBM with a diameter of 13.25 m is used for excavation of a tunnel in length of 4000 m in a mostly silty sand formation.

1. Estimate the amount of bentonite to be added to fresh slurry of 1 m^3 to obtain a slurry density of 1.03 ton/m^3, assuming dry bentonite density of 2.60 ton/m^3 and water density of 1.0 ton/m^3.
2. Estimate the total amount of bentonite to generate slurry required for excavation of the whole tunnel, assuming a slurry replacement rate of 0.75 m^3 slurry per m^3 of excavation.
3. Estimate the total amount of water to generate slurry required for excavation of the whole tunnel, assuming that there is no slurry loss into the ground (no filtrate water) and there is no addition of water to the slurry system from the ground water and TBM flushing.
4. Estimate the slurry flow rate (*SFR*) for obtaining a density of 1.20 ton/m^3 in discharging line, assuming solid's density of 2.60 ton/m^3.
5. Estimate the capacity of slurry discharge pump for the estimated *SFR*.
6. Estimate the inner diameter of the slurry discharge pipe for the critical slurry velocity of 2.25 m/s.

10.7.5.1 Solution of Numerical Example 10.7.5

10.7.5.1.1 Estimation of Amount of Bentonite in 1 m^3 of Slurry

The density of a mixture of different materials is estimated by (in convenient units):

$$\rho_{\text{mixture}} = \frac{\sum_{i=1}^{n} m_i}{\sum_{i=1}^{n} V_i} \tag{10.39}$$

where

ρ_{mixture} = density of the mixture
m_i = mass of the (i)th material
V = volume of the (i)th material

The volume of bentonite in 1.0 m^3 of the slurry is then estimated by

$$\rho_{\text{slurry}} = \frac{m_{\text{bentonite}} + m_{\text{water}}}{V_{\text{bentonite}} + V_{\text{water}}} = \frac{\rho_{\text{bentonite}} \cdot V_{\text{bentonite}} + \rho_{\text{water}} \cdot V_{\text{water}}}{V_{\text{bentonite}} + V_{\text{water}}} \tag{10.40}$$

$$1.03 = \frac{2.60 \cdot V_{\text{bentonite}} + 1.0 \cdot (1 - V_{\text{bentonite}})}{1.0}$$

$$V_{\text{bentonite}} = 0.019 \text{ m}^3$$

The mass of bentonite in 1.0 m^3 of the slurry is estimated as

$$m_{\text{bentonite}} = 2.60 \cdot 0.019 \cdot 1000 \cong 50 \text{ kg}$$

10.7.5.1.2 Estimation of Total Amount of Bentonite Required for Excavation of the Whole Tunnel

The total excavation amount (*TAE* in m^3) is estimated by

$$TAE = L_{\text{tunnel}} \cdot A_{\text{tunnel}} = L_{\text{tunnel}} \cdot \pi \cdot D_{\text{TBM}}^2/4 \tag{10.41}$$

$$TAE = 4000 \cdot \pi \cdot 13.25^2/4 = 551{,}546 \text{ m}^3$$

where

L_{tunnel} = total tunnel length (m)
A_{tunnel} = tunnel cross-section area (m^2)
D_{TBM} = cutterhead (tunnel, excavation) diameter (m)

Total slurry replacement amount (*TSRA* in m^3) is estimated by

$$TSRA = TAE \cdot SRR \tag{10.42}$$

$$TSRA = 55{,}1546 \cdot 0.75 = 413{,}659 \text{ m}^3$$

where *SRR* is slurry replacement rate in m^3 slurry per m^3 excavation. The total bentonite amount (*TBA* in tons) to be used during the excavation of the tunnel is then estimated by

$$TBA = TSRA \cdot m_{\text{bentonite}} \tag{10.43}$$

$$TBA = 413{,}659 \cdot 50/1000 = 20{,}166 \text{ tons}$$

This amount requires a safety margin.

10.7.5.1.3 Estimation of Total Amount of Water Required for Excavation of the Whole Tunnel

Water volume (V_{water}) in 1 m^3 slurry is

$$V_{\text{water}} = 1.0 - V_{\text{bentonite}} = 1 - 0.019 = 0.981 \text{ m}^3$$

Total water volume (TV_{water}) required for excavation of the whole tunnel is

$$TV_{water} = TSRA \cdot V_{water} = 413{,}659 \cdot 0.981 = 405{,}903 \text{ m}^3$$

This amount also requires a safety margin.

10.7.5.1.4 Estimation of the Slurry Flow Rate

SFR is estimated by

$$SFR = \frac{V_{slurry}}{V_{ground}} \tag{10.44}$$

where

V_{slurry} = volume of the slurry in 1.0 m^3 of mixture of excavated ground and slurry (m^3)

V_{ground} = volume of the excavated ground in 1.0 m^3 of mixture of the excavated ground and slurry (m^3)

The volume of the ground (V_{ground}) in 1.0 m^3 of the mixture is then estimated by

$$\rho_{mixture} = \frac{m_{ground} + m_{slurry}}{V_{ground} + V_{slurry}} = \frac{\rho_{ground} \cdot V_{ground} + \rho_{slurry} \cdot V_{slurry}}{V_{ground} + V_{slurry}} \tag{10.45}$$

$$1.20 = \frac{2.60 \cdot V_{ground} + 1.03 \cdot (1 - V_{bentonite})}{1.0} = \frac{2.60 \cdot V_{ground} + 1.03 \cdot (1 - 0.019)}{1.0}$$

$$V_{ground} = 0.108 \text{ m}^3$$

Then, the volume of slurry (V_{slurry}) in 1.0 m^3 of the mixture is

$$V_{slurry} = 1 - 0.108 = 0.892 \text{ m}^3$$

SFR is

$$SFR = \frac{0.892}{0.108} = 8.2 = 8.2 : 1$$

This means that excavation of a unit volume of the excavated ground requires 8.2 units of slurry.

10.7.5.1.5 Estimation of Capacity of Slurry Discharge Pump

The capacity of slurry discharge pump ($Q_{\text{discharge}}$ in m^3/h) can be estimated by

$$Q_{\text{discharge}} = IPR \cdot A_{\text{face}} \cdot (SFR + 1) = IPR \cdot (\pi \cdot D_{\text{TBM}}^2/4) \cdot (SFR + 1) \quad (10.46)$$

$$Q_{\text{discharge}} = 1.25 \cdot (\pi \cdot 13.25^2/4) \cdot (8.2 + 1) = 1586 \text{ m}^3/\text{h}$$

This amount requires a safety margin, for example, around 1.5 times the estimated capacity.

10.7.5.1.6 Estimation of Inner Diameter of the Slurry Discharge Pipe

$$Q_{\text{discharge}} = V_{\text{critical}} \cdot A_{\text{pipe}} = V_{\text{critical}} \cdot (\pi \cdot D_{\text{pipe}}^2/4) \quad (10.47)$$

where

A_{pipe} = cross-section area of the slurry discharge pipe (m^2),
V_{critical} = critical velocity of the mixture through the discharge pipe (m/s).

The inner diameter of slurry discharge pipe (D_{pipe}) is estimated by

$$D_{\text{pipe}} = \sqrt{\frac{4 \cdot Q_{\text{discharge}}}{\pi \cdot V_{\text{critical}}}} = \sqrt{\frac{4 \cdot 1586}{\pi \cdot (2.25 \cdot 3600)}} \cdot 1000 \approx 500 \text{ mm} \approx 50 \text{ cm}$$

10.7.6 Numerical Example on the Estimation of the Torque Requirement of a Half-Filled Cutterhead Chamber

Estimate the torque requirement of a half-filled (with excavated rock) cutterhead chamber for a closed face TBM with diameter of 8.0 m. The internal friction angle of loose rock is 35°. Unit weight of loose rock is 20 kN/m^3. Coefficient of friction between steel plate and loose rock is 0.45.

10.7.6.1 Solution of Numerical Example 10.7.6

Korbin (1998) suggested a theoretical model for these types of problems as follows:

$$Tq_{hf} = 0.5 \cdot \gamma_r \cdot K_a \cdot \mu \cdot R^4 \quad (10.48)$$

$$K_a = \tan^2(45 - \phi/2) \quad (10.49)$$

where

Tq_{hf} = torque required to overcome the frictional resistance of the loose rock in a half-filled cutterhead chamber (kN m)
γ_r = unit weight of loose ground on the excavation chamber (kN/m^3)
K_a = active earth pressure coefficient
μ = coefficient of friction between steel plate and loose ground
R = radius of the cutterhead steel plate in (m), ($R \cong D_{\text{TBM}}/2$)
D_{TBM} = cutterhead (tunnel, excavation) diameter (m)
ϕ = internal friction angle of the loose ground (°)

Thus, the torque required to overcome the frictional resistance of the loose rock in a half-filled cutterhead chamber is estimated as

$$K_a = \tan^2(45 - 25/2) = 0.41$$

$$Tq_{hf} = 0.5 \cdot 20 \cdot 0.41 \cdot 0.45 \cdot 4^4 = 468 \text{ kN m}$$

10.7.7 Numerical Example on Soil Conditioning for EPB-TBMs

An EPB-TBM with diameter of 6.5 m is used for excavation of a tunnel with a length of 5000 m, through a soft ground. Foam expansion ratio (*FER*) is 10 (10:1). Foam injection ratio (*FIR*) is 50%. Surfactant concentration (C_F) is 3.0%. Estimate total amount of surfactant and air to be used for excavation of the tunnel. Assume no plastic compaction in excavated soil and no volumetric decrease in foam under pressure.

10.7.7.1 Solution of Numerical Example 10.7.7

FIR in % is defined as the ratio of foam volume used for in situ unit volume of excavated ground and estimated by (Efnarc 2005):

$$FIR = \frac{V_{\text{foam}}}{V_{\text{soil}}} \cdot 100 \tag{10.50}$$

where

V_{foam} = volume of foam at working pressure (m^3)
V_{soil} = volume of in situ soil to be excavated (m^3)

The total in situ volume of the ground to be excavated (V_{soil} in m^3) is estimated as

$$V_{\text{soil}} = L_{\text{tunnel}} \cdot A_{\text{face}} = L_{\text{tunnel}} \cdot \frac{\pi \cdot D_{\text{TBM}}^2}{4} \tag{10.51}$$

$$V_{\text{soil}} = 5000 \cdot \frac{\pi \cdot 6.5^2}{4} = 165{,}915 \text{ m}^3$$

Then, the total volume of the foam to be used for excavation of the whole tunnel is

$$V_{\text{foam}} = FIR \cdot V_{\text{soil}}/100 = 50 \cdot 165{,}915/100 = 82{,}958 \text{ m}^3$$

FER in % is defined as the ratio of the foam volume used for unit volume of the excavated ground and estimated by (Efnarc 2005)

$$FER = \frac{V_{\text{foam}}}{V_{\text{solution}}} \tag{10.52}$$

where
V_{foam} = volume of foam at working pressure (m^3)
V_{solution} = volume of foaming solution (m^3)

Then, total volume of the foaming solution to be used for excavation of the whole tunnel is

$$V_{\text{solution}} = \frac{V_{\text{foam}}}{FER} = \frac{82{,}958}{10} = 8296 \text{ m}^3$$

The concentration of the solution (C_F in %) is estimated by (Efnarc 2005)

$$C_F = \frac{V_{\text{surfactant}}}{V_{\text{solution}}} \cdot 100 \tag{10.53}$$

where
C_f = concentration of foam in the solution (water + foaming agent) (%)
$V_{\text{surfactant}}$ = volume of surfactant within the solution (m^3)
V_{foam} = volume of solution (m^3)

Then, the total volume of the surfactant to be used for excavation of the whole tunnel is

$$V_{\text{surfactant}} = \frac{C_F \cdot V_{\text{solution}}}{100} = \frac{3 \cdot 8296}{100} \approx 250 \text{ m}^3$$

The volume of air in atmospheric pressure (V_{air} in m^3) to be used for foam generation is estimated by

$$V_{\text{air}} = V_{\text{foam}} - V_{\text{solution}} = 82{,}958 - 8296 = 74{,}662 \text{ m}^3 \tag{10.54}$$

10.7.8 A Numerical Example on Surface Settlement Predictions

By using the parameters given in Problem 10.7.1, estimate the maximum initial (undrained, short term, immediate) surface settlement. Additional parameters are as follows: outer diameter of a lining ring is 6.30 m and average undrained Young's modulus of the ground is 30,000 kPa.

1. Estimate the initial maximum surface settlement by using the empirical method suggested by Schmidt (1969) including suggestion of Arioglu (1992) for estimation of percent volume loss (K).
2. Assuming ground is elastic and no void grouting is applied; estimate elastic ground closures.
3. Estimate initial maximum surface settlement based on elastic ground closures (use average of vertical and horizontal closures) by using volume loss method and Schmidt (1969) method.
4. Estimate initial maximum surface settlements by using volume loss method for grouting case with efficiency of 0.85 (85%).
5. Estimate maximum slope, maximum curvature, maximum horizontal tensile strain, maximum horizontal compressive strain, and point of maximum curvature by using the maximum initial surface settlement value obtained in solution of issue (a) of this problem.
6. Estimate initial maximum surface settlement by using the analytical method developed by Loganathan and Poulos (1998).

10.7.8.1 Solution of Numerical Example 10.7.8

10.7.8.1.1 Estimation of Initial Maximum Surface Settlement by Using Schmidt (1969) Including Suggestion of Arioglu (1992) (Ercelebi et al. 2005; Ercelebi et al. 2011)

Schmidt (1969) suggested an empirical model for estimation of initial maximum surface settlement (S_{max}) for a single tunnel as given

$$S_{max} = 0.0125 \cdot K \cdot \left(\frac{R^2}{i} \right) \tag{10.55}$$

where

S_{max} = maximum initial surface settlement (m), which occurs at the centerline of tunnel on surface and defines the other settlement parameters (maximum slope, maximum curvature, etc.) based on theoretical Gaussian probability curve

K = volume loss (%), which is the ratio of converged ground volume (or area) to total cross-section of excavated face (or excavated volume in unit distance)

R = radius or equivalent radius of tunnel (m) (=D_{TBM}/2 for shielded TBMs),
i = point of inflexion (m), at which the maximum slope of settlement curve occurs; it is symmetrical on both sides of the tunnel axis on horizontal plane; it is assumed that displacements diminish at (3i) from the centerline totaling (6i) of settlement effect distance. Maximum building damages occur at this point, as well.

The value of (i) can be predicted for cohesive soils as given by Glossop (1978) as quoted by O'Reilley and New (1982):

$$i = 0.5 \cdot Z_0 \tag{10.56}$$

where (Z_0) is the depth to tunnel axis, which is 18.25 m in this case.

Arioglu (1992), based on field data, found a relationship between (K) and (N) (stability ratio given in Equation 10.1) for face pressurized TBM cases as given below (Ercelebi et al. 2011):

$$K = 0.87 \cdot \exp(0.26 \cdot N) = 0.87 \cdot \exp\left[0.26 \cdot \left(\frac{\gamma_b Z_0 + \sigma_{Sur} - \sigma_T}{C_U}\right)\right] \tag{10.57}$$

where
γ_b = bulk unit weight of the soil (18 kN/m^3), (ground layer thickness weighted averages can be used),
σ_{Sur} = total surcharge pressure (30 kPa),
σ_T = TBM face pressure (kPa), which is 313 kPa as estimated in solution of Problem 10.7.2,
C_U = undrained cohesion of the soil (40 kPa), (ground layer thickness weighted averages can be used).

Then, S_{max} is estimated as

$$K = 0.87 \cdot \exp\left[0.26 \cdot \left(\frac{18 \cdot (15 + 6.5/2) + 30 - 313}{40}\right)\right] = 1.169\%$$

$i = 0.5 \cdot 18.25 = 9.1$ m

$$S_{max} = 0.0125 \cdot 1.169 \cdot \left(\frac{(6.5/2)^2}{9.1}\right) = 0.017 \text{ m} \approx 17 \text{ mm}$$

10.7.8.1.2 Estimation of Elastic Ground Closures

The reduction in vertical and horizontal diameter of a tunnel due to elastic stress relief after excavation can be estimated as suggested by Poulos and Davis (1974) as quoted by Milligan and Marshall (1995):

$$\delta_v = \frac{(1-v^2)}{E_S} \cdot D_{\text{TBM}} \cdot (3 \cdot \sigma_v + \sigma_h) \tag{10.58}$$

$$\delta_h = \frac{(1-v^2)}{E_S} \cdot D_{\text{TBM}} \cdot (3 \cdot \sigma_h + \sigma_v) \tag{10.59}$$

where

δ_v = vertical closure in tunnel diameter (m)
δ_h = horizontal closure in tunnel diameter (m)
υ = Poisson's ratio (can be taken as 0.5 for undrained cases and 0.2 for drained cases)
E_S = undrained Young's modulus (it can be multiplied by 0.8 for drained cases)
D_{TBM} = cutterhead (tunnel, excavation) diameter (6.5 m)
σ_v = vertical earth pressure at tunnel crown (234 kPa as estimated in solution of Problem 10.7.2)
σ_h = horizontal earth pressure at tunnel springline (293 kPa as estimated in solution of Problem 10.7.2)

These equations were used for microtunnels; it is assumed here that these equations are valid for large diameter tunnels, as well (Copur 2012). The vertical and horizontal closures are then estimated as

$$\delta_v = \frac{(1-0.5^2)}{30{,}000} \cdot 6.5 \cdot (3 \cdot 234 + 293) = 0.1617 \text{ m} \approx 162 \text{ mm}$$

$$\delta_h = \frac{(1-0.5^2)}{30{,}000} \cdot 6.5 \cdot (3 \cdot 293 + 234) = 0.1809 \text{ m} \approx 181 \text{ mm}$$

The average diametrical closure is then estimated as being

$$\delta_{\text{ave}} = \frac{\delta_v + \delta_h}{2} = \frac{162 + 181}{2} = 172 \text{ mm}$$

10.7.8.1.3 Estimation of Initial Maximum Surface Settlement Based on Elastic Ground Closures

Volume of the settled ground or area under the Gauss probability curve (V_S in m^2 or equivalently m^3/m of tunnel advance) is estimated by integrating the theoretical Gauss probability curve and given by

$$V_S = S_{\max} \cdot i \cdot \sqrt{2\pi} \tag{10.60}$$

Then, maximum surface settlement is

$$S_{\max} = \frac{V_S}{i \cdot \sqrt{2\pi}} \tag{10.61}$$

The possible maximum convergence of the ground is based on the difference between the diameter of the excavated tunnel ($D_{\text{TBM}} = 6.5$ m) and the outer diameter of segment rings ($D_{\text{Segm}} = 6.3$ m) and the maximum volume loss without any void grouting (no void injection) can be estimated as

$$V_S = \frac{\pi}{4} \cdot \left(D_{\text{TBM}}^2 - D_{\text{Segm}}^2 \right) \tag{10.62}$$

$$V_S = \frac{\pi}{4} \cdot (6.5^2 - 6.3^2) = 2.01 \text{ m}^3/\text{m}$$

Then the maximum initial surface settlement is estimated as

$$S_{\max} = \frac{2.01}{9.1 \cdot \sqrt{2\pi}} = 0.0881 \text{ m} \approx 88 \text{ mm}$$

However, the average elastic ground closure, in diameter (172 mm), is smaller than the difference between the diameter of the excavated tunnel ($D_{\text{TBM}} = 6.5$ m) and the outer diameter of segment rings ($D_{\text{Segm}} = 6.3$ m) (200 mm). The volume of the elastically settled ground and the maximum settlement can be estimated by

$$V_S = \frac{\pi}{4} \cdot \left[D_{\text{TBM}}^2 - (D_{\text{TBM}} - \delta_{\text{ave}})^2 \right] \tag{10.63}$$

$$V_S = \frac{\pi}{4} \cdot [6.5^2 - (6.5 - 0.172)^2] = 1.74 \text{ m}^3/\text{m}$$

$$S_{\max} = \frac{1.74}{9.1 \cdot \sqrt{2\pi}} = 0.076 \text{ m} \approx 76 \text{ mm}$$

By converting this volume loss into a percentage of the excavated volume (K) and using the Schmidt's equation given in Equation 10.56, the maximum settlement can also be estimated as

$$K = \frac{V_S}{A_{\text{face}}} 100 = \frac{V_S}{\pi \cdot D_{\text{TBM}}^2 / 4} 100 = \frac{1.74}{\pi \cdot 6.5^2 / 4} 100 = 5.2\%$$

$$S_{\max} = 0.0125 \cdot 5.2 \cdot \left(\frac{(6.5/2)^2}{9.1} \right) = 0.076 \text{ m} = 76 \text{ mm}$$

10.7.8.1.4 Estimation of Initial Maximum Surface Settlement for Grouting with Efficiency of 0.85 (85%)

Grouting efficiency (α) of 85% means that 15% of the gap between tunnel wall and the segment outer surface cannot be grouted. Since the possible maximum volume loss estimated by Equation 10.63 should be reduced for a grouting case by

$$V_S = \frac{\pi}{4} \cdot \left(D_{\text{TBM}}^2 - D_{\text{Segm}}^2 \right) \cdot (1 - \alpha) \tag{10.64}$$

$$V_S = \frac{\pi}{4} \cdot \left(D_{\text{TBM}}^2 - D_{\text{Segm}}^2 \right) \cdot (1 - \alpha) = 2.01 \cdot (1 - 0.85) = 0.302 \text{ m}^3/\text{m}$$

Then, the maximum surface settlement is estimated by using Equation 10.62:

$$S_{\max} = \frac{0.302}{9.1 \cdot \sqrt{2\pi}} = 0.0132 \text{ m} \approx 13 \text{ mm}$$

10.7.8.1.5 Estimation of Maximum Slope, Maximum Curvature, Maximum Horizontal Tensile Strain, Maximum Horizontal Compressive Strain, and Point of Maximum Curvature

Theoretical Gauss probability (error function) curve is given by

$$S = S_{\max} \cdot \exp\left(\frac{-x^2}{2i^2} \right) \tag{10.65}$$

where

S = theoretical settlement occurring at any perpendicular distance (x) from the tunnel centerline on the horizontal plane

x = perpendicular distance from the tunnel centerline on the horizontal plane

Equations of maximum slope $(ds/dx)_{\max}$, average slope $(ds/dx)_{\text{ave}}$, maximum curvature (d^2s/dx^2), maximum horizontal tensile strain (ε_t), maximum horizontal compressive strain (ε_c), and point of maximum tensile curvature ($H_{\max\text{-}t}$) are derived from the theoretical equation of Gauss probability curve and are presented below (Arioglu 1992)

$$(ds/dx)_{\max} = 0.606 \cdot \left(\frac{S_{\max}}{i} \right) \tag{10.66}$$

$$(ds/dx)_{\text{ave}} = \frac{S_{\max}}{3i} \tag{10.67}$$

$$d^2s/dx^2 = 0.445 \cdot \left(\frac{S_{\max}}{i^2}\right) \quad \text{at hogging (at point } x = \sqrt{3i}) \tag{10.68}$$

$$d^2s/dx^2 = \left(\frac{S_{\max}}{i^2}\right) \quad \text{at sagging (at point } x = 0\text{-tunnel axis}) \tag{10.69}$$

$$\varepsilon_t = 0.445 \cdot \left(\frac{S_{\max}}{Z_0}\right) \tag{10.70}$$

$$\varepsilon_c = \left(\frac{S_{\max}}{i^2}\right) \tag{10.71}$$

$$H_{\max\text{-}t} = i \cdot \sqrt{3} \tag{10.72}$$

$$S = 0.606 \cdot S_{\max} \text{ (settlement at point } x = i) \tag{10.73}$$

The estimates for 17 mm of maximum surface settlement in the solution of (a) in this problem are given below with parameters:

$$(ds/dx)_{\max} = 0.606 \cdot \left(\frac{0.017}{9.1}\right) = 0.0011$$

$$(ds/dx)_{\text{ave}} = \frac{S_{\max}}{3i} = \frac{0.017}{3 \cdot 9.1} = 0.0006$$

$$d^2s/dx^2 = 0.445 \cdot \left(\frac{0.017}{9.1^2}\right) = 0.0001 \quad \text{(at hogging point)}$$

$$d^2s/dx^2 = \left(\frac{0.017}{9.1^2}\right) = 0.0002 \quad \text{(at sagging point)}$$

$$\varepsilon_t = 0.445 \cdot \left(\frac{0.017}{18.25}\right) = 0.0004$$

$$\varepsilon_c = \left(\frac{0.017}{9.1^2}\right) = 0.0002$$

$$H_{\max\text{-}t} = i \cdot \sqrt{3} = 9.1 \cdot \sqrt{3} = 15.8 \text{ m}$$

$$S = 0.606 \cdot S_{\max} = 0.606 \cdot 0.017 = 0.010 \text{ m} \quad \text{(at point } x = i\text{)}$$

10.7.8.1.6 Estimation of Initial Maximum Surface Settlement by Using an Analytical Model

In the theoretical method suggested by Loganathan and Poulos (1998) for a single tunnel, a theoretical gap parameter (g) is defined based on physical gap in the void, face losses and workmanship value, and then the gap parameter is incorporated to a closed-form solution to predict elastoplastic ground deformations. The undrained gap parameter (g) is estimated by (Lee et al. 1992 as quoted by Loganathan and Poulos 1998)

$$g = G_p + U^*_{3D} + w \tag{10.74}$$

where

G_p = physical gap representing the geometric clearance between the outer skin of the shield and the liner

U^*_{3D} = equivalent 3D elastoplastic deformation at the tunnel face; it is assumed to be zero in this case since a face pressure slightly more than the earth pressure is applied in front of the TBM

w = a value taking into account the quality of workmanship; it is assumed to be ($0.6G_p$) in this case.

The physical gap (G_p) is estimated as

$$G_p = (1 - \alpha) \cdot (2 \cdot \Delta + \delta_c) \tag{10.75}$$

where

α = grouting efficiency and suggested to be 0.90–0.93 for very good applications by Lee et al. (1992) as quoted by Loganathan and Poulos (1998), it is assumed to be 0.93 in this study,

Δ = thickness of the tail shield and assumed to be 0.05 m in this case,

δ = clearance required for erection of the liner and assumed to be 0.05 m in this case.

Then, the physical gap (G_p) is estimated as

$$G_p = (1 - 0.93) \cdot (2 \cdot 0.05 + 0.05) = 0.0105 \text{ m}$$

Then, the gap parameter (g) is estimated as

$$g = G_p + U^*_{3D} + w = 0.0105 + 0 + 0.6 \cdot 0.0105 = 0.017 \text{ m}$$

Short-term surface settlement at any distance (x) from the tunnel centerline (S) is predicted by (Loganathan and Poulos 1998)

$$S = 4 \cdot (1 - v) \cdot R^2 \cdot \left(\frac{Z_0}{Z_0^2 + x^2} \right) \cdot \left(\frac{4 \cdot g \cdot R + g^2}{R^2} \right) \exp\left[\frac{-1.38 \cdot x^2}{(Z_0 + R)^2} \right] \quad (10.76)$$

where υ is the undrained Poisson ratio, which can be assumed as a maximum of 0.5, g is gap parameter (m), which is estimated to be 0.017 m in this study, and x is the transverse distance from the tunnel centerline (m) and it is assumed to be 0 m for the maximum surface settlement. The model yields 24 mm of undrained maximum surface settlement as follows:

$$S_{\max} = 4 \cdot (1 - 0.5) \cdot 3.25^2 \cdot \left(\frac{18.25}{18.25^2 + 0^2} \right) \cdot \left(\frac{4 \times 0.017 \cdot 3.25 + 0.017^2}{3.25^2} \right) \times \exp\left[\frac{-1.38 \cdot 0^2}{(18.25 + 3.25)^2} \right]$$

$$S_{\max} = 0.024 \text{ m} = 24 \text{ mm}$$

References

Abulnaga, B., 2002. *Slurry Systems Handbook*. ISBN 0-07-137508-2, McGraw-Hill.

Aftes, 2005. Recommendations: Slurry for use in slurry shield TBM.GT4R4A1, 20 p.

Arioglu, E., 1992. Surface movements due to tunneling activities in urban areas and minimization of building damages. *Short Course*, Istanbul Technical University, Mining Eng. Dept. (in Turkish)

Ates, U., 2013. A comparative study on the relationships between design parameters of TBMs with two current examples of large section TBMs. Master of Science dissertation, Istanbul Technical University.

Attewell, P.B., Yeates, J., Selby, A.R., 1986. *Soil Movement Induced by Tunneling and Their Effects on Pipelines and Structures*. New York, Chapman & Hall.

Babandererde, S., 1991. Tunneling machines in soft ground: Comparison of slurry and EPB shield systems. *Tunnelling and Underground Space Technology*, 6(2):83–97.

Babandererde, S., 1999. Grouting the shield tail gap. *Tunnels and Tunneling International*, 11:48–49.

Bilgin, N., Copur, H., Balci, C., 2012. Effect of replacing disc cutters with chisel tools on performance of a TBM in difficult ground conditions. *Tunnelling and Underground Space Technology*, 27(1):41–51.

Bilgin, N., Copur, H., Balci, C., Tumac, D., Akgul, M., Yuksel, A., 2008. The selection of a TBM using full scale laboratory tests and comparison of measured and predicted performance values in Istanbul Kozyatagi-Kadikoy metro tunnels. *Proc.*

World Tunnel Congress—Underground Facilities for Better Environment and Safety, eds. Kanjlia, V.K., Ramamurty, T., Wahi, P.P., Gupta, A.C. September 22–24, Agra, India, pp. 1509–1517.

Broms, B.B., Bennermark, H., 1967. Stability of clay at vertical openings. *Journal of ASCE*, 93(SM1):71–94.

Copur, H., 2012. Mechanical Excavation and Mechanization in Soft Ground. Graduate Class Notes. Istanbul Technical University, Mining Engineering Department.

Copur, H., Ercelebi, S.G., Bilgin, N., 2007. Prediction of surface settlements for Istanbul Metro lines excavated by EPB TBMs between Otogar and Basaksehir. *Proc. 2. Symposium on Underground Excavationd for Transportation*, eds. Bilgin, N., Copur, H., Balci, C., Yuce, E., Istanbul, pp. 443–454 (in Turkish).

Copur, H., Bilgin, N., Tuncdemir, H., Balci, C., 2003. A set of indices based on indentation tests for assessment of rock cutting performance and rock properties. Journal of South African Institute of Mining and Metallurgy, 103:9:589–600.

Efnarc, 2005. Specification and guidelines for the use of specialist products for mechanized tunnelling (TBM) in soft ground and hard rock. European Federation Dedicated to Specialist Construction Chemicals and Concrete Systems.

EN ISO 13500, 1998. Petroleum and natural gas industries—Drilling fluid materials—Specifications and tests.

Ercelebi, S., Copur, H., Ocak, I., 2011. Surface settlement predictions for Istanbul Metro tunnels excavated by EPB-TBM. *Environmental Earth Sciences*, 62:357–365.

Ercelebi, S., Copur, H., Bilgin, Feridunoglu, C., 2005. Surface settlement prediction for Istanbul metro tunnels via 3D FE and empirical methods. *Proc. World Tunnel Congress,* eds: Y. Erdem and T. Solak, Istanbul, pp. 163–169.

Gonzales, E.F., Magro, J.L., 2012. Technical parameters of Seattle's mega EPBM. TunnelTalk, December, http://www.tunneltalk.com/

Guglielmetti, V., Grasso, P., Mahtap, A., Xu, S., 2008. *Mechanized Tunnelling in Urban Areas: Design Methodology and Construction Control*. Taylor & Francis, Boca Raton, FL, 528 p.

Herrenknecht, M., Thewes, M., Budach, C., 2011. The development of earth pressure shields: From the beginning to the present. *Geomechanics and Tunnelling*, 4(1):11–35.

Herrenknecht, 2013. http://www.herrenknecht.com/

ITA, International Tunneling Association, 2000. Guidelines for the design of shield tunnel lining. *Working Group No. 2, Tunnelling and Underground Space Technology*, 15(3):303–331.

Jancsecz, S., Krause, R., Langmaack, L., 1999. Advantages of soil conditioning in shield tunneling: Experiences of LRTS in Izmir. *Proc. World Tunnel* Congress, Oslo, Ed. Alten, T., Balkema, Rotterdam, pp. 865–875.

JSCE, Japan Society of Civil Engineers, 2007. *Standard Specification for Tunnelling-2006: Shield Tunnels*. ISBN: 978-4-8106-0568-6, 270 p.

Kanayasu, S., Kubota, I., Shikibu, N., 1995. Stability of face during shield tunneling—A survey on Japanese shield tunneling. *Proc. Underground Construction in Soft Ground*, eds. Fujita, K., Kusakabe, O., New Delhi, pp. 337–343.

Karakus, M., Fowell, R.J., 2003. Effects of different tunnel face advance excavation on the settlement by FEM. *Tunnelling and Underground Space Technology*, 18:513–523.

Korbin, G.E., 1998. Claims and tunnel boring machines: Contributing factors and lessons learned. *Annual Publication of the Tunnelling Association of Canada*, Ed. K.Y. Lo. 6 pp.

Labanov, V.A., Joanknecht, L.W.F., 1980. The cutting of soil under hydrostatic pressure. *Proc. the 9th World Dredging Conference*, October 29–31, Canada, pp. 327–339.

Loganathan, N., Poulos, H.G., 1998. Analytical prediction for tunnelling-induced ground movements in clays. *Journal of Geotechnical and Geoenvironmental Engineering*, September: 846–856.

Lovat, R., 2007. TBM design considerations: Selection of earth pressure balance or slurry pressure balance tunnel boring machines. *BASF TBM Conference*, Istanbul.

Maidl, B., Herrenknecht, M., Anheuser, L., 1996. *Mechanized Shield Tunnelling*. Ernst and Sohn, ISBN: 3-433-01292-X, 427 p.

Maidl, U., 2005. EPB and slurry TBM selection. *Mechanical Tunneling Short Course*, June, Seattle.

Mair, R.J., Taylor, R.N., 1997. Bored tunnelling in the urban environment. State-of-the-art Report and Theme Lecture. *Proc. the 14th Int. Conference on Soil Mechanic and Foundation Engineering*, Hamburg, Balkema, Vol. 4, pp. 2353–2385.

Milligan, G.W.E., Marshall, M.A., 1995. Ground movements due to construction of pipe-jacked tunnels. *Proc. the 11th European Conference on Soil Mechanics and Foundation Engineering*, Copenhagen, Vol. 3, pp. 191–200.

Minguez, F., Gregory, A., Guglielmetti, V., 2005. Best practice in EPB management. *Tunnels and Tunnelling International*, November, 21–25.

O'Reilly, M.P., New, B.M., 1982. Settlement above tunnels in the United Kingdom—Their magnitude and prediction. *Proc. the Tunneling 82 Conference*, Brighton, pp. 173–181.

PJA, Pipe Jacking Association, 1995. *Guide to Best Practice for the Installation of Pipe Jacks and Microtunnels*. London.

Schmidt, B., 1969. A method of estimating surface settlement above tunnels constructed in soft ground. *Canadian Geotechnical Journal*, 20:11–22.

Schmidt, B., 1974. Prediction of settlements due to tunneling in soil: Three case histories. *Proc. Rapid Excavation and Tunneling Conference*, Vol. 2, pp. 1179–1199.

Suwansawat, S., Einstein, H.H., 2006. Artificial neural networks for predicting the maximum surface settlement caused by EPB shield tunnelling. *Tunnelling and Underground Space Technology* 21:133–150.

Tan, W.L., Ranjit, P.G., 2003. Parameters and considerations in soft ground tunnelling. *The Electronic Journal of Geotechnical Engineering*, 8(D): Ppr0344. (http://www.ejge.com/2003/Ppr0344/Abs0344.htm).

Thewes, M., 2007. Shield tunnelling technology to mitigate geotechnical risks. *Proc. the 2nd Symposium on Underground Excavation for Transportation*, eds. Bilgin, N., Copur, H., Balci, C., Yuce, A.E., November 15–17, Istanbul, pp. 49–56.

Thewes, M., Budach, C., 2010. Soil conditioning with foam during EPB tunnelling. *Geomechanics and Tunnelling*, 3(3):256–267.

Thomson, J.C., 1995. *Pipejacking and Microtunnelling*. Blackie Academic & Professional, Glasgow, ISBN: 0-7514-0102-6, 273 p.

11

Microtunnel Boring Machines and Jacking Forces

11.1 General

Utility lines such as gravity sewer lines (sanitary, storm/drainage, combine), gas mains, water mains, long-distance heating lines, long-distance refrigerating lines, pneumatic conveying lines, refuse disposal lines, oil pipelines, ducts, conduits, and cable lines for electricity–telecommunications–signaling are the basic cost items of any urban management. Since urban areas are environmentally sensitive and include some obstacles on surface such as highways, railways, rivers, canals, buildings, and airfields that are on the path of pipe lines, special care should be taken to not disturb the surface structures and obstacles when dealing with infrastructural systems. There are generally two choices to cope with infrastructural needs of an urbanized area: open-cut trenching (cut and cover) and microtunneling (trenchless technology, pipe jacking, no-dig technology).

Microtunneling or trenchless technology in North America (ISTT 2012) is defined as remotely controlled, steerable, continuous pipe jacking in all diameters whether man accessible or not. However, in Europe, man accessible trenchless methods are defined as pipe jacking (ISTT 2012), requiring a minimum diameter of 1–1.2 m, while smaller diameter trenchless operations are defined as microtunneling.

Trenchless technology includes the techniques for the installation, replacement, renovation, and repair–maintenance of pipes, ducts, cable lines, and other underground apparatus with minimum excavation from the ground surface (ISTT 2012). It may also include associated techniques such as leak detection, inspection, and location of existing infrastructure. Applicable diameters are up to 3.5 m (inner diameter), which is currently the maximum available pipe diameter.

Trenchless technology should be considered and is superior to open-cut trenching especially at depths of 5 m or greater, under or near existing buried utilities, under busy roads or industrial/commercial areas, in unstable ground conditions/below water table, and at where settlement is hazardous

TABLE 11.1

Advantages of Trenchless Technology over Cut and Cover

Minimizes disruption to surface/traffic during construction, reduces social cost
Minimizes disruption to existing sewers, utilities, and services
Minimizes risk of settlement (subsidence) and collapse
Minimizes the amount of excavation (only the pipe bore is excavated)
Minimizes reconstruction work to road surfaces
Minimizes restoration work to the buildings
Minimizes the need for man-entry, improving operator/worker safety
Minimizes safety problems in contaminated ground
Avoids the need to dewater the pipe trench, reducing collapse/settlement risk
Accurate installation with line and grade tolerances of better than ± 2.5 cm
Strength of jacking pipe is typically greater than the pipes used in open cut
Smooth internal finish giving good flow characteristics
No requirement for secondary (final) lining
Applicable to the most ground types and depths
Speedier and cost effective construction in favorable conditions

Source: Adapted from ISTT, International Society for Trenchless Technology, 2012. http://www.istt.com

to property or other utilities. Advantages of trenchless construction method over cut and cover construction are summarized in Table 11.1.

11.2 Pipe Line Installation Methods

Methods for installation of new pipe lines can be classified into four general groups based on the excavation method: face excavation (with muck haulage), ground displacement (without muck haulage), horizontal directional drilling (HDD) and combination methods (face excavation + ground displacement + HDD), (modified by Copur 2012 after ISTT 2012). They can also be classified based on steering (guiding) abilities of microtunnel boring machines (MTBMs), man's accessibility to the bore, pipe material, sizes, and so on.

In face excavation method, the face is excavated and the muck should be transferred to the surface. Rigid pipes are used for installation. While a shielded, steerable, remote-controlled MTBM is pushed toward the face, the rigid product pipes are added to each other, and the pipe string and MTBM are pushed together by hydraulic cylinders on the main jacking frame, located in the driving shaft. When the MTBM reaches the exit shaft, it is removed and the pipeline is completed. Face excavation methods can be divided into two general sub-classes: full-face excavation (closed mode: with face pressure in unstable ground, open mode: without face pressure in stable ground, and partly open mode) and part-face (open mode) excavation (Figure 11.1).

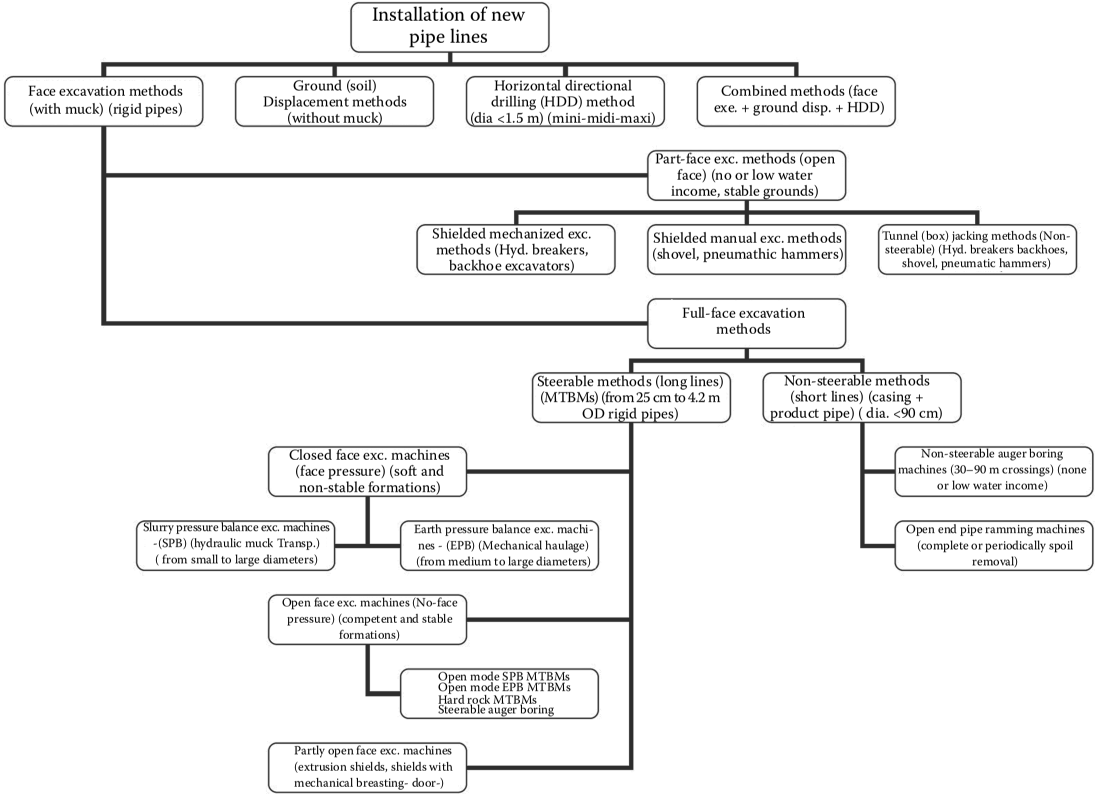

FIGURE 11.1
Generalized classification of new pipeline installation methods. (Modified by Copur, H., 2012. "MAD605E Microtunneling" Class Notes. Istanbul Technical University, Mining Engineering Department after ISTT, International Society for Trenchless Technology, 2012. http://www.istt.com/)

Part-face excavation methods, which cover a very small portion of face excavation methods, usually includes manual excavation (with hand or pneumatic tools) and backhoe excavators. Breasting plates can be used to provide face stability. The microtunnel should be dry or water income should be low for the application of part-face excavation methods.

In ground displacement methods of microtunneling, the face is not excavated and there is no muck to haul. Instead, an opening is created by displacement or compaction of the ground in every direction with special microtunnel heads, which can work in homogeneous soft plastic soils. The method is applicable for shorter distances (<50 m) and smaller diameters (<20 cm) compared to face excavation methods. The head is either pushed or pulled (reaming) toward the ground. The current ground displacement methods are nonsteerable. Nonsteerable ground displacement method includes excavation by percussive (impact) moling machines (also called earth-piercing machines) using a static, hydraulic, or pneumatic hammer, and closed-end pipe ramming machines. Impact moling requires flexible pipes, such as PVC (poly vinyl chloride) and HDPE (high-density poly ethylene) while pipe ramming requires rigid pipes.

HDD is a special steerable pipe installation method and can include fluid boring (excavation), ground displacement, and reaming (enlargement of a pilot hole). HDD machines can be classified as mini, midi, and maxi depending on their size and application range.

In combined new pipeline installation methods, usually a pilot bore is opened by ground displacement method and then the bore is reamed or enlarged by a full face excavation in one or more stages. These methods have limited applications compared to face excavation and ground displacement methods.

Slurry MTBMs and earth pressure balance (EPB) MTBMs are the most widely used full-face MTBMs, which are steerable and have the widest pipe diameter range. With these machines, the earth and water pressures in unstable ground under the water table can be easily counterbalanced by the face pressures given by a special bentonite–water mixture in slurry types and processed (conditioned) muck in EPB types. Muck is transported to the surface by hydraulic transportation in slurry MTBMs and any one of the dry muck haulage systems (rail cars, conveyors, dirt skips) in EPB MTBMs. In stable ground and hard rock conditions, they can be used in open mode without giving face pressure. Technical features of some of the slurry and earth pressure balance MTBMs are summarized in Tables 11.2 and 11.3, respectively.

Compressed air shields and mixshields (polyshields) used in tunneling are not used in microtunneling. Auger boring machines (steerable or nonsteerable) and open-end pipe ramming machines (nonsteerable) are the other full-face type of the MTBMs, requiring steel casing pipes in addition to microtunneling (product) pipes.

A generalized full-face excavation microtunneling system using SPB MTBM is illustrated in Figure 11.2. The pipe installation with MTBMs consists of five major components: a MTBM machine, automated spoils transportation and

TABLE 11.2

Technical Features of Slurry MTBMs

	AVN250XC		AVN300XC		AVN400XC		AVN500XC		AVN600XC		AVN700XC	
	Std	Ext	Std	Ext	Std	Ext	Std	Ext	Std	Ext	Std	Ext
Outer diameter, mm	368	410	410	565	565	665	665	780	780	875	875	975
Pipe OD, mm	360	400	400	550	550	650	650	760	760	860	860	960
Pipe ID, mm	250	300	300	400	400	500	500	600	600	700	700	800
Max. torque, kNm	5.9		9.4		13.4		22.2		33.5		40.1	
Revolution LH/RH, rpm	0–44		0–27		0–19		0–15		0–13		0–11	
Rated power, kW	45		45		45		45		45		55	
Steering cylinders	3		3		3		3		3		3	
Force per cylinder/oil pressure, kN/bar	116/500		245/500		245/500		311/500		311/500		383/500	
Stroke per cycle, mm	10		15		15		25		25		30	
Pipe jacking drive length (recommended), m	80		100		100		120		140		140	
Waterproofness, bar	3		3		3		3		3		3	
Slurry line diam., mm	55		55		80		100		100		100	

Source: Adapted from Herrenknecht, 2012. http://www.herrenknecht.com/. With permission.
Note: Std, standard; Ext, extended.

TABLE 11.3

Technical Features of Earth Pressure Balance MTBMs

	EPB1400TB Std Ext	EPB2200TB Std Ext	EPB2600TB Std Ext	EPB1600AE	EPB2200AE	EPB2600AE
Outer diameter, mm	1740 1810	2725 3025	3125 3625	1970	2725	3125
Pipe OD, mm	1720 1780	2700 3000	3100 3600	1940	2700	3100
Pipe ID, mm	1400 1500	2200 2400	2600 3000	1600	2200	3000
Max. torque, kNm	236	820	1200	175	500	560
Revolution LH/RH, rpm	0–6	0–5	0–5	0–3.5	0–3	0–3
Rated power, kW	110	250	315	44	88	120
Steering cylinders	4	8	8	4	8	8
Force per cycle/oil pressure, kN/bar	752/500	770/500	1005/500	1005/500	770/500	1005/500
Stroke per cycle, mm	60	150	150	60	150	150
Drive length (recommended), m	400	1100	1100	700	1100	1100
Waterproofness, bar	3	3	3	3	3	3

Source: Adapted from Herrenknecht, 2012. http://www.herrenknecht.com/. With permission.
Note: Std, standard; Ext, extended.

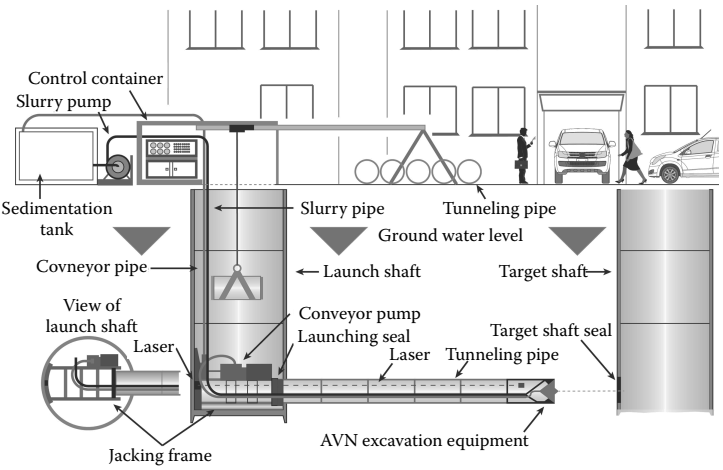

FIGURE 11.2
Generalized microtunneling system. (Adapted from Herrenknecht, 2012. http://www.herrenknecht.com With permission.)

excavation rate controls, a steering system capable of maintaining accuracy sufficient to directly install the rigid product pipe, a remote control system, and a guidance (usually laser) system that continuously confirms the position of boring machine.

11.3 Some Design Considerations and Planning in Microtunneling

Rigid pipes should be used with the face excavation method. Concrete is the most common material used as a pipe material for microtunneling with a range of diameters from about 30 cm upwards. However, pipes of steel, fiber glass (GRP, Hobas), and clay (in smaller diameters) are also used. The choice of material can be influenced by diameter, length of drive and in some cases, by ground conditions or the intended end use of the pipe. The pipes of composite manufacture, for example, concrete and GRP, have been produced to meet exceptional conditions. Guidance on jointing techniques together with advice on joint packing should be obtained from the manufacturer. The available sizes for different types of pipe materials are summarized in Table 11.4.

The main jacks for pushing the pipes and shielded excavation machine should be mounted in a jacking frame. The MTBM is pushed forward by the jacks, advancing a successive string of connected pipes toward the receiving shaft. The jacking equipment is better to have a capacity slightly higher than the maximum allowable jacking force, which is basically dependent upon

TABLE 11.4

Available Sizes for Different Types of Pipe Materials

Type of Pipe	Inner Diameter Range (mm)	Pipe Section Length Range (m)
Reinforced concrete pipe (RCP)	300–3600	0.9–3
Glass-fiber reinforced thermosetting resin pipe (GRP)	300–2700	3–6
Vitrified clay pipe (VCP)	150–600	0.9–1.2
Ductile iron pipe	100–600	Up to 6
Steel pipe	75–3600	2.4–12

Source: Adapted from Chung et al. 2004. *Journal of Construction Engineering and Management*, 130(6):835–843.

pipe strength. The jacking system should distribute the jacking loads uniformly on the pipe. The extension rate of the hydraulic cylinders should be matched to the excavation rate of the MTBM.

A pipe lubrication system can be used to reduce the friction between the outer surface of pipe and the ground. Usually bentonite slurry (water + bentonite) is used as lubrication material, which can be injected at the rear of the MTBM shield or through lubrication ports on pipes.

Intermediate jacking stations are used when the jacking force for the required drive length is expected to exceed the capacity of the main jacks or the strength limit of the jacking pipe. Diameters of intermediate jacking stations usually start from 90 cm. Their length is usually around 140 cm. The number of intermediate jacking stations should be kept to a minimum (mostly 3–4), since increasing the number of intermediate jacking stations would result in misalignment of MTBM. Typical main jack and intermediate jacking station capacities are presented in Table 11.5.

TABLE 11.5

Typical Main Jack and Intermediate Jacking Station Capacities

Pipe Inner Diameter (mm)	Main Jack Capacity (Short Tons[a])	Intermediate Jacking Station Capacity (Short Tons)
250/450	150/200	—
500/665	200/300	300
600/760	240/300	300
800/865	300/400	300/400
900/1100	300/400	300/400
1000/1285	400/550	400/550
1200/1535	400/550	400/550
1500/1965	600/850/100	600/850
1800/2145	850/1000/1200	850/1000/1200

Source: Adapted from Ozdemir, L., Coss, T., 1998. *Microtunneling. Short Course*. Colorado School of Mines, Golden, CO-USA. Section: "Ancillary equipment" by T. Coss.

[a] 1 short ton = 0.907 metric ton (ton).

General recommendations for planning a microtunneling project are summarized in Table 11.6. Changing pipe diameters may require a different MTBM or a complete system. Minimizing the number of pipe diameters may reduce the overall equipment requirements for a particular project. A pipeline depth that will provide the most favorable geotechnical conditions and the least risk of encountering an obstruction should be selected.

Utilizing a drive shaft for multi-drives minimizes the number of drive shafts required for a given project. This will result in time and money saved because receiving shafts are smaller in diameter. The location of shafts should be planned so that areas difficult to access contain only a reception shaft wherever possible.

The achievable length of the drive is dependent upon the jacking force, pipe material, and pipe size. The jacking force is a function of many variables including the drive length, soil conditions, depth of the pipeline, annular space between the pipe and the soil, lubrication of the pipe (by a water–bentonite mixture of slurry), water table location, overburden (earth–water–surcharge) loads, installation time, and pipe material–diameter–strength. The minimum depth of cover to the top of the installed pipe using this process should be one to three times the outside diameter of the pipe being installed, or around 2 m, whichever is greater depending on the soil conditions.

Longer drives are possible when larger diameters are utilized because larger pipe diameters provide greater cross-sectional surface area for the axial jacking forces to be transmitted and when the pipe diameters permit person entry, then, intermediate jacking stations can be employed. Also, pipe breakages, which cause long delays thereby reducing machine utilization time, are less prone in larger diameters for the same jacking distance. Therefore, estimation of jacking forces prior to construction is very important.

A detailed site investigation for technical (design and planning) and economical (cost estimations, financing, risk assessment) purposes, as well

TABLE 11.6

General Recommendations for Planning a Microtunneling Project

Minimize the number of pipe diameters
Allow a combination of pipe materials for the project
Plan the project so that microtunnel drives can be constructed in both directions from a given driving shaft
Maximize drive lengths consistent with pipe size, type of microtunneling system being used, and geotechnical conditions
Planner should evaluate different depths, pipe sizes, and gradients
Evaluate several alignments so that an optimal alignment can be selected which requires the fewest number of shafts without exceeding the practical drive lengths of the microtunneling system and pipe being considered for the project

Source: Adapted from Ozdemir, L., Coss, T., 1998. *Microtunneling. Short Course*. Colorado School of Mines, Golden, CO-USA. Section: "Site layout and logistics" by T. Iseley.

as safety concerns (stability and other hazards), is always a priority for a successful microtunneling project.

Shaft design is also important in microtunneling (face excavation methods), since all the loads from jacking frames are transferred to the ground by the shafts. Jacking, earth, and surcharge loads play a very important role on shaft design.

11.4 Performance Predictions for MTBMs

Predicting performance of steerable full-face MTBMs is quite similar to the ones of TBMs, especially for hard rock applications, since their mechanical structures are quite similar (Figure 11.3). The basic difference lies in the jacking forces, which becomes very important for microtunneling operations. Therefore, the numerical examples on predicting microtunnel jacking forces will be mentioned in the next section.

11.5 Numerical Examples on Estimation of Jacking Forces

11.5.1 Jacking Force Estimation by Using the Method of Chapman and Ichioka

Estimate total jacking force by using empirical method developed by Chapman and Ichioka (1999). Draw graphically the variation of jacking force based on the parameters given below:

Excavation machine: slurry MTBM

Depth (overburden): 9 m

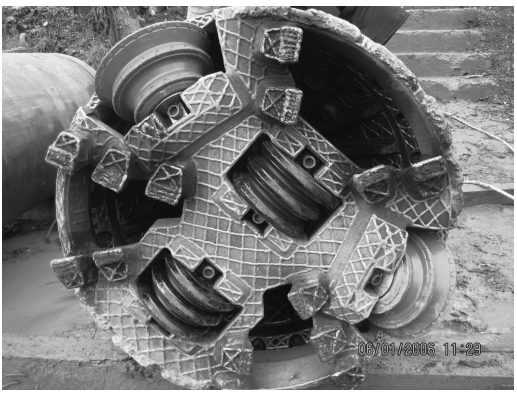

FIGURE 11.3
Picture of a slurry-type microtunneling machine.

Lubrication: well lubricated

Microtunnel length (jacking distance), $L = 140$ m

Formation: 40 m of sand-gravel, 40 m of sand, 60 m of clay (in the excavation order)

Outer diameter of concrete jacking pipe, $D_p = 1.20$ m

Excavation diameter, $D_0 = 1.22$ m

Face pressure, $P_0 = 70$ tonf/m^2

11.5.1.1 Solution of Numerical Example 11.5.1

Chapman and Ichioka (1999) statistically examined 189 slurry machine cases. Their method is applicable/valid for slurry MTBMs with a 360–1200 mm outer diameter (250–1000 mm inner diameter, 375–1220 mm excavation diameter), maximum overburden of 15 m and well-lubricated microtunnels.

The general form of the model (Chapman and Ichioka 1999) for estimating jacking forces (either total or at a position) is given by Equation 11.1 for slurry MTBMs:

$$F = f_0 + \pi \cdot D_p \cdot P \cdot L \tag{11.1}$$

where

F = jacking force in tonf
f_0 = primary resistance (face pressure force) in tonf
P = frictional resistance along the pipe run in tonf/m^2
L = jacking distance in meters
D_p = outer diameter of the jacking pipe in meters

The face resistance f_0 is estimated by Equation 11.2:

$$f_0 = \pi \cdot D_0^2 \cdot P_0/4 \tag{11.2}$$

where

D_0 = excavation diameter in meters
P_0 = face resistance (pressure) in tonf/m^2. It is usually between 50 tonf/m^2 for 60% coverage and 90 tonf/m^2 for 90% coverage of the collected data for establishment of the model. For this problem, it is selected to be 70 tonf/m^2.

Frictional resistance along the pipe run P can be estimated by Equation 11.3:

$$P = a + 0.38D_p \tag{11.3}$$

where a is a constant based on soil types excavated. The value of a can be taken as 0.153 for clays, 0.243 for sands and 0.343 for sand and gravel mixed soil type.

If only total jacking force is to be estimated, the last formation (clay) in the excavation order is considered and the total jacking distance of 140 m is used. By using Equation 11.2, the face resistance f_0 is estimated to be 82 tonf by taking D_0 of 1.22 m and P_0 of 70 tonf/m^2. By using Equation 11.3, the frictional resistance P along the pipe run is estimated to be 0.61 tonf/m^2 by taking D_p of 1.2 m and a of 0.153. Total jacking force of 403 tonf is then estimated by Equation 11.1.

If the variation of jacking forces should be estimated, then, all the formation types in the excavation order should be considered by taking a and L values as follows:

$$a_{\text{sand\&gravel}} = 0.343$$
$$a_{\text{sand}} = 0.243$$
$$a_{\text{clay}} = 0.153$$
$$L_{\text{sand\&gravel}} = 40 \text{ m}$$
$$L_{\text{sand}} = 80 \text{ m}$$
$$L_{\text{clay}} = 140 \text{ m}$$

Then, P and F values for different formations are estimated to be

$$P_{\text{sand\&gravel}} = a_{\text{sand\&gravel}} + 0.38D_{\text{p}} = 0.343 + 0.38 \cdot 1.20 = 0.80 \text{ tonf/m}^2$$
$$P_{\text{sand}} = a_{\text{sand}} + 0.38D_{\text{p}} = 0.243 + 0.38 \cdot 1.20 = 0.70 \text{ tonf/m}^2$$
$$P_{\text{clay}} = a_{\text{clay}} + 0.38D_{\text{p}} = 0.153 + 0.38 \cdot 1.20 = 0.61 \text{ tonf/m}^2$$

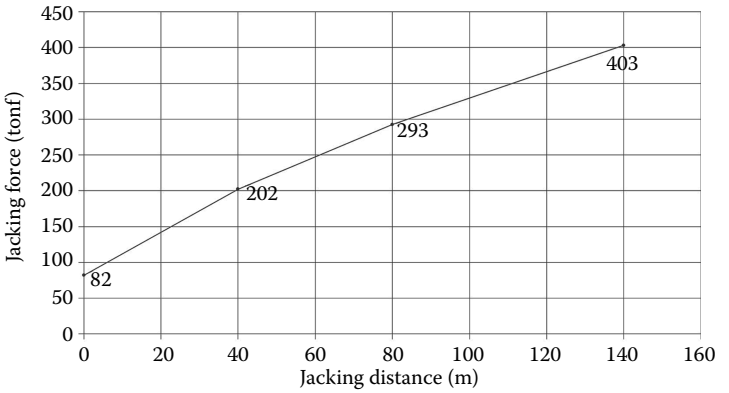

FIGURE 11.4
Variation of jacking force along the drive.

$$F_{\text{sand\&gravel}} = f_0 + \pi \cdot D_{\text{p}} \cdot P_{\text{sand\&gravel}} \cdot L_{\text{sand\&gravel}} = 82 + \pi \cdot 1.20 \cdot 0.80 \cdot 40 = 202 \text{ tonf}$$

$$F_{\text{sand}} = f_0 + \pi \cdot D_p \cdot P_{\text{sand}} \cdot L_{\text{sand}} = 82 + \pi \cdot 1.20 \cdot 0.70 \cdot 80 = 293 \text{ tonf}$$

$$F_{\text{clay}} = f_0 + \pi \cdot D_p \cdot P_{\text{clay}} \cdot L_{\text{clay}} = 82 + \pi \cdot 1.20 \cdot 0.61 \cdot 140 = 403 \text{ tonf}$$

Jacking force of 403 tonf estimated for clay formation is also total jacking force. Variation of jacking force along the drive is presented in Figure 11.4.

11.5.2 Jacking Force Estimation by Using the Method of Bennett and Cording for Sand

Estimate frictional jacking force by using empirical method developed by Bennett and Cording (2000) based on the parameters given below:

Excavation machine: Any full face excavation type of MTBM
Lubrication: lubricated
Microtunnel length (jacking distance), $L = 100$ m
Formation: dry sand
Internal friction angle of sand, $\phi_{\text{sand}} = 30°$
Unit weight of sand, $\gamma_{\text{sand}} = 1.6$ tonf/m^3
Outer diameter of concrete jacking pipe, $D_p = 1.20$ m

11.5.2.1 Solution of Numerical Example 11.5.2

The model developed by Bennett and Cording (2000) suggests Equation 11.4 for estimation of frictional jacking forces:

$$F_F = C_a \cdot \gamma_n \cdot \pi \cdot D_p{}^2 \cdot L \cdot \tan(C_f \cdot \phi) \tag{11.4}$$

where
F_F = frictional force in tonf
C_a = a constant for taking into account for ground arching
γ_n = bulk unit weight of the soil in tonf/m^3
D_p = outer diameter of the pipe in meters
L = jacking distance in meters
C_f = a constant for taking into account for friction between pipe and ground
ϕ = residual internal friction angle of the soil in degrees

For an upper bound solution, they suggest C_a, C_f and γ_n values for granular soils (especially sands) as follows:

$C_a = 1.5$, $C_f = 1$, $\gamma_n \Rightarrow \gamma_n$ for nonlubricated dry (or dewatered) sands,

$$C_a = 1.5,\ C_f = 2/3,\ \gamma_n \Rightarrow \gamma_n \quad \text{for lubricated dry sands,}$$

$$C_a = 1,\ C_f = 1,\ \gamma_n \Rightarrow (\gamma_n - \gamma_w) \quad \text{for nonlubricated wet sands,}$$

$$C_a = 1,\ C_f = 2/3,\ \gamma_n \Rightarrow (\gamma_n - \gamma_w) \quad \text{for lubricated wet sands,}$$

where, γ_w is the unit weight of water and can be taken as 1 tonf/m^3 for practical purposes. Based on the given parameters, Equation 11.5 can be rewritten as follows:

$$F_F = 1.5 \cdot 1.6 \cdot \pi \cdot 1.2^2 \cdot 100 \cdot \tan(0.67 \cdot 30) = 397 \text{ tonf}$$

Then, the frictional force acting on the pipeline is estimated to be a 397 tonf. For conservative designs, the estimated value should be increased by 1/3 for delays, misalignment, and so on, giving an estimation of 528 tonf.

A reasonable face resistance force should also be added to the frictional force to estimate total jacking force. In small diameter microtunnels, the face resistance force is quite small compared to the frictional force and can be ignored; however, it can be a large value for larger diameters. Face resistance force can be estimated by Equation 11.5 as given in Atalah et al. (1994):

$$F_R = P_1 + P_2 \tag{11.5}$$

where

F_R = Face or penetration resistance force in tonf.
P_1 = Cutterhead front plate contact pressure force in tonf. P_1 should be between the limit face pressures (active and passive earth pressures).
P_2 = Excavation chamber hydraulic (face) pressure force in tonf.

P_1 and P_2 are estimated by Equations 11.6 and 11.7:

$$P_1 = \pi \cdot D_C^2 \cdot P_{CC}/4 \tag{11.6}$$

$$P_2 = S_M \cdot D_S^2 \cdot P_w/4 \tag{11.7}$$

where

D_C = Cutterhead diameter in meter
P_{CC} = Cutterhead contact pressure in tonf/m^2
S_M = Safety margin, it is usually between 1.1 and 1.2, average 1.15
D_S = Shield diameter in meter
P_w = Hydrostatic water pressure at the bottom of pipe in tonf/m^2

It can be estimated by Equation 11.8:

$$P_w = \gamma_w \cdot h_w \tag{11.8}$$

where

γ_w = Unit weight of water, 1 tonf/m^3 for practical purposes
h_w = Height of water column over the pipe bottom, in meters

The approach given in Equation 11.5 does not include the effect of cutting the soil by knife/wedge/ripper cutters. The normal force coming from the cutting tools can be found by using the results of either theoretical models or laboratory experiments and can be incorporated into Equation 11.5, although it is a small fraction of the face resistance in soft ground.

On the other hand, in Chapman and Ichioka (1999), a face pressure for slurry shields or slurry MTBMs up to 1.2 m diameter is given between 50 and 90 tonf/m^2. Face resistance can just be estimated by multiplying the excavated cross-section area by the given face pressure.

11.5.3 Jacking Force Estimation by Using the Method of Bennett and Cording for Clay

Estimate frictional jacking force by using empirical method developed by Bennett and Cording (2000) based on the parameters given below:

Excavation machine: any full face excavation type of MTBM

Lubrication: lubricated

Microtunnel length (jacking distance), L = 100 m

Formation: stiff clay

Internal friction angle of stiff clay, $\phi_{\text{clay}} = 10°$

Unit weight of stiff clay, γ_{clay} = 2.4 tonf/m^3

Outer diameter of concrete jacking pipe, D_p = 1.20 m

11.5.3.1 Solution of Numerical Example 11.5.3

The model developed by Bennett and Cording (2000) suggests Equation 11.4 for estimation of frictional jacking forces. For an upper bound solution, they suggest C_a, C_f and γ_n values for cohesive soils as follows (notations are the same as in Problem 11.5.2):

$C_a = 1$, $C_f = 1$, $\gamma_n \Rightarrow \gamma_n$ for nonlubricated dry or wet stiff to hard clays and soft to medium silts and clays,

$C_a = 2/3$, $C_f = 2/3$, $\gamma_n \Rightarrow \gamma_n$ for lubricated dry or wet stiff to hard clays

$C_a = 3$, $C_f = 1$, $\gamma_n \Rightarrow \gamma_n$ for lubricated dry or wet soft to medium silts-clays

On the basis of the given parameters, Equation 11.4 can be rewritten as follows:

$$F_F = 0.67 \cdot 2.4 \cdot \pi \cdot 1.2^2 \cdot 100 \cdot \tan(0.67 \cdot 10) = 85 \text{ tonf}$$

Then, the frictional force acting on the pipeline is estimated to be an 85 tonf. For conservative designs, the estimated value should be increased by 1/3 for delays, misalignment, and so on, then estimated as being a 113 tonf.

The normal force coming from the cutting tools can be found by using the results of either theoretical models or laboratory experiments and can be used for estimation of face resistance and, then, of total jacking force.

11.5.4 Jacking Force Estimation by Using U.S. Army Corps of Engineers for Dry Formation

Estimate frictional force due to vertical earth pressures acting on concrete pipeline by using the model suggested by the U.S. Army Corps of Engineers (1998) based on the parameters given below:

Microtunnel length (jacking distance), L = 300 ft (90 m)
Formation: clay (dry)
Unit weight of clay, γ_{clay} = 18850 N/m^3 (120 pcf)
Cohesion of clay, c_{clay} = 4790 N/m^2 (100 psf)
Internal friction angle of clay, ϕ_{clay} = 10°
Soil Constant (for clay), $K\mu'$ = 0.130
Excavation diameter, B_t = 1.2 m (4 ft)

11.5.4.1 Solution of Numerical Example 11.5.4

The general form of the model suggested by the U.S. Army Corps of Engineers (1998) for estimating vertical earth loads is given by Equation 11.9 for slurry MTBMs:

$$W_t = C_t \cdot \gamma \cdot B_t^2 - 2 \cdot c \cdot C_t \cdot B_t \tag{11.9}$$

where
W_t = vertical earth load under tunneled or jacked (dry) conditions in N/m
C_t = load coefficient for tunneled or jacked pipe (unitless)
γ = unit weight of the soil in N/m^3
B_t = excavation diameter in meters
c = cohesion of soil in N/m^2, (given in U.S. Army Corps of Engineers (1998) as a tabulated list for all soil types)

Load coefficient for tunneled or jacked pipe (C_t) is estimated by Equation 11.10:

$$C_t = 1 - \frac{e^{-2 \cdot K\mu' \cdot (H/B_t)}}{2 \cdot K\mu'} \tag{11.10}$$

where

e = base of the natural logarithms,
$K\mu'$ = Soil constant (unitless), (0.165 for sand and gravel, 0.150 for saturated top soil, 0.130 for clay, and 0.110 for saturated clay)
H = overburden (height of soil layer or fill) above the crown of the tunnel

Load coefficient is estimated to be 0.8509 by using Equation 11.10 as follows:

$$C_t = 1 - \frac{e^{-2 \cdot 0.130 \cdot (15/1.20)}}{2 \cdot 0.130} = 0.8509$$

Earth load per meter of jacked pipe (W_t) is estimated to be 13314 N/m (= 13.3 kN/m = 1.33 tonf/m = 953 lbf/ft) by using Equation 11.9 as follows:

$$W_t = 0.8509 \cdot 18850 \cdot 1.20^2 - 2 \cdot 4790 \cdot 0.8509 \cdot 1.20 = 13314 \text{ N/m}$$

The frictional force (F_F) due to vertical earth load can be estimated by multiplying W_t value by the length of drive (L) as in Equation 11.11:

$$F_F = W_t \cdot L \tag{11.11}$$

By using Equation 11.11, the frictional force is estimated to be 1,198,295 N (= 1198 kN = 121 tonf).

The face resistance force coming from the cutterhead area should be added to the frictional force for estimation of total jacking force. The method does not include any effect of lubrication of the void between pipes and tunnel perimeter.

11.5.5 Jacking Force Estimation by Using the Method of Shimada et al.

Estimate total jacking force by using the empirical method developed by Shimada et al. (2004) based on the parameters given below:

Excavation machine: slurry MTBM

Lubrication: well lubricated

Microtunnel length (jacking distance), L = 100 m

Applied face pressure, P_w = 80 kPa

Cohesion between pipe and mud (lubrication) slurry, C = 5 kPa

Coefficient of kinematic friction between pipe and mud (lubrication) slurry, μ = 0.15

Outer diameter of concrete jacking pipe, D_p = 1.20 m

11.5.5.1 Solution of Numerical Example 11.5.5

The model developed by Shimada et al. (2004) for well-lubricated stable bores suggests Equation 11.12 to estimate the total jacking forces required for slurry MTBMs:

$$F_T = P_w \cdot (D_p/2)^2 \cdot \pi + \pi \cdot D_p \cdot (P_w \cdot \mu + C) \cdot L \tag{11.12}$$

where
F_T = total jacking force in kN
P_w = slurry pressure in kPa
D_p = outer diameter of the pipe in meters
μ = coefficient of kinematic friction between pipe and mud slurry
C = cohesion between pipe and mud slurry in kPa
L = jacking distance in meters

On the basis of the given parameters, the total jacking force is estimated to be 6545 kN (655 tonf) by using Equation 11.12 as follows:

$$F_T = 80 \cdot (1.2/2)^2 \cdot \pi + \pi \cdot 1.2 \cdot (80 \cdot 0.15 + 5) \cdot 100 = 6545 \text{ kN} \cong 655 \text{ tonf}$$

11.5.6 Jacking Force Estimation by Using Theoretical Methods

Estimate total jacking force using theoretical methods suggested in the standards of Japan, the United Kingdom, and Germany, based on the parameters given below (Figure 11.5):

Excavation machine: slurry MTBM

Lubrication: nonlubricated

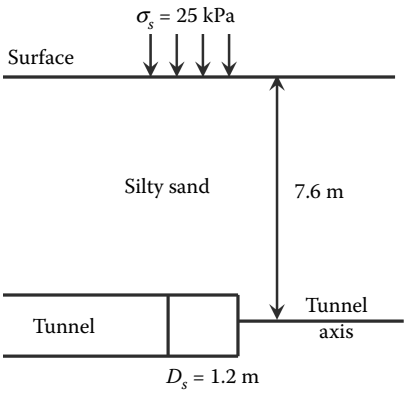

FIGURE 11.5
Geometry for Numerical Example 11.5.6.

Overburden to tunnel crown, $h = 7$ m
Microtunnel length (jacking distance), $L = 100$ m
Formation: silty sand (dry)
Bulk unit weight of silty sand, $\gamma_{soil} = 20$ kN/m^3
Internal friction angle of silty sand, $\phi_{soil} = 30°$
Surcharge pressure, $\sigma_S = 25$ kPa $= 25$ kN/m^2
Outer diameter of concrete jacking pipe, D_p (~D_S, shield diameter) $= 1.2$ m

11.5.6.1 Solution of Numerical Example 11.5.6

The total jacking force is a summation of face resistance force and frictional force as given in Equation 11.13 (Pellet-Beaucour and Kastner 2002):

$$F_T = F_P + F_F \tag{11.13}$$

where
F_T = total jacking force in kN
F_P = jacking force requirement due to face resistance in kN
F_F = jacking force due to frictional resistance between earth and pipes in kN

Face resistance force can be simply estimated (ignoring the contact pressure between the cutterhead plate and the soil, and forces coming from the cutters ripping the soil) by Equation 11.14:

$$F_P = \pi \cdot D_p^2 \cdot \sigma_h / 4 \tag{11.14}$$

where
D_p = outer diameter of the pipe in meters
σ_h = horizontal earth pressure in kPa

Herzog suggests an approach for estimation of frictional jacking force as presented in Equation 11.15 (Thomson 1995):

$$F_F = \pi \cdot D_p \cdot L \cdot f_2 \cdot \left(\frac{\sigma_v + \sigma_h}{2} \right) \tag{11.15}$$

where
D_p = outer diameter of the pipe in meters
L = jacking distance in meters
f_2 = coefficient of friction between pipe and ground (it varies between 0.2 and 0.3 for interaction between clays and concrete pipes; it can be taken as 0.25 for nonlubricated case)

σ_v = equivalent vertical earth pressure uniformly acting at pipe crown in kPa
σ_h = equivalent horizontal earth pressure uniformly acting at the level of tunnel axis in kPa

Vertical and horizontal earth pressures can be estimated by using Terzaghi's theoretical model developed especially for granular soils (Stein et al. 1989). The general form of the theoretical model suggested by Terzaghi (Stein et al. 1989) for estimating vertical earth pressure can be given in Equation 11.16 for dry ground conditions:

$$\sigma_v = \kappa \cdot \sum_{i=1}^{n} \gamma_i \cdot h_i + \sigma_S \tag{11.16}$$

where
κ = stress reduction factor due to silo effect
γ_i = bulk unit weight of the (i)th soil layer in kN/m^3
h_i = height (thickness) of the (i)th soil layer in meters
σ_S = uniformly acting surcharge pressures on the surface (can be estimated by using any standard or can be assumed for a region) in kN/m^2

Stress reduction factor κ can be estimated by Equation 11.17 (Stein et al. 1989):

$$\kappa = \frac{1 - e^{-2K_0 \tan(\delta)(h/b_s)}}{2K_0 \tan(\delta)(h/b_s)} \tag{11.17}$$

where
e = base of natural logarithms
K_0 = coefficient of lateral earth pressure at rest
δ = angle of wall friction (of load prism) in degrees
h = depth of cover (overburden) to pipe crown in meters
b_s = width of load prism acting on pipe in meters

Once the equivalent vertical earth pressure uniformly acting at the level of pipe crown is estimated, the equivalent horizontal earth pressure uniformly acting at the level of the tunnel axis can be estimated for dry conditions by using Equation 11.18 (Stein et al. 1989; Thomson 1995):

$$\sigma_h = K_0 \cdot \left(\sigma_v + \frac{D_p}{2} \cdot \gamma_n \right) \tag{11.18}$$

where, γ_n is bulk unit weight of the (n)th soil layer (at level of tunnel axis) in kN/m^3.

TABLE 11.7

Soil Parameters Used in Standards of Japan, Germany, and the United Kingdom

Parameter	Japan (Terzaghi)	Germany (ATVA 161)	UK (PJA)
b_s	$D_p\,(1 + 2 \cdot \tan(\pi/4 - \phi/2))$	$D_p\sqrt{3}$	$D_p \tan(3\pi/8 - \phi/4)$
δ	ϕ	$\phi/2$	ϕ
K_0	1	0.5	$(1-\sin\phi)/(1+\sin\phi)$

Source: Adapted from Pellet-Beaucour, A.L., Kastner, R., 2002. Experimental and analytical study of friction forces during microtunneling operations. *Tunnelling and Underground Space Technology,* 17:83–97.

Note: D_p, pipe (or shield) diameter (m), ϕ, (undrained) internal friction angle of soil (°).

Scientists and standards differ from each other on selection of the parameters b_s, δ, and K_0 given above. Soil parameters used by Japan, Germany, and the United Kingdom are presented in Table 11.7.

On the basis of the parameters given, the estimated stress reduction factors (Equation 11.17), vertical earth pressures (Equation 11.16), horizontal earth pressures (Equation 11.18), face resistance force (Equation 11.14), frictional force (Equation 11.15), and total jacking forces (Equation 11.13) for different standards are summarized in Table 11.8.

11.5.7 Jacking Force Estimation by Using the U.S. Army Corps of Engineers (1998) for Wet Formation

Estimate total jacking force by using the method suggested by the U.S. Army Corps of Engineers (1998) based on the parameters given below (Figure 11.6):

Excavation machine: slurry MTBM
Lubrication: nonlubricated
Overburden to tunnel crown, $h = 7$ m
Dry height of overburden, $h_i = 2$ m
Wet height of overburden to crown, $h_w = 5$ m
Microtunnel length (jacking distance), $L = 100$ m
Formation: silty sand (wet)
Bulk unit weight of silty sand, $\gamma_{soil} = 20$ kN/m^3
Internal friction angle of clay, $\phi_{soil} = 30°$
Surcharge pressure, $\sigma_S = 25$ kPa $= 25$ kN/m^2
Outer diameter of concrete jacking pipe, D_p (~ D_S, shield diameter) = 1.2 m
Friction coefficient between soil and concrete jacking pipe, $f_2 = 0.3$

TABLE 11.8

Estimated Soil Parameters and Total Jacking Forces

Parameter	Unit	Japan (Terzaghi)	Germany (ATVA 161)	UK (PJA)
b_s	m	2.59	2.08	2.08
δ	°	30.0	15.0	30.0
K_0	—	1.00	0.50	0.33
κ	—	0.31	0.66	0.56
σ_v	kPa	68	117	103
σ_h	kPa	80	65	38
F_P	kN	90	73	44
F_F	kN	6957	8568	6689
F_T	kN	7048	8641	6732
F_T	tonf	719	881	686

11.5.7.1 Solution of Numerical Example 11.5.7

If the pipeline is under the water table, the U.S. Army Corps of Engineers (1998) suggests Equation 11.19 for the estimation of vertical earth pressure:

$$\sigma_v = \sigma_S + \sum_{i=1}^{n} \gamma_i \cdot h_i + \sum_{j=1}^{k} (\gamma_j - \gamma_w) \cdot h_j + \gamma_w \cdot h_w \tag{11.19}$$

where

σ_v = vertical earth pressure under tunneled/jacked (wet) conditions in kN/m²

σ_S = surcharge pressure in kN/m²

γ = unit weight in kN/m³, indices i = soil layers over the ground water level, j = soil layers under the ground water level, w = water

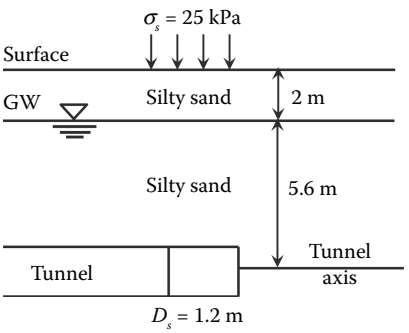

FIGURE 11.6
Geometry for Numerical Example 11.5.7.

h = soil height to crown in meters, indices i = soil layers over the ground water level, j = soil layers under the ground water level, w = height of water column over the crown

Horizontal earth pressure at the level of tunnel axis in this case is estimated by using soil weights for the appropriate moisture conditions and full hydrostatic pressure (US Army Corps of Engineers 1998), as can be estimated in Equation 11.20:

$$\sigma_h = \sigma_V + (\gamma_k - \gamma_w) \cdot D_p/2 + \gamma_w \cdot D_p/2 \tag{11.20}$$

where, σ_h is horizontal earth pressure under tunneled or jacked (wet) conditions in kN/m^2.

Vertical (at crown) and horizontal (at axis) earth pressures are estimated to be 165 and 177 kN/m^2 by using Equations 11.19 and 11.20, respectively:

$$\sigma_v = 25 + 20 \cdot 2 + (20 - 10) \cdot 5 + 10 \cdot 5 = 165 \text{ kN/m}^2$$

$$\sigma_h = 165 + (20 - 10) \cdot 1.2/2 + 10 \cdot 1.2/2 = 177 \text{ kN/m}^2$$

Equations 11.13 through 11.15 can also be applied for this problem. By using these equations, the total jacking force is estimated to be 19,540 kN (1993 tonf).

$$F_P = \pi \cdot 1.2^2 \cdot 177/4 = 200 \text{ kN}$$

$$F_F = \pi \cdot 1.2 \cdot 100 \cdot 0.3 \cdot \left(\frac{165 + 177}{2} \right) = 19340 \text{ kN}$$

$$F_T = 200 + 19340 = 19540 \text{ kN}$$

11.5.8 Jacking Force Estimation by Using the Method of Roark and Young

Estimate the total jacking force for a stable ground (hard rock or stiff cohesive soils) using the theoretical method of Roark and Young in 1976 suggested by Milligan and Norris 1996 based on the parameters given below:

Excavation machine: Any type of MTBM

Lubrication: unlubricated

Microtunnel length (jacking distance), L = 100 m

Formation: Any hard rock or stiff cohesive soil

Diameter of bore, D_1 = 1.554 m

Outer diameter of concrete pipe, D_2 = 1.530 m

Elastic modulus of soil, E_1 = 48 MPa

Elastic modulus of concrete pipe, $E_2 = 40{,}000$ MPa
Poisson's ratio of soil, $v_1 = 0.2$
Poisson's ratio of concrete pipe, $v_2 = 0.2$
Self-weight of pipe, $P_U = 17.7$ kN/m

11.5.8.1 Solution of Numerical Example 11.5.8

Milligan and Norris (1996) suggested a model using a solution for estimating contact stresses in stable bores (such as hard rock and stiff cohesive soils) obtained from the elastic solution for a solid elastic cylinder resting in a cylindrical cavity (Figure 11.7). The contact width is given as in Equation 11.21:

$$b = 1.6 \cdot (P_U \cdot k_d \cdot C_e)^{0.5} \tag{11.21}$$

where
b = contact width between the pipe and bore in meters
P_U = contact force (self-weight of the pipe) per unit length in kN/m

k_d and C_e are estimated by Equations 11.22 through 11.23:

$$k_d = \frac{D_1 \cdot D_2}{(D_1 - D_2)} \tag{11.22}$$

$$C_e = \frac{(1 - v_1^2)}{E_1} + \frac{(1 - v_2^2)}{E_2} \tag{11.23}$$

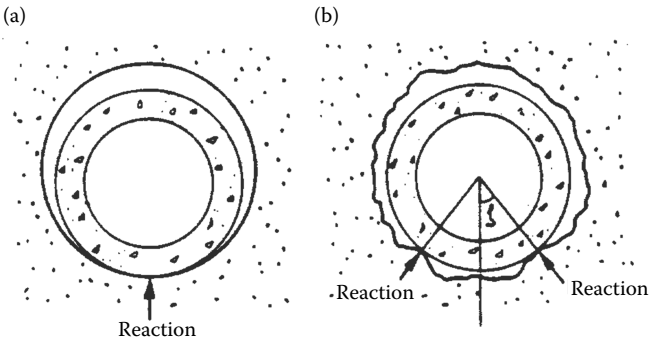

FIGURE 11.7
Case for a stable microtunnel bore. (a) Assuming perfectly circular excavation. (b) Real situation (As quoted by Milligan and Norris 1996 after O'Reilly, M.P. and Rogers, C.D. 1987. Pipe jacking forces. *Proceedings of the International Conference on Foundation and Tunnels*, eds. Forde, M.C., Edinburgh Engineering Technics Press, Vol. 2.)

where
D_1 = diameter of the bore in meters
D_2 = outer diameter of the pipe in meters
v_1 = Poisson's ratio of the soil
v_2 = Poisson's ratio of the concrete pipe
E_1 = elastic modulus of the soil in kPa
E_2 = elastic modulus of the concrete pipe in kPa

The contact normal stress distribution (p) is given by Equation 11.24:

$$p = \frac{2 \cdot P_U}{\pi \cdot (b/2)} \cdot \left(1 - \frac{x^2}{(b/2)^2}\right)^{0.5} \tag{11.24}$$

where, x is the distance to either side of the center line of the area of contact. When the given parameters are substituted into Equations 11.22 through 11.23, k_d and C_e are estimated to be 99.1 and 2×10^{-5}, respectively, as follows:

$$k_d = \frac{1.554 \cdot 1.530}{(1.554 - 1.530)} = 99.1$$

$$C_e = \frac{(1 - 0.2^2)}{48{,}000} + \frac{(1 - 0.2^2)}{40{,}000{,}000} = 2 \cdot 10^{-5}$$

The contact width b is estimated to be 0.3 m by using Equation 11.21:

$$b = 1.6 \cdot (17.7 \cdot 99.1 \cdot 2 \cdot 10^{-5})^{0.5} = 0.30 \text{ m}$$

When the value of x is taken to be zero (at the centerline of the bore, at which the stress is a maximum), the contact stress (p) acting on the pipe bottom is estimated to be 75.2 kPa/m^2 of the pipe length by using Equation 11.24:

$$p = \frac{2 \cdot 17.7}{\pi \cdot (0.3/2)} \cdot \left(1 - \frac{0^2}{(0.3/2)^2}\right)^{0.5} = 75.2 \text{ kPa/m}^2$$

Since the surface area of the contact between pipe and soil for 100 m of driving length is estimated to be 30 m^2, jacking force due to friction between pipe and the soil is estimated to be 2254 kN (230 tonf), assuming the contact stress (p) is the same along contact length (b).

In these types of problems, the face pressure force coming from cutting tools becomes very important, especially in hard rocks and large diameter microtunnelling machines. Assuming eight of the small diameter multi-row

disk cutters are used on the cutterhead of a microtunneling machine and the bearing capacity of each disk cutter being a 10 tonf, the maximum force acting on the cutterhead is estimated to be a 80 tonf. In this condition, the total jacking force is estimated to be around 310 tonf, which is the sum of 230 tonf of frictional force and 80 tonf of face resistance force. Appropriate lubrication and misalignment effects can also be added to the solution of this problem.

It should be noted here that the force capacity of disk cutters depends on their diameters and can be learned from the manufacturer. It should also be noted that operators usually apply the maximum force (sometimes more than the capacity, not suggested to protect the cutters) to the cutters. In fact, the force to be applied to the cutters should be estimated for optimum cutting geometry obtained from linear cutting tests. Also, it should be kept in mind that the force requirement of the other types of cutting tools such as blades (wedge, knife, ripper tools) and conical tools would be different from the disk cutters.

The uplift force due to the buoyancy effect of lubrication fluid should also be considered in these types of stable bores. If the pressure of the lubricant fluid is high enough, then the pipeline would float over the lubricant. In this case, the buoyant weight of the pipeline and a suitable frictional coefficient (which is usually around a low 0.05) should be simply used when estimating the frictional forces.

11.5.9 Jacking Force Estimation by Using the Method of O'Reily and Rogers

Estimate the total jacking force for a stable ground using the method suggested by O'Reily and Rogers (1987), (as quoted by Thomson 1995) based on the parameters given in Problem 11.5.8.

11.5.9.1 Solution of Numerical Example 11.5.9

O'Reily and Rogers (1987) suggested using a solution for estimating frictional force in stable bores (such as hard rock and stiff cohesive soils) The frictional force is given as in Equation 11.25 (Thomson 1995):

$$F_F = \frac{W_P \cdot \tan(\delta_P)}{\cos(\zeta)} \cdot L \tag{11.25}$$

where

F_F = frictional force in kN.

W_P = weight of the pipeline in kN/m.

δ_P = coefficient of friction between pipe and ground in degrees. When there is no experimental data, δ_P can be taken as 40° for conservative estimations.

ζ = offset of reaction from vertical. When there is no experimental data, ζ can be taken as 30° for conservative estimations.
L = microtunnel length (jacking distance).

For the given parameters, the frictional force acting on the pipeline is estimated to be 1715 kN (174 tonf) as follows:

$$F_F = \frac{17.7 \cdot \tan(40)}{\cos(30)} \cdot 100 = 1715 \text{ kN} = 174 \text{ tonf}$$

It should also be noted that the appropriate face resistance force should be considered, based on the principles of rock-cutting mechanics, when estimating total jacking force. Assuming eight of the small diameter multi-row disk cutters are used on the cutterhead of the microtunneling machine and the bearing capacity of each disk cutter being a 10 tonf, the maximum force acting on the cutterhead is estimated to be an 80 tonf. In this condition, the total jacking force is estimated to be around 254 tonf, which is the sum of 175 tonf of frictional force and 80 tonf of face resistance force. Appropriate lubrication and misalignment effects can also be added to the solution of this problem.

11.5.10 Numerical Example on Positioning of Intermediate Jacking Stations

Position the intermediate jacking stations (IJS) by using the method suggested by Coller et al. (1996), based on the parameters given below:

Excavation machine: Any full-face excavation type of MTBM
Microtunnel length (jacking distance), $L = 350$ m
Estimated maximum total jacking force, $F_T = 1500$ tonf
Maximum allowable axial force acting on pipes, $F_{\text{allowable}} = 550$ tonf
Capacity of main jacking frame, $F_{\text{capacity}} = 550$ tonf
Face resistance force, $F_P = 50$ tonf
Pipe section length, $P_{SL} = 2$ m

11.5.10.1 Solution of Numerical Example 11.5.10

The location of the first IJS (L_1) is estimated by using Equations 11.26 through 11.28 (Coller et al. 1996):

$$L_1 = \left(\frac{F_{\text{capacity}} - F_P}{F_{\text{pipe/m}}} \right) - SR_1 = 0.80 \cdot \left(\frac{F_{\text{capacity}} - F_P}{F_{\text{pipe/m}}} \right) \tag{11.26}$$

$$F_{\text{pipe/m}} = 1.15 \cdot \frac{F_T}{L} \tag{11.27}$$

$$SR_1 = 0.20 \cdot \left(\frac{F_{\text{capacity}} - F_P}{F_{\text{pipe/m}}} \right) \tag{11.28}$$

where
L_1 = the location of the first IJS in meters
F_{capacity} = capacity of main jacking frame in tonf
F_P = face resistance force in tonf
$F_{\text{pipe/m}}$ = force acting per meter of pipe in tonf/m (1.15 is safety factor)
F_T = estimated total jacking force in tonf
SR_1 = safety reduction for the first IJS in meters
L = microtunnel length (jacking distance) in meters

The location of the second IJS (L_2) is estimated by using Equations 11.29 through 11.30 (Coller et al. 1996):

$$L_2 = \left(\frac{F_{\text{capacity}}}{F_{\text{pipe/m}}} \right) - SR_2 = 0.90 \cdot \left(\frac{F_{\text{capacity}}}{F_{\text{pipe/m}}} \right) \tag{11.29}$$

$$SR_2 = 0.10 \cdot \left(\frac{F_{\text{capacity}}}{F_{\text{pipe/m}}} \right) \tag{11.30}$$

where
L_2 = the location of the second IJS in meters; this is also the location of the 3rd, 4th, and maybe the 5th IJSs if necessary
SR_2 = safety reduction for the second IJS in meters

The force acting per meter of pipe is estimated to be 4.93 tonf/m by using Equation 11.27:

$$F_{\text{pipe/m}} = 1.15 \cdot \frac{1500}{350} = 4.93 \text{ tonf/m}$$

The location of the first IJS is estimated by using Equations 11.26:

$$L_1 = 0.80 \cdot \left(\frac{550 - 50}{4.93} \right) = 81.1 \text{ m} = 80 \text{ m}$$

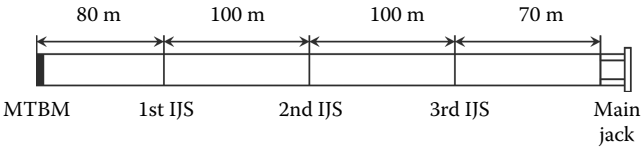

FIGURE 11.8
Positioning of the intermediate jacking stations.

Since the pipe section length is 2 m, the location of the IJS is defined by truncating the estimated L_1 to the nearest lower integer number that can be divided by the pipe section length of 2 m. Therefore, L_1 is taken to be 80 m.

The location of the second intermediate jacking station is estimated by using Equations 11.29:

$$L_2 = 0.90 \cdot \left(\frac{550}{4.93} \right) = 100.4 \text{ m} = 100 \text{ m}$$

The estimated location of the second intermediate jacking station (100 m) is also the location of the 3rd intermediate jacking station. The remaining 70 m is pushed by the main jacking frame, as seen in Figure 11.8.

The positions of the second and third IJSs can be set at 90 m intervals, reducing forces at IJS locations.

References

Atalah, A.L., Bennett, D., Iseley, T., 1994. Estimating the required jacking force. *No-Dig 1994 Conference*, April, Dallas, Paper D2.

Bennett, D., Cording, E.J., 2000. Jacking loads and ground deformations associated with microtunneling. *No-Dig 2000 Conference*, April 9–12, California, pp. 19–35.

Chapman, D.N., Ichioka, Y., 1999. Prediction of jacking forces for microtunneling operations. *Tunnelling and Underground Space Technology, Trenchless Technology Research*, 14(1):31–41.

Chung et al. 2004. Decision support system for microtunneling applications. *Journal of Construction Engineering and Management*, 130(6):835–843.

Coller, P., Staheli, K., Bennett, D., Post, R., 1996. A review of jacking forces by both theoretical and empirical methods as compared with 20 years of practical experience. *Proceedings of International No-Dig'96*, April, New Orleans, pp. 126–150.

Copur, H., 2012. *"MAD605E Microtunneling" Class Notes*. Istanbul Technical University, Mining Engineering Department.

Herrenknecht, 2012. http://www.herrenknecht.com/

ISTT, International Society for Trenchless Technology, 2012. http://www.istt.com/

Milligan, G.W.E., Norris, P., 1996. Site based research in pipe jacking-objectives, procedures and a case history. *Trenchless Technol. Res.*, 11(1):3–24.

O'Reilly, M.P. and Rogers, C.D. 1987. Pipe jacking forces. *Proceedings of the International Conference on Foundation and Tunnels*, ed. Forde, M.C., Edinburgh Engineering Technics Press, Vol. 2.

Ozdemir, L., Coss, T., 1998. *Microtunneling. Short Course*. Colorado School of Mines, Golden, CO-USA. Section: "Ancillary equipment" by T. Coss.

Ozdemir, L., Coss, T., 1998. *Microtunneling. Short Course*. Colorado School of Mines, Golden, CO-USA. Section: "Site layout and logistics" by T. Iseley.

Pellet-Beaucour, A.L., Kastner, R., 2002. Experimental and analytical study of friction forces during microtunneling operations. *Tunnelling and Underground Space Technology,* 17:83–97.

Shimada, H., Khazaei, S., Matsui, K., 2004. Small diameter excavation method using slurry pipe-jacking. *Geotechnical and Geological Engineering*, 22:161–186.

Stein, D., Mollers, K., Bielecki, R., 1989. *Microtunnelling—Installation and Renewal of Nonman-Size Supply and Sewage Lines by the Trenchless Construction Method*. Ernst & Sohn, Berlin, ISBN: 3-433-01201-6, 352 p.

Thomson, J.C., 1995. *Pipejacking and Microtunnelling*. Blackie Academic & Professional, Glasgow, ISBN: 0-7514-0102-6, 273 p.

US Army Corps of Engineers, 1998. Conduits, culverts, and pipes. *CECW-ED Engineer Manual*, No. 1110-2-2902.

12

Shaft and Raise Boring Machines

12.1 Background

The raise boring technology was developed to meet the demands of the underground mining industry, but has also found numerous applications in tunneling or infrastructural projects for ventilation purposes even in very hard rock formations or in opening deep shafts like in the Gothard Tunnel in Switzerland. Raise boring provides a safe means of excavating a shaft between two levels of a mine without the use of explosives. Raise boring machines operate on the principle of first drilling a small pilot hole and then reaming the hole, in one or more stages to the desired size.

The breakthrough of using continuous tunneling machines in the 1950s has provided a completely new method of mechanized shaft boring, which thereby eliminated the need for drilling and blasting in some cases. However, as Stack (1995) stated in his voluminous work, "The first major breakthrough in raise boring came in 1949 from a German engineer, Herr Bade. He conceived of a brilliant method of raise driving which he hoped to eliminate the necessity for the presence of workmenship within the shaft during the dangerous period of raise driving. Basically this equipment consisted of a robe winch, a borer and a control point." Developments in this area came very quickly: work on the Robbins raise boring machine was initiated in 1950 by Robert E. Cannon; testing the first Robbins machines at the International Nickel Company (INCO) Ontario division occurred during 1962–1963; the use of large-diameter Ingersoll-Rand raise boring machines were developed in INCO during 1973; in 1979, Ingersoll-Rand was taken over by the Robbins Company; in 1993, the Robbins Company was purchased by Atlas Copco thereby splitting the Robbins raise boring product line; and in 1998, it was transitioned to Atlas Copco RDE & RDT in Sweden.

In 1960, about the same time as the Cannon and Robbins Company, Hugh B. Williams Manufacturing Company produced its first raise boring machine for Mather Mine. Initially, a pilot hole of 32 cm was first drilled from the lower to the upper level and then, back-reamed downwards by a machine of 122 cm diameter. In 1963, Wirth Company of Germany

introduced an electrohydraulic raise drill, which followed the Cannon principle. It should be mentioned here that several other companies also contributed to the development of raise boring systems and applications of mechanical excavation systems for shaft boring have increased tremendously since then.

The first blind-hole or boxhole raise borer was introduced by the Calweld–Smith Company in 1967 for New Mexico uranium fields; the same company produced BH-80 machine in 1974 for gold mines in South Africa. The Robbins Company produced 51R and 52R blind-hole raise drills for mining companies in South Africa. It is reported that these machines worked successfully in hard and abrasive rock formations. Since the introduction of the first Calweld Smith machine in 1967, blind-hole raise drills improved considerably (Stack 1995).

Serious developments on large-diameter shaft drills were carried out in Germany by TURMAG in 1954 and further developed by Wirth Company after 1971 with successful applications in coal mines.

Raise boring was also used in coal mines in Europe to diameters up to 8 m (Bruemmer and Wollers 1976; Grieves 1981; Muirhead 1982).

Herrenknecht AG has developed a vertical shaft-sinking machine (VSM), which can excavate in medium soft rock, in soil, or even in water-bearing soils. The ground is excavated by a roadheader boom. The muck is removed by a slurry system or a pneumatic system in combination with hoisting of skips. These machines have been applied successfully on shafts down to 100 m. For deep hard rock shafts, a new shaft boring system (SBS) has also been developed by Herrenknecht AG in collaboration with Rio Tinto. The SBS is a development for the mechanized excavation of deep vertical blind shafts in hard rock conditions. The semi-full-face sequential excavation process is based on the use of a rotating cutting wheel excavating the full shaft diameter in a two-stage process for one complete stroke (Frenzel et al. 2010a,b).

12.2 Classification and Working Principles

A raise boring machine (Figure 12.1) is set on the upper level to drill a pilot hole, through to the level below. The diameter of this hole is typically 230–350 mm, large enough to accommodate the drillstring. Once the drill has broken through, the pilot bit is removed and is replaced by a reamer head (Figure 12.2) and the drill cuttings from the reamer head fall to the bottom of the shaft.

Excavating shafts with mechanical excavation technologies may be divided into four types as explained below and given in Figures 12.3 and 12.4.

FIGURE 12.1
A raise boring machine. (Courtesy of Atlas Copco.)

FIGURE 12.2
A reaming head. (Courtesy of Atlas Copco.)

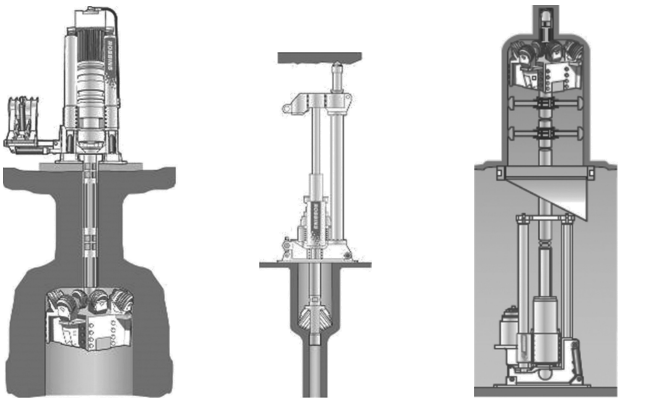

FIGURE 12.3
Conventional raise boring, down reaming, and boxhole boring. (Courtesy of Atlas Copco.)

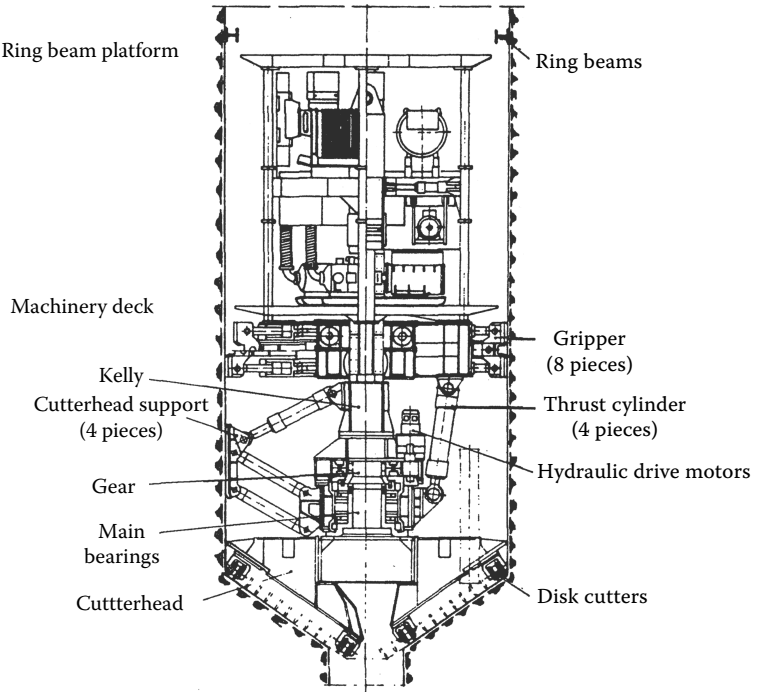

FIGURE 12.4
A V mole or vertical shaft boring system. (After Raine, A.G., 1984. *Large Diameter Mine Shaft Construction, Stabilitiy in Underground Mining* 2. SME-AIME, New York, pp. 97–109.)

12.2.1 Raise Boring

In this system, the pilot hole is drilled down to a lower level; once the pilot drilling operation is finished, the drill bit is removed and a reamer or raise head is attached to the drill rod. The broken rock falls to the lower level by gravity. This system operates with the drill string in tension.

12.2.2 Down Reaming

In this system, the pilot hole is drilled downwards until it connects to a lower access level. The drill string is retrieved and then a reamer is pushed downwards. This method uses drill string in compression and usually stabilizers must be installed to eliminate the potential of the drill string buckling.

The decision whether to drill raises from the top or bottom usually depends on the access point in a mine.

12.2.3 Boxhole

The boxhole borer is a variant of a raise borer that is used when there is not enough space on the higher of the two levels to be connected. A pilot hole is drilled to an upper level up from the raise borer. Once the pilot hole drilling is accomplished, the drill string is retrieved, and a reamer attached and pushed upwards. The broken rock falls down onto a special collection chute attached to the top of the raise borer. Precautions have to be taken to redirect falling drill cuttings away from the machine, and to reinforce the drill string.

12.2.4 Drilling Blind Shafts with V Moles

A typical large-diameter shaft drill is seen in Figure 12.4. The V mole is a horizontal TBM modified for shaft boring. Wirth is pioneering in this field and machines developed by this company may excavate shafts up to 7 m diameter. The gripper assembly serves to resist to the thrust and torque required for rock boring. Hydraulic pressure of thrust cylinders is controlled by the operator to provide the required penetration rate. Rotary motion is transmitted from grippers to a cutterhead trough, a Kelly. Shaft lining is realized using a working platform located above a gripper assembly. Muck is removed to a pilot hole by scrapers located on the cutterhead. In shaft reaming machine (SB) the excavated muck falls through the pilot hole to a lower level. The pilot hole of 1–2 m diameter can be excavated with the raise boring machine. If a pilot hole is not possible, a blind-shaft boring machine (VSB) needs to be used, where the excavated material is transported through the shaft to the surface.

In 2009, Wirth became a fully controlled subsidiary of Aker Solutions, a Norwegian-owned company. Wirth Maschinen und Bohrgeräte-Fabrik GmbH changed its name to Aker Wirth GmbH, reflecting the change of ownership.

12.3 Advantages and Disadvantages of Raise Boring

The main advantages may be cited as follows:

Workers are not needed to access the raise while it is under construction and using explosives is eliminated.

Continuous operation provides a faster advance rate than other methods.

Less total manpower, less rock to handle, and less construction time provide less cost.

Raise boring creates a shaft with smooth walls, which usually does not require lining. The hole is more stable than a drilled and blasted raise and has better air flow, making it ideal for ventilation raises.

The main disadvantages may be cited as follows:

Raise boring is a convenient method in competent rock; however, several problems are faced in geological formations where geological discontinuities are dominant. In such cases, shaft boring time extends to several months for supporting shaft walls. In strong rocks without geological discontinuities, usually no support is required; otherwise, shotcrete rock fractures, bolts, wire mesh, or steel lining may be needed.

Capital cost is high, and in most cases, companies specializing in shaft boring see a preference for the short length of shafts.

Assembly and disassembly time may be long in some cases.

12.4 Design and Technical Features

There are two main systems of powering raise boring machines: electric drive through gear reducers, or hydraulic drive with primary power from electric motors. If electric drive is used, electric motors of 0–125 HP are directly geared to the cutterhead main bearing.

One should be careful in selecting cutters in raise boring, since cutter cost may be one of the major components in raise boring operational costs. Disk cutters and strawberry cutters with tungsten carbide bits are the main cutting tools. As will be explained in the numerical examples given in this chapter, disk cutters provide higher boring rates. However, strawberry cutters are preferred in most cases since they have a much longer life, although their penetration is comparatively low, giving small chips and smooth shaft walls.

The machine is composed of a rigid plate with drilling assembly, hydraulic, and electrical equipment. The pilot hole is drilled with stabilizers to ensure directional accuracy of the pilot hole.

Starting the shaft (collaring) is a critical operation and may damage the cutterhead due to an uneven surface. The operator should pay special attention for collaring, and slow rotational speed and low reaming forces are necessary at the beginning.

There is a variety of machines available in the market designed for different geological formations. Typical characteristics of the machines are drill pipe diameter, reaming torque, reaming thrust, and type of drive (electrical or hydraulic). The characteristics of some rise boring machines are given in Tables 12.1 through 12.5.

TABLE 12.1

Characteristics of Some Robbins–Atlas Copco Raise Boring Machines

	Diameter		Depth				
Robbins Model	**Nominal (m)**	**Range (m)**	**Nominal (m)**	**Maximum (m)**	**Thrust (kN)**	**Torque (kN m)**	**Installed Power Drive + Thrust (kW)**
34RH-Low	1.2	0.6–1.5	340	610	1285	64	110–160
34RH-Std	1.2	0.6–1.5	340	610	1285	64	110–160
34RH-Wide	1.2	0.6–1.5	340	610	1285	64	110–160
44RH	1.5	1.0–1.8	250	610	2000	75	150
53RH	1.8	1.2–2.4	490	650	3550	156	225
53RH-EX	1.8	1.2–2.4	490	650	3550	156	225
73RAC	2.1	1.8–2.4	550	700	4159	173	215
73RH	2.4	1.8–3.1	550	700	4159	225	305
73RVF	2.4	1.8–3.1	550	700	4159	225	305
83RH	4.0	2.4–4.5	500	1000	6124	407	445
97RL-DC	4.0	2.4–5.0	600	1000	6845	447	375
91RH	4.0	2.4–5.0	600	1000	6700	450	500
123RH	4.0	3.1–5.0	920	1100	8923	450	500
123RVF	5.0	3.1–6.0	920	1100	8923	540	525
191RH	5.0	4.5–6.0	1000	1400	11,600	814	750

TABLE 12.2

Characteristics of Some Aker Wirth Raise Boring Machines

	HG 100	**HG 160-2**	**HG 250-2**	**HG 330-SP**	**HG 380-SP**
Power (kW)	112	160	250	400	550
Torque (kNm)	31.2	70.0	167	540	710
Thrust (kN)	1079	2000	2700	8350	12,000
Diameter up to (m)	1.4	2.4	3.0	6.0	7.0
Raises up to (m)	150	250	300	1000	1300

TABLE 12.3

Characteristics of Some Aker Wirth Large-Diameter Shaft Reaming (SB) and Blind-Shaft Boring Machines (VSB)

	SB VI	SB VII	VSB VI	VSB VII
Installed power (kW)	492	740	600	1050
Operating torque (kNm)	745	1140–1508	860–1075	1920–2290
Advance power raising (kN)	5400	8500	6360	10,550
Diameter (m)	5.0–6.5	6.5–8.5	5.8–7.5	8.0–9.5

TABLE 12.4

Some Examples of Sandvik Reaming Heads

Type	Diameter (mm)	Number of Cutters	Weight (kg)
CRH 3	1060	4	2700
CRH 4	1420	6	3400
CRH 6	1829	10	5100
CRH 8	2440	14	6850
CRH 10D	3094	16	11,050
CRH 10SE	3696	20	15,325
CRH 12E	4500	24	28,000
CRH 12E	5100	26	30,550
CRH 12E	5875	32	38,450

TABLE 12.5

Characteristics of Some Terratek Raise Boring Machines

		TDR600	TDR2000	DR3000	TDR6000
Maximum diameter (mm)	Raise boring	1500	2400	3000	6000
Maximum diameter (mm)	Down reaming	720	1800	–	–
Power (kW)		97.5	242	352	704
Torque (kNm)	Pilot hole drilling	8.6	31	78	135
Torque (kNm)	Reaming	43.4	175	237	675
rpm	Pilot hole drilling	0–120	0–60	0–42	0–42
rpm	Reaming	0–23	0–14	0–10	0–8
Thrust (kN)	Down reaming	550	1647	1600	1600
Thrust (kN)	Up reaming	985	3100	4500	13,300
Derrick weight (kg)		9300	19,350	17,200	29,000

12.5 Performance Predictions of Raise Boring Machines

Performance predictions of raise boring machines in different geological formations are explained using numerical examples given in Section 12.6. Table 12.6 gives some data obtained from raise boring projects in different rocks.

TABLE 12.6

Some Data from Raise Boring Projects

Project, Year	Type of Shaft	Construction Months	Length (m)	Inclination Degree	Pilot Hole Deviation (m)	Diameter (m)	Rock MPa
Kiruna Mine, Sweden, 1976	Ore pass	2.5	242	90	0.4	1.83	Syenite 350
Ravliden Mine, Sweden, 1977	Ore pass	1.5	136	54	0.4	2.14	Quarzite 150–200
Plandertunnel, Austria, 1977	Pilot shaft	1	310	90	2.0	1.52	Marl Limestone 50–80
Seelisburg Tunnel, Switzerland, 1978	Ventilation	1	178	90	0.8	2.14	Marl Limestone 50–80
Edelo Pover Station, Italy, 1978	Shaft	1.5	148	45	0.4	2.14	Granite 200–250
Edelo Power Station, Italy, 1978	Shaft	1.5	210	48	0.55	2.14	Micashist 75–200
Pampur Power Station, Guatemala, 1979	Shaft	2	215	90	–	2.44	Limestone 100–200
Fortuna Power Station, Panama, 1980	Shaft	4	425	90	1.4	1.83	Andesite 100–200
Fortuna Power Station, Panama, 1982[a]	Penstock	15	405	57	–	2.14	Tufite and Andesite

Source: Swanska brochure, Product code no. 89.

[a] The raise was immediately supported behind the reamer with steel ribs due to unfavorable rock conditions. This was realized with Alimak lift.

12.6 Numerical Examples

12.6.1 Numerical Example 1: Application of (V)-Type Disk Cutters

With a raise boring machine (Robbins 73 RH), a shaft of 200 m in length and a diameter of 2.4 m will be opened between –100/–300 levels of a mine. The rock formation is limestone having compressive strength of 80 MPa with high RQD values. A disk cutter of (V) type having a 30-cm disk diameter with an edge angle of 90° and a bearing capacity of 180 kN is selected since the rock is medium strength and nonabrasive. It is considered that maximum thrust force

applied to one disk will be in the order of 75% of the bearing capacity, that is, 135 kN. Mine management decided to work with two shifts being 8 h each shift. The characteristics of the machine are given below. Calculate theoretical net advance rate, number of days to complete the shaft, and torque and power of the machine, and discuss whether calculated values are within the limits of the installed values. Machine utilization time of raise boring machine is expected to be 50%. The characteristics of the machine are given below:

Rotational speed at reaming: 0–16 rpm
Rotational speed at pilot hole drilling: 0–50 rpm
Maximum running torque: 225 kN m at 7.5 rpm
Reaming thrust: 4159 kN
Raise diameter: 2.4 m
Nominal raise length: 550 m
Installed power: 305 kW
Derrick weight: 11,500 kg
Cutterhead weight: 8000 kg
Drill pipe weight: 290 kg/m

12.6.1.1 Solution

1. Penetration for one revolution of the cutterhead or for one revolution of the disk cutter is calculated using Equation 4.9 given in Chapter 4:

$$F_N = 4 \cdot \sigma_c \cdot \tan\frac{\varphi}{2}\sqrt{Dp^3 - p^4} \tag{4.9}$$

   In this equation, $F_N = 13{,}500$ kgf (75% of the bearing capacity of one disk cutter), $\sigma_c = 800$ kgf/cm^2, φ is the disk edge angle as 90°, and D is the disk diameter as 30 cm.

   Penetration (p) is calculated as approximately 0.85 cm/rev, or 0.9 cm/rev.

2. Theoretical net advance rate is calculated as explained below.

   Mean rotational speed is taken as 7 rpm, and net advance rate per hour is calculated as

$$\begin{aligned}\text{Net advance rate} &= \text{penetration (cm/rev)} \cdot \text{rotational speed (rev/h)} \\ &= 0.9 \cdot 7 \cdot 60 \text{ cm/h} \\ &= 3.78 \text{ m/h}\end{aligned} \tag{12.1}$$

   Theoretical mean advance rate per day is calculated as 3.78 (m/h) · 16 (h/day) · 0.5 (machine utilization time) or 30.2 m/day.

Number of days taken for reaming is 200 m (length of the shaft)/33.6 m per day = 6.6 days.

However the following items should be taken into account to calculate the time to finish the shaft:

Transportation and preparation of the machine = 4 days

Drilling of pilot hole = 7 days

Fixing the reaming head = 1 day

Delays for different reasons = 2 days

Dismantling of the machine = 2 days

Total time to finish the shaft = 23 days

3. Checking the trust of the raise boring machine.

   Number of disk cutters in the cutterhead may be calculated as dividing reamer head radius by the cutter spacing. Cutter spacing is usually 8.5 cm and number of disk cutters is calculated as (240/2)/8.5 or 14 cutters.

$$\begin{aligned}\text{Reaming thrust} = {} & \text{Total thrust force of the disk cutters for a} \\ & \text{predetermined penetration} \\ & + \text{the maximum weight of drill string} \\ & + \text{the weight of reaming cutterhead}\end{aligned}$$

$$\text{Reaming thrust} = 14 \cdot 13{,}500 \text{ kgf} + 290(\text{kgf/m}) \cdot 200 \text{ m} + 8000 \text{ kgf}$$

$$\text{Reaming thrust} = 255{,}000 \text{ kgf}$$

   Calculated reaming thrust of 2550 kN; this value is lower than then installed reaming thrust, so the machine is not thrust limited.

4. Checking the torque and power of the raise borer.

   Torque of the raise borer will be calculated using the following equation given by Home (1978) as

$$\text{Torque} = 0.66 \cdot r \cdot \text{number of cutters} \cdot f \cdot \text{disk thrust force} \qquad (12.2)$$

   where r is the radius of the reamer head and f is the ratio of rolling force to thrust force. For disk cutters, $f = 0.15$, and for button or strawberry cutters, $f = 0.08$.

$$\text{Theoretical torque of the machine} = 0.66 \cdot 1.2 \text{ m} \cdot 14 \cdot 0.15 \cdot 135 \text{ kN}$$

$$\text{Theoretical torque of the machine} = 224.5 \text{ kN} \cdot \text{m}$$

   The calculated torque is smaller than installed torque value, so the machine is not torque limited.

5. Checking the power of the raise borer.

   The power of the machine may be calculated using the equation given below:

$$\text{Power} = 2 \cdot \pi \cdot N \cdot T/\eta \tag{12.3}$$

   where N is the rotational speed of the machine, T is the torque of the machine, and η is the efficiency.

$$\text{Power} = 2 \cdot \pi \cdot (7/60) \cdot 224.5/0.7$$

$$\text{Power} = 235.1 \text{ kW}$$

   The calculated power value is less than the installed value, so the machine is not power limited.

12.6.2 Numerical Example 2: Application of (CSS) Disk Cutters

Solve the above problem if the rock is abrasive and has a compressive strength of 120 MPa and a tensile strength of 8 MPa.

Constant cross-section disk cutters (CCS) should be used in hard and abrasive rock formations. 432 mm CCS disk cutters with 15.9 mm of tool width having bearing capacity of 220 kN will be used. It is considered that maximum thrust force applied to the disk cutter will be in the order of 75% of the bearing capacity, that is, 165 kN.

1. For CCS disk cutters, penetration for one revolution of the cutterhead or for one revolution of the disk cutter is calculated using Equation 4.18 given in Chapter 4.

   Penetration (p) is calculated as approximately 0.7 cm/rev.

2. The theoretical net advance rate is calculated as explained below. Mean rotational speed is taken as 7 rpm, and net advance rate per hour is calculated as

$$\text{Net advance rate} = \text{penetration (cm/rev)} \cdot \text{penetration (rev/h)}$$

$$= 0.7 \cdot 7 \cdot 60 \text{ cm/h}$$

$$= 2.94 \text{ m/h}$$

   Theoretical mean advance rate per day is 2.94 (m/h) · 16 (h/day) · 0.5 (machine utilization time) or 23.5 m/day.

   Number of days taken for reaming is 200 m (length of the shaft)/23.5 m per day = 8.5 days.

   However, 16 days are necessary for auxiliary items as explained in numerical example 1, so 25 days are necessary to complete the job.

3. Check the thrust of the raise boring machine.

   The number of disk cutters in the cutterhead may be calculated by dividing the reamer head radius by the cutter spacing. Cutter spacing is usually 8.5 cm and the number of disk cutters is calculated as (240/2)/8.5 or 14 cutters.

   $$\begin{aligned}\text{Reaming thrust} &= \text{total thrust force of the disk cutters for a predetermined penetration} \\ &\quad + \text{the maximum weight of drill string} \\ &\quad + \text{the weight of reaming cutterhead} \\ \text{Reaming thrust} &= 14 \cdot 16{,}500 \text{ kgf} + 290(\text{kgf/m}) \cdot \text{m} + 8000 \text{ kgf} \\ \text{Reaming thrust} &= 297{,}000 \text{ kgf}\end{aligned}$$

   The calculated reaming thrust of 2970 kN is lower than the installed reaming thrust, so the machine is not thrust limited.

4. Check the torque and power of the raise borer.

   The torque of the raise borer will be calculated using the following equation given by Homes as:

   $$\text{Torque} = 0.66 \cdot r \cdot \text{number of cutters} \cdot f \cdot \text{disk thrust force}$$

   $$\text{Theoretical torque of the machine} = 0.66 \cdot 1.2 \text{ m} \cdot 14 \cdot 0.15 \cdot 165 \text{ kN}$$

   $$\text{Theoretical torque of the machine} = 274.4 \text{ kN} \cdot \text{m}$$

   The calculated torque is greater than the installed torque value, so the machine is torque limited and should be worked with less penetration, that is, 0.6 cm/rev.

12.6.3 Numerical Example 3: Application of Tungsten Carbide Bit Cutters

Solve the above problem if the rock is very abrasive and has a compressive strength of 250 MPa.

For a diameter of 2.4 m, the number of cutter found is 14 from Table 12.4. It is estimated that there are 80 button bits in one cutter and 9% of the cutter in contact at the same time. Machine utilization time is 50%.

Strawberry cutters with tungsten carbide buttons, as seen in Figure 12.5, are mainly used in hard and abrasive rocks, since they do not require frequent replacements. These types of cutters may also be preferred in other types of rocks as a smooth cutting face is obtained, eliminating unnecessary lining operations of the shaft.

Penetration index obtained from indentation tests should be used for strawberry cutters to estimate the raise boring performance (Bilgin 1989).

FIGURE 12.5
Cutter preferred to use in hard and abrasive rocks.

Penetration index (α) is obtained by pushing one bit upon a rock sample under a hydraulic press in the laboratory and it is the slope of load penetration versus load curve or F/d, F being the applied load and d the penetration. Penetration index is mainly dependent on rock properties and the geometry of the indenter bit. The values given in Table 12.7 are for an indenter having a tip radius of 3 mm.

12.6.3.1 Solution

1. Estimating daily advance rate

   Total number of effective bits (N) that are in contact with the rock is calculated as

$$N = N' \cdot 0.09 \tag{12.4}$$

   where N' is the total number of carbide inserts.

$$N = 80 \cdot 14 \cdot 0.09 \quad (N \text{ is calculated for 14 cutters})$$

$$N = 100$$

TABLE 12.7
Penetration Index Values for Different Rock Types

Rock Compressive Strength (MPa)	Penetration Index (kgf/mm) if Grain Size Is Less than 3 mm	Penetration Index (kgf/mm) if Grain Size Is Greater than 3 mm
30–80	1500–2000	1500–2000
80–150	2000–3000	2000–2500
150–250	3000–4000	25000–3500

Total thrust force (T) for 1 mm of penetration is calculated as

$$T = N \cdot F/d$$

$$T = 100 \cdot 3000 \text{ kgf/mm or } 300{,}000 \text{ kgf/mm}$$

$$T = 3000 \text{ kN/mm}$$

Penetration per revolution is calculated as

$$T_{max} = T \cdot p \tag{12.5}$$

where T_{max} is the maximum thrust or reaming thrust of the raise borer (4159 kN) and p is the penetration for one revolution of the cutterhead.

$$p = 4159/3000 \text{ or } 1.4 \text{ mm}$$

Daily advance rate (AR) is calculated as

AR = penetration · rpm · daily working hours · machine utilization

$AR = 1.4 \cdot 7 \cdot 60 \cdot 16 \cdot 0.5$

$AR = 4704$ mm/h or 4.7 m/h

2. Calculate the torque of the machine

   Torque is calculated from the equation given by Home (1978) as explained above.

   Torque = 0.66 · r · number of cutters · f · disk thrust force

   Torque = 0.66 · 1.2 m · 14 · 0.08 · 220 kN or 195.2 kN · m

   Torque = 195.2 kN · m

   The machine is not torque limited.

12.6.4 Critical Remarks to the Results of the Numerical Examples

The above numerical examples are only to explain the methodology in estimating the performance of raise boring machines. The penetration index for tungsten carbide inserts given in Table 12.7 are only for rocks having compressive strength up to 250 MPa. However, as noted by Oosthuizen (2004), in Kloof Gold Mine, South Africa, the lava formation has a compressive strength ranging between 600 and 750 MPa. In such cases, laboratory indentation tests are necessary to be carried out for more accurate performance prediction.

Penetration rates of cutters equipped with tungsten carbide inserts (strawberry cutters) are always less than disk cutters. However the size of the chips obtained with these types of cutters are less than the others, producing smoother shaft walls and making them the inevitable choice for most types of rock formations, when an advance rate is not more important than wall smoothness.

Rock formations have several geological discontinuities that can be considered risk factors, prolonging the termination of the shaft boring process (Visser 2009). In such cases, a detailed geotechnical evaluation or "raise bore rock quality assessment" based on the McCracken and Stacey method is recommended in the case of deep and/or large-diameter shafts (Peck and Lee 2008).

References

Aker Wirth product catalogues.

Atlas Copco–Robbins product catalogues.

Bilgin, N., 1989. *Applied Rock Cutting Mechanics for Civil and Mining Engineers*. Birsen Publishing Company, Istanbul, ISBN 975-511-010-0, p. 192.

Bruemmer, K.H., Wollers, K., 1976. Experience with shaft boring and new developments in German Coal Mines. *Rapid Excavation and Tunnelling Conference*, Nevada, pp. 126–147.

Frenzel, C., Burger, W., Delabbio, F., 2010a. Shaft boring systems for mechanical excavation of deep shafts. *Newsletter Australian Center for Geomechanics*, 34, 1–4.

Frenzel, C., Delabbio, F., Burger, W., 2010b. Shaft boring systems for mechanical excavation of deep shafts. *Proceedings of the Second International Symposium on Block and Sublevel Caving*, ed. Potvin, Y. Australian Centre for Geomechanics, Perth, Australia.

Grieves, M., 1981. Shaft sinking today, a boring business tomorrow. *Mining Engineer*, December:1705–1709.

Home, L.W., 1978. Limiting factors on economical use of a raise drill, *Proceeding of the 3rd Australian Tunnelling Conference*, Sydney, pp. 90–98.

McCracken, A., Stacey, T.R., 1989. Geotechnical risk assessment of large diameter raisebored shafts. *Trans. Instn. Min. Metall.* (September–December), pp. A145–A150.

Muirhead, I.R., 1982. Mechanized excavation in mining, a challenge for tomorrow. *14th Canadian Rock Mechanics Symposium*. The Canadian Institute for Mining and Metallurgy, Vancouver, pp. 68–75.

Oosthuizen, M., 2004. Large diameter vertical raise drilling and shaft boring techniques as an alternative to conventional shaft sinking techniques. *SANIRE 2004—The Miner's Guide through the Earth's Crust*, South African National Institute of Rock Engineering, pp 149–162.

Peck, W.A., Lee, M.F., 2008. Application of the Q-System to Australian Underground Mines. *Proceedings of the International Workshop on Rock Mass Classification in Underground Mines, U.S Department of Health and Human Services CDC/NIOSH Office of Mine Safety and Health Services*, Pittsburg, USA, pp 129–140.

Raine, A.G., 1984. *Large Diameter Mine Shaft Construction, Stabilitiy in Underground Mining 2*. SME-AIME, New York, pp. 97–109.

Sandvik product catalogues.

Stack, B., 1995. *Encyclopaedia of Tunnelling, Mining and Drilling Equipment*, Hobart, Tasmania, Muden Pub. Co. 3 Volumes. ISBN 0 9587711 1 1.

Swanska Catalogue Product Code No. 89.

Terratek product catalogues.

Visser, D., 2009. Shaft sinking methods based on the towlands ore replacement project-rise boring. *The Southern African Institute of Mining and Metallurgy Shaft Sinking and Mining Contractors Conference*, Capetown, p. 13.

This page intentionally left blank

13

Large-Diameter Drill Rigs

13.1 Large-Diameter Drill Rigs for Pile Construction in Civil Engineering

13.1.1 Background and Technical Features

Pile constructing in civil engineering has been in use for many years as a technology for the foundation of buildings, bridges, and other structures. Rotary boring techniques offer larger-diameter piles than other piling methods, and permits pile construction in hard rocks. This chapter is intended to explain to the readers the basic working principles of large-diameter drill rigs for pile construction, particularly in hard rocks. This chapter will also give a numerical example concerning the application of the basic principles or rock-cutting mechanics for the design of the drill rigs and estimation of drilling performance. A typical large-diameter drill rig used in Istanbul is shown in Figures 13.1 and 13.2. Technical features of some available machines constructed by different manufacturers are given in Table 13.1.

13.1.2 Working Principles and Operations: A Typical Example in Istanbul

Conical cutters or chisel cutters are widely used in large-section drill rigs. This section is intended to show the validity of the cutter force predictor equations given in Table 4.4 in Chapter 4. It will also show the performance prediction and design of large-section drilling drums as shown in Figures 13.3 through 13.5. The equations given below were developed by Bilgin et al. (2006) based on cutting of 24 different rock samples in the laboratory with conical cutters. The predictor Equations 13.1 through 13.3 for normal force *FN* and cutting force *FC* are given below. In these equations, *FC* and *FN* values are in kgf, depth of cut d in cm, and σ_c in kgf/cm^2. The rotary drill rig, Bauer BG 36 shown in Figure 13.1, is used in one construction site in Istanbul with three different drilling drums (Figures 13.3 through 13.5) related to the strength of geologic formation consisting of Fresh Diorite, Weathered Diorite, and Flysch or Greywacke, each having compressive strength values

FIGURE 13.1
Rotary drill rig, Bauer BG 36 used in Istanbul in one construction site. (Adapted from the archive of Bilgin, N., 2006. A large-diameter drill rig study in Cifteler construction site in Istanbul. Istanbul Technical University, p. 30.)

FIGURE 13.2
Cutting debris and dust generation when pulling out the drilling drum. (Adapted from the archive of Bilgin, N., 2006. A large-diameter drill rig study in Cifteler construction site in Istanbul. Istanbul Technical University, p. 30.)

TABLE 13.1

Technical Features of Some Available Large-Diameter Drill Rigs, Lower and Upper Values

Drill Rig Characteristics	Bauer BG-12–48	Wirth PBA 408–1245	Liebherr 125–255	Yutong YTR160–260
Drill diameter (m)	1.2–3.0	1.3–4.0	—	Up to 1.5–2.0
Operating weight (ton)	40–250	64–300	46–80	52–80
Rotational speed (rpm)	—	44–22	—	—
Maximum thrust force (kN)	—	400–550	200–450	—
Maximum pull back (kN)	—	600–2450	200–450	—
Torque (kN · m)	125–482	81–403	120–300	160–260
Engine power (kW)	153–570	150–364	450–670	125–261

of 124, 73.5, and 40.7 MPa, respectively. The characteristics of the drill rig are given in Table 13.2. Drilling depth, drilling time, peak torque, and thrust values of the drill rig were measured using a data acquisition system and the results are plotted in Figure 13.6. The aim of the numerical example is to show how thrust and torque values of a large-diameter drill rig may be calculated using the predictor equations given below.

Mean normal force for relieved cutting:

$$\frac{FN}{d} = 0.752\,\sigma_c^{1.051} \tag{13.1}$$

FIGURE 13.3
Drilling drum type A used in Bauer BG36. (Adapted from the archive of Bilgin, N., 2006. A large-diameter drill rig study in Cifteler construction site in Istanbul. Istanbul Technical University, p. 30.)

FIGURE 13.4
Drilling drum type B used in Bauer BG36. (Adapted from the archive of Bilgin, N., 2006. A large-diameter drill rig study in Cifteler construction site in Istanbul. Istanbul Technical University, p. 30.)

Mean normal force for unrelieved cutting:

$$\frac{FN}{d} = 1.217\sigma_c^{1.014} \tag{13.2}$$

Mean cutting force for unrelieved cutting:

$$\frac{FC}{d} = 0.826 \cdot \sigma_c + 21.76 \tag{13.3}$$

FIGURE 13.5
Drilling drum type C used in B36. (Adapted from the archive of Bilgin, N., 2006. A large-diameter drill rig study in Cifteler construction site in Istanbul. Istanbul Technical University, p. 30.)

TABLE 13.2

Characteristics of Rotary Drill Rig, Bauer BG 36

Overall height (m)	24.2
Torque (kNm) first gear	367
Torque (kNm) second gear	117
Rotational speed maximum first gear (rpm)	23
Rotational speed maximum second gear (rpm)	48
Power unit (kW)	365
Maximum drilling depth (m)	60.5
Operating weight (ton)	115

13.1.3 A Numerical Example of the Large-Section Drills Equipped with Conical Cutters

After calculation of the cutting rate when cutting fresh diorite, the mean drilling rate was found to be 8/5 m/h. This value was found by dividing drilling depth between points *d*1 and *d*2 in Figure 13.6 by drilling time. Thrust and torque values given in Figure 13.6 are for peak values.

During site investigation, it was observed that half of the mean drilling time was used to get out the debris and for cleaning the drill hole, so it was estimated that the net cutting drilling rate is double that of the mean drilling rate, that is, = 2.8/5 m/h; 2.8/5×60 m/min and the net drilling rate was found as 5.3 cm/min.

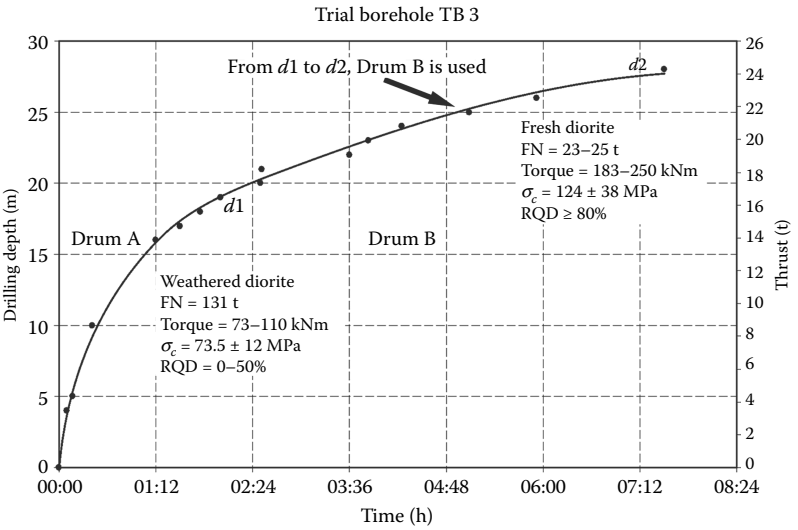

FIGURE 13.6
The relationships between drilling depth and drilling time for trial borehole TB3. (Adapted from the archive of Bilgin, N., 2006. A large-diameter drill rig study in Cifteler construction site in Istanbul. Istanbul Technical University, p. 30.)

When drilling diorite, a rotational speed was observed to be 10 rpm. The cutting depth for one revolution of the drilling drum is 5.3/10 cm. The drilling or cutting depth for one revolution of the drilling drum is 5.3 mm, for a thrust force of 24 t and torque of 200 kNm. These are peak values recorded during field measurements.

For trial borehole TB3, cutting depth of 0.5 cm is calculated as shown above.

Problem: Calculate the thrust force of the drill rig and torque of the drum equipped with 19 conical cutters, using the empirical equation given above. Discuss the applicability of force predictor equations in relieved and unrelieved cutting mode for design and the performance prediction of large-diameter grill rigs.

13.1.3.1 Solution

For relieved cutting, calculate the drill rig thrust

$$\frac{FN}{d} = 0.752\,\sigma_c^{1.051} \quad \text{as given in Equation 13.1}$$

for $d = 0.5$ cm and $\sigma_C = 1240$ kgf/cm^2

$$FN = 0.5 \cdot 0.752 \cdot 1240^{1.051}$$

$$FN = 0.5 \cdot 0.752 \cdot 1783 \text{ kgf} \quad \text{or} \quad 670.4 \text{ kgf}$$

$$\sum_{i=1}^{i=19} FN = 19 \cdot 670.4 \text{ kgf} \quad \text{or} \quad 12,738 \text{ kgf}$$

F'N is peak normal force and is assumed to be double the mean force.

$$\sum_{i=1}^{i=19} F'N = 2 \cdot 19 \cdot 670.4 \text{ kgf} \quad \text{or} \quad 25,476 \text{ kgf}$$

For unrelieved cutting, calculate drill rig thrust

$$\frac{FN}{d} = 1.217\sigma_c^{1.014}$$

for $d = 0.5$ cm and $\sigma_c = 1240$ kgf/cm^2

$$FN = 0.5 \cdot 1.217 \cdot 1370 \text{ kgf}$$

$$FN = 833 \text{ kgf (for one conical cutter)}$$

for 19 conical cutters

$$\sum_{i=1}^{i=19} FN = 19 \cdot 833 \quad \text{or} \quad 15,840 \text{ kgf}$$

Peak forces are always double the mean forces

$$\sum_{i=1}^{i=19} F'N = 2 \cdot 19 \cdot 833 \quad \text{or} \quad 31,650 \text{ kgf}$$

If predicted mean and peak thrust forces are compared based on Figure 13.6, it may be concluded that the conical cutters work in relieved cutting mode during field studies, since the measured values are close to the calculated values corresponding to the relieved mode. This is important since in relieved mode, specific energy is usually less than unrelieved mode.

Calculate the torque.

For drill drum (B), the torque is the sum of these values.

T_1 = torque for the 11 conical cutters from the center to the periphery of the drum

T_2 = torque for the 8 conical cutters around the periphery of the drum

T_3 = torque for the weight of the drum and the accessories

$$\frac{FC}{d} = 0.826 \cdot \sigma_c + 21.76 \quad \text{as given in Equation 13.3}$$

$$FC = 0.5 \cdot (0.826 \cdot 1240 + 21.76)$$

$$FC = 523 \text{ kgf}$$

$$F'C = 2 \cdot 523 \text{ kgf} \quad \text{or} \quad 1046 \text{ kgf}$$

$$T_1 = \frac{11 \cdot 1046 \cdot 0.5 \text{ (drum radius)} \cdot 1.35 \text{ (friction)}}{2 \cdot 0.7 \text{ (efficiency)}} \text{kgf} \cdot \text{m}$$

$$T_1 = 5548 \text{ kgf} \cdot \text{m} \quad \text{or} \quad 55.48 \text{ kN} \cdot \text{m}$$

T_1 is divided by 2 since all conical cutters may be assumed to be located at a half distance drum diameter from the drum center.

$$T_2 = \frac{8 \cdot 1046 \cdot 0.5 \text{ (drum radius)} \cdot 1.35 \text{ (friction)}}{0.7 \text{ (efficiency)}} \text{kgf} \cdot \text{m}$$

$$T_2 = 8069 \text{ kgf} \cdot \text{m} \quad \text{or} \quad 80.69 \text{ kN} \cdot \text{m}$$

T_2 is not divided by 2 since all conical cutters are located at the periphery of the drum. For T_3, drum weight is 2000 kg.

$$T_3 = \frac{4000 \cdot 1.35 \cdot 1}{0.7 \cdot 2} \quad \text{or} \quad T_3 = 3857 \text{ kgf} \cdot \text{m} \quad \text{or} \quad 38.6 \text{ kN} \cdot \text{m}$$

$$\text{Total torque} = T_1 + T_2 + T_3$$

$$\text{Total torque} = (5548 + 8069 + 3857) \text{ kgf} \cdot \text{m}$$

$$\text{Total torque} = 17{,}474 \text{ kgf} \cdot \text{m} \quad \text{or} \quad 175 \text{ kN} \cdot \text{m}$$

As will be noticed from Figure 13.6, the calculated values are very close to the measured values, showing clearly that the predictor equations given above may be used for drill rigs equipped with conical cutters.

13.2 Large-Diameter Drill Rigs Used in Mining Industry and Possibilities of Using Drilling Specific Energy for TBM Selection

13.2.1 Background

Large-diameter drill rigs are widely used, in surface mining for blasting operations to increase the productivity, in well drilling, in geotechnical site investigations, and so on. This section is mainly aimed to show the readers the possibilities of using drilling specific energy to have some preliminary information on the classification of the rock formation for excavability or possible estimates of TBM performance or the performance of any mechanical excavators. Proper selection of a TBM for tunnel excavation needs a detailed site investigation and a large explanatory drilling program for site characterization. Core drilling is necessary. Sometimes it is carried out for certain levels of tunnel overburden close to the tunnel axis to speed the site investigation work and the rest of the location is drilled with other drilling techniques. Research works carried out in the past showed clearly that if the drilling parameters such as drilling rate, thrust, torque, rotational speed, and drill bit wear are recorded carefully during the site investigation program, it is possible to estimate some of the geotechnical properties of the strata to some extent (Rabia 1982; Muftuoglu 1987; Celeda et al. 2009).

13.2.2 Concept of Drilling Specific Energy and Drilling Tests Carried Out in TKI (Turkish Coal Enterprises)

Test results reported by Bilgin et al. (1993) are used to estimate the drilling specific energy. Ingersol Rand or Reedrill rotary drill rigs equipped with

25.1 cm toothed or button-studded tricone bits were used throughout *in situ* tests. A typical drill rig used is shown in Figure 13.7.

Equation 13.4, developed by Teale (1965), is used to estimate drilling specific energy:

$$SE = FT/A + 2 \cdot \pi \cdot N \cdot T/NPR \tag{13.4}$$

where SE is the specific energy, MJ/m^3; FT is the drill bit thrust, MN; A is the area of drill hole m^2; N is the rotational speed of the drill bit, revolution per second; T is the torque, MN · m; and NPR is the net production rate in drilling, m^3/h.

The relation between thrust and torque of the drill rig is given in Equation 13.5:

$$T\ (\text{kN} \cdot \text{m}) = 0.0408\ FT\ (\text{kN}) + 1.01 \tag{13.5}$$

In situ drilling experiments were carried out in 11 different coal mines of Turkish Coal Enterprises, where compressive strength of the strata ranged from 10.5 to 88.7 MPa. Test results and calculated drilling specific energy values are given in Table 13.3. Calculated specific energy values are plotted against rock compressive strength in Figure 13.8. This figure clearly shows that there is a trend of increasing specific energy with increasing rock compressive strength values.

FIGURE 13.7
A typical rotary drill used in Orhaneli Lignite Mine. (Adapted from the archive of Bilgin, N., 2006. A large-diameter drill rig study in Cifteler construction site in Istanbul. Istanbul Technical University, p. 30.)

TABLE 13.3

Results of *In Situ* Drilling Tests Carried Out with 25.1 cm Drill Bits in Different Coal Mines

Location	Rock	Compressive Strength (MPa)	Drill Thrust (kN)	RPM	Net Drilling Rate (m/h)	SE (MJ/m^3)	SE (kWh/m^3)
ELI Isiklar	Marn	88.7	50.3	119	44.1	62.5	17.4
Isiklar	Limestone	77.5	50.3	119	58.2	47.7	13.3
Sarikaya	Marn	69.2	42.6	118	39.9	62.2	17.3
Kisrakdere	Marn	82.4	54.2	120	36.6	80.4	22.4
GELI Sekkoy	Marn	21.6	38.7	118	80.8	29	7.9
Tinaz	Marn-limestone	59.4	34.1	118	85.5	25.4	7.1
MLI Orhaneli	Tufite	24.2	54.2	118	76.8	38	10.6
Orhaneli	Marn	45.4	46.4	118	93.9	28.1	7.8
Orhaneli	Marn	40.4	46.4	119	118.8	22.5	6.3
Keles	Marn-limestone	61.5	50.3	119	91.2	30.6	8.5
SLİ	Marn	10.5	50.3	118	153	18.5	5.1

Source: Adapted from Bilgin, N. et al., 1993. Drillability studies in TKI and optimum use of the drill bits, ITU School of Mines, p. 200.

Note: ELI, Aegean Lignite Mine; GELI, Southern Aegean Lignite Mine; MLI, Marmara Lignite Mine; SLI, Seyitomer Lignite Mine.

13.2.3 Concept of Rock-Cutting Specific Energy and the Effect of Rock Compressive Strength on Specific Energy

Specific energy is the energy spent to excavate a unit volume of rock and it is one of the most important factors in determining the efficiency of rock excavation and it may be used to estimate net or instantaneous production

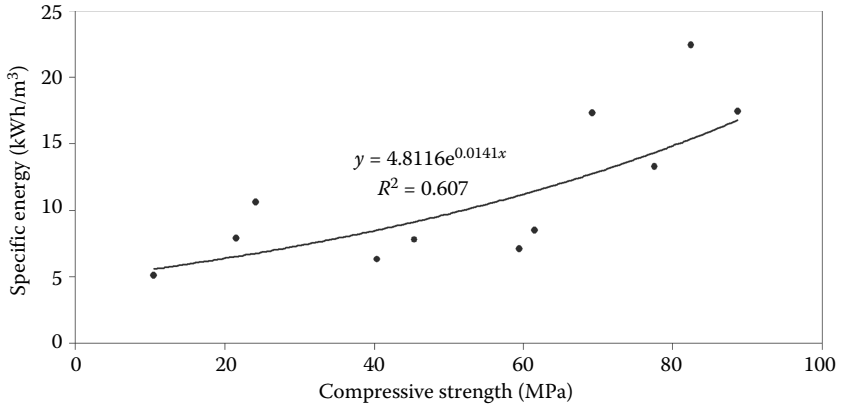

FIGURE 13.8
The relationship between drilling specific energy and rock compressive strength.

rate of TBM's or roadheaders, and so on. Specific energy values are determined experimentally using a full-scale laboratory cutting rig as explained in Chapter 5 or in the field as given in Equation 13.6. TBM's and optimum specific energy may be used to calculate the net production rate of any mechanical excavator as given in Equation 13.7 (Rostami et al. 1994; Balci 2009; Copur et al. 2001). Laboratory studies showed that optimum specific energy was related to rock compressive strength as explained in Chapter 9, Figure 9.15.

13.2.4 Numerical Example to Predict TBM Performance from Large-Diameter Drilling Results

A drill rig of 25 cm diameter is used for preliminary site investigation. The following drilling parameters are obtained: drill thrust is $55 \cdot 10^{-3}$ MN, rpm 110, net drilling rate 40 m/h, and torque $3.3 \cdot 10^{-3}$ MN · m. Discuss the energy spent for applying thrust force and torque.

13.2.4.1 Solution

1. Calculate drilling specific energy and rock compressive strength.
   Equations 13.4 and 13.5 gives

   $$SE = FT/A \text{ (}SE\text{ for thrust)} + 2 \cdot \pi \cdot N \cdot T/IPR \text{ (}SE\text{ for torque) and} \quad (13.6)$$

   $$SE = 55.10^{-3}\ \text{MN}/0.0495\ \text{m}^2 + 2 \cdot \pi \cdot 110/60\ (\text{rev/s}) \cdot 3.310^{-3}\ \text{MN} \cdot \text{m}/(0.011\ (\text{m/s}) \cdot 0.0495\ \text{m}^2)$$

   $$SE = 1.1\ \text{MJ/m}^3 + 69.8\ \text{MJ/m}^3 \text{ or } 70.9\ \text{MJ/m}^3 \text{ equivalent to } 19.7\ \text{kWh/m}^3$$

   As noted from the above calculation, *SE* for thrust is only 1% of the SE for torque.

   From Figure 13.8, compressive strength of the rock is estimated to be 100 MPa.

2. Using the above calculated value of rock compressive strength, roughly calculate the daily advance rate of a hard rock TBM used in this formation, for a machine utilization time of 45% and daily working time of 20 h.

   From Equation 9.15, optimum *SE* is found to be 6.8 kWh/m^3.

   As explained in Section 9.3.4 and Equation 9.4, the cutting power of the TBM in 6 m diameter is

   $$P = 80 \cdot 6 = 480\ \text{kW}$$

Net excavation rate is estimated as given in Equation 13.7 (Balci 2009)

$$\text{Net excavation rate} = 0.8 \cdot P/SE \tag{13.7}$$

Net excavation rate is $0.8 \cdot 480/6.8 = 56.5$ m^3/h

Daily advance rate = 20 h · 0.45 machine utilization time · 56.5 (m^3/h)/28.3 m^2 (tunnel area)

Daily advance rate = 18 m/day

However, one should be careful of using this method of calculation, since the methodology needs further research.

References

Balci, C., 2009. Correlation of rock cutting tests with field performance of a TBM in a highly fractured rock formation: A case study in Kozyatagi-Kadikoy Metro Tunnel, Turkey. *Tunnelling and Underground Space Technology*, 24:423–435.

Bilgin, N., 2006. A large-diameter drill rig study in Cifteler construction site in Istanbul. Istanbul Technical University, p. 30.

Bilgin, N., Demircin, M.A., Copur, H., Balci, C., Tuncdemir, H., Akcin, N., 2006. Dominant rock properties affecting the performance of conical picks and the comparison of some experimental and theoretical results. *International Journal of Rock Mechanics and Mining Sciences*, 43(1):139–156.

Bilgin, N., Eskikaya, Ş., Dincer, T., Kahraman, S., 1993. Drillability studies in TKI and optimum use of the drill bits, ITU School of Mines, p. 200.

Celada, B., Galera, J.M., Munoz, C., Tardaguilla, I., 2009. The use of specific drilling energy for rock mass characterization and TBM driving during tunnel construction. *World Tunnelling Congress, Budapest, Proceedings*, 9:05–06.

Copur, H., Tuncdemir, H., Bilgin, N., Dincer, T., 2001. Specific energy as a criterion for use of rapid excavation systems in Turkish mines. *Transactions of The Institution of Mining and Metallurgy Section A–Mining Technology*, 110:A149–157.

Muftuoglu, Y., 1987. Recording drilling parameters of drill rigs. Turkish 10. *Scientific and Technical Congress* (in Turkish). Ankara, ss. 253–270.

Rabia, H., 1982. Specific energy as a criteria for drill performance prediction. *International Journal of Rock Mechanics and Mining Sciences & Geomechanics Abstacts*, 19:39–42.

Rostami, J., Ozdemir, L., Neil, D.M., 1994. Performance prediction: A key issue in mechanical hard rock mining. *Mining Engineering*, 11:1263–1267.

Teale, R., 1965. The concept of specific energy in rock drilling. *International Journal of Rock Mechanics and Mining Sciences*, 2:57–73.

14

Mechanical Excavation in Coal Mines

14.1 Background

Coal plays an important role in power generation. As seen from Figure 14.1, 40% of the world's electricity comes from coal. This may continue for decades (International Energy Agency 2012). At current production levels, proven coal reserves are estimated to last 150–200 years or more. Coal reserves of some countries, and annual productions at the end of 2009 are given in Table 14.1 (International Energy Agency 2012).

Nearly 64% of world anthracite and bituminous coal production in 2005 came from underground mining with different productivity values in tons per man shift as 35 in the United States, 16 in Australia, 14 in South Africa, 2.6 in Russia, 1.5 in China, 1 in Ukraine, and 0.07 in India (Johnson 2007). There is always an increasing trend in productivity with an increasing degree of mine mechanization technology. Longwall, and room and pillar methods are the two main underground mining methods using shearers, ploughs, and continuous miners.

Almost half of the world underground coal production comes from longwall mining methods. The panel and face length change between 600–2500 and 100–300 m, respectively. The coal faces having length between 50 and 150 m are usually called short walls. Primary excavating machines are shearers and ploughs, moving mechanically back and forth across the coal seam. The excavated coal falls onto armored face conveyor (AFC) for removal from the work area. Longwall systems have their own hydraulic roof supports for overlying the rock that advances with the machine as mining progresses. As the longwall mining equipment moves forward, the roof and the rock are usually allowed to fall behind the operation in a controlled manner. The supports make it possible to have high levels of production and safety. In 2009, the average U.S. coal production per longwall mine was $4 \cdot 10^6$ tons; 417 employees having a production efficiency of 4.4 tons per employee hour (Weir 2009). Typical plan view of a mechanized coal face is seen in Figure 14.2.

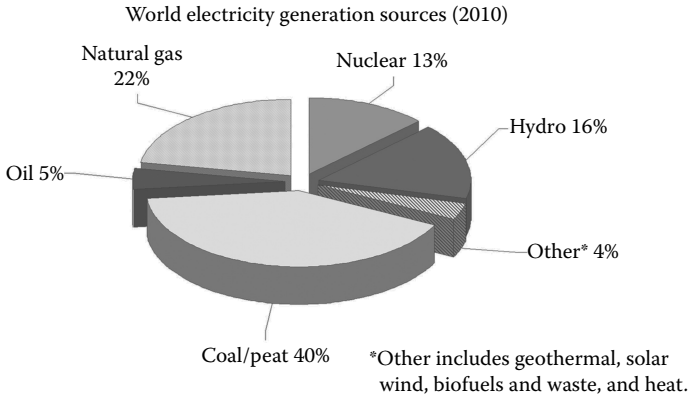

FIGURE 14.1
Total world electricity generation by fuel in 2010. (Adapted from International Energy Agency, 2012. *Key World Energy Statistics*, Paris, France, p. 88.)

TABLE 14.1

Proved Coal Reserves and Production at the End of 2009 (10^6 Tons)

Country	Anthracite and Bituminous	Subbituminous and Lignite	Total	Share of Total %	Production	Share of Total %
United States	108,950	129,358	238,308	28.9	973.2	15.8
Russian Federation	49,088	107,922	157,010	19.0	298.1	4.1
China	62,200	52,300	114,500	13.9	3050.0	45.6
Australia	36,800	39,400	76,200	9.2	409.2	6.7
India	5400	4600	58,600	7.1	557.6	6.2
Ukraine	15,351	18,522	33,873	4.1	73.7	1.1
Kazakhstan	28,170	3130	31,300	3.8	101.5	1.3
South Africa	30,408	–	30,408	3.7	250.0	4.1
Others	79,954	59,448	139,402	10.3	1227.3	15.1
World Total	411,321	414,680	826,001	100	6940.6	100

Source: Adapted from International Mining, 2010, August, World Coal.

14.2 Shearers

A typical shearer is seen in Figure 14.3 and some technical features from different manufacturing companies are summarized in Table 14.2.

Shearers can operate in weak and hard coal seams having a thickness between 1.5 and 7.0 m and having longitudinal and transversal inclinations up to 20°. Shearers can easily adapt their height in seams with changeable height. They have installed power up to 2590 kW. Specific energy ranges between 0.7 and 10 MJ/m^3 according to coal hardness. Shearers can cut coal with velocities up to 40 m/min and cut with a web between 0.8 and 1.2 m

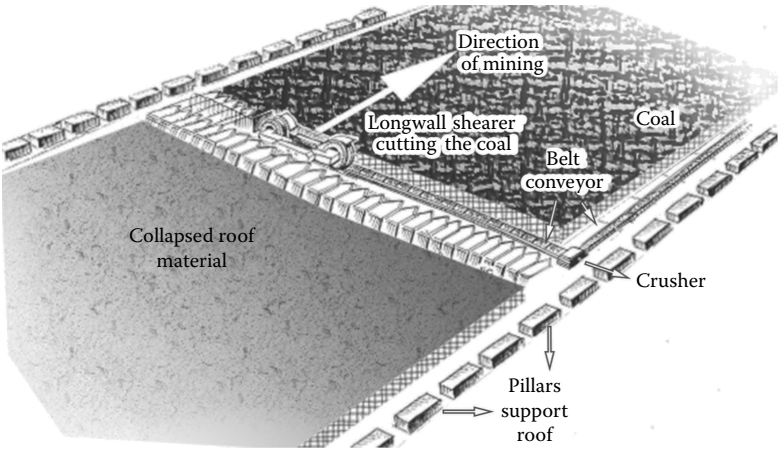

FIGURE 14.2
Plan view of a mechanized coal longwall face.

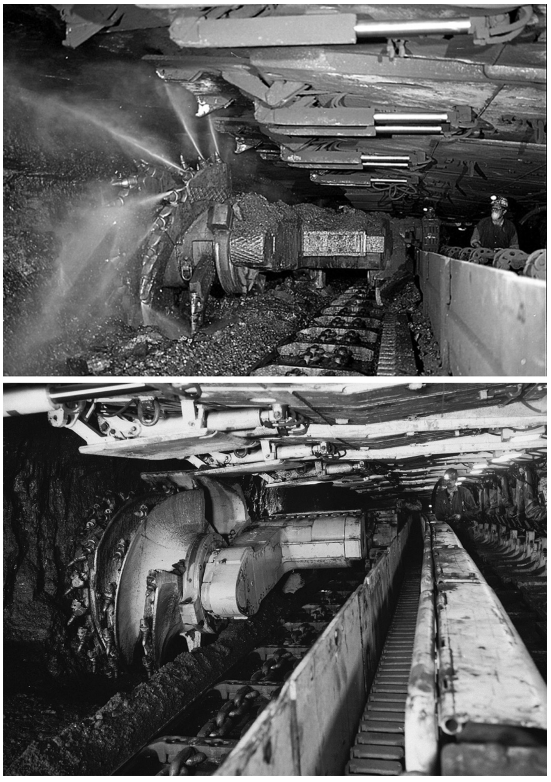

FIGURE 14.3
Eickhoff SL300 shearers with and without water spray. (Courtesy of Eickhoff.)

TABLE 14.2

Technical Features of Some Shearers Available in the Market

			Eickhoff	
Shearer	**TM 570E**	**FAMUR**	**SL300**	**SL1000**
Seam thickness (m)	1–3	1.8–4.3	1.4–4.0	2.7–7
Drum diameter (m)	1–1.5	1.6–4.3	1.4–4.0	–
Drum width (m)	0.8	0.8	0.8	–
Rotational speed (rpm)	47–60	34–45		32–50
Haulage speed (m/min)	0–11.5	0–25	0–10	0–50
Haulage force (kN)	2×300	2×436	–	
Cutting power (kW)	2×250	2×300		
Haulage power (kW)	2×30	2×60	1–80	–
Total power (kW)	567.5	1065	2×300	2590
Weight (t)	25	65	40	110–155

(Myszkowski and Paschedag 2008). The volume of the excavated coal is regulated by setting a required shearer haulage speed. Machine utilization time changes between 40% and 60%.

In bidirectional cutting, the shearer cuts coal in both directions with two sumping operations at the face ends in a complete cycle. In unidirectional cutting, the shearer cuts the coal in one direction. On the return trip, the floor is cleaned and there is only one sumping operation.

14.3 Ploughs

Ploughs are moving devices with cutting tools that shear off coal and push it into the face conveyor. A typical coal plough is seen in Figure 14.4 and technical features of some coal ploughs available in the market are given in Table 14.3.

Ploughs were widely used in the German coal mining industry between the 1950s and the 1980s. Thereafter, shearers developed very quickly and were used more. Ploughs are used in moderately medium-strength coal with seam heights from 0.6 up to 2.3 m and they may operate in faces with a longitudinal inclination up to 45°. Generally, in seams below 1.0 m of height, base plate ploughs are used, while in seams thicker than 1 m, gliding ploughs are used. Today's plough systems have up to 1600 MW of installed cutting power and have a tendency to cut harder rocks. Specific energy ranges between 1 and 10 MJ/m^3. In the conventional method, the plows travel in both directions, slower than the AFC with a relatively high cutting depth of cut. In the overtaking method, the plow travels in both directions, faster

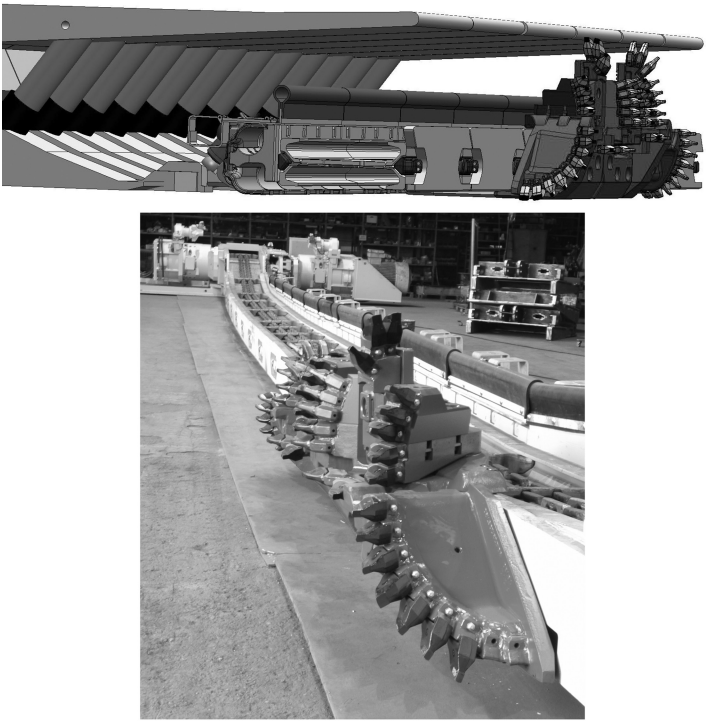

FIGURE 14.4
A drawing (upper) and view (lower) of a plough. (Courtesy of Halbach and Braun.)

than AFC, with a relatively smaller depth of cut. The plough speed is generally adjusted between 0 and 3 m/s. Ploughs always cut the seam in both directions. In coal seams having low strength, the height of the plough is less than the coal seam. Machine utilization time is less than shearers. Cutting depths of ploughs range between 4 and 20 cm, according to coal

TABLE 14.3

Technical Features of Some Coal Ploughs Available in the Market

Plough	Bucyrus GH800 Sliding Plough	Bucyrus GH1600 Sliding Plough	Bucyrus RHH 800 Base Plate	Zhangj Akou
Seam thickness (m)	0.9–2	1–2.3	0.6–1.6	0.8–1.8
Maximum seam inclination (degree)	60	60	60	25
Maximum power (kW)	2×400	2×800	2×400	–
Maximum plow speed (m/s)	3.0	3.6	2.5	1,7
Maximum cutting depth (mm)	150	250	150	120
Weight (ton)	–	–	–	92–225

hardness. Ploughability of coal developed by the German Research Institute DMT GmbH as described by an average cutting force F_S is described as given below (Myszkowski and Paschedag, 2008):

Good ploughable: $F_S < 1.5$ kN
Normal ploughable: 1.5 kN $< F_S <$ 2.0 kN
Hard ploughable: 2.0 kN $< F_S <$ 2.5 kN
Very hard ploughable: 2.5 kN $< F_S$

14.4 Room and Pillar Mining Method and Continuous Miners

In the room and pillar method, the mine is divided into a series of 6–10 m rooms with pillars up to 30 m wide. The method is commonly used in the United States. Production per shift is usually between 300 and 500 tons. Continuous miners (Figure 14.5) account for about 45% of the underground coal production in the room and pillar mining method. They also utilize conveyors to transport the removed coal from the seam. They may excavate coal seams from 0.8–6 m high. Remote-controlled continuous miners are used in a variety of difficult seams and conditions and robotic versions controlled by computers are becoming increasingly common. Some information about different products are given in Table 14.4.

FIGURE 14.5
A continuous miner. (Courtesy of Joy Inc.)

TABLE 14.4

Characteristics of Different Joy Continuous Miners

Series	Drum Diameter (m)	Drum Width (m)	Weight (ton)	Minimum Cutting Height (m)	Maximum Cutting Height (m)	Total Power (kW)	rpm
14 CM9A	0.57	3.35	53.6	0.81	2.3	550	62
14 CM9E	0.57	3.32	55.0	1.22	3.3	600	60
12 CM15D	0.57	3.30	59.0	2.16	4.6	610	60
12 HM36	0.57	4.12	95.0	2.10	4.6	840	42

14.5 Performance Prediction and Numerical Examples

14.5.1 Numerical Example for Continuous Miners

A continuous miner has a cutting power of 200 kW and a maximum thrust of 90 kN. The diameter of the cutting drum is 1 m and the rotational speed is 30 rpm. Laboratory cutting experiments carried out on rock samples representing the excavation site showed that the ratio of normal force to cutting force is 0.6. Find out if the machine's thrust is limited or not for the given power.

14.5.1.1 Solution

Cutting power of a continuous miner may be calculated as given below:

$$PCM = 2 \cdot \pi \cdot N \cdot T / \eta \tag{14.1}$$

where
PCM = power of the continuous miner (kW)
N = rotational speed of the cutting drum (rpm)
T = torque (kNm), and $\eta = 0.8$

$$200 = 2 \cdot \pi \cdot \frac{30}{(60 \times 0.8)} \cdot T$$

$$T = 50.9 \text{ kNm}$$

$$\text{Torque} = \text{total cutting force} \cdot \text{ radius of cutting drum} \tag{14.2}$$

$$T = FC \cdot r \tag{14.3}$$

FC = 50.9 kNm/0.5 m

Total cutting force FC = 101.8 kN

Total normal force $FN = 101.8 \cdot 0.6$ kN

FN = 61.08 kN

Maximum thrust of the machine is given as 90 kN, so the machine is not thrust limited.

14.5.2 Numerical Example for Plough

Objective of the numerical example is the application of coal-cutting mechanics in designing and planning of a mechanized coal longwall using ploughs (Figure 14.4). Data obtained from Ruhr District Colliery, Germany are used throughout the problem to compare the calculated values with in situ values.

Mine data and operating results are

Seam thickness = 2–2.1 m

Seam dip = 4°

Face length = 224

Plough speed = 2 m/s

Conveyor speed = 0.65 m/s

Panzer conveyor used = M-500

Plough driving power = 2 × 120 kW

Operating results are

Saleable output = 3600 t/day

Rate of advance = 5.65 m/day

Assumptions are

Coal tensile strength = 10 kgf/cm^2

Height of the plough used = 140 cm

The weight of the plough = 3 t

The weight of chain = 15 kgf/m

Rake angle and width of chisel pick = 10°, 20 mm

Working shift per day = 3

Plough utilization = 20%

Calculate the following operational parameters:

1. Calculate the numbers of chisel picks used in plough using basic optimum specific energy concept.

2. Calculate the force to pull the plough using Evans cutting theory.
3. Calculate the driving power of the plough.
4. Calculate the driving power of the chain conveyor.
5. Calculate mean daily advance and production rate of the coal face.

14.5.2.1 Solution

1. It is well known from the basic cutting mechanics that optimum specific energy SE_{opt} for coal is obtained for the ratio of cutter spacing/cutting depth ratio (s/d) of 2.

$$\text{For coal, } s/d = 2$$

where
s = cutter spacing
d = depth of cut

Depth of cut of the plough changes from 10 cm (for medium-strength coal) to 7 cm (for high-strength coal). Depth of cut may be taken as 5 cm for the coal seam concerned.

$$\frac{s}{5} = 2; \quad s = 10 \text{ cm}$$

Number of chisel picks may be calculated as given below:

$$N_C = \frac{H_P}{s + w} + N_{GC} \tag{14.4}$$

where
N_C = number of cutters
H_P = height of the plough
N_{GC} = number of gauge cutters
w = width of the cutter

Taken the given values, $w = 2$ cm and $s = (10 + 2) = 12$ cm.
$N_{GC} = 2$
N_C is calculated as

$$N_C = \frac{140}{12} + 2 = 14$$

2. Peak cutting force for one cutter may be calculated after Evans cutting theory as given in Equation 14.5:

$$F'C = \frac{2 \cdot \sigma_t \cdot d \cdot w \cdot \sin \frac{1}{2}\left(\frac{\pi}{2} - \alpha\right)}{1 - \sin \frac{1}{2}\left(\frac{\pi}{2} - \alpha\right)} \tag{14.5}$$

where
σ_t = tensile strength of coal
α = rake angle of chisel cutter
$F'C$ = 360 kgf

$$\text{Mean cutting force } FC = \frac{F'C}{2} = 180 \text{ kgf}$$

Pulling force of the plough, P_{FP}, without considering the weight of the machine itself:

$$P_{FP} = FC \cdot N_C \tag{14.6}$$

$$\sum_{N_C=1}^{N_C=14} 180 \cdot 14$$

$$P_{FP} = 2520 \text{ kgf} \quad \text{or} \quad 25.2 \text{ kN}$$

3. Driving power of the plough is calculated using the following equation:

$$P_P = (S_P \cdot P_{FP} \cdot (1 + \mu) + W_P \cdot S_P \cdot \mu)/\text{eff} \tag{14.7}$$

where
P_P = power to move the plough
P_{FP} = force to pull the plough
S_P = speed of the plough
W_P = plough weight
μ = friction coefficient
eff = efficiency

$$P_P = \frac{25.2 \text{ kN} \cdot 2 \text{ m} \, (1 + 0.2)}{0.8 \text{ s}} + \frac{30 \text{ kN} \cdot 2 \text{ m} \cdot 0.2}{0.8 \text{ s}}$$

$$P_p = 75.6 \text{ kW} + 15 \text{ kW}$$

$$P_p = 90.6 \text{ kW}$$

4. Driving power of the chain conveyor

   Driving power of the chain conveyor may be calculated using the following equation:

$$P_{CC} = P_{COAL} + P_{CHAIN} \tag{14.8}$$

$$P_{COAL} = L_{CC} \cdot A_{CC} \cdot S_{CC} \cdot \gamma_{COAL} / \text{eff} \tag{14.9}$$

$$P_{CHAIN} = L_{CC} \cdot S_{CC} \cdot \gamma_{CHAIN} \cdot \mu / \text{eff} \tag{14.10}$$

   where
   P_{CC} = total power to move chain conveyor
   P_{COAL} = power to move the coal on the chain conveyor
   P_{CHAIN} = power to move the chain of the panzer conveyor
   L_{CC} = length of the chain conveyor
   A_{CC} = cross section of the panzer conveyor
   γ_{COAL} = density of the coal (1300 kgf/m^3)
   S_{CC} = speed of the chain conveyor
   γ_{CHAIN} = mass of the unit length of chain material, 15 kgf/m

   Cross section of M-500 chain conveyor 0.054 m^2.

$$P_{COAL} = 224 \text{ m} \cdot 0.054 \text{ m}^2 \cdot 0.65 \text{ m} \cdot 13 \text{ kN} / (0.8 \cdot \text{s} \cdot \text{m}^3)$$

$$P_{COAL} = 127.7 \text{ kW}$$

$$P_{CHAIN} = 224 \text{ m} \cdot 0.65 \text{ m} \cdot 0.15 \text{ kN} \cdot 0.2 / (0.8 \cdot \text{s} \cdot \text{m}^3)$$

$$P_{CHAIN} = 5.5 \text{ kN}$$

$$P_{CC} = 133.2 \text{ kW}$$

5. Mean daily advance and production rate of the coal face

$$Ar = n \cdot d \tag{14.11}$$

$$n = WT_p \cdot Uf \cdot S_p / Lf \tag{14.12}$$

   where
   Ar = daily advance rate
   n = travel period of the plough per day
   WT_p = working time of the plough

Uf = utilization factor of the plough (20%)
S_p = speed of the plough
Lf = length of the coal face
d = depth of slice cut in one pass of plough

$$Ar = 16 \cdot 3600 \text{ s} \cdot 0.2 \cdot 2 \text{ m} \cdot 0.05 \text{ m}/(\text{day} \cdot \text{s} \cdot 224 \text{ m})$$

$$Ar = 5.14 \text{ m/day}$$

$$Pr = Ar \cdot Lf \cdot Sh \cdot \gamma_{\text{Coal}}$$

where
Pr = production rate of plough
h = height of the coal seam
γ_{coal} = density of coal seam

$$Pr = 5.14 \text{ m} \cdot 224 \text{ m} \cdot 2 \text{ m} \cdot 1.3 \text{ t}/(\text{day} \cdot \text{m}^3)$$

$$Pr = 2994 \text{ t/day}$$

14.5.3 Application of Linear Cutting Test Results to Preliminary Calculation of Power Requirement of a Shearer–Loader

Check the power requirement of the shearer–loader selected for excavation of a thick coal seam in Amasra Coal Field, Turkey, after the coal-cutting experiments are carried out in a linear cutting machine. The technical specifications of the shearer–loader selected are given in Table 14.5.

TABLE 14.5

Technical Properties of the Selected Shearer–Loader

Type of shearer–loader	Double drum ranging arm
Cutting height	3.85 m
Drum cutting diameter	1.8 m
Web width including clearance plate	0.85 m
Maximum speed of drum rotation	27 rpm
Haulage speed capacity	0–11 m/min
Haulage force capacity	245 kN
Cutting power capacity	2 × 200 kW
Haulage power capacity	2 × 60 kW
Total power	538 kW
Total mass	422 kN
Tool type	Conical tools
Tool reach for 48° attack angle	6 cm
Vane (start, sequence) number	3 vanes
Tool number per cutting line	3 tools/line

The following numerical example is of the authors (Bilgin et al. 2010); for details of the shearer drum design, the readers should consult Brooker (1979a,b), Somanchi et al. (2005), Roxborough and Phillips (1981), Hekimoglu and Tiryaki (1998), Hekimoglu et al. (2002), Hurt and McStravic (1988).

It is assumed that the speed of drum rotation (*RPM*) is 27 rpm and the required haulage speed (H_S) is 4.0 m/min. Conical cutters are going to be used for excavation. Full-scale linear cutting experiments performed on blocks of coal samples by using a conical cutter at single scroll cutting pattern and different line spacings and depths of cut indicate that the optimum line spacing to depth of cut ratio $(s/d)_{opt}$ is around 2.0. Cutting (*FC*) and normal (*FN*) forces acting on the tools by cutting perpendicular to the cleat planes are given in Equations 14.13 and 14.14 depending on the depth of cut (per revolution) for line spacing of 10 cm:

$$FC = 1.96 \cdot d^{0.50} \tag{14.13}$$

$$FN = 0.98 \cdot d^{0.70} \tag{14.14}$$

FC and *FN* are in (kN) and *d* is in (cm) in these equations.

14.5.3.1 Solution

Advance per revolution of the drum is estimated to be 15 cm/rev by using Equation 14.15:

$$APR = H_S/RPM \tag{14.15}$$

where
APR = advance per revolution of the drum (cm/rev)
H_S = haulage speed of the shearer–loader (cm/min)
RPM = rotational speed of the drum (revolution/min, rpm)

Since there are three tools per cutting line, nominal penetration of each tool at middrum height for each revolution of the drum (d) is estimated to be 5 cm/tool/rev by using Equation 14.16:

$$d = APR/V_N \tag{14.16}$$

This value of d is below 6 cm of tool reach. Since the optimum ratio of line spacing (s) to depth of cut (d) is around 2.0 as in Equation 14.17, the line spacing between the tools is estimated to be around 10 cm:

$$(s/d)_{opt} \cong 2.0 \tag{14.17}$$

Since the drum/web width (D_W) is 85 cm, the number of vane tools per sequence or vane (N_{TPS}) is estimated to be 9 tools/sequence by using Equation 14.18:

$$N_{TPS} = D_W/S \tag{14.18}$$

Since the number of vanes or sequences (V_N) on the drum is 3, total number of vane tools (N_{VT}) is estimated to be 27 tools by using Equation 14.19:

$$N_{VT} = N_{TPS} \cdot V_N \tag{14.19}$$

If it is assumed that the number of tools on the face plate/clearance ring is 9, then the total number of tools (N_{TT}) on the drum is estimated to be around 36 tools by using Equation 14.20:

$$N_{TT} = N_{VT} + 9 \tag{14.20}$$

Cutting power of a drum (P_{CUT}) is estimated by using Equation 14.21:

$$P_{CUT} = 2 \cdot \pi \cdot N \cdot T \tag{14.21}$$

where N is the drum rotational speed per second ($RPM/60$) and T is the torque requirement of the drums for cutting. Torque (T) is estimated by using Equation 14.22:

$$T = N_{TC} \cdot FC \cdot R_D \tag{14.22}$$

where

T = torque requirement of the drum for cutting (kNm)
N_{TC} = number of tools in contact with coal
FC = cutting force acting on a tool (kN)
R_D = radius of the drum (m)

Since the half of a drum sumps into the coal, the number of tools in contact with coal is $0.5 \cdot N_{TT} = 18$ tools per drum for the selected problem. Since there are two ranging drums on the shearer–loader, (N_{TC}) is estimated to be $2 \cdot 18 = 36$ tools. The drum radius is $R_D = D_D/2 = 1.8/2 = 0.9$ m. It is assumed that the tools placed on face plate/clearance ring are closely spaced so that the tool forces acting on them are almost equal to the forces acting on the vane tools.

The shape of the area cut by a tool, as the drum rotates and moves forward, approximates a cissoid (crescent). The depth of cut (penetration) of a tool is almost zero at the beginning of a cut. It becomes a maximum, when the tool reaches at middrum height. The maximum depth of cut at middrum height for this problem is 5 cm/rev. The average depth of cut can be calculated as 0.64 of the maximum (Roxborough and Phillips 1981), which yields 3.25 cm/rev of average depth of cut. For this depth of cut value, FC is estimated to be 3.5 kN and FN is estimated to be 2.2 kN by using Equations 14.13 and 14.14.

On the basis of these considerations and estimations, the net cutting power of two drums ($P_{CUT\text{-}N}$) are estimated as 320 kW by using Equation 14.23:

$$P_{CUT\text{-}N} = 2 \cdot \pi \cdot N \cdot T = 2 \cdot \pi \cdot (\text{RPM}/60) \cdot N_{TC} \cdot FC \cdot (D_D/2) \tag{14.23}$$

$$P_{CUT\text{-}N} = 2 \cdot \pi \cdot (27/60) \cdot 36 \cdot 3.5 \cdot (1.8/2) = 320\,\text{kNm/s} = 320\,\text{kW}$$

If the efficiency of the drum power transmission is assumed to be 0.8, the output (gross) power of the drums for cutting should be (320/0.8) = 400 kW, which is almost the same as the installed cutting power of the drums, meaning that the powers of the drums are good enough to achieve the required performance.

Net power requirement of the shearer–loader for pulling over the armored face conveyor ($P_{\text{PULL-N}}$) is estimated by using Equation 14.24:

$$P_{\text{PULL-N}} = P_{\text{THRUST-N}} + P_{\text{MOVE-N}} \tag{14.24}$$

where

$$P_{\text{THRUST-N}} = N_{\text{TC}} \cdot FN \cdot (H_S/60) \tag{14.25}$$

$$P_{\text{MOVE-N}} = W \cdot f \cdot (H_S/60) \tag{14.26}$$

where W is the force acting on the mass center of the shearer–loader and f is the friction coefficient between the shearer–loader and the armored face conveyor (which can be assumed to be 0.3 for this problem). Therefore

$$P_{\text{THRUST-N}} = 36 \cdot 2.2 \cdot (4/60) = 5.3\,\text{kW}$$

$$P_{\text{MOVE-N}} = 422 \cdot 0.3 \cdot (4/60) = 8.4\,\text{kW}$$

$$P_{\text{PULL-N}} = 5.3 + 8.4 = 13.7\,\text{kW}$$

If the efficiency of the power transmission of haulage motors is assumed to be 0.8, the output power for haulage should be (13.7/0.8) = 17.1 kW, which is well below the installed haulage power of 2×60 kW, meaning that the haulage power of the shearer–loader is good enough to achieve the required performance. Power requirement of the vanes for loading is ignored in this study, since it is quite small (1–2% of the total) compared to power requirement for cutting.

Total net power requirement of the shearer–loader ($P_{\text{TOTAL-N}}$) is estimated to be 333.7 kW by using Equation 14.27:

$$P_{\text{TOTAL-N}} = P_{\text{CUT-N}} + P_{\text{PULL-N}} \tag{14.27}$$

Total gross power requirement of the shearer–loader is estimated to be (333.7/0.8) = 417 kW.

The haulage force acting on the shearer–loader (FH) can be estimated to be 206 kN, which is lower than the haulage force capacity of the shearer–loader (meaning that the haulage force capacity of the shearer–loader is good enough to achieve the required performance), by using Equation 14.28:

$$FH = N_{\text{TC}} \cdot FN + W \cdot f \tag{14.28}$$

This special example does not include the effect of any particular operational conditions such as working uphill or downhill, geological irregularities on the floor, partings, and so on, and only accounts for a rough estimation of power requirement of the shearer–loader. Loading capacity of the vanes should also be checked. Detailed analysis of force balance of the drums should also be analyzed by computer simulations of drums.

References

Bilgin, N., Temizyurek, I., Copur, H., Balci, C., Tumac, D., 2010. Cuttability characteristics of TTK Amasra thick seam and some comments on mechanized excavation. *Proceedings of the 17th Coal Congress of Turkey*, eds. Colak, K., Aydin, H. June 2–4, Zonguldak, TMMOB Chamber of Mining Engineers of Turkey, pp. 217–229 (in Turkish).

Brooker, C.M., 1979a. Theoretical and practical aspects of cutting and loading by shearer drums. Part-I. *Colliery Guardian Coal International*, January:9–16.

Brooker, C.M., 1979b. Theoretical and practical aspects of cutting and loading by shearer drums. Part-II. *Colliery Guardian Coal International*, April:41–50.

Bucyrus product catalogue.

Eickhoff product catalogue.

Famur product catalogue.

Hekimoglu, O.Z., Tiryaki B., 1998. In-situ investigations on shearer drum design. *CIM Bulletin*, 91(1018):225–228.

Hekimoglu, O.Z., Tiryaki, B., Ayhan, M., 2002. Reducing respirable dust and fines through shearer drum design in coal mines. *CIM Bulletin*, 95(1059):119–123.

Hurt, K.G., McStravic, F.G., 1988. High performance shearer design. *Colliery Guardian*, December:428–429.

International Energy Agency, 2012. *Key World Energy Statistics*, Paris, France, p. 88.

International Mining, 2010, August, World Coal.

Joy product catalogue.

Johnson, D., 2007. Latest technology and performances in the global underground coal mining industry. Asia Pacific Economic Co-operation APEC, Clean Fossil Energy Technical and Policy Seminar, Hanoi, Vietnam, pp.1–38. *Joy Mining Machinery*, 38.

Myszkowski, M., Paschedag, U., 2008. Longwall mining in seams of medium thickness, comparison of plow and shearer performance under comparable conditions, Bucyrus, p. 28.

Roxborough, F.F., Phillips, H.R., 1981. Applied rock and coal cutting mechanics. *Workshop Course 156/81*, May 11–15, Australian Mineral Foundation, Adelaide.

Somanchi, S., Kecojevic, V., Kozminski, T., 2005. Advance design of lacing and breakout patterns for shearers. *Mining Technology (Trans. Inst. Min. Metall. A)*, June, 114:A118–A124.

Weir, 2009. Weir International, Inc. Mining, Geology and Energy Consultants, USA longwall mining statistics, p. 8.

15

Chain Saw Machines

15.1 Background

Chain saw machines are used for the extraction of natural (dimensional) stones such as travertine and marble. They are used for cutting low- to medium-abrasive and soft- to medium-strength natural stones in both underground and surface quarrying operations, as well as in squaring operations. They cut relatively thin slots vertically or horizontally and are usually used in combination with diamond wire-cutting machines (Primavori 2006). Adding only one chain saw to the equipment fleet, in addition to diamond wire-cutting machines, improves the overall performance of a mid-size quarry by about 20% (Copur et al. 2006). They eliminate time losses and labor for drilling boreholes for wire insertion when using with diamond wire-cutting machines, especially in high benches more than 6–7 m (eliminate collimation problems). They reduce production and time losses due to their ability of sumping horizontally or vertically to enter a new bench. They result in a directly saleable stone. They create an excellent working environment (regular and planar surfaces) for quarrying. They produce less dust and waste material compared to diamond-wire cutting machines (Sariisik and Sariisik 2010). The basic limitation of these machines is that they cannot cut hard, abrasive, and fractured stone deposits.

15.2 Technical Features of Chain Saw Machines

Basic modules of a chain saw machine are presented in Figure 15.1. The chain saw machines move along a rail system by an electrohydraulic or electric motor. Their arm lengths vary from 2 m up to around 8 m. The arm thicknesses (cutting widths) are usually either 38 or 42 mm, depending on the manufacturer. Cutting tools are bolted to tool holders mounted on sockets (Figure 15.2). The sockets are connected to each other, making an endless chain sliding over the arm by an electrohydraulic or electric motor after

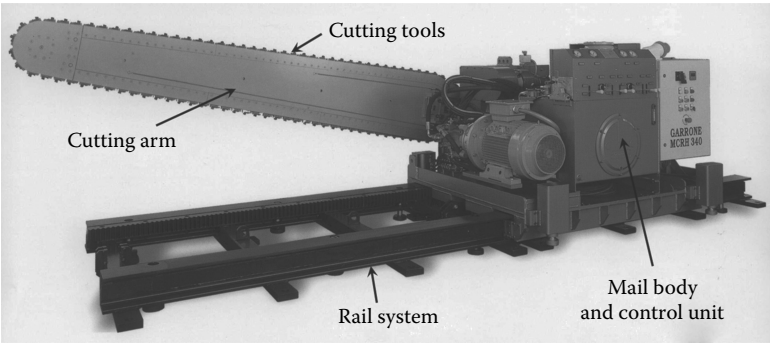

FIGURE 15.1
Basic modules of a chain saw machine. (Courtesy of Garrone, Product Catalogues. With permission.)

giving a certain pretension. Grease is used to reduce the sliding friction and the torque requirement of the arm rotation. Technical properties of some of the chain saw machines used in the natural stone industry are summarized in Table 15.1.

Chisel (wedge)-type cutting tools made of tungsten carbide with rectangular prism geometry are the most widely used tools with chain saw machines. There are different cutting tool designs in terms of geometry, composition, and metallurgical features (Figures 15.3 and 15.4). The tools are rotated after a certain amount of wearing to obtain a sharp edge on operation. All the tools should be rotated at the same time to get a better excavation performance, excluding prematurely broken tools. Cutting profile, tool lacing, metallurgical properties of the tools, and stone abrasivity determine the type, shape, and amount of cutting tool wear.

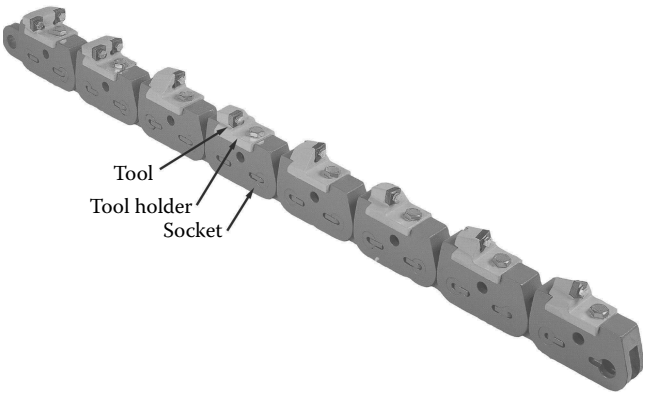

FIGURE 15.2
A picture of a sequence of cutting tools. (Courtesy of Garrone, Product Catalogues. With permission.)

TABLE 15.1

Specifications of Some of the Chain Saw Machines

Manufacturer	Garrone	Fantini	Demmak
Model	MCRH 340	MOD70 RA/P-S	ZK 3400
Weight (ton)	6	10	7.5
Driving unit	Electrohydraulic	Electrohydraulic	Electric
Electric voltage (V)	380	380	380
Total installed power (kW)	50	55	45
Maximum reach (cm)	340	740	340
Chain speed (m/s)	0–1.8	0–0.9	0–1.5
Feed motion speed (cm/min)	0–20	0–13	0–18
Cutting width (mm)	42	38	42
Grease tank capacity (liter)	220	300	250
Chain rotation pressure (bar)	350	240	–
Cart movement pressure (bar)	50	50	–
Arm rotation (degrees)	360	360	360

Source: Adapted from Garrone, Fantini, and Demmak Product Catalogues.

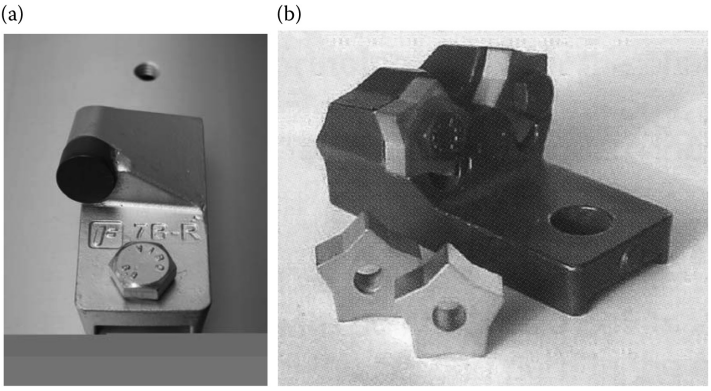

FIGURE 15.3
Circular (a) and star-shaped (b) tool geometries. (Courtesy of Fantini.)

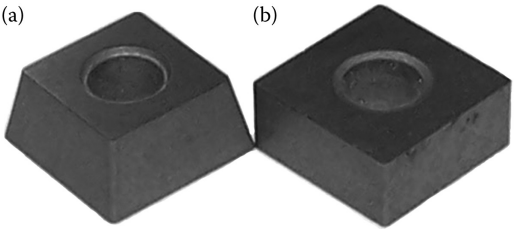

FIGURE 15.4
Rectangular prism tools: four-edge tool (a) and eight-edge tool (b).

15.3 Design of Chain Saw Machines

There are different designs of cutting sequences, depending on the manufacturer. A cutting sequence can be composed of different numbers of sockets (usually 8–10) depending on cutting conditions. Usually two to three of the tool holders located at the end of a sequence include two tools and the others only one tool. Tools on a sequence are usually located symmetrically to counterbalance the forces acting on the arm for avoiding uneven wear of tools and arm plate, as well as deviations from intended cutting line. Cutting action of a sequence of tools is repeated by the following sequences. Total number of sequences on a chain depends on the arm and/or chain length. An example of a tool lacing (layout) is presented in Figure 15.5. An example of a cutting profile is presented in Figure 15.6.

Tool (line) spacing along the cutting profile is usually smaller at the edges and larger around the center (Figure 15.7). However, the tool spacing along the cutting trajectory is constant and depends on the socket length; for example, it is 90 mm in Figure 15.5. Angular positions of each tool (sideways angle) is usually between 45° and –5°, being at maximum on the center and getting gradually smaller at the sides of the profile. Levels (altitudes) of strike points of each tool also vary in a sequence.

15.4 Performance Prediction of Chain Saw Machines

Parameters affecting the performance of chain saw machines are summarized in Table 15.2. There are a few models published for the prediction of chain saw machines. The empirical prediction models are presented in the next section of this chapter when solving a numerical example. A recently developed deterministic model, which can also be used for the design of chain saw machines, is summarized below.

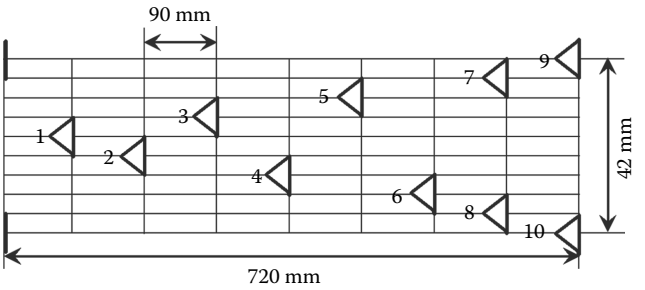

FIGURE 15.5
An example of tool lacing in a sequence.

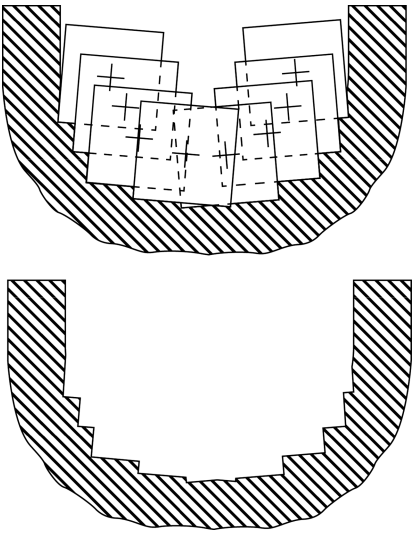

FIGURE 15.6
An example of cutting profile.

A deterministic model, presented below, for up-cutting mode can be considered as a semitheoretical model based on the results of linear cutting experiments and kinematics of the chain saw machines (Copur et al. 2008a,b, 2010, 2011a; Copur 2010). Symbols used in up-cutting mode are illustrated in Figure 15.8 (Mellor 1976).

The arm angle or cutting angle (ϕ) is commonly close to and less than 90°, and the chain tends to propel the machine. The cutting depth of arm (H) is the depth of penetration of the arm. The longitudinal tool spacing (S) is the distance between tracking tools along the chain; in other words, it is the

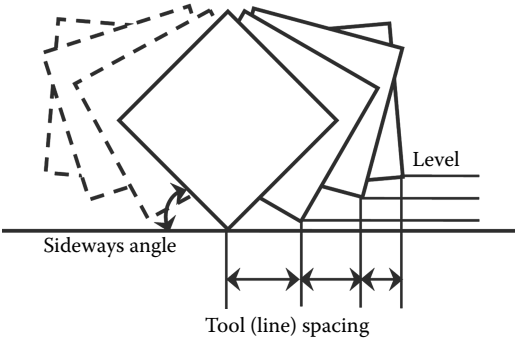

FIGURE 15.7
Variable tool (line) spacing, sideways angles, and levels. (Adapted from Copur, H., 2010. *International Journal of Rock Mechanics and Mining Sciences*, 47(1):104–120.)

TABLE 15.2

Parameters Affecting Performance of Chain Saw Machines

Geology	Joint set number and frequency
	Dip and direction of the deposit
	Bedding and foliation
	Cuttability, strength, elasticity, abrasivity properties
	Petrographical and texture properties
Machine	Torque–power–thrust capacities
	Driving unit and weight
	Arm length and thickness
	Lacing design of the cutting tools
	Metallurgical and geometrical properties of the cutting tools
Operational	Arm cutting depth and angle
	Cart movement speed
	Chain rotation speed
	Pretension of chain
	Grease use on the chain
	Cutting dry or water feeding
	Cutting vertical or horizontal
	Quality of labor and material availability

Source: Adapted from Copur, H. et al., 2008a. Optimization of cutting performance of chain saw machines used for natural stone quarrying. Project report submitted to TUBITAK, Project No: 105M017. Istanbul Technical University, Mining Engineering Department.

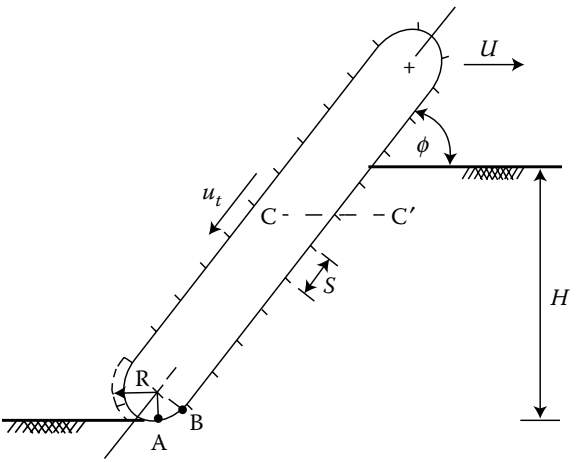

FIGURE 15.8
Symbols used in kinematics analysis of chain saw machines. (Adapted from Mellor, M., 1976. Mechanics of cutting and boring, part 3: Kinematics of continuous belt machines. CRREL (US Army, Cold Regions Research and Engineering Laboratory, Hanover, New Hampshire), Special Report, No: 76-17.)

length of a sequence. Each tool enters the work at point A with a depth of cut (chipping depth) being close to 0, then, increases steadily through the curved portion of the nose AB, until it reaches a steady maximum value (d), which would be maintained throughout the rest of the working sweep. However, the change of depth of cut in this transition region can be ignored in many cases, since it is only a small portion of the arm.

Cutting depth of a tool (d) is determined by the forward movement speed of the machine (U) during the time interval Δt ($\Delta t = S/u_t$) between successive tool passes through a given horizon such as C–C′ in Figure 15.8. Here, (u_t) is tangential (linear) speed of tool. In the same time interval, the traverse motion gives the whole chain a horizontal displacement of ($U\Delta t$), so that the horizontal (nominal) penetration of the tool is (SU/u_t). The effective cutting depth of a tool (d) (normal to the face of the arm or of the stone surface being cut) is estimated by Equation 15.1 (Mellor 1976):

$$d = \frac{U}{u_t} \cdot S \cdot \sin\phi \tag{15.1}$$

The areal net cutting rate ($ANCR$) of the machine per unit time can be estimated by Equation 15.2:

$$ANCR = H \cdot U \tag{15.2}$$

The length of the chain in contact with stone (H_C), ignoring the nose section, can be estimated by

$$H_C = H/\sin\phi \tag{15.3}$$

The number of sequences in contact with the stone (S_C) can be estimated by

$$S_C = H_C/S \tag{15.4}$$

The number of tools in contact with the stone (T_C) can be estimated by

$$T_C = S_C \cdot T_S \tag{15.5}$$

where (T_S) is the number of tools on a sequence.

Forces acting on the tools of a sequence are estimated based on results of linear cutting experiments, by using the relationships between effective depth of cut (d) and tool forces and specific energy:

$$FN_i \text{ (or } FC_i) = A_i \cdot d^{B_i} \tag{15.6}$$

$$SE_i = C_i \cdot e^{D_i d} \tag{15.7}$$

where
- FN = average normal force
- FC = average cutting force
- SE = specific energy
- i = the subscript of tool number on a sequence, which defines the position, sideways angle, and cutting pattern of the tools starting from 1 up to (T_S)
- e = base of natural logarithm
- A_i and B_i = experimental constants for tool forces
- C_i and D_i = experimental constants for specific energy

Total forces ($\sum FN$ and $\sum FC$) acting on the arm can be estimated by

$$\sum FN \text{ (or } FC) = t \cdot S_C \cdot \sum_{i=1}^{T_S} FN_i \text{ (or } FC_i) \tag{15.8}$$

where (t) is a coefficient to take into account for different cutting conditions. The value of (t) can be estimated by

$$t = t_1 \cdot t_2 \cdot t_3 \tag{15.9}$$

where
- t_1 is the multiplier for wearing (dullness) of tools and can be taken to be 1.3 for average conditions (Roxborough and Rispin 1973; Takaoka et al. 1974; Copur et al. 2008a; Copur 2010).
- t_2 is the multiplier for groove deepening (incremental cutting) action of the tools and can be assumed to be 3.0 for both normal and cutting forces for lower rake angles, such as in chain saw machines (Morrell and Wilson 1983; Roxborough 1988).
- t_3 is the multiplier for a rake angle, which can be used if the results of the cutting experiments have to be adapted to a different rake angle (in this case, it is taken to be 0.85 to adopt the results from –5° to 0° rake angle) (Whittaker 1962; Pomeroy 1964).

Torque requirement of the machine for only cutting the stone (T_{CUT}) can be determined by

$$T_{CUT} = \frac{\sum FC}{\cos(\lambda)} \cdot r \tag{15.10}$$

where
- r = radius of chain driving sprocket
- λ = chain rib (ridge) angle

Field measurements of hydraulic pressures of cart movement and chain rotation motors indicate that the frictional losses due to cart movement

and free chain rotation with a constant pretension are generally about 20% and 15%, respectively, compared to maximum capacity cutting conditions (allowed maximum ampere or maximum hydraulic pressure) (Copur et al. 2008a). A frictional loss coefficient of (f_L) due to chain rotation with only pretension (without cutting, $d = 0$ mm) can be taken to be 1.15 for estimation of total torque.

Frictional effect of total normal (thrust) force ($\sum FN$) acting perpendicular to the arm guide on the chain torque should be taken into account for estimation of total torque by multiplying it with a frictional coefficient (f_f). The frictional coefficient (f_f) between the chain and arm guide can be taken as 0.05 for very well-lubricated chains and 0.15 for poorly lubricated chains (Mancini et al. 1992, 1994).

Total torque requirement of the machine (T_{TOT}) can then be estimated by

$$T_{\text{TOT}} = \left(f_L \cdot \sum FC + f_f \cdot \sum FN\right) \cdot \frac{r}{\cos(\lambda)} \tag{15.11}$$

Total power consumption of the machine (P_{TOT}) for cutting the stone and frictional losses can be determined by

$$P_{TOT} = 2 \cdot \pi \cdot N \cdot T_{\text{TOT}} \tag{15.12}$$

where (N) is the rotational speed of the chain sprocket wheel. This power estimation does not include the power consumption for cart movement and any efficiency factor for estimation of gross power requirement.

Total horizontal force acting on the machine body (F_H), which is balanced by the weight of the machine and determines the total thrust requirement of the machine, is estimated as the sum of the horizontal components of ($\sum FN$) and ($\sum FC$) by

$$F_H = \sin\phi \cdot \sum FN + \cos\phi \cdot \sum FC \tag{15.13}$$

Total vertical force acting on the machine body (F_V) is estimated as the sum of the vertical components of ($\sum FN$) and ($\sum FC$) by

$$F_V = \cos\phi \cdot \sum FN - \sin\phi \cdot \sum FC \tag{15.14}$$

Field observations and measurements indicate that (F_H) had to be equal to or less than the mass of the machine for a secure operation and breakage-free machine components (Simsek 2008). This can be considered as design and optimization criteria for chain saw machines. (F_H) and (F_V) values can also be used for structural design of chain saw machines. A design criterion for checking if there is any limitation for available haulage volume of the chain should also be applied in such a model (Mellor 1976).

15.5 Numerical Examples on the Performance Prediction of Chain Saw Machines

15.5.1 Numerical Example on Deterministic Performance Prediction of Chain Saw Machines

A chain saw machine with arm length of 3.4 m is going to be used for the production of marble in a quarry. Technical features of the chain saw machine are presented in Table 15.3. The tool lacing design of a sequence used for performance prediction is illustrated in Figure 15.5. Results of the full-scale linear cutting tests for simulation of the marble cutting operation by chain saw machines are presented in Table 15.4. Estimate the *ANCR* of the chain saw machine by using deterministic modeling for cutting the given marble. Also, estimate forces acting on the arm of the chain saw machine.

15.5.1.1 Solution of Numerical Example 15.5.1

After several trials by modifying the input parameters of the deterministic model, it is seen that when effective depth of cut (d) is selected as 0.33 mm, the arm cutting depth (H) should be kept around 2.50 m to not exceed the thrust capacity of the machine.

If the arm cutting depth (H) of 2.50 m and arm angle (ϕ) of 80° are taken, then the length of the chain in contact with the stone (H_C) is estimated to be 2.54 m (Equation 15.3):

$$H_C = 2.5/\sin(80°) = 2.54 \text{ m}$$

Since the length of the sequence (S) is 0.72 m and the number of tools on a sequence (T_S) is 10 (Figure 15.5), the number of sequences (S_C) and the tools (T_C) in contact with the stone are 3.5 sequences (Equation 15.4) and 36 tools (Equation 15.5), respectively:

$$S_C = H_C/S = 2.54/0.72 = 3.53 \text{ m}$$

TABLE 15.3

Technical Features of the Chain Saw Machine

Weight	5.5 tons
Electric voltage	380 V
Total installed power	50 kW
Maximum reach	340 cm
Chain speed	0–1.8 m/s
Feed motion speed	0–20 cm/min
Cutting width	42 mm

TABLE 15.4

Results of the Full-Scale Linear Cutting Tests

Tool No.	Sideways Angle[a]	Cutting Series	Average Normal Force Coefficients		Average Cutting Force Coefficients		Specific Energy Coefficients	
			A_i	B_i	A_i	B_i	C_i	D_i
1	30	U	45.114	0.9239	16.441	1.4333	59.266	–0.1333
2	30	S	37.146	0.3483	12.998	1.0944	33.075	–0.0851
3	15	O	51.235	0.2425	19.961	0.5716	89.061	–0.5028
4	15	O	51.235	0.2425	19.961	0.5716	89.061	–0.5028
5	15	S	41.358	0.3356	16.686	0.7769	72.020	–0.3558
6	15	S	41.358	0.3356	16.686	0.7769	72.020	–0.3558
7	0	S	224.90	0.3508	57.454	0.9325	72.245	–0.3989
8	0	S	224.90	0.3508	57.454	0.9325	72.245	–0.3989
9	0	K	308.91	0.2755	105.54	0.8281	87.673	–0.2123
10	0	K	308.91	0.2755	105.54	0.8281	87.673	–0.2123

Source: Adapted from Copur, H. et al., 2008a. Optimization of cutting performance of chain saw machines used for natural stone quarrying. Project report submitted to TUBITAK, Project No: 105M017. Istanbul Technical University, Mining Engineering Department.

Note: These coefficients result in normal and cutting forces in (kgf) and specific energy in (MJ/m^3). To convert from kgf to *N*, kgf is multiplied by 9.80665. To convert from MJ/m^3 to kWh/m^3, MJ/m^3 is divided by 3.6.

[a] Approximate values.

$$T_C = S_C \cdot T_S = 3.53 \cdot 10 = 35.3 \cong 36 \text{ tools}$$

The effective depth of cut (d) of the tools is estimated to be 0.33 mm (Equation 15.1) for cart movement speed (U) of 2.0 m/h (0.56 mm/s) and chain rotational speed (u_t) of 1.2 m/s:

$$d = \frac{0.56}{1.2} \cdot 0.72 \cdot \sin(80°) = 0.33 \text{ mm}$$

The *ANCR* of the machine is estimated to be 5.0 m^2/h (Equation 15.2) for given operational parameters:

$$ANCR = H \cdot U = 2.5 \cdot 2.0 = 5.0\,\text{m}^2/\text{h}$$

The lacing design given in Figure 15.5 is used for the estimation of tool forces. Tool forces are estimated for a sequence of tools by using the relationships between the depth of cut and tool forces and specific energy obtained from linear cutting experiments and are summarized in Table 15.4. The results of individual tool force and specific energy estimates are summarized for 0.33 mm of effective depth of cut in Table 15.5 and Figure 15.9. As seen in Table 15.5, total normal force (Equation 15.6), cutting force (Equation

TABLE 15.5

Results of the Estimations of Tool Forces and Specific Energy

Tool No.	Line Spacing[a] (mm)	Swept Spacing[a] (mm)	Average Normal Force (kgf)	Average Normal Force (kN)	Average Cutting Force (kgf)	Average Cutting Force (kN)	Specific Energy (kWh/m³)	Specific Energy (MJ/m³)
1	–	5	16.1	0.16	3.3	0.03	15.76	56.73
2	5	5	25.2	0.25	3.8	0.04	8.93	32.16
3	5	5	39.1	0.38	10.6	0.10	20.98	75.51
4	5	5	39.1	0.38	10.6	0.10	20.98	75.51
5	5	5	28.5	0.28	7.0	0.07	17.80	64.08
6	5	5	28.5	0.28	7.0	0.07	17.80	64.08
7	0	4.25	59.9	0.59	8.0	0.08	17.60	63.38
8	0	4.25	59.9	0.59	8.0	0.08	17.60	63.38
9	–	1.75	62.6	0.61	11.6	0.11	22.71	81.77
10	–	1.75	62.6	0.61	11.6	0.11	22.71	81.77
Total		42	422	4.13	81	0.80	17.63[b]	63.46[b]

[a] Approximate values.
[b] Weighted average based on swept spacing by each tool.

15.6), and average specific energy (Equation 15.7) of each sequence are 4.13 kN (422 kgf), 0.80 kN (81 kgf), and 63.46 MJ/m³ (17.63 kWh/m³), respectively. As seen in Figure 15.9, the current tool lacing has some unbalanced tool force distribution, which should be redesigned for a proper balance.

The coefficients (t_1) of 1.3, (t_2) of 3.0, and (t_3) of 0.85 generate a total (t) value of 3.3 (Equation 15.9). Total forces acting on the arm are estimated to

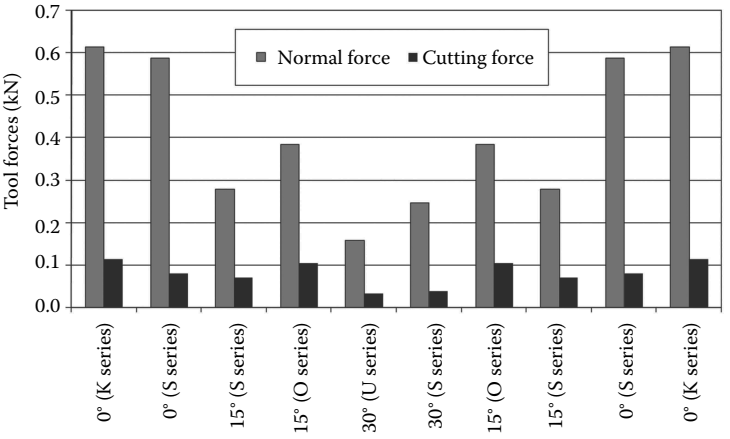

FIGURE 15.9
Variation of tool forces on a sequence of tools.

be 48.3 kN (4927 kgf) for normal force and 9.3 kN (952 kgf) for cutting force (Equation 15.8):

$$t = t_1 \cdot t_2 \cdot t_3 = 1.3 \cdot 3.0 \cdot 0.85 = 3.3$$

$$\sum FN = t \cdot S_C \cdot \sum_{i=1}^{T_S} FN_i = 3.3 \cdot 3.53 \cdot 4.13 = 48.3 \text{ kN}$$

$$\sum FC = t \cdot S_C \cdot \sum_{i=1}^{T_S} FC_i = 3.3 \cdot 3.53 \cdot 0.80 = 9.3 \text{ kN}$$

Total horizontal (F_H) and vertical (F_V) components of tool forces acting on the machine are 49.2 kN (5017 kgf) (Equation 15.13) and −0.78 kN (79 kgf) (Equation 15.14), respectively. Note that the negative sign indicates the direction of the vertical force.

$$F_H = \sin(80°) \cdot 48.3 + \cos(80°) \cdot 9.3 = 49.2 \text{ kN}$$

$$F_V = \cos(80°) \cdot 48.3 - \sin(80°) \cdot 9.3 = -0.78 \text{ kN}$$

The estimated total horizontal force (49.2 kN) should be balanced by the machine mass of 54 kN (5500 kgf) showing that the machine works close to its thrust capacity in this case. This shows that the machine works in just under its thrust limit so that its *ANCR* cannot be increased to the over 5.0 m²/h for this type of operation.

Total cutting force of 9.3 kN (952 kgf) determines the machine torque. If the radius of the chain driving sprocket (r), the chain rib angle (λ), the frictional loss coefficient due to pretension (f_L), and the frictional coefficient between chain and arm guide (f_f) are 0.1 m, 20°, 1.2, and 0.05 (very well lubricated), respectively, the total torque requirement of the chain saw machine (T_{TOT}) is estimated to be 1.45 kNm (Equation 15.11).

$$T_{TOT} = \left(1.2 \cdot 9.3 + 0.05 \cdot 48.3\right) \frac{0.1}{\cos(20°)} = 1.45 \text{ kNm}$$

For this torque requirement, the total consumed machine power (P_{TOT}) is estimated to be 17.4 kW (Equation 15.12); by estimating the rotational speed of the chain driving sprocket (N) being 115 revolution per minute for 1.2 m/s of chain speed (u_t).

$$P_{TOT} = 2 \cdot \pi \cdot \left(\frac{115}{60}\right) \cdot 1.44 = 17.4 \text{ kW}$$

Torque and power requirement for just cutting (T_{CUT} (Equation 15.10) and P_{CUT} excluding frictional losses and cart movement) are 1.0 kNm and 12.0 kW, respectively.

$$T_{CUT} = \frac{9.3}{\text{Cos}(20°)} \cdot 0.1 = 1.0 \text{ kNm}$$

$$P_{CUT} = 2 \cdot \pi \cdot \left(\frac{115}{60}\right) \cdot 1.0 = 12.04 \text{ kW}$$

15.5.2 Numerical Example on Empirical Performance Prediction of Chain Saw Machines

A chain saw machine with arm length of 3.4 m, weight of 5.5 tons, and arm thickness of 42 mm is going to be used for the production of marble in a quarry. The uniaxial compressive strength of the marble is 85 MPa. Estimate the *ANCR* of the chain saw machine by using two empirical models (based on specific energy and chain saw penetration index) for cutting the given marble. Estimate the tool consumption rate based on the chain saw tool consumption index.

The relationship between specific energy (*SE*, in kWh/m^3) obtained by linear cutting experiments in unrelieved cutting mode with a standard chisel tool and effective depth of cut (*d*, in mm) is presented in Equation 15.15:

$$SE = 14.832 \cdot e^{(-0.238d)} \tag{15.15}$$

15.5.2.1 Solution of Numerical Example 15.5.2

A model based on specific energy is given in Equation 15.16 for predicting the *ANCR* of a chain saw machine without considering arm length (Copur et al. 2008a; Copur 2010):

$$ANCR = \frac{k \cdot P_{\text{cutting}} / (1.3 \cdot SE)}{T} \tag{15.16}$$

where

P_{cutting} is the power consumed for only cutting the stone in kW. For the arm lengths between 3.4 and 7.4 m, a value can be assigned between 11.4 and 15.6 kW by linear extrapolation. In this case, it is taken to be 11.4 kW for arm length of 3.4 m.

T is the arm thickness (cutting width) of chain saw machine in m. In this case, it is 0.042 m.

k is the coefficient related to mechanical miner type and cutting geometry (usually around 0.3 for chain saw machines (Copur et al. 2008a; Copur 2010)).
SE is the specific energy value obtained for a certain effective depth of cut in unrelieved cutting mode with a standard chisel tool in kWh/m^3.

It was shown that the specific energy can be estimated for effective depth of cut (d) values between 0.3 and 0.7 mm (or 0.5 mm as an average) without considering the specifications of the chain saw machine used. If d is taken to be 0.5 mm, *SE* is estimated to be 13.2 kWh/m^3 by using Equation 15.15:

$$SE = 14.832 \cdot e^{(-0.238 \cdot 0.5)} = 13.17 \text{ kWh/m}^3$$

The *ANCR* is then estimated to be 4.76 m^2/h by using Equation 15.16.

$$ANCR = \frac{0.3 \cdot 11.4/1.3 \cdot 13.17}{0.042} = 4.76 \text{ m}^2/\text{h}$$

A model based on the chain saw penetration index is given in Equations 15.17 and 15.18 for predicting the ANCR of a chain saw machine (Copur et al. 2011b):

$$ANCR = 5.18 \cdot CSPI + 3.68 \tag{15.17}$$

$$CSPI = \frac{W \cdot H}{UCS} \tag{15.18}$$

where
CSPI is the chain saw penetration index.
W is the force vector of the chain saw weight acting on the mass center of the machine in tonf. In this case, it is 5.5 tonf.
H is the useful cutting depth of the arm in m. It is usually around 3.0 m for arm lengths of 3.4 m.
UCS is the uniaxial compressive strength of the stone in MPa. It is 85 MPa.

The *ANCR* for the given operational conditions is estimated to be 4.82 m^2/h by using Equations 15.18 and 15.17:

$$CSPI = \frac{5.5 \cdot 3.4}{85} = 0.22 \text{ tonf . m/MPa}$$

$$ANCR = 5.18 \cdot 0.22 + 3.68 = 4.82 \text{ m}^2/\text{h}$$

Daily marble (block) production rates can be estimated by assuming machine utilization time of 35% for a midsize quarry.

Tool consumption rates (*TCR*, in tools/m^3) can be estimated by using Equations 15.19 and 15.20 (Copur et al. 2011b):

$$TCR = 0.024 \cdot CSTCI + 0.111 \tag{15.19}$$

$$CSTCI = \frac{UCS}{W \cdot H} \tag{15.20}$$

where *CSTCI* is chain saw tool consumption index and the other parameters are the same as mentioned above. By using Equations 15.19 and 15.20, the tool consumption rate for the given operational conditions is estimated to be 0.220 tools/m^3 for the four-edge chisel tools made of tungsten carbide, without considering the water feeding condition during cutting.

$$CSTCI = \frac{85}{5.5 \cdot 3.4} = 4.55\,\text{MPa/tonf . m}$$

$$TCR = 0.024 \cdot 4.55 + 0.111 = 0.220\,\text{tools/m}^3$$

References

Copur, H., 2010. Linear stone cutting tests with chisel tools for identification of cutting principles and predicting performance of chain saw machines. *International Journal of Rock Mechanics and Mining Sciences*, 47(1):104–120.

Copur, H., Balci, C., Bilgin, N., Tumac, D., Avunduk, E., Saracoglu, M.A., Serter, A., 2011a. A deterministic model for predicting and optimizing performance of chain saw machines. *Proceedings of the 22nd World Mining Congress and Expo*, September 11–16, Istanbul, Vol. 2, pp. 175–181.

Copur, H., Balci, C., Bilgin, N., Tumac, D., Feridunoglu, C., Dincer, T., Serter, A., 2006. Cutting performance of chain saws in quarries and laboratory. *Proceedings of the 15th International Symposium on Mine Planning and Equipment Selection*, eds. Cardu, M., Ciccu, R., Lovera, E., Michelotti, E. September 20–22, Turin, Italy, pp. 1324–1329.

Copur, H., Balci, C., Tumac, D., Bilgin, N., 2011b. Field and laboratory studies on natural stones leading to empirical performance prediction of chain saw machines. *International Journal of Rock Mechanics and Mining Sciences*, 48(2):269–282.

Copur, H., Balci, C., Tumac, D., Bilgin, N., Avunduk, E., 2010. Field and laboratory studies on performance of chain saw machines. *Proceedings of European Rock Mechanics Symposium (EUROCK 2010)*, eds. Zhao, J., Labiouse, V., Duth, J.P., Mathier, J.F. June 15–18, Lausanne-Switzerland, CRC Press/Balkema, Taylor & Francis Group, pp. 823–826.

Copur, H., Bilgin, N., Balci, C., Tumac, D., 2008a. Optimization of cutting performance of chain saw machines used for natural stone quarrying. Project report submit-

ted to TUBITAK, Project No: 105M017. Istanbul Technical University, Mining Engineering Department.

Copur, H., Balci, C., Bilgin, N., Tumac, D., 2008b. Laboratory cutting tests for performance prediction of chain saw machines. *Proceedings of the 21st World Mining Congress and Expo 2008*, September 7–12, Poland, Krakow-Katowice-Sosnowiec, pp. 97–107.

Demmak, Product Catalogues.

Fantini, Product Catalogues.

Garrone, Product Catalogues.

Mancini, R., Cardu, M., Fornaro, M., Linares, M., Peila, D., 1992. Analysis and simulation of stone cutting with microtools. In: *Proceedings of the III Geoengineering Congress, Rock Excavation: The Future and Beyond*, December 1–2. Torino, Italy, pp. 227–236.

Mancini, R., Linares, M., Cardu, M., Fornaro, M., Bobbio, M., 1994. Simulation of the operation of a rock chain cutter on statistical models of inhomogeneous rocks. *Proceedings of the 9th International Symposium on Mine Planning and Equipment Selection*, eds. Pasamehmetoglu, G., Karpuz, C., Eskikaya, S., Hızal, T., Istanbul, pp. 461–468.

Mellor, M., 1976. Mechanics of cutting and boring, part 3: Kinematics of continuous belt machines. CRREL (US Army, Cold Regions Research and Engineering Laboratory, Hanover, New Hampshire), Special Report, No: 76-17.

Morrell, R.J., Wilson, R.J., 1983. Toward Development of a Hard-Rock Mining Machine—Drag Cutter Experiments in Hard, Abrasive Rocks. USBM, RI 8784.

Primavori, P., 2006. Uses for the chain saw. *Marmo Macchine International*, 53:80–102.

Pomeroy, C.D., 1964. Breakage of coal by wedge action—Factors affecting tool design—2. *Colliery Guardian*, July 24, pp. 115–121.

Roxborough, F.F., 1988. Multiple pass sub-interactive rock cutting with picks and discs. *Proceedings of the CARE '88 (Conference on Applied Rock Engineering)*, Newcastle upon Tyne, pp. 183–191.

Roxborough, F.F., Rispin, A., 1973. The mechanical cutting characteristics of the lower chalk. *Tunnels and Tunneling*, 5:45–67.

Sariisik, A., Sariisik, G., 2010. Efficiency analysis of armed-chained cutting machines in block production in travertine quarries. *The Journal of Southern African Institute of Mining and Metallurgy*, 110:473–480.

Simsek, A., 2008. Personnel communication. DEMMAK Demireller Marble Machinery Co, Research and Development Manager. 2008.

Takaoka, S., Hayamizu, H., Misawa, S., Kuriyagawa, M., 1974. Mechanical fracture characteristics of rock with a cutter bit and a disk cutter. *Proceedings of the 3rd International ISRM Congress*, Denver, Vol. 1, Part B, pp. 1723–1729.

Whittaker, D., 1962. Effect of pick shape on cutting forces. *Colliery Guardian*, August 23, pp. 242–244.

This page intentionally left blank

16

Emerging Mechanical Excavation Technologies

16.1 Background

The overall reviews of the rock fragmentation/excavation techniques available today show that the major methods are still drill and blast and mechanical excavation methods. The novel rock fragmentation/excavation techniques, such as thermal energy (laser, electric), ultrasound or microwave energy, chemical energy, and water-jet cutting, do not currently offer a profitable rock excavation method due to very high specific energy requirements. The novel methods might be utilized as an auxiliary method in combination with mechanical excavation and drill and blast, may be for kerf cutting or precision cutting, not for excavation of the whole face. Water-jet cutting is the most promising method among the novel methods when used in combination with mechanical cutting tools.

The drill and blast method has maintained its position in underground mining and tunneling applications due to, basically, the flexibility and the mobility of the equipment, and the ability to excavate any shape and size of openings in any rock type. Automation and application of higher-efficiency drills are the dominant area of improvement in the drill and blast techniques. However, it looks like it is not possible to get rid of the cyclic nature of the drill and blast method, in opposition to the continuous nature of mechanical excavation that makes it prone to automation. All the attempts so far have resulted in making the cycle shorter to create a semicontinuous operating environment.

The application and market share of mechanical miners in both mining and civil underground construction are gradually growing in parallel to the improved efficiency, reliability, automation, and capability of the machines, creating a cost advantage to mechanical excavation over the drill and blast. In addition to inherent advantages of mechanical mining, environmental restriction on the usage of explosives, especially for excavation operations in urbanized areas, is the other reason that is causing growth of the mechanical excavation market. However, the development of mechanical excavation

technologies, especially for underground operations, has been at a slow pace compared to surface operations, as well as other technologies.

Since there is no space limitation in surface operations, many mechanical excavation techniques (such as excavators, draglines, and surface miners) have been specially developed for softer rocks and these systems could be improved for higher productivity, while the problems of excavating harder rocks and natural stones (such as production of granite blocks) remain unresolved. Although drill and blast still dominates the hard rock excavation operations in surface mining, the use of machine mining is increasing especially for softer rocks as they are capable of economically producing large amounts of material in an environmentally friendly manner.

Since space is always limited in underground operations, it is difficult to develop excavation systems that can fit in small openings while trying to meet some of requirements of underground operations, such as mobility (easiness of relocation, decreased dimension and weight, thus decreased cost), flexibility (operational adaptability, turning radius, working gradients, flat floor requirement, etc.), selective mining/cutting ability (part face excavation, easiness of access to the face, fast maintenance, reduced ore dilution, etc.), and hard and abrasive rock-cutting ability. Therefore, the main challenge to the excavation industry is to develop a "truly mobile hard rock excavator" (Friant et al. 1994).

The competitiveness of the drill and blast method will continue for a while, especially in surface mining operations in hard rock, underground stoping, short tunnels in rock, noncircular openings in hard rock, and excavation in very hard and abrasive rocks. On the other hand, the mechanical excavation would remain unchallenged in soft rock mining. The tunneling industry has already shown the trend of using TBMs as the standard excavation equipment for any hard rock applications. However, development of a mobile hard rock excavator for tunneling noncircular openings remains as a main challenge. Development of a versatile tunneling machine that can cope with all types of grounds (including hard rock and soft ground under the water table) encountered in especially urbanized areas is still a target to reach for excavation industry, although very capable mix-shield TBMs are gradually improving. Mechanized excavation of vertical or inclined openings (shafts) needs still to be improved, especially for muck removal systems. Also, mechanical excavation of narrow veins (reefs) in deep hard rock mines is still to be improved.

The emerging (new) mechanical excavation techniques mainly have two objectives: to increase productivity and degree of automation in soft ground excavation and develop a truly mobile hard rock excavation system. In addition to these, the other areas of objectives are to increase the machine mechanical reliability and availability, reduce maintenance requirement and time for changing parts, and increase machine utilization time. This is basically provided by equipping the machines with self-diagnostic systems, programmable logic control systems to allow for optimum usage of machine capabilities, and more automation to reduce stoppage hours, as well as improving new materials and methods especially for cutting tools. Attempts

are also underway to increase the utilization time by simultaneous installation of ground support and using continuous haulage systems to avoid the unnecessary interruptions.

The basic route of a new development requires a scientific basis followed by laboratory testing and field testing of a prototype. The following hard rock excavation machines/technologies/techniques have been developed by different manufacturers and tested on a limited basis either in the laboratory or in the field. None of these systems has been widely accepted so far by the underground hard rock excavation industry, but they are considered as promising or emerging developments.

16.2 Developments in Cutting Tool Technology

Improvement of the hard rock cutting abilities of mobile machines such as roadheaders cannot be achieved unless the cutters used with them are improved, since the most important limiting factor for hard rock excavation is the cutting tools used for excavation. Single disk cutter, which is a type of roller cutter, is the most efficient hard rock cutting tool. However, drag-type tools are not durable enough to cut hard and abrasive rocks due to their attacking mechanism (dragging, scratching) to the rock surface being cut and their overall strength. The most important developments in the last decade on cutter technology that can improve tool life and cutting ability are minidisk, dual-property tungsten carbide, smart*cut, polycrystalline diamond composite (PDC), and oscillating disk cutter technologies. These technologies will be briefly introduced in this section.

16.2.1 Minidisk Cutters

The single disk cutters are proven to be the most efficient hard rock-cutting tools. The current single disks are too large and heavy, and require thrust forces too high to be used on small-sized, mobile machines. Since the disk force requirements decrease with decreasing disk diameter, reducing the disk diameter would allow reduction of the thrust requirement that results in lower machine weights and more mobile and flexible machines. Based on this theoretical idea, the Excavation Engineering and Earth Mechanics Institute of the Colorado School of Mines in conjunction with the Excavation Engineering Associates Inc. of Seattle, Washington, has developed a new type of small-size disk cutter in 1992, which is called minidisk cutter (Friant and Ozdemir 1994a; Friant et al. 1994; Ozdemir and Rostami 1995).

The minidisk incorporates a new pedestal mounting assembly compared to the regular saddle mount disk cutters available in the industry. A simplified drawing of the minidisk assembly is shown in Figure 16.1. This system

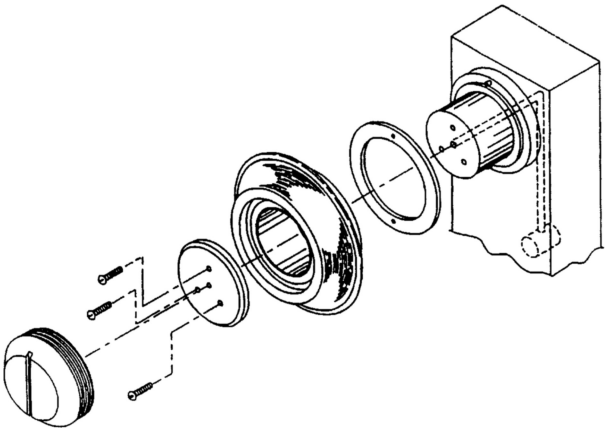

FIGURE 16.1
Simplified drawing of minidisk cutter assembly. (Adapted from Friant, J.E., Ozdemir, L., 1994a. Development of the high thrust minidisc cutter. *Proceedings of Institute of Shaft Drilling Technology Annual Technical Conference*, April 18–21, Las Vegas, Nevada, 12 p.; Friant, J.E., Ozdemir, L., 1994b. Development of the high thrust mini-disc cutter for microtunneling applications. *No-Dig Engineering*, June:12–16.)

offers several advantages such as the ease of change, lower number of parts, less consumable parts, stiffer shaft, and higher load capacity for the same disk diameter. While disk cutters currently on the market have more than 20 parts, the minidisk has only 5 parts, including a seal/wear ring. When the minidisk wears out, the ring is pulled off the shaft and discarded and the hubcap is replaced. Since the minidisk is a cantilever design, the shaft can be built as an integral part of the cutterhead. A well is burned out in the forward plate of the cutterhead and the cutter shaft is welded into the cutterhead structure. In this way, the cutter is both recessed and protected.

There are two types of minidisk cutters: carbide-tipped and hardened steel. A carbide-tipped minidisk cutter is mainly manufactured for very hard and abrasive rock conditions to increase the cutter life. Carbide-tipped minidisk cutters have almost three times more cutter life than the hardened steel minidisk cutters. They can be used in cutterheads as small as 7.875 in diameter. Several sizes from 3.25 to 10 in have been tested in the field for different applications such as longwall drum shearer, continuous miner, drill bit, roadheader, and open-pit surface miner. This new technology was used in microtunneling industry for excavation of relatively soft rocks. Application of this technology to the hard rock cutting requires improvements on its bearing system. Pictures of hardened steel minidisk cutters are presented in Figure 16.2.

16.2.2 Dual-Property Tungsten Carbide Technology

Sandvik has developed a different carbide manufacturing technology, which is called dual property. Dual-property carbide has three layers. The external

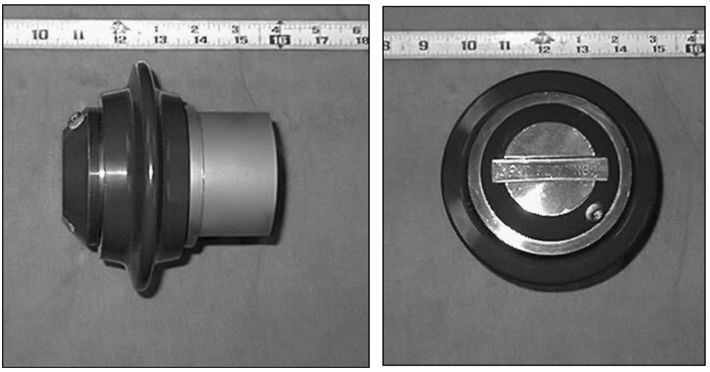

FIGURE 16.2
Five-inch minidisk cutter.

and internal layers are harder than the intermediate layer. The intermediate layer (tougher) absorbs the shocks. The external and internal layers are harder (wear resistant) layers. This structure enables both increased hardness and toughness. The regular tungsten carbide structure does not allow increasing both hardness and toughness, since they are inversely proportional to each other. This technology is being used with drilling machines using button carbide. The implementation of the technology to the conical cutters is still under research (Anonymous 1995; Icacutrock 1998).

16.2.3 Polycrystalline Diamond Composite Tool Technology

The PDC cutter consists of a thin layer (0.001–0.04 in) of polycrystalline diamond integrally sintered at ultra high pressure and temperature to a cemented tungsten carbide substrate. The thin layer of PDC is very sensitive to high temperatures, although it is highly wear resistant, 300 times as wear resistant as carbide. The presence of cobalt in the PDC layers catalyzes the transformation of diamond to graphite. Thus, PDC cutters should not be exposed to temperatures in excess of 700°C for any sustained period of time. The PDC drill bits are being widely used in the oil and gas industry in medium-soft to medium-hard formations where the lithology is well known. The experience showed that in hard rock formations cutter degradation could lead to sudden tool failure (Schafer and Glowka 1994). Laboratory studies showed that using this technology with high pressured water jets might give a possibility of applying this technology to mining cutter tools (Thimons et al. 1991).

16.2.4 Smart*Cut Technology

Super material abrasive-resistant tools (smart*cut) technology uses thermally stable diamond composites (TSDC) in the design and manufacture of

cutting tools (Ramazanzadeh and Hood 2010; Li et al. 2011). The two key features of smart*cut technology are replacement of conventional tungsten carbide with TSDC as the cutting tip of the tool and a CSIRO (Commonwealth Scientific and Industrial Research Organization)-patented bonding technology to attach the TSDC tip to the steel tool body. These types of tools can be used in temperatures higher than 1200°C. This technology was tested in the laboratory and expected to be tested in the field.

16.2.5 Undercutting Disk Cutter Technology

The undercutting concept was originally developed by CMTE (Cooperative Research Center for Mining Technology and Equipment) in Australia to cut the rock in tension/shear rather than compression as in the typical application of disk cutters (CMTE 1998). For this purpose, an edge is created by the cutters and the rock is cut toward a free face (Figure 16.3). This action reduces the tool forces up to 2.5 factors. However, the side loads acting on this type of cutting action limits their applicable rock strength, causing wear and damage on the tools and low penetrations. The basic application area of this technology is considered as narrow vein (reef) mining and a prototype of such a machine has already been manufactured and tested in the field by Wirth and Sandvik-Voest Alpine.

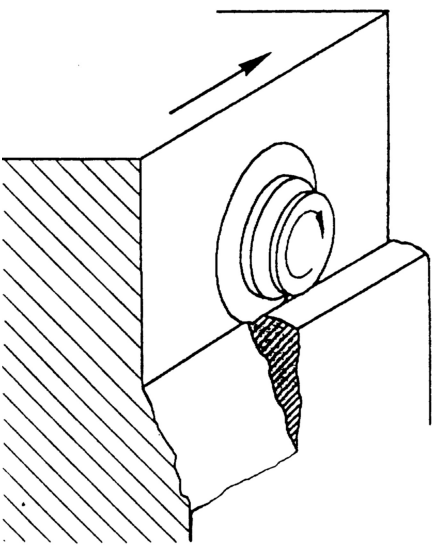

FIGURE 16.3
Under cutting disk cutter. (Adapted from Ramazanzadeh, A., Hood, M., 2010. *International Journal of Mining and Environmental Issues*, 1(1):29–39.)

16.2.6 Oscillating (Activated) Undercutting Disk Cutter Technology

The basic concept of oscillating disk cutters is to generate fatigue damage on rock by cyclic loading, which is an easier way to break it. Laboratory studies indicated that oscillating an undercutting disk reduced the tool forces (Hood et al. 2005; Ramazanzadeh and Hood 2010), although some problems encountered in field testing of this concept originated from disk bearing and activation mechanism.

16.3 Emerging Mobile Machines for Hard Rock Excavation

16.3.1 Robbins Mobile Miner

Robbins Company developed the first mobile miner excavation machine in the mid-1980s (Robbins 1985). Mobile miner is a partial-face machine and cuts arched or near rectangular cross sections with elliptical-shaped walls. This is a crawler-mounted excavator, which features a rotating wheel fitted with disk and roller cutters and mounted on a swinging boom. This wheel is mounted vertically on the swing arm and rotates around a horizontal axis. Rock excavation is accomplished by sumping the rotating cutting wheel into the rock and slewing it sideways. A mobile miner with a ranging wheel is also a new concept providing more flexibility to the mobile miner. This system is capable of moving the ranging arm vertically to complement the horizontal movements and enable the machine to create a horseshoe-shaped opening. A picture of a mobile miner is presented in Figure 16.4.

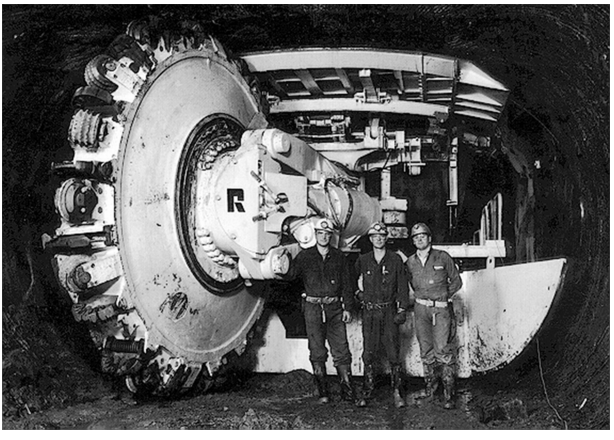

FIGURE 16.4
Robbins mobile miner. (Courtesy of Robbins, Product catalogues. With permission.)

This machine has been the only successful emerging partial-face excavator. However, it is hardly mobile with its weight reaching over 300 ton. One of the main problems with this cutting concept is the criss-crossing of the cuts. In other words, the cutters in each swing cross the cuts made in the previous pass. This is an inefficient process reducing the success of the concept and needs to be fixed.

16.3.2 Aker–Wirth Mobile Tunnel Miner

The first version of this concept was developed by Wirth and HDRK and the current development attempts are performed by Aker–Wirth. The excavation process is accomplished by cutting arms fitted with large-diameter disk cutters working in an undercutting concept. The arms are hinge-mounted on a rotating support plate. As the plate rotates, the arms are swung out to create spiral cuts to break the rock. The center arm creates a pilot hole by slewing toward the center of the bore. Once this free face is created, the other arms start cutting spiral tracks outwards toward the gage. This provides an undercutting action. When the arms reach the maximum inner circular profile of the tunnel, they can be extended farther to cut the corners to the desired final shape of the opening. This is all accomplished under computer control, allowing for different sizes and shapes of openings. A picture of this machine is presented in Figure 16.5.

16.3.3 Hard Rock Roadheaders

There were several attempts to manufacture a hard rock roadheader. In most of these attempts, the manufacturers usually concentrated on structural

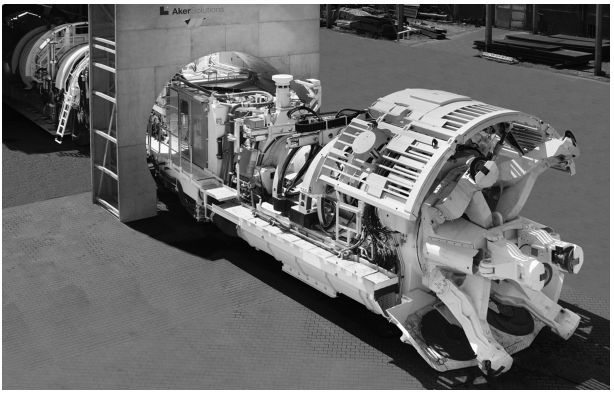

FIGURE 16.5
Aker-Wirth mobile tunnel miner with six arms. (Adapted from Aker-Wirth, 2013. http://www.wirth-erkelenz.de)

improvements such as heavier machines and more cutterhead power. However, it is known that hard rock cutting ability of roadheaders is limited due to the drag-type cutters they use. Therefore, most of those prototypes did not find any attention by the excavation industry. One of the most promising hard rock roadheader concepts was created by Earth Mechanics Institute of Colorado School of Mines (Ozdemir and Rostami 1995; Rostami et al. 1995). The laboratory studies verified the concept of using mini disks with a roadheader cutterhead; however, the concept should still be tested in field (Figure 16.6). The other successful testing of a prototype roadheader equipped with dual-property drag tools was performed by Voest Alpine; the excavation rate increased and tool wear was reduced in the prototype tests (Icacutrock 1998).

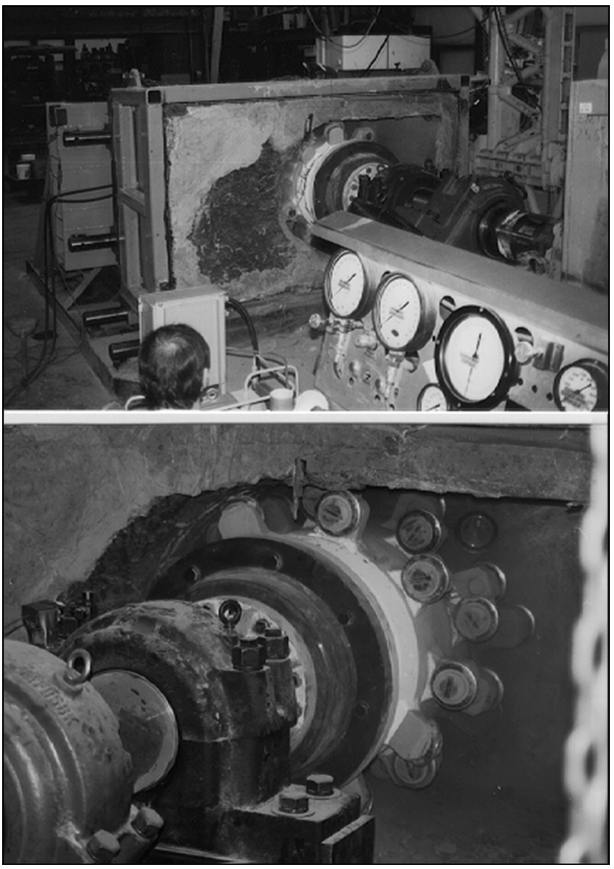

FIGURE 16.6
Minidisk equipped roadheader cutterhead during sumping test. (Adapted from Rostami, J., Ozdemir, L., Asbury, B., 1995. Mini-disc equipped roadheader technology for hard rock mining. *Proceedings of the 3rd International Symposium on Mine Mechanization and Automation*, eds. Ozdemir, L., Hanna, K., June 12–14. Golden, Colorado School of Mines, Vol. 2, pp. 16-1–16-12.)

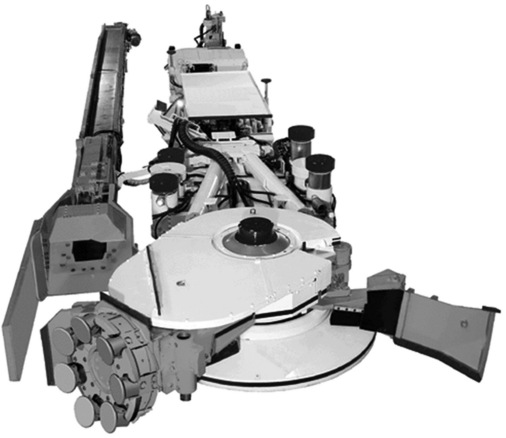

FIGURE 16.7
Sandvik reef miner. (Courtesy of Sandvik, 2013. http://construction.sandvik.com)

16.3.4 Sandvik Reef (Narrow Vein) Miner

Sandvik manufactured prototypes of reef miners equipped with undercutting disks and tested them in South Africa (Moxham 2004). The tests were encouraging for these machines in use for excavation of narrow hard veins, although the system had disadvantages of an undercutting concept. A picture of this machine is presented in Figure 16.7.

16.3.5 Other Developments on Hard Rock Excavation Machines and Systems

There were/are some other attempts to develop hard rock excavation machines and systems, of which some of them are in a conceptual or laboratory testing stage, while others are in the stage of field testing of prototypes. Some of them are Ramex impact kerfing cutter (Handewith et al. 1989), impact miner (Pickering and Haase 1995), radial and radial-axial splitters (Paraszczak and Hadjigeorgiou 1994; Lombardi 1995; Breeds and Conway 1992), and large-diameter stope coring/diamond core boring (Stacey 1982). Studies on deep sea mining machines are also still under development (Jones 2011).

16.4 Developments in Blind Shaft Excavation

There is quite a limited development in the field of blind shaft excavation technologies. There are a few conceptual designs of partial-face shaft boring machines (Robbins 1985; Snyder 1991; Frenzel et al. 2010) for hard rock

excavation. There has been almost no improvement in the concept since the muck removing problem could not be solved. However, a new system of shaft excavation was developed by Herrenknecht Company in Germany especially for soils under the water table, and also for soft rocks (Herrenknecht 2013). The vertical shaft sinking machine (VSM) uses a boom-type machine similar to a roadheader with a telescoping boom attached to the side walls of the shaft by anchoring arms that can also work under water (as submerged) to excavate the blind shaft, and a slurry system is used for transportation of excavated materials to a slurry separation plant. The shaft can be lined with precast concrete segments, in situ concrete, steel segments or, provided the soil is free from groundwater, also lined with rock anchors, steel mats, and shotcrete. The completed shaft can be used, for example, as a launch shaft for microtunneling or as an access shaft for existing caverns. The system was successfully used in a few countries for excavation of shafts up to 70 m depth and 9 m diameter.

16.5 Water-Jet-Assisted Mechanical Excavation

Combined water-jet–mechanical rock fragmentation has been one of the most widely researched hybrid excavation methods. Extensive laboratory and field trials have been performed for water-jet-assisted mechanical excavation, including demonstration projects with roadheaders and TBMs. The combination of mechanical energy and fluid energy can be in two forms: water-jet-assisted mechanical fragmentation and mechanically assisted water-jet cutting (Hood et al. 1989; Hood 1993; Summers 1995). The water-jet-assisted rock fragmentation has shown better results and consequently has been adopted by the industry. This system has the potential for achieving major advances in rock excavation. For mechanically assisted water-jet rock fragmentation, uniformly spaced kerfs are first created by water jets (principal source of energy) and then mechanical tools are used to remove rock ridges. Since the kerfs promote crack growth, this fragmentation method leads to chip formation with reduced bit forces. This method is not as attractive as water-jet-assisted mechanical rock fragmentation. This is mostly because the water-jet rock cutting still needs more energy than mechanical rock cutting. The main problem of using water jets with roadheaders is low machine utilization because of excessive water jet maintenance and excessive water amounts on the working area.

References

Aker-Wirth, 2013. http://www.wirth-erkelenz.de

Anonymous, 1995. Rock fracture: Cemented carbide still has more to offer. *World Mining Equipment*, April:35–36.

Breeds, C.D., Conway, J.J., 1992. Rapid excavation. Chapter 22.1. In *SME Mining Engineering Handbook*, ed. Hartman, H.L., U.S. Society of Mining Engineers, Littleton, Denver, Colorado, 2nd Edition, Vol. 2, pp. 1871–1907.

CMTE, 1998. Annual Report 1997–1998.

Frenzel, C., Burger, W., Delabbio, F., 2010. Shaft boring systems for mechanical excavation deep shafts. *Newsletter, Australian Centre for Geomechanics*, 34:1–4.

Friant, J.E., Ozdemir, L., 1994a. Development of the high thrust minidisc cutter. *Proceedings of Institute of Shaft Drilling Technology Annual Technical Conference*, April 18–21, Las Vegas, Nevada, 12 p.

Friant, J.E., Ozdemir, L., 1994b. Development of the high thrust mini-disc cutter for microtunneling applications. *No-Dig Engineering*, June:12–16.

Friant, J.E., Ozdemir, L., Ronnkvist, E., 1994. Mini-cutter technology—The answer to a truly mobile excavator. *Proceedings of North American Tunneling '94 Conference and Exhibition*, eds. Ozdemir, L., Brierly, G., June, Denver, Colorado, pp. 2B-49–2B-56.

Handewith, H.J., Coski, W.D., Thimons, E.D., 1989. Development of a prototype hard rock excavating machine. *Proceedings of the Rapid Excavation and Tunneling Conference*, Los Angeles, pp. 769–787.

Herrenknecht, 2013. http://www.herrenknecht.com

Hood, M., 1993. The use of water jets for rock excavation. *Rock Engineering*, 4(9):229–260.

Hood, M., Guan, Z., Tiryaki, N., Li, X., Karekal, S., 2005. The benefits of oscillating disc cutting. *Australian Mining Technology Conference*, Perth, September 27–28, pp. 267–275.

Hood, M., Knight, G.C., Thimons, E.D., 1989. A review of water-jet-assisted rock cutting. U.S. Bureau of Mines, IC 9273, 17 pp.

Icacutrock, 1998. Research report "Icacutrock" project cutting systems for hard rock conditions. *Sandvik-Tamrock-Voest Alpine*.

Jones, G.R., 2011. Deep sea mining—Nautilus Minerals Bismarck Sea development project. *The 22nd World Mining Congress and Expo*, September 11–16, Istanbul, Vol. 3, pp. 129–137.

Li, X.S., Tiryaki, B., Cleary, P.W., 2011. Hard rock cutting with smart*cut technology. *Proceedings of the World Mining Congress*, Istanbul, pp. 725–732.

Lombardi, J.A., 1995. An overview of drill-split excavation mining system potentials. *Proceedings of the 3rd International Symposium on Mine Mechanization and Automation*, eds. Ozdemir, L., Hanna, K., June 12–14, Golden, Colorado School of Mines, Vol. 2, pp. 15-1–15-11.

Moxham, K.A., 2004. A hard rock narrow reef mining machine—ARM 1100. *International Platinum Conference 'Platinum Adding Value'*. The South African Institute of Mining and Metallurgy, Johannesburg, pp. 207–214.

Ozdemir, L., Rostami, J., 1995. Roadheader development for hard rock mining. SME Annual Meeting, Denver, Colorado, March 6–9, 8 p.

Paraszczak, J., Hadjigeorgiou, J., 1994. Rock splitting as a primary excavation technique. *Proceedings of the North American Tunneling '94 Conference and Exhibition*, ed. Ozdemir, L., June, Denver, Colorado, pp. 2B-35–2B-48.

Pickering, R.G.B., Haase, H., 1995. Non-explosive mechanized mining in narrow, flat dipping reefs. *Proceedings of the 3rd International Symposium on Mine Mechanization and Automation*, eds. Ozdemir, L., Hanna, K., June 12–14. Golden, Colorado School of Mines, Vol. 2, pp. 15-27–15-37.

Ramazanzadeh, A., Hood, M., 2010. A state of the art review of mechanical rock excavation technologies. *International Journal of Mining and Environmental Issues*, 1(1)29–39.

Robbins. Product catalogues.

Robbins, R.J., 1985. What lies ahead for mechanized excavation. *Underground Space*, 9:93–96.

Rostami, J., Ozdemir, L., Asbury, B., 1995. Mini-disc equipped roadheader technology for hard rock mining. *Proceedings of the 3rd International Symposium on Mine Mechanization and Automation*, eds. Ozdemir, L., Hanna, K., June 12–14. Golden, Colorado School of Mines, Vol. 2, pp. 16-1–16-12.

Sandvik, 2013. http://construction.sandvik.com

Schafer, D.M., Glowka, D.A., 1994. An overview of the Department of Energy's advanced synthetic-diamond drill bit program. PD-Vol. 56, Drilling Technology, ASME, pp. 175–180.

Snyder, L., 1991. Design concepts for a partial face shaft boring machine. *Proceedings of the 1st International Symposium on Mine Mechanization and Automation*, eds. Ozdemir, L. King, R., Hanna, K., June 10–13, Golden, Colorado School of Mines, Vol. 2, pp. 7-15–7-24.

Stacey, T.R., 1982. Mechanical mining of strong brittle rock by large diameter stopecoring—Rock mechanics investigations. *Proceedings of the 14th Canadian Rock Mechanics Symposium on Rock Breaking and Excavation. CIM Special*, Vancouver, 30, 96–99.

Summers D.A., 1995. *Waterjetting Technology*. E & FN SPON, Chapman & Hall, Oxford, ISBN 0 419 19660 9, 882 p.

Thimons, E.D., Kogelmann, W.J., Virgona, J.E., 1991. A new hard rock cutting technology. *Underground Mining*, June:36.

This page intentionally left blank

MINING

Mechanical Excavation in Mining and Civil Industries

The secret to streamlined scheduling of mining and civil engineering projects is a solid understanding of the basic concepts of rock cutting mechanics. Comparing theoretical values with experimental and real-world results, **Mechanical Excavation in Mining and Civil Industries** thoroughly explains various rock cutting theories developed for chisel, conical, disc, and button cutters. The authors provide numerical examples on the effect of independent variables on dependent variables, as well as numerical and solved examples from real-life mining and civil engineering projects using equipment such as:

- Hard- and soft-ground tunnel boring machines (TBMs)
- Roadheaders
- Shearers
- Ploughs
- Chain saws
- Raise borers
- Impact hammers
- Large-diameter drill rigs
- Microtunnel boring machines

This book assists students and practicing engineers in selecting the most appropriate machinery for a specific job and predicting machine performance to ensure efficient extraction, and offers background information on rock cutting mechanics and different mechanical miners.

CRC Press
Taylor & Francis Group
an **informa** business
www.crcpress.com

6000 Broken Sound Parkway, NW
Suite 300, Boca Raton, FL 33487
711 Third Avenue
New York, NY 10017
2 Park Square, Milton Park
Abingdon, Oxon OX14 4RN, UK

K19055
ISBN-13: 978-1-4665-8474-7
90000
9 781466 584747